043
MIS
4235

Dissertation

on

STUDIES OF THE IONOSPHERIC IRREGULARITIES AT LOW LATITUDES

Presented

by

RAJIV KUMAR MISRA

for

the degree of

DOCTOR OF PHILOSOPHY

of

THE GUJARAT UNIVERSITY

043
B4235

RY
ATORY
80009.

October, 1971

PHYSICAL RESEARCH LABORATORY

AHMEDABAD

043
MIS
4235

P R E F A C E

Immediately after the decision of the Indian National Committee on Space Research for establishing a rocket station near equator (at Thumba) plans were made to start ionospheric investigations under the supervision of Dr.K.G.Rastogi. Ionospheric drift measurements were started in January 1964, using closely spaced receiver technique originated by MITRA (1949). An ionosonde (CRPL model C4) was also put into operation in October, 1964. The daytime horizontal drifts and the parameters of the ground diffraction pattern for 1964-65 were studied by Mr.M.R. Deshpande. In May 1967, additional receiving aerials were installed in the north-south direction and the observations were extended whenever possible over the night-time hours. The results of the second epoch were discussed by Mr. Harish Chandra in his Ph.D. thesis.

With the increasing sunspot number, it was felt that a high power transmitter was required to compensate the increasing absorption in the lower ionosphere. A completely new and independent ionospheric drift unit involving higher transmitter power and various other modifications in the recording unit was developed and constructed by the author at Physical Research Laboratory during 1966-67 and was

was installed at Thumba in January 1968. Additional receiving aerials were added in north south direction increasing the antenna separation to about one thousand metres. This new unit enabled uninterrupted round the clock observations of the F-region as well as on some nights for the E-region .

With the two independent transmitter, receiver and recording units being available and with a system of ten receiving aerials, various special observations were possible, namely simultaneous recording of drifts at two heights, on different multiples of the same frequency, at six different aerials etc.

The main scope of the present work was, besides, the solar cycle variation of drift, the special observations and analyses of the drift records which would clarify the significance of the drift measurements at the magnetic equator. Due to a continuous series of data, it has been now possible to correlate the drift with geomagnetic field changes at the equator and thereby to show a close association between the drift measurements and the equatorial electrojet currents.

During the course of observations, it was noticed that the E-region echoes in the nighttime were significantly

prominent only during the periods of thunderstorm activity and an investigation of the thunderstorm effect on equatorial ionosphere has been discussed.

The observations at Thumba for the period 1968-69 were taken by the author. The analysis of the data was later done by him at Physical Research Laboratory during 1970-71, using the facilities of the IBM 1620 computer.

R G Rastogi

(R.G.RASTOGI)
Professor-in-charge

R. K. Misra

(R.K.MISRA)
Author

R K Misra

LIST OF PUBLICATIONS

1. Ionospheric drift measurements at Thumba during 1964-68 - Proc. Third International Symp. on Equatorial Aeronomy (1969).

2. Ionospheric irregularities and their drifts at Thumba during 1964-68 - Ind. J. Pure and App. Phys.,8,548 (1970).

3. Daily variation of E-region drifts at the dip equator during 1968-69 - J.I.T.E. (1970) in press.

4. Solar cycle effects in the electron drifts over the magnetic equator - Journal of Geomag. Geoelect. (1971) in press.

5. Equatorial ionospheric drifts and the electrojet - Planetary Space Science (1971) in press.

6. Geomagnetic field variations and the ionospheric drift - Proc. Symp. on Equatorial Ionosphere, PRL Ahmedabad (1970).

7. Effect of magnetic activity on electron drifts in equatorial electrojet region - Nature (1971).

8. Height variation of F-region horizontal drifts - J. Atmos. Terr. Phys., 32, 967 (1970).

9. Horizontal and vertical electron drifts in the F-region at Thumba, J.I.T.E. (1971) in press.

10. The features of the ionospheric drift over the magnetic equator - Proc. COSPAR Meeting (1971).

11. Thunderstorm and the equatorial sporadic-E - Ind. J. Pure and App. Phys. (1971) in press.

12. Solar cycle variations of noon critical frequency of the E-layer- Proc.Third International Symp. on Equatorial Aeronomy (1969).

LIST OF FREQUENTLY USED SYMBOLS

t_x, t_y - Mean time lag between the similar fades in the eastwest and northsouth directions respectively.

ξ_o, η_o - Antenna separation in eastwest and northsouth direction respectively.

V' , ϕ' - Apparent drift velocity and direction derived by Mitra's similar fades method, direction measured in degrees east of magnetic north.

V_a, ϕ_a - Apparent drift speed and direction derived from the shift of the maximum of cross-correlation curves.

V , ϕ - True or steady drift speed and direction by full correlation analysis ϕ measured east of magnetic north.

V'_c - Fading velocity of the pattern.

V_c - The characteristic or random drift speed of the pattern.

r - Axial ratio of the characteristic ellipse.

b - Semi-minor axis of the characteristic ellipse.

ψ - Tilt of the major axis of the characteristic ellipse, east of magnetic north.

χ - Tilt of the line of maximum aplitude to the direction perpendicular to the direction of motion.

All the times used are in IST which is $5\frac{1}{2}$ hours ahead of GMT unless otherwise mentioned.

ACKNOWLEDGEMENTS

The author is greatly thankful to Prof.R.G.Rastogi for his guidance and supervision during the entire course of present investigations.

Thanks are also due to Prof.K.R.Ramanathan for his continuing interest and suggestions. The author feels pleasure in acknowledging thanks to the other members of the ionospheric group at Physical Research Laboratory (i) to Dr.J.S.Shirke for helpful discussions (ii) to Dr.M.R.Deshpande for his help during the development of the equipments at Ahmedabad (iii) to Dr.Harish Chandra for his assistance in the later stages of the work (iv) to Mr.R.P.Sharma for his help during the preparation of the thesis.

Thanks are also due to Computing Division at Thumba and at Physical Research Laboratory for their cooperation during the analysis of the data and to Mr.S.S. Deshikachar for his assistance in the computational work.

It is a pleasure to acknowledge thanks to Prof.V.A. Sarabhai, Chairman Indian National Committee on Space Research for the facilities at the Thumba Equatorial Rocket launching station to conduct these experiments.

The author is happy for his association with Dr.B.V. Krishnamurthy Dr.Ramnath and other members of the Space Physics Division of SSTC during his stay at Thumba. The author was recepient of the research fellowship from the Ministry of Education for the period of first three years during the course of the work.

Finally the author is deeply indebted to his parents whose continued encouragement has enabled him to achieve this goal.

C O N T E N T S

	Page
Preface	i
List of publications	iv
List of symbols	v
Acknowledgements	vi
CHAPTER I - INTRODUCTION TO EQUATORIAL IONOSPHERE AND THE IONOSPHERIC DRIFT MEASUREMENTS	
1.1 Geomagnetic variations at low latitudes	1
1.2 Electrical conductivities at the ionospheric heights	3
1.3 Ionospheric variations at low latitudes	6
1.4 Electromagnetic Drift of the ionization	8
(a) Martyn's theory	8
(b) Predictions of Martyn's theory for ionospheric drifts	9
1.5 Ionospheric drifts and its measurements	
1.6 Experimental set up at Thumba for Drift measurements	18
(a) Transmitter unit	18
(b) Receiving unit	21
(c) Recording system	25
(d) Antenna system	27

Page

CHAPTER II - FADING CHARACTERISTICS OF IONOSPHERIC ECHOES AND SIMILAR FADES METHOD FOR DRIFT COMPUTATIONS

2.1 Ratcliffe's theory of fading of radio-waves reflected from the ionosphere and further extensions by McNicol and others 31

2.2 Typical amplitude distribution and power spectrum of ionospheric echoes observed at Thumba 33

2.3 Diurnal, seasonal and solar-cycle variations of the fading rate of the reflected signal at Thumba 34

2.4 Similar fades method of analysis for drift from spaced antenna fading records 36

2.5 Results of apparent drift parameters at Thumba for the period 1964-69 39

2.6 Statistical errors in V' and its day-to-day fluctuations at a particular solar hour 49

2.7 Effect of solar cycle on the apparent drift at Thumba 50

2.8 Latitudinal variation of drift and anisotropy parameters 50

(a) Magnitude of apparent drift 50

(b) Diurnal and semi-diurnal drift vectors 51

2.9 Conclusions 52

CHAPTER III - FULL-CORRELATION METHOD OF ANALYSIS OF FADING RECORDS AT SPACED RECEIVERS

3.1 Method of Briggs, Phillips and Shinn and its extension by Phillips - Spencer and Fooks. 59

3.2 Optimization of the method of the present analysis 72

(a) Sampling theory 72

Page

(b) Criterion for the sampling interval and length of the record 74

3.3 Results of steady and random drift components at Thumba

3.4 Results of anisotropy parameters of ionospheric irregularities over Thumba 82

3.5 Solar cycle effect on drift and anisotropy parameters 89

(a) Steady and random drift speeds 89

(b) Anisotropy parameters 90

3.6 Occurrence of negative V_c^2 and r^2 at Thumba 91

3.7 Latitudinal dependence of drift and anisotropy parameters 94

3.8 Conclusions 96

CHAPTER IV - IONOSPHERIC DRIFTS IN RELATION TO THE EQUATORIAL ELECTROJET DURING MAGNETICALLY QUIET AND DISTURBED CONDITIONS

4.1 Equatorial ionospheric drift and the electrojet 106

4.2 Effect of magnetic activity on electron drifts in the equatorial electrojet 106

4.3 Steady and random drift parameters during magnetically quiet and disturbed days 106

4.4 Anisotropy parameters of the ground diffraction pattern during magnetically quiet and disturbed days 107

		Page
4.5	Reversal of drift and disappearance of sporadic-E during the short-term depressions in H.	108
4.6	Drifts during magnetic storms	110
4.7	Conclusions	111
CHAPTER V -	THE COMPARISON OF VARIOUS METHODS OF ANALYSIS AND THEIR VALIDITY	
5.1	Futter's method	114
5.2	Method of Briggs - Page and Spencer (probability distribution of time lags)	115
5.3	Banerji's statistical method for anisometric and turbulent patterns	116
	(a) Isometric turbulent pattern	116
	(b) Anisometric turbulent pattern	117
5.4	Method of Lyon, Morris and Bamgboye using standard deviation of time lags	118
5.5	Sprenger and Schminder's method (Variant-2)	122
5.6	Six point correlation method of Yerg and its modification by Keneshea and by Fedor for 3-D case	123
	(a) Yerg's method	123
	(b) Best fit correlation method	125
	(c) Statistical determination of the three dimensional ionospheric drifts	126
5.7	Briggs spatial correlation method of analysis	130

Page

5.8 Validity of correlation analysis 131

5.9 Results and comparison of various methods of analysis for Thumba (0.6°S dip) 132

5.10 Conclusions 138

CHAPTER VI - ON THE SPECIAL FEATURES OF THE IONOSPHERIC DRIFTS

6.1 Height gradient of the horizontal drift and anisotropy parameters in E and F regions of the ionosphere at Thumba 143

6.2 Vertical ionospheric drift in E and F regions at Thumba 145

(a) Introduction 145

(b) Experimental technique 146

(c) Method of analysis 147

(d) Results 148

6.3 Reversal of drift direction at Thumba 150

(a) Introduction and observations schedule 150

(b) Rate of fading and drift vector around reversal 151

(c) Morning reversal and the size of irregularities 154

(d) Evening reversal and height of the E-layer 154

(e) Reversal of drift in F-region and the appearance and disappearance of sporadic E layer 154

Page

(f) Reversal of drift and short-term fluctuations in H 155

(g) Conclusions 155

6.4 Drift and anisotropy parameters at Thumba during spread-F conditions 156

(a) Introduction 156

(b) Fading characteristics during spread-F 157

(c) Results for V', ϕ, V, ϕ, V_c, V, b r and γ 158

6.5 Occurrence of opposite drifts in E and F-regions at Thumba 161

6.6 Dependence of the drift and anisotropy parameters of the ground diffraction pattern at the equator on the E-W and N-S extent of antenna separation 162

(a) Introduction 162

(b) Special observations 163

(c) Results 165

(d) Interpretation of results 168

(e) Discussion 17

6.7 Effect of solar flares on the drifts at Thumba 172

6.8 Drift and anisotropy parameters from first and second order reflections recorded at spaced aerials 173

(a) Introduction 173

(b) Specular and diffusive reflection mechanisms 174

Page

(c) Experimental arrangements 176

(d) Apparent drifts 178

(e) Steady and random drifts 178

(f) Anisotropy parameters of the diffraction pattern 179

(g) Autocorrelation functions 179

(h) Discussion 180

CHAPTER VII - DISPERSIVE PROPERTIES OF THE IONOSPHERIC DRIFTS

7.1 Power spectrum analysis of fading records at Thumba 183

(a) Method of analysis 185

(b) Application to Thumba drift records 187

7.2 Power spectrum results for drifts at other stations 191

7.3 Interpretation of results 194

7.4 Comparison of apparent drift speed as determined by similar fades method and from the shift of the maxima of cross-correlogram 202

7.5 Skewness of the cross-correlograms 204

7.6 Analysis of frequency filtered drift records 206

7.7 Variation in the shape of the cross-correlation curves with the receiver separation 209

7.8 Conclusions 214

Page

CHAPTER VIII - THUNDERSTORM AND THE OCCURRENCE OF NIGHT-TIME SPORADIC E AT THUMBA

8.1 Introduction 215

8.2 Ionospheric soundings during thunderstorm activity 217

8.3 Conclusions 221

8.4 Discussions 222

References 224

CHAPTER - I

INTRODUCTION TO EQUATORIAL IONOSPHERE AND THE IONOSPHERIC DRIFT MEASUREMENTS

1.1 Geomagnetic variations at low latitudes

The solar daily variation on magnetically quiet days (S_q) of three components of the geomagnetic field, namely X (the northward), Y (the eastward) and Z (vertically downward) at various latitudes are shown in Fig.1.1 (VESTINE, 1960). It is seen that the variations are largest around 1100 hr local time. The curves for the X-component show that the amplitude of the variation decreases with increasing latitude on either side of the dip equator. It is also seen that the amplitude of S_q is abnormally large at Huancayo (- 0.6° dip), which was first noted by McNISH (1937). EGEDAL (1947, 1948) found that this abnormally large amplitude of $S_q(H)$ occurs at all the equatorial stations within a narrow belt (a few degrees of latitudinal width) around the dip equator (Fig.1.2). This phenomenon was interpreted by McNISH (1937) as due to locally concentrated eastward electric currents. This concentration of electric currents flowing eastward in a narrow zone over the equator in the sunlit hemisphere was named 'equatorial

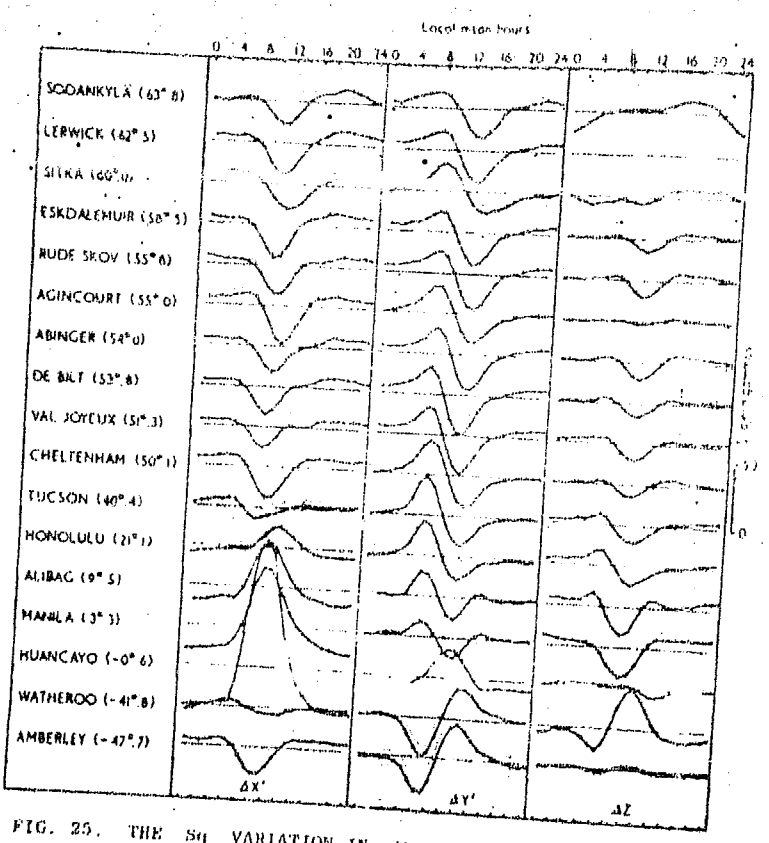

FIG. 25. THE Sq VARIATION IN ΔX, ΔY AND ΔZ AT VARIOUS LATITUDES (after Vestine, 1960).

FIGURE 1.1

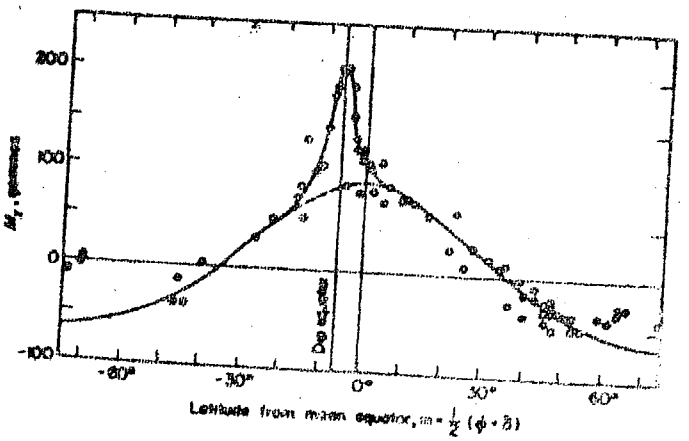

FIGURE 1.2

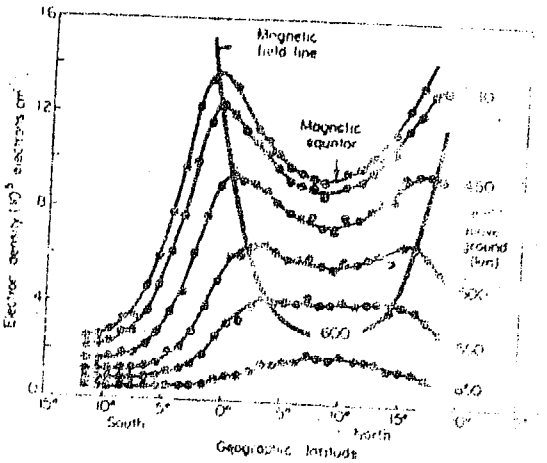

FIGURE 1.3

electrojet' by CHAPMAN (1951a). Further studies of the electrojet (RASTOGI, 1962; 1963) showed that it is most intense in the American zone and weakest in the Indian zone. Recent rocket measurements have shown that the peak current density of the electrojet is approximately 7.0 x 10^{-6} Amp/m^2 over Peru (MAYNARD, 1967; DAVIS ET AL.,1967) and approximately 4.0 x 10^{-6} Amp/m^2 over Thumba (SASTRY,1968), thus confirming the earlier results of RASTOGI (1962, 1963). The electrojet shows a solar cycle variation, being greater in the high sunspot period (RAO ET AL., 1965). Also the strength of electrojet is greater in equinoxes than in solstices (CHAPMAN and RAJARAO, 1965).

In order to explain the geomagnetic quiet daily variations, STEWART (1882) proposed that the upper atmosphere behaves like an electric conductor which moves across the earth's main geomagnetic field under the action of convective motion of air caused by solar heating. This would induce the electric currents in the conducting upper atmosphere. This theory of S_q (and L) variations is known as the dynamo theory and has been greatly modified since then (CHAPMAN, 1913,1919 ; HIRONO, 1950a,b,1952 ; MAEDA, 1951,1952; BAKER and MARTYN, 1952, 1953; CHAPMAN, 1956). These currents flow at a level where the electrical conductivity is largest. Hence a brief discussion of electrical conductivity is given.

1.2 Electrical conductivities at the ionospheric heights

In the presence of the magnetic field, the electrical conductivity of a lightly ionized gas, such as ionosphere, is anisotropic in character and is described below:

(i) Direct or longitudinal conductivity:

When the electric field (E) is parallel to the magnetic field (B), the conductivity, independent of magnetic field, is known as direct conductivity and is given by:

$$\sigma_0 = \sum \frac{n_r e_r^2}{m_r \nu_r} \qquad \text{-----(1)}$$

where m_r, n_r, e_r and ν_r are the mass, number density, charge (plus and minus for positive ions and electrons respectively) and the collision frequency with the neutrals of the r^{th} species of the charged particles.

(ii) Pedersen conductivity:

When E is perpendicular to B, the conductivity σ_1 is given by:

$$\sigma_1 = \sum \frac{n_r \nu_r e_r^2}{m_r (\nu_r^2 + \omega_r^2)} \qquad \text{----(2)}$$

where $\omega_r = \frac{e_r B}{m_r}$, gyrofrequency of the r^{th} species of the charged particles.

(ii) Hall conductivity:

In case of crossed electric and magnetic fields, the current flows perpendicular to both E and B. The conductivity denoted by σ_2 is given by:

$$\sigma_2 = -\sum \frac{n_r \omega_r e_r^2}{m_r (\nu_r^2 + \omega_r^2)} \qquad ----(3)$$

when the medium is bounded in the direction of hall current (i.e. the E x B direction), the flow of this current results in polarization which opposes further flow of current. In the ionosphere, hall current leads to polarization which easily leaks away along the lines of geomagnetic field except over the magnetic equator, where the geomagnetic field is entirely horizontal.

The conductivities σ_0, σ_1 and σ_2 are functions of n_r, m_r and ν_r which depend on neutral particle density. These parameters vary with time and space, horizontally and vertically. The height distributions of σ_0, σ_1 and σ_2 show that σ_1 or σ_2 are smaller than σ_0 and reach maximum at 110 - 140 Km (E-region). The ratio of σ_2/σ_1 is about 10 around 100 Km during the daytime (MAEDA and MATSUMOTA, 1962).

From this it is clear that the S_q currents flow mainly in the E-region. The existence of these currents has since been confirmed by rocket borne magnetometers (SINGER ET AL., 1951; CAHILL, 1959; DAVIS ET AL.,1965; SASTRY,1968).

At the magnetic equator, the geomagnetic field lines are horizontal and the electric field E is in the eastwest direction. Therefore the direction of hall current is vertical (E x B). Since the electrical conductivity is low below 70 Km and above 140 Km, the intermediate region is bounded in the direction of hall current. Thus the hall polarization field (E_p) completely inhibits the Hall current ($\sigma_2 E$) i.e. $\sigma_2 E = \sigma_1 E_p$ or $E_p = (\sigma_2/\sigma_1)E$. This polarization field E_p gives rise to additional current density along the direction of the original field E. The total current along E therefore becomes:

$$j = \sigma_1 E + \sigma_2 E_p = (\sigma_1 + \sigma_2^2/\sigma_1)\, E = \sigma_3 E$$

where σ_3 is known as cowling conductivity. As described earlier, the ratio (σ_2/σ_1) approximately 10 at about 100 Km. σ_3 is therefore very much larger than σ_1. This increased conductivity in the east-west direction accounts for the large currents of the equatorial electrojet. Since then this theory has been subject to modification by various workers (ONWUMECHILLI, 1959; SAGUIRA and CAIN,1966;

UNTIED, 1967; SUGIURA and POROS, 1969; COOK and PRICE, 1969).

1.3 Ionospheric variations at low latitudes

In 1931 Chapman gave a theory of ionospheric layer formation, according to which the maximum ionization of an ionospheric layer should vary with solar zenith angle, being maximum at noon and greater in summer than winter. E and F_1 layers are found to obey Chapman theory to some extent and exhibit strict solar control. On the other hand F_2 region shows various anomalies.

It was shown by BERKNER and WELLS (1934) that there is a noon bite-out in the daily curve of f_oF_2 at Huancayo, i.e. the peak of f_oF_2 is reached in morning and again in the late afternoon with a trough near noon. This bite-out effect was found to be typical of all the equatorial stations (HIRONO and MAEDA, 1954).

Another important feature of the equatorial F-region is the well known equatorial anomaly. A plot of noon values of f_oF_2 as a function of magnetic latitude shows a pronounced trough centered on the magnetic dip equator with crests 15 to 20° north and south (APPLETON 1946; BAILEY, 1948). The trough is also found in plots of electron density at fixed heights below (CROOM ET AL., 1959) and above (KING, 1954) (see Fig.1.3), the F_2 peak.

Further studies of the anomaly showed that the anomaly exists during most of the day, being most pronounced in the afternoon hours and disappears at about 20-21 hr (RASTOGI, 1959; LYON and THOMAS, 1963; RAO and MALHOTRA, 1964). The anomaly shows rather different features in different longitudes, seasons and different parts of the sunspot cycle.

A theory to explain the equatorial anomaly was first proposed by MARTYN (1947) and it makes the use of electro-magnetic drift (see section 1.3). According to this theory eastward electric field exists during the day at equator and produces an upward plasma drift in conjunction with the northward magnetic field. The plasma lifted in this way then diffuses down the magnetic field lines away from the equator causing an accumulation of electrons to the north and south. This explanation is now well known as the ' fountain effect' and has been further confirmed by the calculations of HANSON and MOFFET (1966) and BRAMELEY and PEART (1965).

Equatorial E_s

Ionosonde often detect dense layers or patches of ionization in the E-region at heights of 100-120 Km which is known as the sporadic E or E_s. Generally E_s

appears as a patchy and partially transparent layer while sometimes it appears in sheets which completely blankets the overlying F-layer.

Near the magnetic equator a distinctive type of 'equatorial E_s' is observed which is patchy and transparent to waves reflected from higher levels. It is a predominantly daytime phenomenon and is strongly associated with the equatorial electrojet current (MATSUSHITA, 1951; SKINNER and WRIGHT, 1957). KNECHT ET AL (1962) showed that the equatorial E_s occurs in a belt of width of about 700 Km which agrees very well with the width of the equatorial electrojet deduced from the geomagnetic observations. Further, the equatorial E_s irregularities seem to be aligned with the geomagnetic field (BOWLES ET AL.,1960) and may be caused by plasma instability arising from the flow of the large electrojet current (FARLEY, 1963). Recently MISRA and RASTOGI (1971) showed that the isolated thunderstorms sometimes produce an equatorial sporadic-E even in the night-time.

1.4 Electromagnetic Drift of the Ionization

(a) Martyn's theory:

Electromagnetic drift of ionisation was first suggested by MARTYN (1947, 1948) to explain the tidal

oscillations and the abnormal behaviour of F-region of the ionosphere. These drifts are caused by the electrodynamic forces associated with the magnetic variations, and have both vertical and horizontal components.

The equation of motion of a charged particle in the presence of electric field E and the earth's magnetic field B is given as:

$$u = \frac{J \times B}{\sum_r n_r m_r \nu_r} \qquad \text{(MARTYN, 1953 and KATO, 1959)} \qquad \text{- - - - (4)}$$

where J is the electric current density and u is the velocity of the charged particle with respect to neutrals.

In F-region, collision frequency is much smaller than the gyrofrequency and assuming that the vertical current vanishes at equator, we get for the component velocities:

$$\left.\begin{aligned} u_x &= -(E_y/B)\ \text{Sin I} \\ u_y &= (E_x/B)\ \text{Cosec I} \\ u_z &= (E_y/B)\ \text{Cos I} \end{aligned}\right\} \qquad \text{- - - (5)}$$

where I is the dip-angle and x,y,z are southward, eastward and vertically upward directions respectively.

(b) Predictions of Martyn's theory for ionospheric drifts

MARTYN (1953) studied the drift of ionization

under the influence of an electric-field and the atmospheric wind and derived the relations for the horizontal and vertical drift of ionization at all latitudes in a thin shell of ionosphere, in which the vertical electric currents are prohibited. His results can be summarized as follows:

(i) In the lower E-region, the ionization will move horizontally with substantial local wind velocity

(ii) In the upper E-region, the horizontal motion of ionization may differ substantially in magnitude and direction from that of the local wind velocity.

(iii) In the F-region, ionization cannot be moved by the neutral winds transverse to earth's magnetic field. A local north-south wind causes the F-region ionization to move along the direction of the earth's magnetic field. Strong eastwest drift is produced in F-region at the equator when the north-south electric field (E_x) is transferred from the dynamo region as a vertical electric field (E_z) in the F-region given by equation.

$$E_z = - E_x \text{ Cos } I$$

The eastward drift in F-region will therefore be given by:

$$u_y = (E_x \text{ Sin } I - E_z \text{ Cos } I) / B \quad - - - - (6)$$

and at equator

$$u_y = -E_z/B_x \qquad \text{---------- (7)}$$

(iv) The vertical drift velocities due to either winds or fields are small below 100 Km, except in the immediate vicinity of the equator, where the E-W electric fields can produce large vertical drifts at the heights of 90 Kms and above.

(v) Notable vertical drifts in F-region are produced by the E-W electric fields transferred from dynamo region crossing with earth's magnetic field (horizontal) or by the local N-S winds blowing the ionization along the field lines.

MAEDA (1963) obtained the complete solar daily variation of the three components u_x, u_y and u_z of the ionospheric drift speed and a world-wide distribution of the horizontal drifts, using the Martyn's theory. According to this the N-S component is zero at the equator and increases towards the pole, reaching a maximum of about 50 m/s. It is northward during daytime and southward during nighttime for low latitudes while at high latitudes it is northward beforenoon and southward after moontime. E-W component is towards west during day and east during night at low latitudes and reverse at the high latitudes with

the changeover occurring around 40-50° lat. The E-W component is maximum at the equator (~ 200 m/s) and decreases steadily to zero at the S_q focus beyond which it again increases but slowly. The vertical drift is highest at the equator and decreases slowly towards the poles. All the three components of drift in F-region show predominently a diurnal variation. The daily reversal of drift is sudden at the equator whereas at middle and high latitude, the drift vector goes through a slow rotation.

1.5 Ionospheric Drifts and its measurements

Introduction: - Existence of winds in the upper atmosphere was first noticed in 1923, when the changes occurred in the distribution of haze in the upper atmosphere following Krakatoa eruption. The visual observations of the noctilucent clouds provided the most direct evidence of the winds in the upper atmosphere. STORMER (1932, 1933 and 1935) studied horizontal drifts of such clouds and found average speeds of the order of 30-80 m/s in the height range of 80-90 Kms. Another evidence of winds in the heights around 100 Km was obtained from the drift of visual meteor trials. Both photographic and radio methods have been used to study the meteor trails (LILLER and WHIPPLE, 1953 and HEY, 1947 respectively). This method is limited to the height range of 80-110 Km. Both these

methods relate to the neutral winds in the upper atmosphere. The drift of ionization in the ionosphere was first noticed indirectly by RATCLIFFE and PAWSEY (1933) and PAWSEY (1935), while studying the amplitude fluctuations (fading) of a radio echo returned from the ionosphere. They concluded from the study of the fading records at two spaced receivers that the cause of fading was the interference of radio waves reflected from scattering centres in the ionosphere. PAWSEY (1935) was also first to notice a consistent time delay of the order of a second between fading records at two receivers. He attributed this to the horizontal movement in the ionosphere. MITRA (1949) and KRAUTKRAMER (1950), using the idea of RATCLIFFE and PAWSEY (1933) devised a technique to measure the ionospheric movements. A pulsed transmitter was used by **Mitra** at vertical incidence and the reflected signals fluctuations were recorded at three spaced receivers situated at the vertices of a right angled triangle of sides 100 metres each. From the time shifts between the maxima of similar fades the drift speed was determined. Radio stars have also been used as the source of radio waves instead of using ground based pulse transmitter. The radio star method gives the integrated drift of the entire ionosphere unlike the ground based transmitter method, giving the value of drift speeds at fixed levels of the ionosphere supposedly the level of reflection of the transmitted frequency.

Various techniques of drift measurements:

Various techniques employed for exploring the winds and drifts in the upper atmosphere have recently been reviewed by KENT and WRIGHT (1968). Following table gives the list of these alongwith the height range over which they are applicable:

Motion of Neutral Atmosphere		Height range of application
Ground based	1.Radio Meteor	80-110 Km.
	2.Airglow	75-105 Km and 190-260 Km.
	3.Noctilucent clouds	80-90 Km.
	4.Satellite drag	200-300 Km.
	5.Aurorae	100-120 Km
Vehicle borne	1.Chemical trail	80-200 Km.
	2.Ejected sensors	70-90 Km.
	3.Pilot tube	85-110 Km.
	4.Acoustic waves	85-95 Km.
Mass Motion of Plasma		
	1.Back-scatter	250-350 Km.
	2.Plasma ejection	100-200 Km.
Motion of irregularities in Plasma		
	1.Closely spaced receiver (D_1)	85-120 Km and 200-400 Km.
	2.Meteor trail method (D_2)	95-105 Km and 250-400 Km.
	3.Radio star scintillation(D_3) (for the patches of irregularities).	100-110 Km and 270-400 Km.
	4.Widely spaced receivers (D_4) (for large scale irregularities)	100-200 Km.

The first four techniques have been named as D_1, D_2, D_3 and D_4 by the international committee on drift measurements. The methods dealing with the motion of ionospheric irregularities are described below in brief:

(1) Closely spaced receiver techniques:

This is one of the most widely employed method to measure the drifts of the small scale irregularities of electron density. The basic technique is to record the amplitude pattern of the reflected signal simultaneously at three closely spaced points on the ground (MITRA, 1949). The radio waves are transmitted vertically upwards from a pulse transmitter. When these waves travel through these irregularities, phase modulation takes place and the returned waves form a diffraction pattern on the ground. The movement of these irregularities results in the movement of the ground diffraction pattern too, giving rise to amplitude variations at a particular point on the ground, with respect to the time. The time delays between similar fades at two set of receivers give the magnitude of drift speed of the ground diffraction pattern in that direction.

Drifts have been measured for E and F regions using Mitra's technique at large number of high latitude

stations since 1949 and a review is given for these results by BRIGGS and SPENCER (1954). A number of low latitude stations started functioning in the last decade.

The method of analysis for the determination of drifts from the spaced receiver fading records have since been modified by a number of workers. BRIGGS, PHILLIPS and SHIN (1950) were first to use full correlation method to derive the steady and random drift speeds. PHILLIPS and SPENCER (1955) modified it so that the anisotropy parameters of the diffraction pattern could also be derived. The statistical methods of analysis were later proposed by BRIGGS and PAGE (1955), PUTTER (1955) and BANERJI (1959,1960) to derive all these parameters from the time shifts data itself. DATTA (1968), SPRINGER (1969) and LYON (1969) have modified some of these methods.

(2) Doppler shift technique:

Motions of irregularities have been estimated from the doppler shifts in the radio echoes from them, using very high frequencies. Sporadic E irregularities in the equatorial and auroral regions have been detected by this method (COHEN and BOWLES, 1963; COLE,1963). CALVERT and COHEN (1961) and CLEMSHA (1964) have employed this technique to study the spread-F irregularities in the F-region. They reported an east-west dimension of the

order of 150-300 Km for these irregularities and a speed of 100-200 m/sec. in the eastward direction during nights. CLEMSHA (1964) in Africa reported an east-west dimension of about 400 Km and a mean rate of drift of about 100 m/sec. This is of the same order as that of the small scale irregularities.

(3) Widely spaced receiver technique:

The large scale irregularities are studied by the use of widely spaced receivers with a central transmitter or widely spaced transmitters with a central receiver. A separation of the order of several tens of kilometers is used. The waves received at three points travel in different paths and occasionally a similar anomaly is noticed on the three records with a definite time delay. These anomalies arise due to the passage of large scale irregularities across the three paths of travel, through the reflection points. These large scale irregularities are generally restricted to F-region, except for sporadic E layers of high ionization. MUNRO (1948, 1950 and 1953) studied the p - t traces at fixed frequency and noticed abnormalities appearing as peaksor dips of virtual height, crossing ordinary and extra-ordinary components. From the time delays between such abnormalities on different records, the drift speed of large scale irregularities can be derived.

(4) Radio star scintillation method:

Radio star scintillation have been employed by SPENCER (1955) and LITTLE ET AL. (1962) at high latitudes and by KOSTER (1963) at equator to study the drifts and size of the large patches of irregularities in the F_2 region. Scintillation of satellite signal after it traverses through the ionosphere, was first observed by SLEE (1958). MUNRO (1963) and KENT and KOSTER (1966) have described in detail the work on satellite scintillation technique.

1.6 Experimental set up at Thumba for Drift measurements

The experimental set up at Thumba Rocket Range for the measurement of ionospheric drift broadly consists of four parts:-

(a) Pulsed transmitter
(b) Receiving system
(c) Recording system
(d) Antenna system.

(a) Transmitter unit:

A new transmitting unit working on several frequencies was designed by the author on the pattern of CRPL-4 ionosonde so as to achieve a wide-band characteristic for the power stage. The aim was to achieve higher

BLOCK DIAGRAM OF THE TRANSMITTER

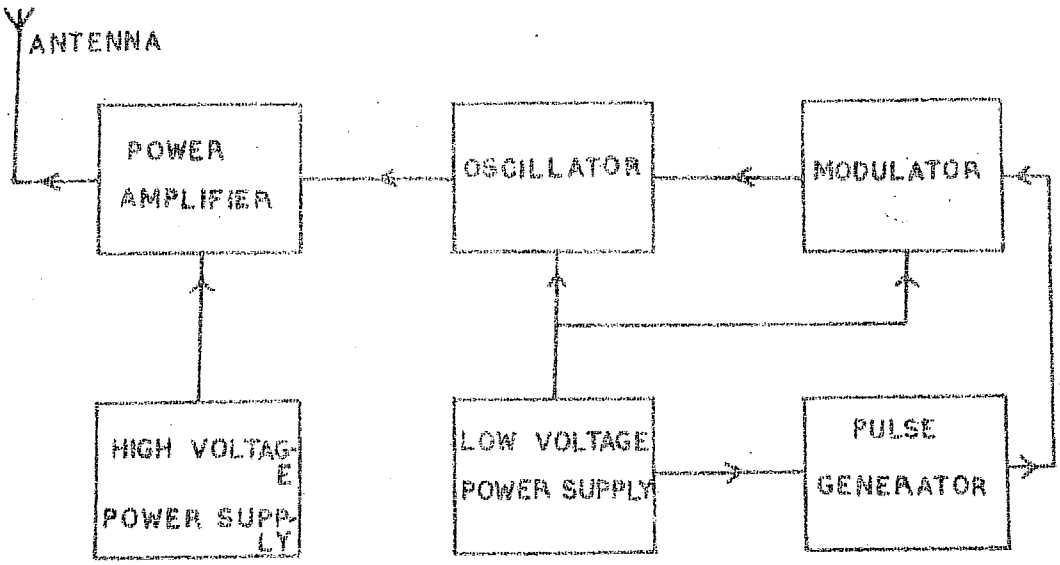

FIGURE 1.4a

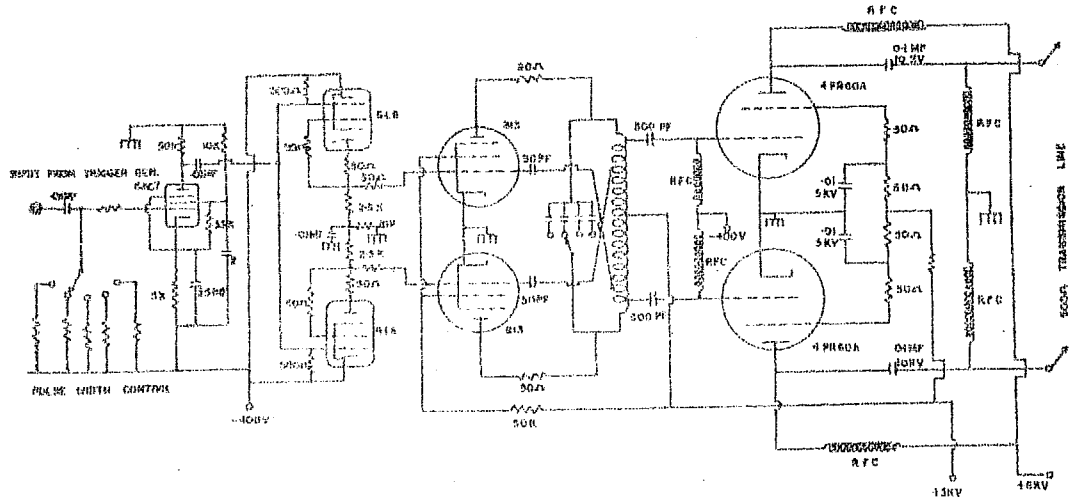

WIDEBAND PULSED TRANSMITTER

FIGURE 1.4b

power output at all the frequencies including 2.0 mc/s so that good reflections could be obtained from sporadic E layer. Fig.1.4a gives the schematic block diagram of the transmitter and Fig.1.4b gives the full details of the circuit. The basic characteristics of the transmitter are as follows:

Peak power	:	5 - 10 KW
Band width	:	2 - 10 mc/s
Pulse repetition rate	:	50- c/s
Pulse width	:	100 - 350 microseconds in steps of 50 micro-seconds.
Frequency range of operation	:	2 - 6 mc/s

It consists of the following basic units:

(i) Mains triggered pulse generator
(ii) Modulator
(iii) Master oscillator
(iv) Power amplifier

These are described below:

(i) Mains triggered pulse generator:

Fig.1.5 gives the circuit diagram of this unit. A sine-wave output of about 20V r.m.s. is derived from the step-down transformer T1, the phase of which can be varied with the help of a potentiometer R in the RC network. The square wave thus generated is differentiated

which triggers a one shot cathode-coupled multivibrator. The negative and positive pulses are obtained from the plates of V_2A and V_2B and used to trigger the transmitter.

(ii) Modulator:

In Fig.1.4b the tubes 6AC7 and 6L6 constitute the modulator section. The output of the mains triggered pulse generator is fed to the modulator unit. The pulse width is controlled at this stage by means of differentiating RC circuit. Five different resistors are provided to achieve pulse widths from 100 to 350 microseconds in steps of 50 microseconds. The negative pulse output of 6AC7 is applied to the grids of the modulator tubes. The plate loads of these two tubes are the grid leaks of the two tubes of master oscillator (4PR60P) which are normally biased beyond cut off. The negative pulse from 6AC7 momentarily cuts off the modulator tubes and the bias is removed from the oscillator, which is thus allowed to oscillate for the duration of modulator pulse.

(iii) Master oscillator:

This consists of two 813 tubes in the push-pull connection of a Hartley circuit. The oscillator is grid modulated and operates only during the duration of the pulse. A 3KV plate voltage and 800V screen voltage is employed.

(iv) Power amplifier:

A broad band power amplifier stage on the pattern of CRPL-4 ionosonde was designed. This consists of two 4PR60A tubes with 60 watts dissipation power, in the push-push connection. Radio frequency chokes in the plate circuit are used as the loads. A 6KV plate voltage and 1.25 KV screen voltage is employed for the best efficiency of the system. The grid of these tubes are normally biased to cut-off with - 400V. D.C. coupling is used for the antenna connection. The output impedence of the power amplifier is 600 ohms over 2-6 mc/s and it is matched to the input impedence of the wide-band transmitting aerial by means of a 600 ohms transmission line.

(b) Receiving unit

Schematic block diagram of the receiving unit is shown in Fig.1.6. The complete system consists of the following parts:

(i) Trigger generator
(ii) Delayed Pulse generators
(iii) Electronic switch and step wave generator
(iv) Sweep generator
(v) Pulse receiver

These are described below in detail:

(i) Trigger generator:

This is the basic circuit which gives rise

TRIGGER UNIT

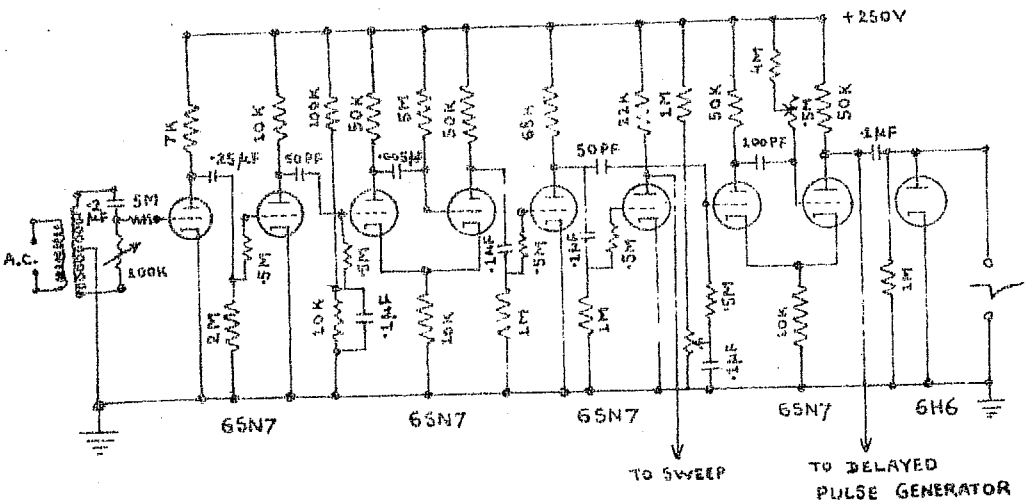

FIGURE 1.5

BLOCK DIAGRAM OF RECEIVING & RECORDING SYSTEM

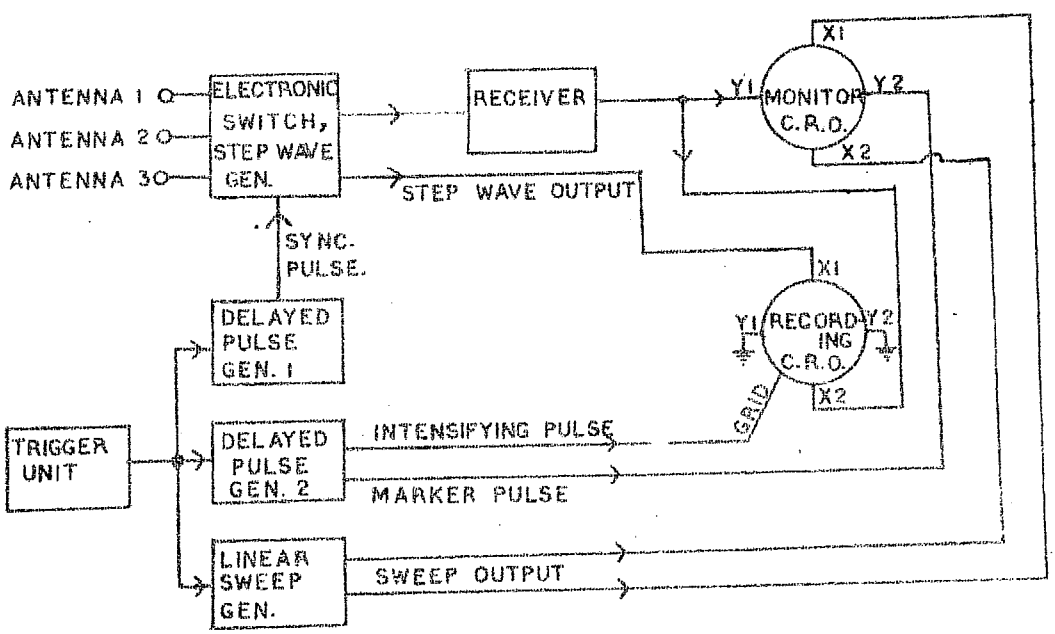

FIGURE 1.6

to 50 c/s pulses required to trigger various subsequent circuits in the receiving unit and is similar in design to the one described in connection with the transmitter. The positive pulse output is fed to the delayed pulse generator and the negative pulse output is fed to the linear sweep generator. The circuit diagram is given in Fig.1.5.

(ii) Delayed pulse generator:

In order to select out a pa rticular echo for recording its fading, a gating circuit is used which gives a pulse whose phase can be varied with respect to the ground pulse. Two such circuits are used, one for synchronizing the electronic switch and another for generating two pulses, one of 15V which is fed to the monitoring scope for the visual selection of the echo by varying its phase and another of 150V and of the same phase, to intensity modulate the recording oscilloscope during the period of the pulse in which the desired echo appears. The schematic circuit diagram is shown in **Fig.**1.7. The phase and the width of these pulses are controlled by the potentiometers P1 and P2 respectively, put in the grid circuit of the tubes V1 and V2. The final output is taken through a cathode follower stage V4, to avoid the loading.

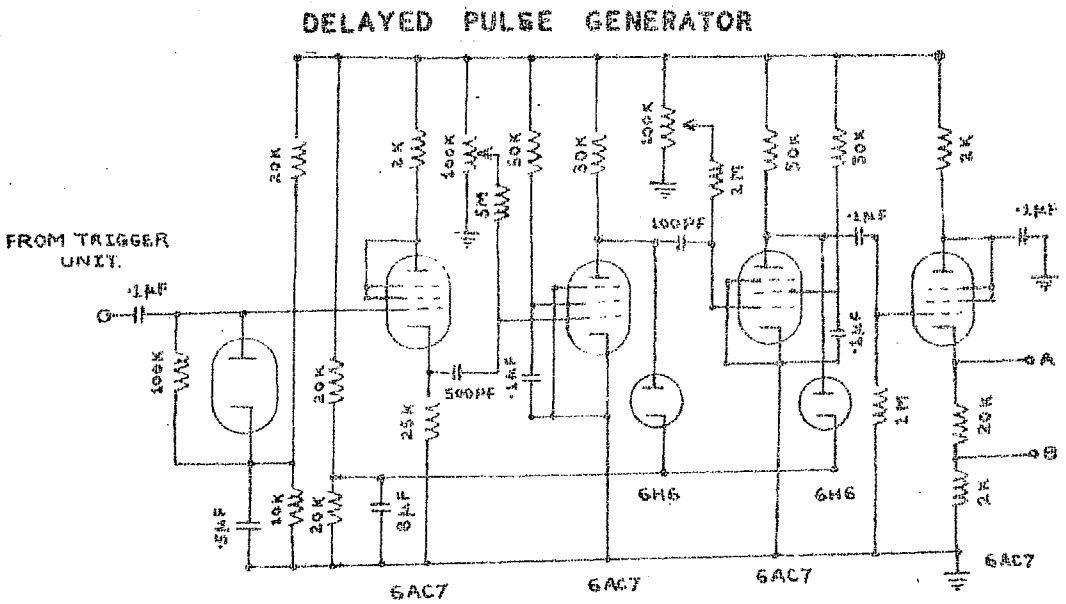

FIGURE 1.7

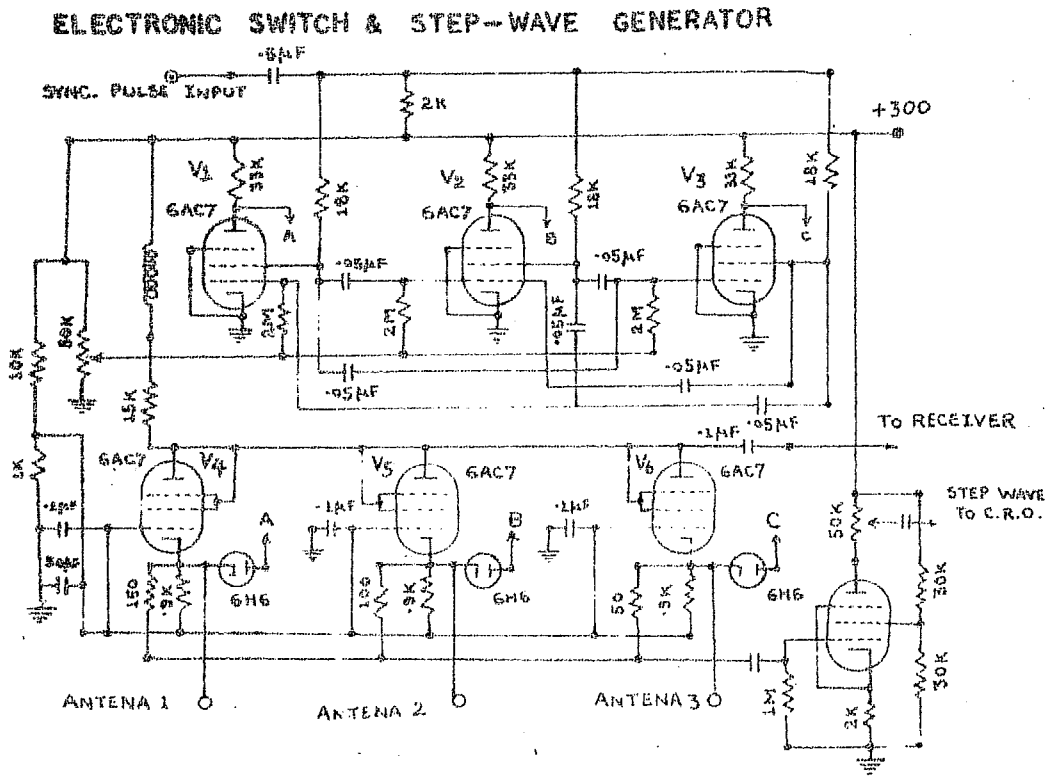

FIGURE 1.8

(iii) Electronic switch and step-wave generator:

This unit provides the switching sequence for the three aerials in succession to a receiver. The circuit diagram is given in Fig.1.8. It also provides a step wave output enabling the separate recording of the signals from the three aerials.

The grids of V1, V2 and V3 are used to produce the multivibrator action and the output is taken from the plates. The wave forms at A, B and C switch the grounded grid high frequency amplifier tubes V4, V5 and V6. These wave-forms are applied to the cathodes through the diodes V7,V8 and V9. During the lower voltage level of the wave-forms at A,B and C, the tubes V4, V5 and V6 conduct, thus connecting the antenna to the receiver in equal sequential order. The wave-forms at the cathode of V4,V5 and V6 are similar to that at A,B and C. By combining these pulses with the loads in the ratio of 1:2:3, a step-wave is generated which is amplified by V10. This wave, when fed to the X-plates of recording C.R. tube, gives rise to three distinct spots on the screen, whose relative separation and overall coverage can be controlled by two potentiometers on the front panel - one is in the plate circuit of the amplifier tube and the other is one of the combining load resistances.

(iv) Linear sweep generator:

Fig.1.9 gives the schematic circuit diagram for this unit. A sanatron type circuit is used to generate a single stroke linear sweep. The circuit also provides a rectangular pulse, having precisely the same duration as the sweep, which is used to brilliance the monitoring oscilloscope during this period only, thereby avoiding the appearance of flyback. The sanatron consists of the Miller integrating circuit of V4 linked with V2 to form one semistable stage. The coupling of a similar tube V5 with V4 enables to get the push-pull output of the sweep wave form. This is to ensure perfect linearity of the sweep on the monitor scope. The output is d.c. coupled to the X-plates of the monitor scope.

(v) Pulse receiver:

BC-348 CW receiver was modified suitably for the pulse operation by removing its AVC and using high gain 6AC7 tubes in the two RF stages. Further the band-width was increased by suitable damping of the primary and secondary coils of IF transformers with proper resistances. The detector (6H6) was operated in linear portion of its characteristic curve and the detected output was video amplified in a 6AC7 tube and fed to the recording and monitoring CR-tubes in X and Y plates respectively.

TIME BASE UNIT

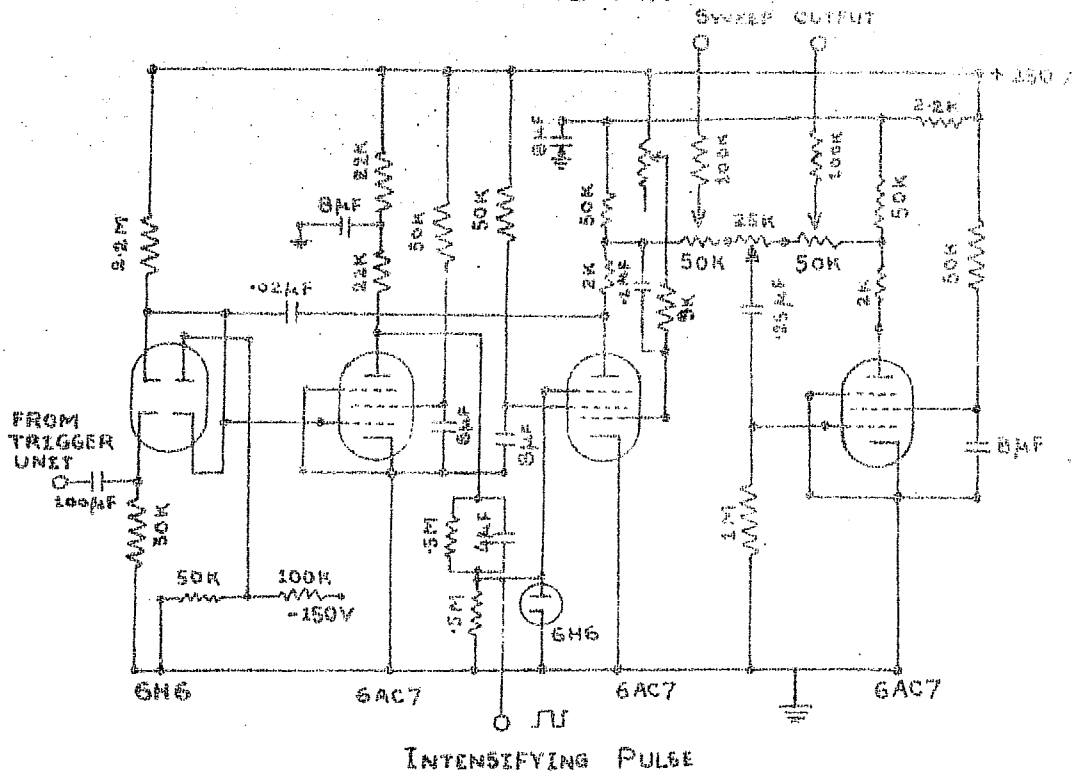

FIGURE 1.9

RECEIVER

R.F. AMP. & MIXER SECTION

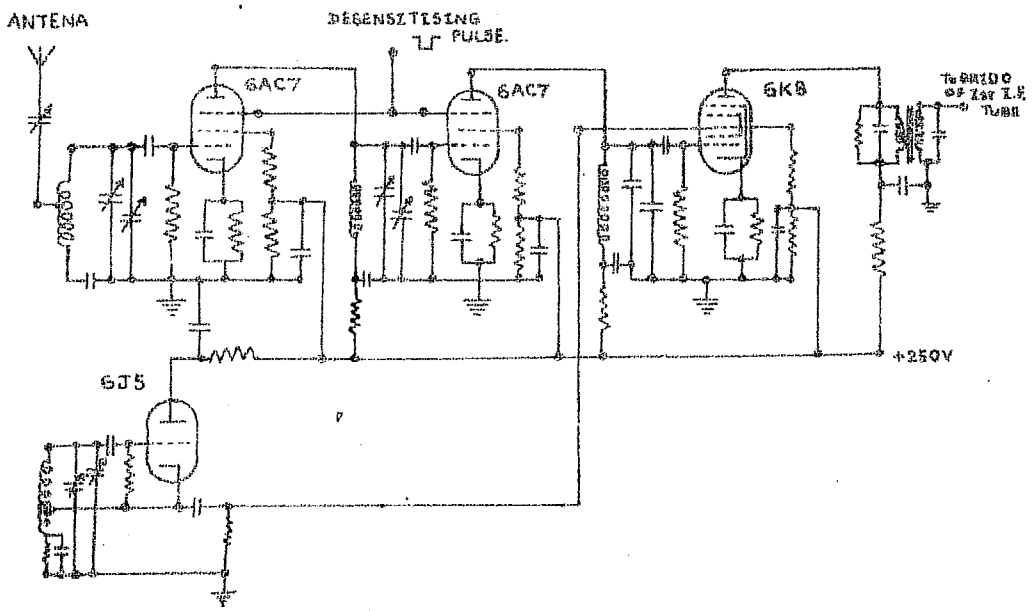

FIGURE 1.10

Figs. 1.10 and 1.11 give the complete modified circuit diagrams for the R.F. and I.F. stages of the pulse receiver. The linearity of the receiver response with respect to strength of the input signal was also ensured (see Fig.1.13).

(c) Recording system

(i) Monitoring and Recording Units:

A green screen tube 5BP1 and a blue screen tube 5LP11 are used for the monitoring and recording oscilloscopes respectively. The recording tube's pattern is also displayed on the front panel by connecting another 5LP11 tube in its parallel. The X and Y shifts are controlled by means of ganged 500K potentiometers. Fig.1.12 gives the details of the circuit connections. The sweep output is fed to the X-plates of the monitoring CR-tubes and the received output to its one of the Y-plates. The delayed pulse (gating pulse of 15V) is fed to the other Y-plate. The intensifying pulse from the sweep generator (150V) is applied to the grid of the monitoring tube 5BP1.

The step wave output is connected to the X1-plate of the recording 5LP11 tube. The receiver output is connected to the X2 plate of the tube. Theintensity of the trace on the recording oscilloscope is kept out off in the normal condition and is intensified by 150V pulse only

RECEIVER

I.F. AMP. 2ND DET. & VIDEO AMP. SECTION

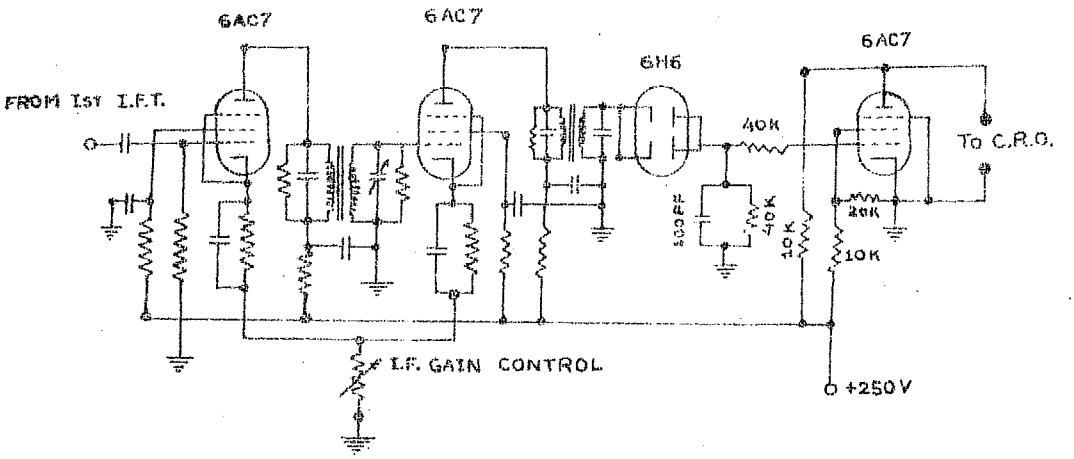

FIGURE 1.11

DISPLAY UNIT

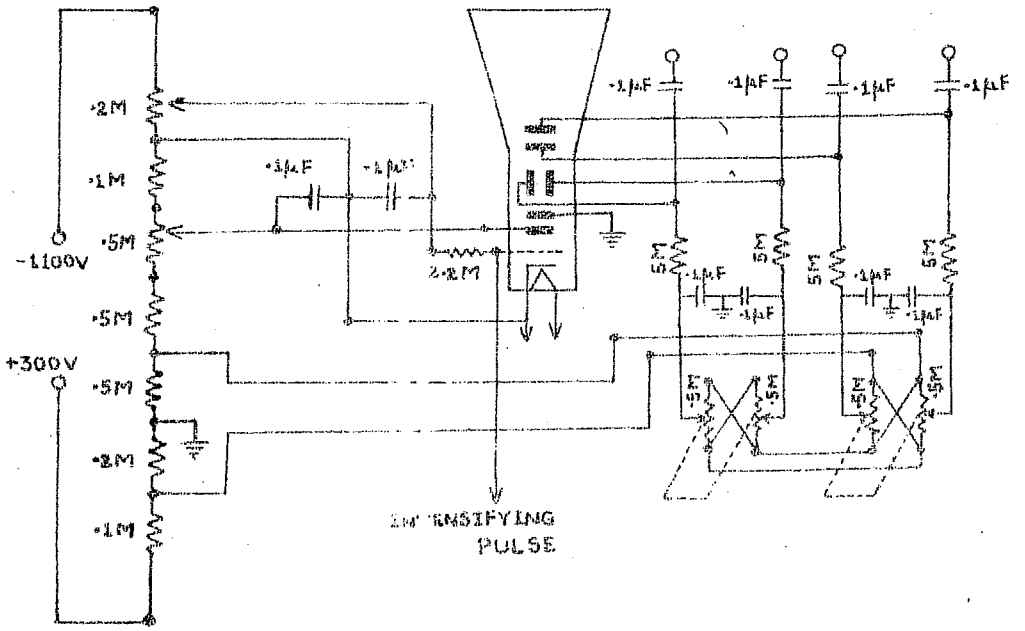

FIGURE1.12

during the portion of gating time, which is same as 15V pulse phase. The pulse is applied to the grid of the recording tube.

(ii) Camera system:

A Camera system was designed to record the fading patterns at three or more aerials on the same 35 mm film at various fading rates. The film speed could be controlled from 5 cm/minute to 100 cm/minute in the steps of five cm/minute. Very slow as well as very fast fading could therefore be recorded at appropriate film speeds. This was achieved by using various combinations of the gears between the 1RPM synchronous motor and the 35 mm toothed drum. End of the film indicator was also designed using a rolling type of microswitch.

(iii) Height marker:

A height marker circuit was designed using a crystal oscillator of Harteley type. The sinusondal output of this 3 Kc/s oscillator was squared in an over driven amplifier and then differentiated. The negative sharp pulses were then clipped off by taking the output through a crystal diode and the sharp positive pulses were fed to the Y-plate of the monitoring oscilloscope. 50 Km height markers were thus obtained and used to record the height of the echo,

which is selected for the drift measurement.

(iv) Time marker:

All the drift records were time marked at the intervals of 12 secs in the form of transparent vertical lines on the film, by cutting of the intensifying pulse from the recording oscilloscope for the fraction of a second using a microswitch and a cranked wheel arrangements. The wheel was moved at the rate of one revolution per minute by means of a synchronous motor.

(d) Antenna system

Half wave centre fed dipoles oriented along magnetic N-S were used to receive the signals. Eight such aerials were used as depicted in Fig.1.14. Four were in the north-south direction, with an overall separation of 960 metres between extreme aerials and four in eastwest direction. The relative disposition of these aerials is shown in the figure. The suffixes denote the distance in the unit of λ (i.e. 120 metres for 2.5 mc/s). Each aerial was a quarter wave dipole for 2.5 mc/s. Aerials N4,N2, C and S4 were accurately alined in N-S line and W2,W1, $W\frac{1}{2}$, C and $E\frac{1}{2}$ were accurately alined in E-W direction.

The transmitting aerial consisted of a wide-band double folded dipole, with an input impedence of 600 ohms

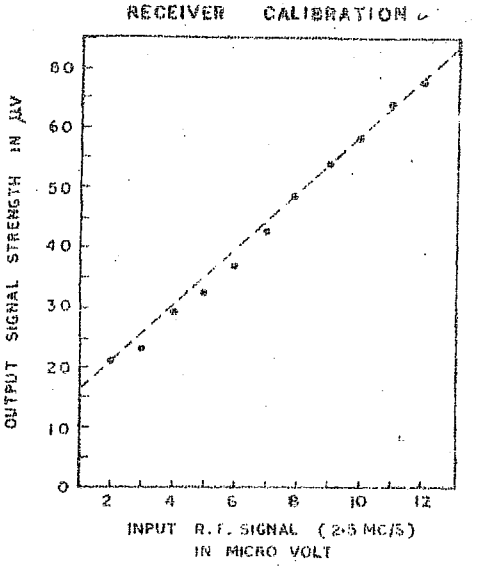

FIGURE 1.13

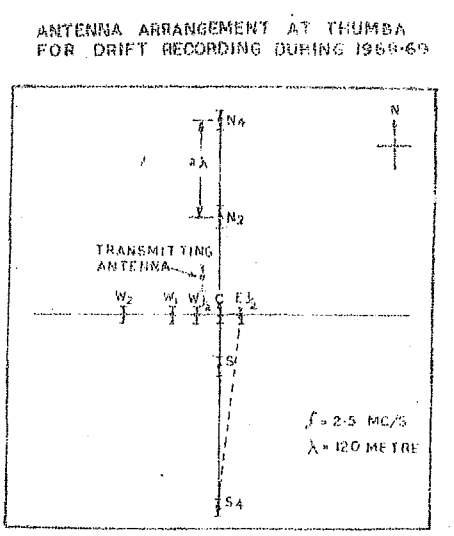

FIGURE 1.14

THUMBA F-REGION (6·0MHz)

DRIFT RECORDS WITH SIMPLE AND DIRECTIONAL TRANSMITTING AERIALS

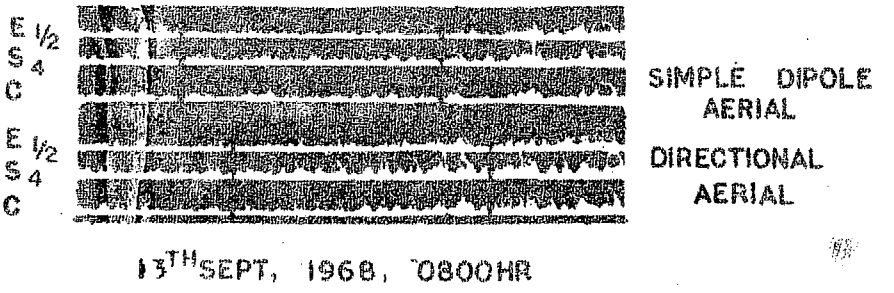

FIGURE 1.15

for 2-6 mc/s and located near the W1 receiving dipole. A 600 ohms transmission line was used to feed the transmitter output.

Two more transmitting dipoles for the fixed frequency operation at 2.2 and 4.7 mc/s were also used. Two central receiving dipoles were installed in order to take simultaneous drift observations at two frequencies or two triangles.

Coupling between aerials

The signal received by one aerial may be reradiated and received by the other. ROSSITER (1970) on the basis of nearly equal cross-correlation between the parallel and perpendicularly aligned receiving aerials separated by the same distance apart, showed that the orientation of the aerials relative to one another is not important. The correlation between the records at orthogonal aerials at the same point should be unity but was found to be 0.92. It is shown that this depression arises not due to the coupling of the aerials but due to the other experimental factors such as the unequal amplifications and the digitizing errors.

Directivity of the aerials

The radiation pattern of a simple dipole aerial is a main lobe of about 60° solid angle. A very wide area of

the E and F regions of the ionosphere is therefore illuminated by the simple dipole transmitting aerials. Even-though a gating mechanism is used for the selection of the echo so that the radio waves reflected only from a limited area of the layer may contribute to the fading record, the possibility of the contamination of the drift records by the flant echoes coming from much wider portion of the ionosphere is not ruled out. In such a case, as the drift of the irregularities may not be the same over such a wide area of a few hundreds of Kms, different fading frequencies may lead to different values of drift velocity and there will be an imposed or artificial dispersion in the observed drift. Such an effect can be reduced to some extent by using more directional transmitting and receiving aerials. As a large number of receiving aerials have to be used, it was found easier to use a more directional transmitting aerial. A parasitic type of reflector was used to increase the directivity of the transmitting aerial. The directivity with this arrangement was expected to be about 20°. Fig. 1.15 shows drift records taken with and without directional transmitting aerials. Very little effect was however felt on the fading characteristic and the drift parameters, showing that a directivity of 20° is also not sufficient. A better directivity could however not be achieved for such low frequencies as 2 to 6 MHz as the erection of an array required a very large area on the ground.

CHAPTER - II

FADING CHARACTERISTICS OF IONOSPHERIC ECHOES AND SIMILAR FADES METHOD FOR DRIFT COMPUTATIONS

A radio wave reflected from the Ionosphere is found to fluctuate in intensity when received at a ground station. This phenomenon is called the fading of the signal. The fading could be caused by the following processes:

(a) the interference between the reflected and the ground wave,

(b) the interference between the multiply reflected waves,

(c) the interference between the waves reflected from different regions of the ionosphere,

(d) the interference between the magneto-ionic components.

By using short pulses of radio waves and the gated receiver, it is possible to isolate a single downcoming wave (as described in chapter I). One of the magneto-ionic component can be supressed by the use of polarized aerial. The signal is still observed to fade. The experiments conducted by APPLETON and RATCLIFFE (1927) and RATCLIFFE and PAWSEY (1933) showed that the fading rate was roughly proportional to the frequency of the radio-wave and the fadings recorded at two points on the ground were uncorrelated at a separation of more than one wave length. From

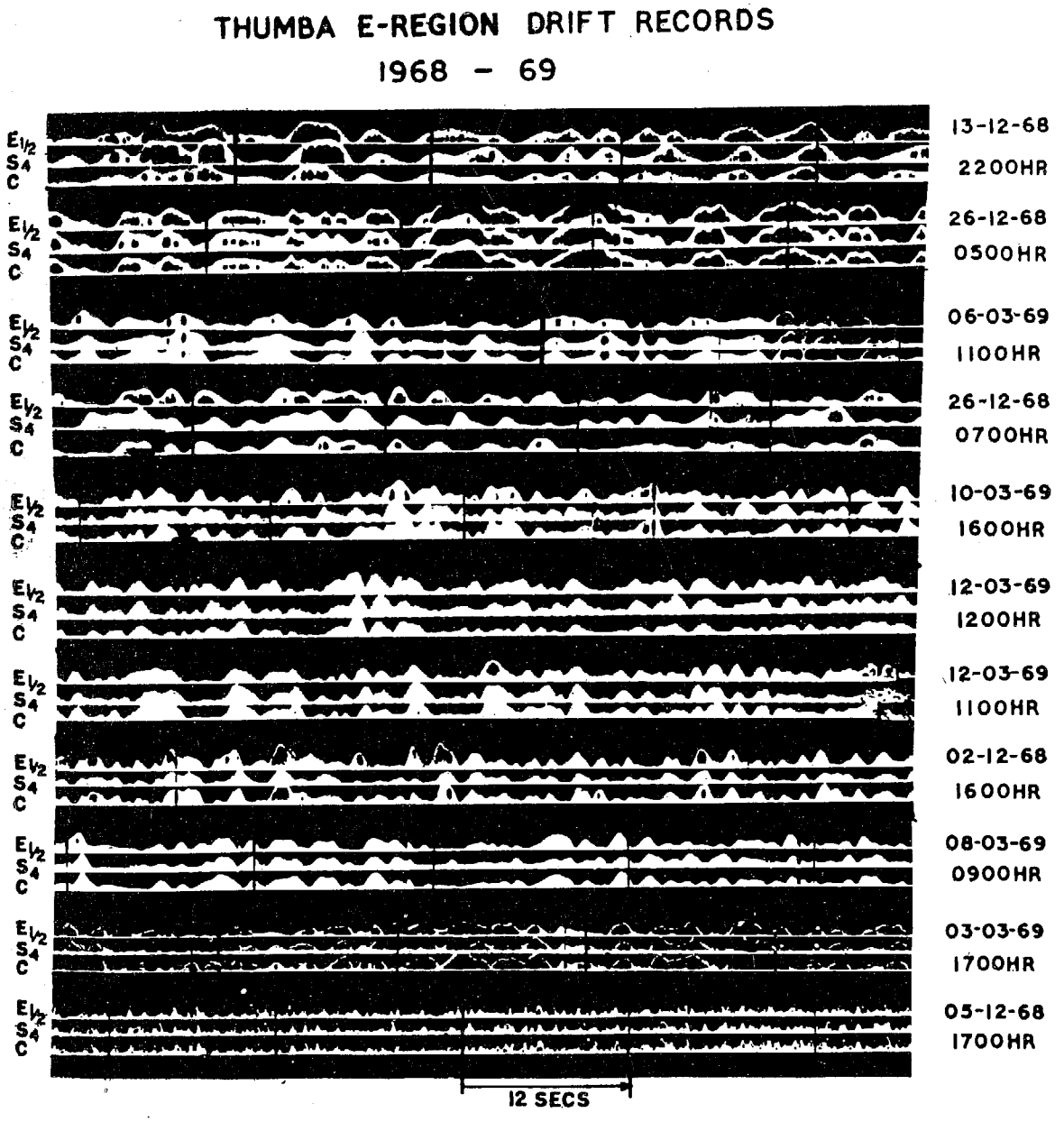
THUMBA E-REGION DRIFT RECORDS
1968 - 69
E½
S4
C
13-12-68
2200HR
26-12-68
0500HR
06-03-69
1100HR
26-12-68
0700HR
10-03-69
1600HR
12-03-69
1200HR
12-03-69
1100HR
02-12-68
1600HR
08-03-69
0900HR
03-03-69
1700HR
05-12-68
1700HR
12 SECS

Figure 2.1

the measurements of the angle of deviations of the waves, RATCLIFFE and PAWSEY (1933) concluded that the fading is due to the interference at the ground of the waves scattered from a series of diffracting centres distributed over an area of ionosphere at least 20 Km in radius in their experiment.

2.1 Ratcliffe's theory of fading of radio-waves reflected from the ionosphere and further extensions by McNicol and others

Based on above experimental findings, RATCLIFFE (1948) gave a theory of fading of the radio waves considering the ionosphere as a diffractive screen. It is assumed that there exist several scattering centres distributed approximately in a horizontal plane and that each centre scatters the same power from the incident wave. As the centres are randomly distributed, the phases of the various scattered waves may be assumed to be randomly distributed. The resultant signal strength at ground will therefore consist of components of different frequencies. He showed that the power within a frequency range df is shown to be:

$$W(f)\,df = \frac{}{\sigma\sqrt{2\pi}} \exp\left(-(f^2-f_o^2)/2\sigma^2\right) \qquad \ldots\ (1)$$

where $\sigma = 2 f_o V_o/c = 2 V_o/\lambda$, V_o being the velocity of scattering centres in the line of sight and the wave

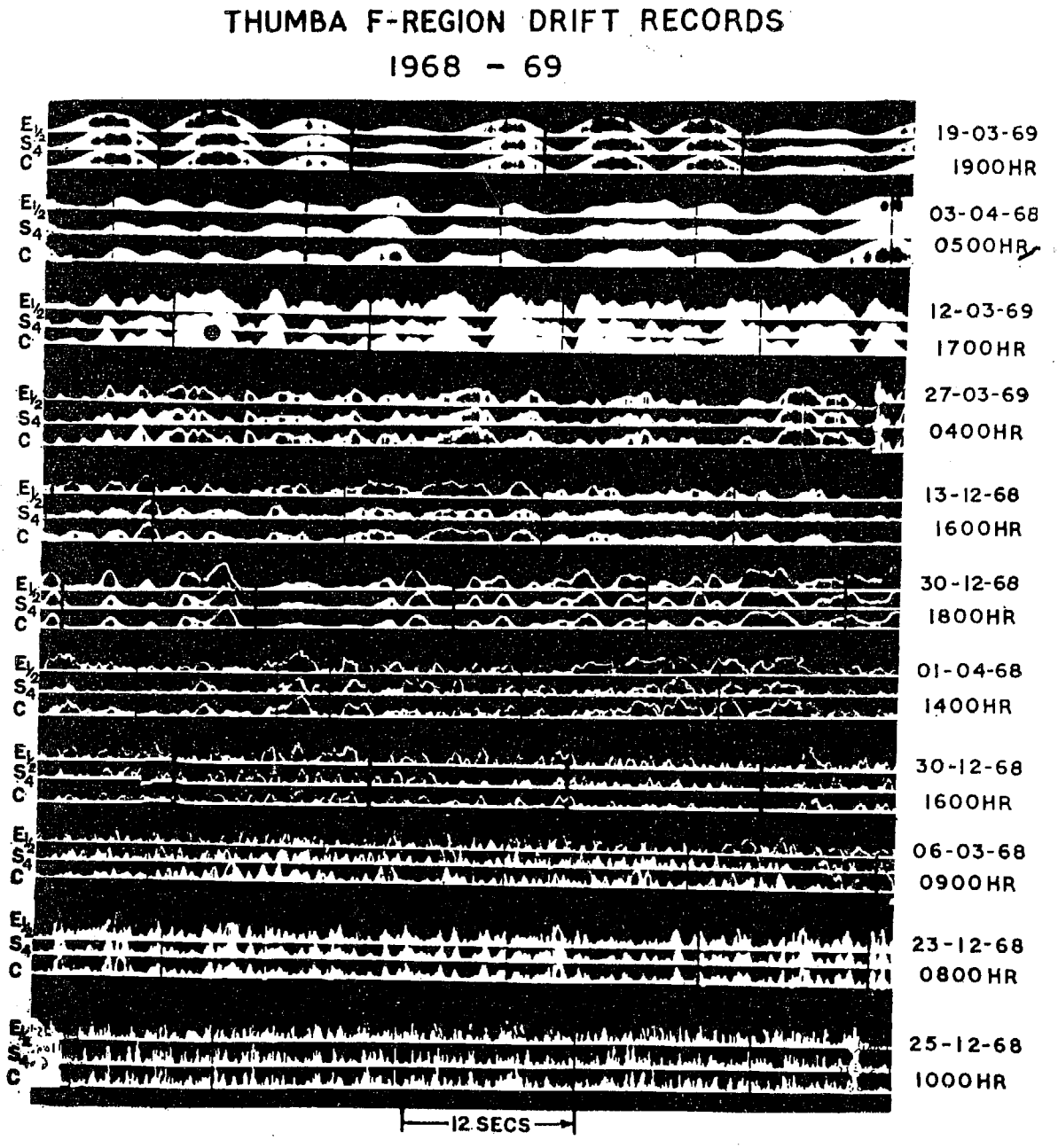
THUMBA F-REGION DRIFT RECORDS
1968 - 69
E½
S4
C
19-03-69
1900HR
03-04-68
0500HR
12-03-69
1700HR
27-03-69
0400HR
13-12-68
1600HR
30-12-68
1800HR
01-04-68
1400HR
30-12-68
1600HR
06-03-68
0900HR
23-12-68
0800HR
25-12-68
1000HR
12 SECS

Figure 2.2

length used. Also $\psi = \int_0^\infty W(f)\,df$ = total power in the wave. FÜRTH and MCDONALD (1947) had shown that in a power pass filter of this characteristic, the amplitude R of the output signal is distributed according to Rayliegh law and the probability distribution P(R) for the range R and R+dR is given by:

$$P(R) = \frac{R}{\psi} e^{-R^2/2\psi} \qquad \ldots\ldots(2)$$

The mean amplitude $R = \sqrt{\pi\psi}/2$ and most probable value of the amplitude, $R_m = \psi^{1/2}$.

McNICOL (1949), using the method suggested by RICE (1945), has worked out the probability distribution of amplitude where there is a steady movement of the scattering centres besides the random movement. If B is the amplitude of the steady signal and R is that of random signal, then the resultant amplitude, we have $Q = (B^2 + R^2)^{\frac{1}{2}}$. McNICOL (1949) showed that the probability distribution of Q i.e.P(Q) is of Rayleigh type when the ratio $b = B/\sqrt{\psi}$ (i.e.the steady to most probable random signal) is less than one and of Gaussian type when $b \gg 1$. The theoretical curves for different values of the parameter 'b' are shown in the Fig.2.3.

ALPERT (1960) has given another way of defining this ratio of steady to random signal. According to this, the ratio of the average square of the amplitude to square of the average amplitude is given by:

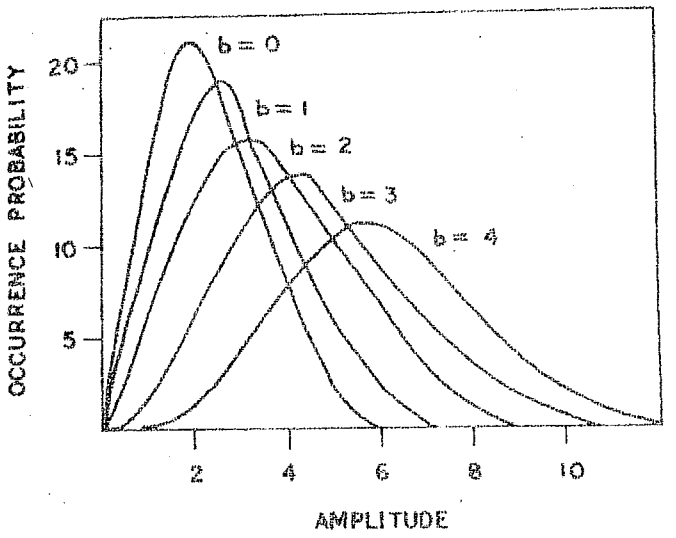

FIGURE 2.3

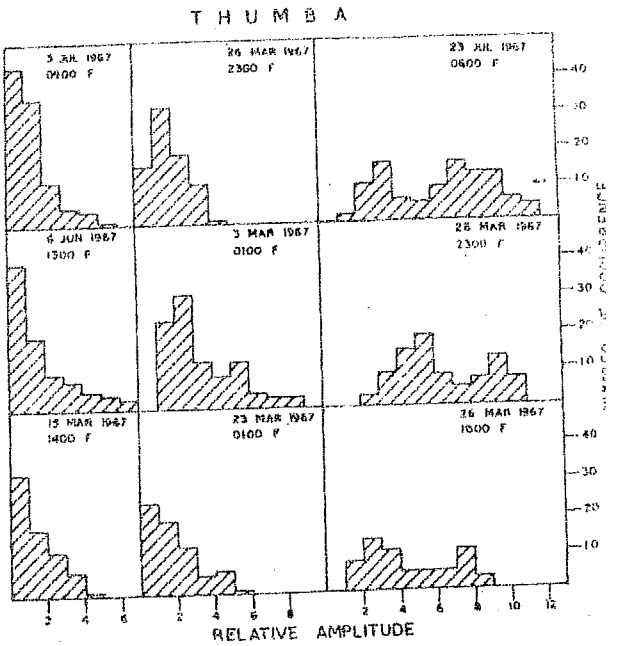

FIGURE 2.4

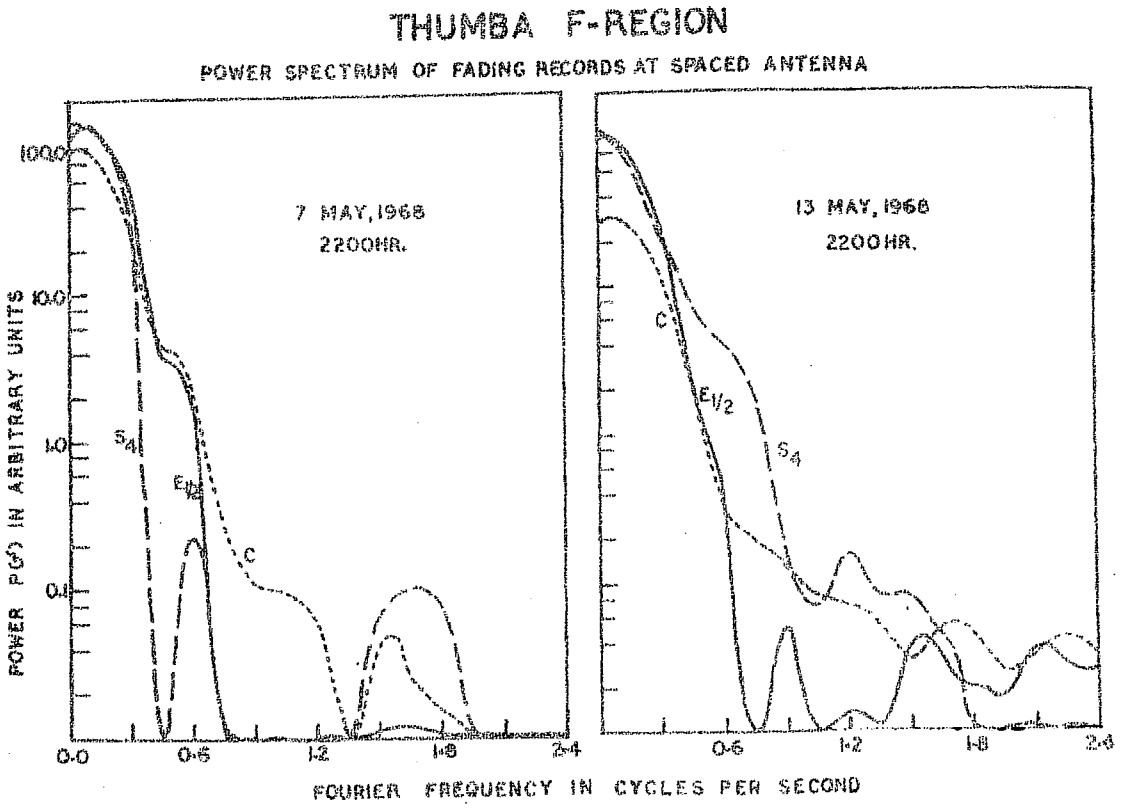

FIGURE 2.5

$$\overline{R^2}/\bar{R}^2 = r(1+b)^2 \, e^{b^2} / \pi\left[(1+b^2) \, I_o (b^2/2) + b^2 I_1 (b^2/2)\right]^2 \quad \ldots\ldots (3)$$

where I_o and I_1 are the Bessel functions with imaginary arguments. The limiting values of this ratio are:

$$\overline{R^2}/\bar{R}^2 \simeq 4/\pi = 1.27 \qquad \text{for } b \longrightarrow 0$$

and

$$\overline{R^2}/\bar{R}^2 = 1.0 \qquad \text{for } b \longrightarrow \infty$$

Hence, theoretically, this ratio must range between 1.00 and 1.27 from a Rayleigh to a normal distribution.

2.2 Typical amplitude distribution and power spectrum of ionospheric echoes observed at Thumba

Fig.2.4 gives a few of the typical amplitude distributions for the fading records at Thumba. Most of the day time records show a distribution which is neither a normal distribution nor a Rayleigh type but it is more similar to an exponential type. Very slow fading records, namely those obtained in the early morning or evening and the night gave a Rayleigh type distribution of amplitudes.

On a few occasions when the fading is very slow a two peaked distribution was observed. This may be due to different distributions centred at different most probable amplitude levels. A steady of $\overline{R^2}/\bar{R}^2$ was also made for both

E and F region records of Thumba for 1967 (CHANDRA, 1969) and most of the times this ratio exceeded $4/\pi$. Mean value was found to be 1.96 for day-time E region and 1.92 for day and night-time F-region. This abnormally high value of $\overline{R^2}/\bar{R}^2$ seems to be resulting from high rates of fading at Thumba. This ratio was found to increase with the fading rate.

The power spectrum of the signal strength at three spaced aerials were worked out by the author for a number of Thumba drift records. Two of them are shown in Fig.25. It is seen that though the most of the power is in the low frequency range and is common at all the three aerials, the secondary power peaks at higher frequencies of fading are sometimes shifted from one another. This could be the cause of slightly different fading characteristics at the spaced aerials. The reducing similarity between the records of fading at spaced aerials with increasing separation can therefore also result due to the presence of different higher fading frequencies at different points on the ground, besides the well-known changing shape of the pattern. Such an effect can arise from the dissimilar antenna characteristics.

2.3 Diurnal, seasonal and solar-cycle variations of the fading rate of the reflected signal at Thumba

The fading characteristics of the daytime E and F region echoes for 1965-65 have been studied by DESHPANDE(1966).

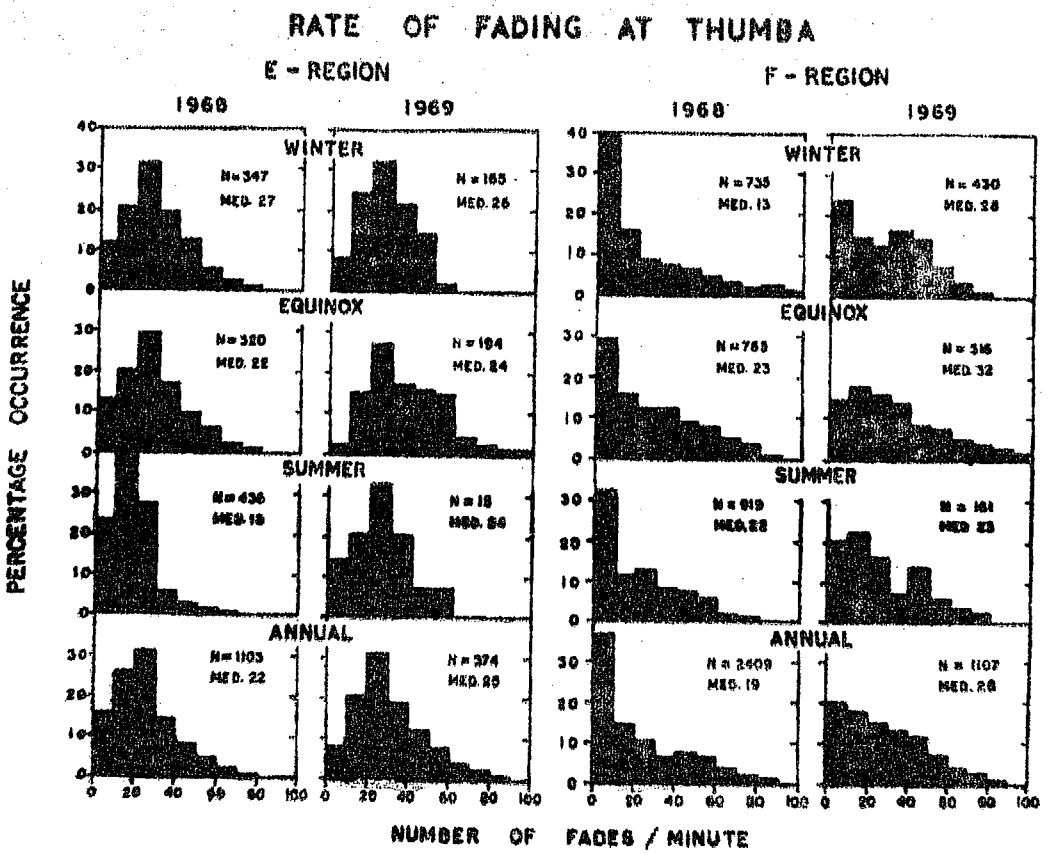

FIGURE 2.6

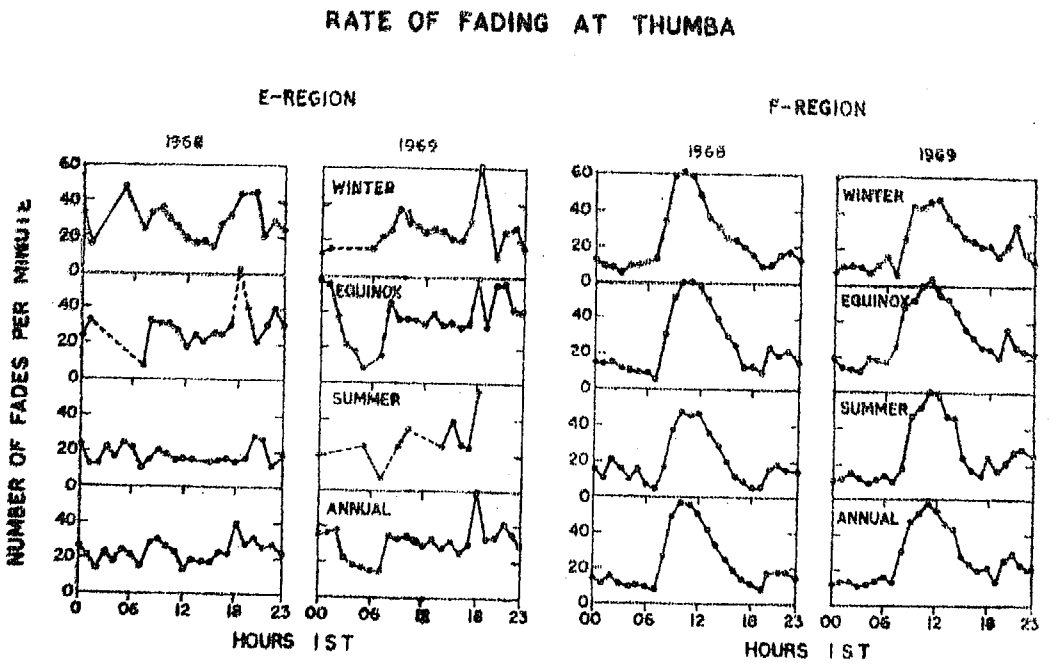

FIGURE 2.7

The fading records were found to be impulsive in nature with short bursts of signal intensity occurring in the background. The rate of fading is found to be much higher than that at higher latitude stations. A few sample records for E and F regions are reproduced in Figs. 2.1 and 2.2. The percentage occurrence of the rate of fading 'N' for different seasons of the year 1968-69 is shown in Fig.2.6 and is found to be least during the summer. The diurnal variation of N during different seasons of the period 1968-69 is shown in Fig.2.7 and that for different months of the year 1968 is shown in Fig.2.8. At times the signal is found to fade as fast as hundred fades per minute for F-region and sixty fades per minute for E-region. F-region shows a broad maximum around noon and E-region shows two maxima, one around 0900 hr and the another around 1800 hr, the later being much stronger than the former. A minor secondary peak is observed around 21-22 hr for F-region, and it occurs slightly later in summer. The peaks of the fading rate are well related to the drift velocity as shown later on. This is expected on the basis of the results of MITRA (1950).

E-region fading rate does not show a significant solar cycle variation. There is a slight tendency of decreasing N in equinoxes and summer but not in winter.

The higher sunspot years show a stronger evening peak for winter and equinoxes. The F-region fading increases considerably with increasing solar activity for each of the three seasons. The nature of the diurnal variation is same for each season of different years, with maxima occurring around 1100 hr when the mean rate of fading is as high as 80 to 90 fades per minute for 1967-68.

2.4 Similar fades method of analysis for drift from spaced antenna fading records

MITRA (1949) and KRAUTKRAMER (1950) gave a simple method of estimating drifts of ionospheric irregularities, which basically consists in comparing the similar features of three closely spaced fading records. This is also known as 'similar fades method' or 'time delay method' or also as 'Mitra's method'.

Considering the ionospheric irregularities to be fixed in space, one would obtain a spatial distribution of amplitude of the echo on the ground, not varying with time at any point. But if the irregularities do not change themselves and move uniformly with velocity V, then the diffraction pattern on the ground will move with a velocity 2V in the same direction as the motion of irregularities, and will give rise to temporal variation of amplitude at a point. Fading could also be produced by an irregularity

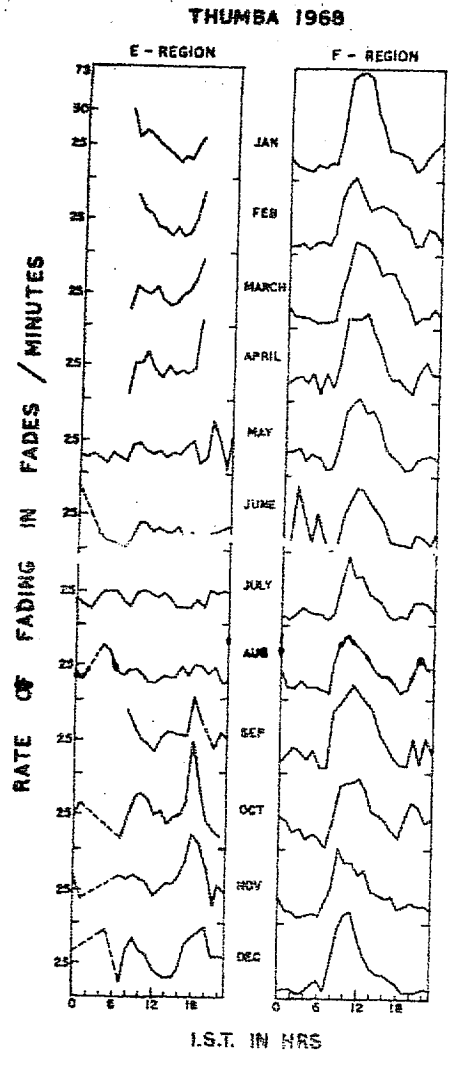

FIGURE 2.8

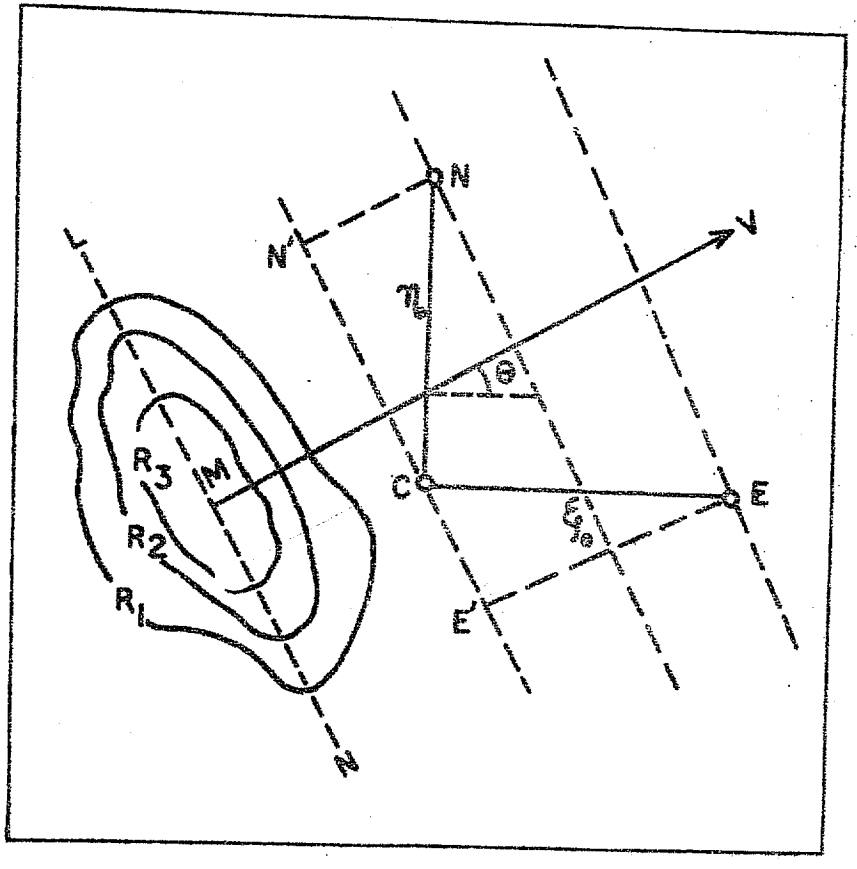

FIGURE 2.9

which is changing in shape but not moving.

MITRA (1949) derived a set of equations for the drift speed and direction, from the simple geometrical considerations, under the following basic assumptions:

(1) The ground diffraction pattern is moving with a uniform velocity V', during the course of an observation.

(2) The diffraction pattern on the ground does not change in shape as it moves.

(3) The diffraction pattern is isometric i.e. its average characteristics remain same in all the directions.

(4) The spacing of three receivers is small compared to size of the diffraction pattern.

Let us represent the diffraction pattern on the ground by means of the contours of constant amplitudes R_1, R_2, R_3 etc. moving with a uniform speed V in a direction which makes an angle ϕ' with X-axis (Fig.2.9). Let N,C and E be the three receiving sites. As different contours pass over these sites, the signal strength at these sites will fluctuate with time. A maximum of signal strength will be recorded at any aerial when a contour passes over the receiver tangentially. The locus of the tangential points along the direction of drift is called the line of maximum

amplitude (RATCLIFFE, 1954) and it is shown in Fig.2.9 by dotted line. Under the above assumptions, this line would be a straight line, perpendicular to the direction of movement.

The contours of constant amplitude can be in the case of maxima of amplitudes, replaced by the line of maximum amplitude and following relations can be written from the simple trigonometrical considerations.

If T_x and T_y be the time lags between the similar fades of aerials C and E and the aerials C and N respectively, then

$$T_x = \frac{\xi_o \cos \phi'}{V'}$$

$$T_y = \frac{\eta_o \sin \phi'}{V'} \qquad \ldots\ldots (4)$$

where ξ_o and η_o are the distances CE and CN.

Writing $\xi_o/T_x = V'_x$ and $\eta_o/T_y = V'_y$, we have

$$\frac{\cos \phi'}{V'} = \frac{1}{V'_x}$$

$$\frac{\sin \phi'}{V'} = \frac{1}{V'_y} \qquad \ldots\ldots (5)$$

Hence $$\frac{1}{V^2} = \frac{1}{V'^2_x} + \frac{1}{V'^2_y} \qquad \ldots\ldots (6)$$

and $$\phi' = \tan^{-1} (V'_x/V'_y)$$

$$\text{if } \xi_0 = \eta_0 = a$$

$$V' = a/(T_x^2 + T_y^2)^{\frac{1}{2}}$$

$$\text{and } \phi' = \tan^{-1}(T_y/T_x) \qquad \ldots\ldots (7)$$

The speed V' thus obtained is the speed with which the ground diffraction pattern moves and it must be divided by a factor of two to get the drift of the irregularities of the ionization at the level of reflection. These velocities are uncorrected for the anisotropy and turbulence of the diffraction pattern and are called Apparent drift velocities. K.SHIN ET AL. (1970) have modified Mitra's method to a case where the first assumption fails i.e. when the drift speed fluctuates during the course of an observation.

2.5 Results of apparent drift parameters at Thumba for the period 1964-69

The regular drift observations at Thumba (0.6°S dip) were first started in January 1964, using 2.2 MHz and 4.7 MHz for the E and F-regions respectively. Only daytime records were taken between 07 hr and 18 hr at each hour. The F-region night observations were not possible due to the disappearance of the echo after midnight in low sunspot year (CHANDRA, 1970). No night-time E-region records were possible due to low power of the transmitter and also the

rare occurrence of nighttime sporadic-E near the magnetic equator. The main results for apparent drift parameters for the year 1964 are discussed by DESHPANDE and RASTOGI (1966a). The average drift speed was 132 m/s for E and 161 m/s for F-region and the average drift direction was within 270° ± 15° on about 65% of the occasions for both the regions. Seasonal study showed the highest drift in equinoxes and least in summer for both E and F regions. The F-region drift was found to reverse from westward to eastward in the night (DESHPANDE and RASTOGI, 1968).

Regular night-time F-region drift observations were also started in January 1967. A few more receiving aerials were added in May 1967. The main daytime results for period 1964 to 1967 are summarized by CHANDRA and RASTOGI (1969). The mean and median values of daytime E-region drifts were found to be 125 m/s and 114 m/s respectively while for the F-region, the mean and median drifts were 160 m/s and 150 m/s. The direction was predominantly westward. The night-time F-region drifts were eastward, with the change-overs occurring around 06 hr and 20 hr (CHANDRA, 1969).

A new drift recording equipment designed and tested by the author at Ahmedabad during 1966-67, was installed at Thumba in January 1968. This system incorporated a

number of modifications over the existing system (as discussed in detail in chapter I) besides much increased power of the transmitter. This enabled the detection of night-time sporadic-E at Thumba on several occasions and it was found to be associated with the isolated thunderstorms (MISRA and RASTOGI, 1971). Night-time E-region drifts were therefore recorded at Thumba for the first-time, whenever possible. Both E and F region hourly drift observations for all the twenty-four hours of all mondays, wednesdays (regular world day) and fridays were made by the author for the period 1968-69 and the results for apparent drift parameters are summarized below.

Nearly three thousand F-region records and two thousand E-region records are used in the present results. The seasonal grouping of the data is made as follows:

Winter - consisting of November, December, January and February in one continuation.

Equinoxes - consisting of March, April, September and October of the same year.

Summer - consisting of May, June, July and August of the same year.

The day and night-time division of the data was made as 08 hr to 16 hr for day and 20 hr to 04 hr for night, excluding the periods around the changeover of drift direction, which usually occurs around 06 - 07 hr and 19 - 20 hr, as clear from the previous study.

Fig.2.10 gives the overall picture of Thumba drift speed and direction during day and night-times, over the two years, for both E and F regions. Over one thousand records for E-region and two thousand five hundred records for F-region were used to obtain this diagram. It is seen from this that the drift speed in E-region ranges from 50 - 300 m/s during day and from 50-250 m/s during night, with median drift speeds being 120 and 122 m/s. For the F-region the drift speed ranges from 50 - 300 m/s during day and from 50 - 280 m/s during night with median drift speeds equal to 148 and 90 m/s respectively. Night-time E-region drifts at equator were estimated for the first-time and a clear difference was noticed in its direction as compared to F-region night-time drifts. Although in 90% cases the drift was 90° $\pm$ 15° east of north in F-region during night, 40% cases for E-region showed a 270° $\pm$ 15° east of the north drifts. During day-time however, both E and F-regions have 90 to 95% cases of westward drifts i.e. (270° $\pm$ 15°) east of north.

Histograms of percentage occurrences were computed for speed as well as direction for each season for the two years 1968 and 1969, combined. Weighted means were used for the computation. Fig.2.11 gives the speed histograms and Fig.2.12 gives the direction histograms for the E and

THUMBA 1968-69

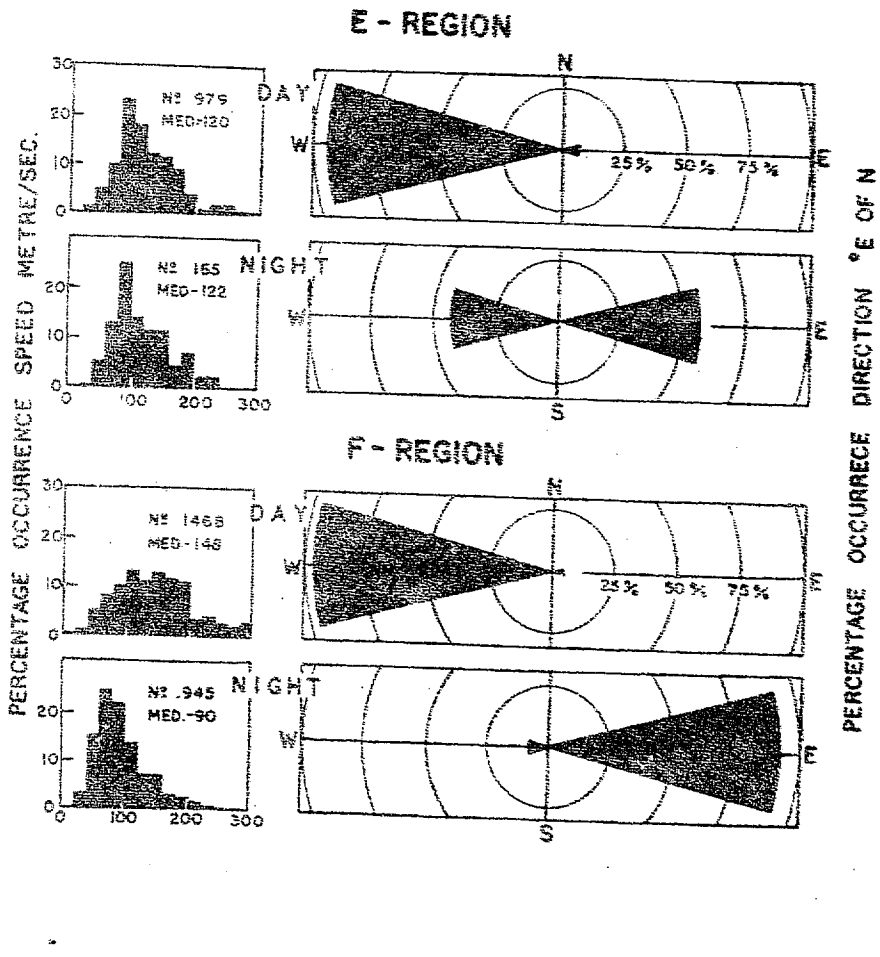

FIGURE 2.10

THUMBA APPARENT DRIFTS DIRECTION 1968–1969

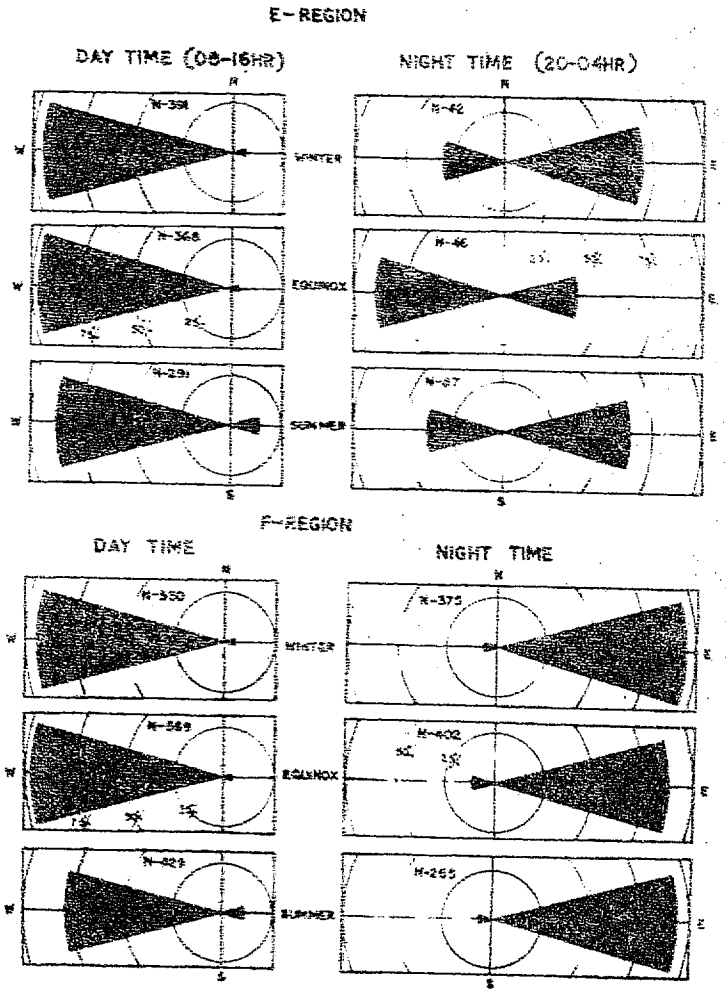

FIGURE 2.11

F regions during Day and Night times. For E-region, 130, 120 and 110 m/s are the median values for drift speed in daytime and 116, 134 and 100 m/s are the median values for drift speed in night-time, during winter, equinox and summer respectively. For the F-region, 155, 152 and 130 m/s are the median values of drift speed during day and 89, 93, 87 m/sec for the night-time during winter, equinox and summer respectively.

Drift directions (Fig.2.12) for E-region during day are predominantly westward with slight tendency for eastward drift during summer. During night hours however, E-region drift directions show an special characteristic. The drift is never entirely towards east, unlike F-region for the same period and there is more tendency for a westward drift during night time in E-region during the equinoxes. 30% cases during winter, 65% during equinoxes and 40% during summer show a westward drift during night-time.

F-region drift is predominantly westward during day and eastward during night for all the three seasons with only a slight scatter during summer day-time directions.

Diurnal variation of drifts at Thumba during 1968-69

The apparent drift speed was resolved into eastward and northward components and diurnal plots were made for

THUMBA APPARENT DRIFT SPEED FOR 1968-1969

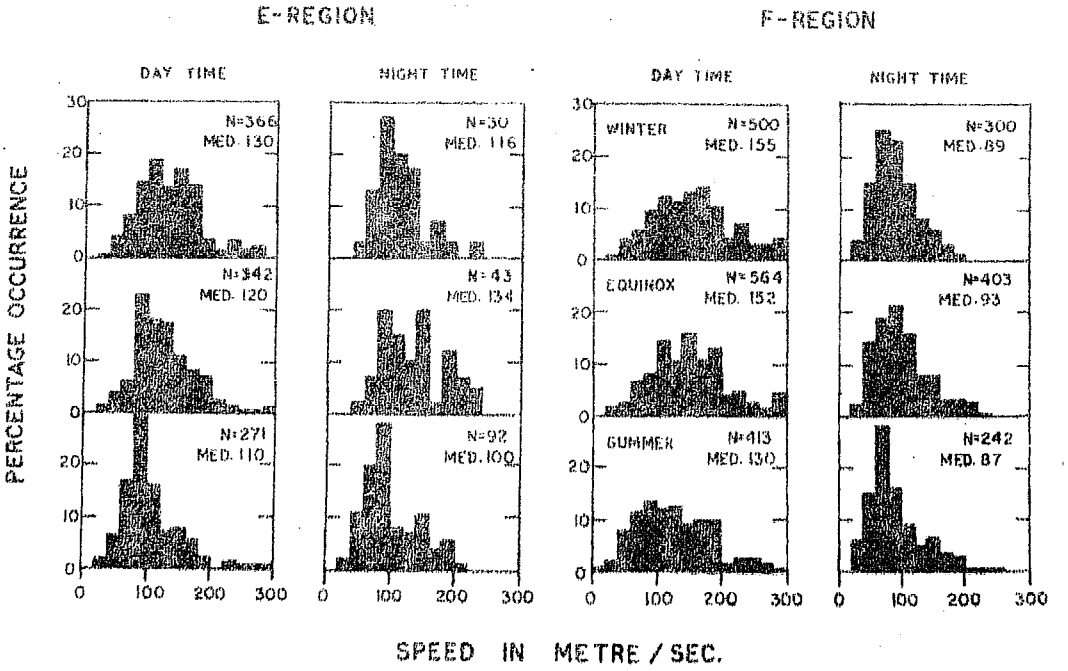

FIGURE 2.12

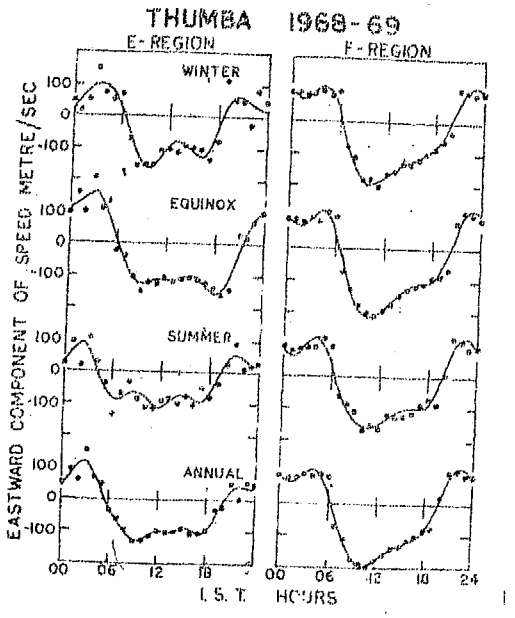

FIGURE 2.13

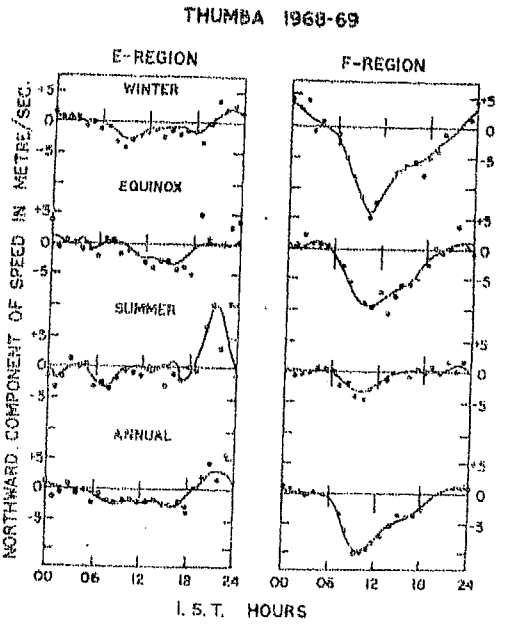

FIGURE 2.14

0645 hr in the morning and 2000 hr, 1930 hr and 1940 hr in the evening. The times of morning reversal are therefore fairly fixed in the case of F-region drifts unlike the E-region where the reversal from east to west takes place much earlier during summer season. The times of evening reversals are quite different in the three seasons for F-region, being latest during equinoxes. The reversal of F-region drift in relation to the electrojet, the size of the irregularities, the height of F-layer and a few other effects is discussed in detail in Chapter VI.

The E-region evening reversal from west to east occurs very late during equinoxes. This particular feature indicates the residual effect of electrojet at Thumba till late in the evening (MISRA and RASTOGI, 1971).

The north-south component of ionospheric drift at Thumba has been studied for the first-time in the present work. Fig.2.14 and table II give the daily curves of the northward component of drifts at Thumba for the period 1968-69 and the four harmonic coefficients alongwith the time of reversals. The E-region does not show much tendency for a northward drift, as is expected from the electrojet consideration. The F-region drift however shows northward drift of the order of 10 - 15 m/s, being maximum in winter and least in summer. BAMGBOYE and LYON (1968) have also

measured the N-S drift velocity for Ibadan using extended N-S aerials separated by 5 λ and found a strong ($\sim$ 100 m/s) southward drift in day and northward drift in the night. RAO and RAO (1963) have shown the existence of strong N-S drift at Waltair, being northward in night and southward in day. However, the simple theory of electrodynamic drift predicts a strong E-W and zero N-S (meridional) drift in this region. RISHBETH (1967) and BRAMLEY and YOUNG (1968) have recently discussed the possibility of meridional winds connected with the development of equatorial anomaly.

Fig.2.15 gives a composite picture of eastward and northward components of drifts at Thumba for E and F-regions during 1968-69 on the harmonic dial. The steady diurnal and semi-diurnal components are plotted and highly elongated ellipses are obtained as far as the diurnal component is concerned. The steady drift is westward, with slight tendency for south. The times of maxima for diurnal component are 1100hr in the westward direction, and 2200 hr in the eastward direction for E-region and 1130 hr in the westward and 2330 hr in the eastward direction for F-region.

Months to month variations

Month to month diurnal plots of V' for E and F regions for the year 1968 are shown in Fig.2.29. The E

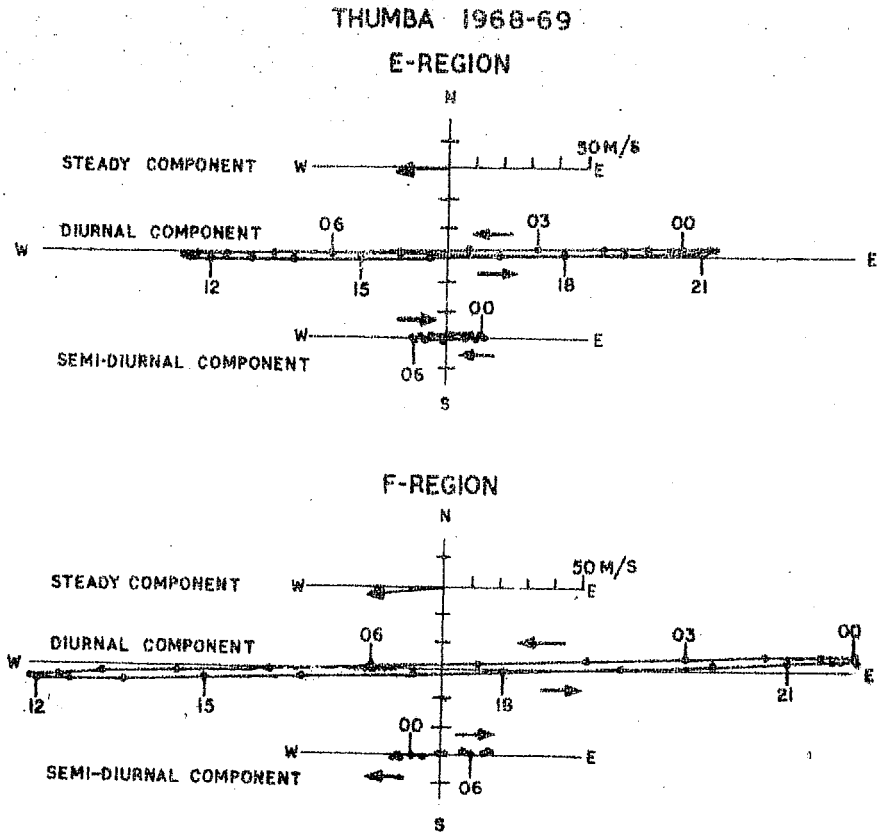

FIGURE 2.15

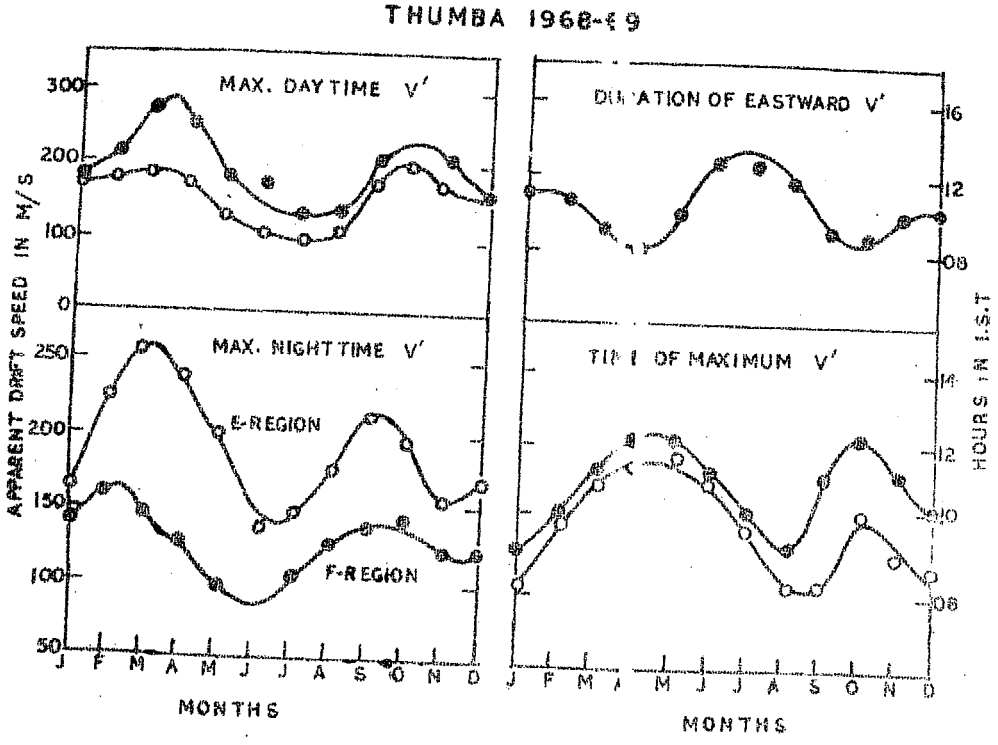

FIGURE 2.16

as well as F region drift speed shows an equinoxial maximum excepting the month of May, when the values are exceptionally high for E-region. This phenomenon is discussed at length in chapter IV. The secondary night-time peak of V' in F-region is more clear during summer season when the spread-F is also more. This point is discussed in chapter V in relation to other parameters of drift during spread-F conditions.

Fig.2.16 gives the month to month variation of the maximum day and night-time drift, the duration of eastward drift and the time of maximum drift, for both E and F regions for the period 1968-69. The equinoxial peak is clearly manifested in the maximum drift as well as the time of its occurrence, suggesting a strong electrojet control. The duration of eastward drift is most in summer and least in equinoxes, as expected from the electrojet control of drifts.

Comparison of E and F region drifts

Fig.2.17 is a vector plot of all the observations common between E and F regions, in different hour groups. The tendency of more scatter of points in the E-region, particularly in night hours is clearly brought out. During the daytime the drifts in both E and F regions are west-

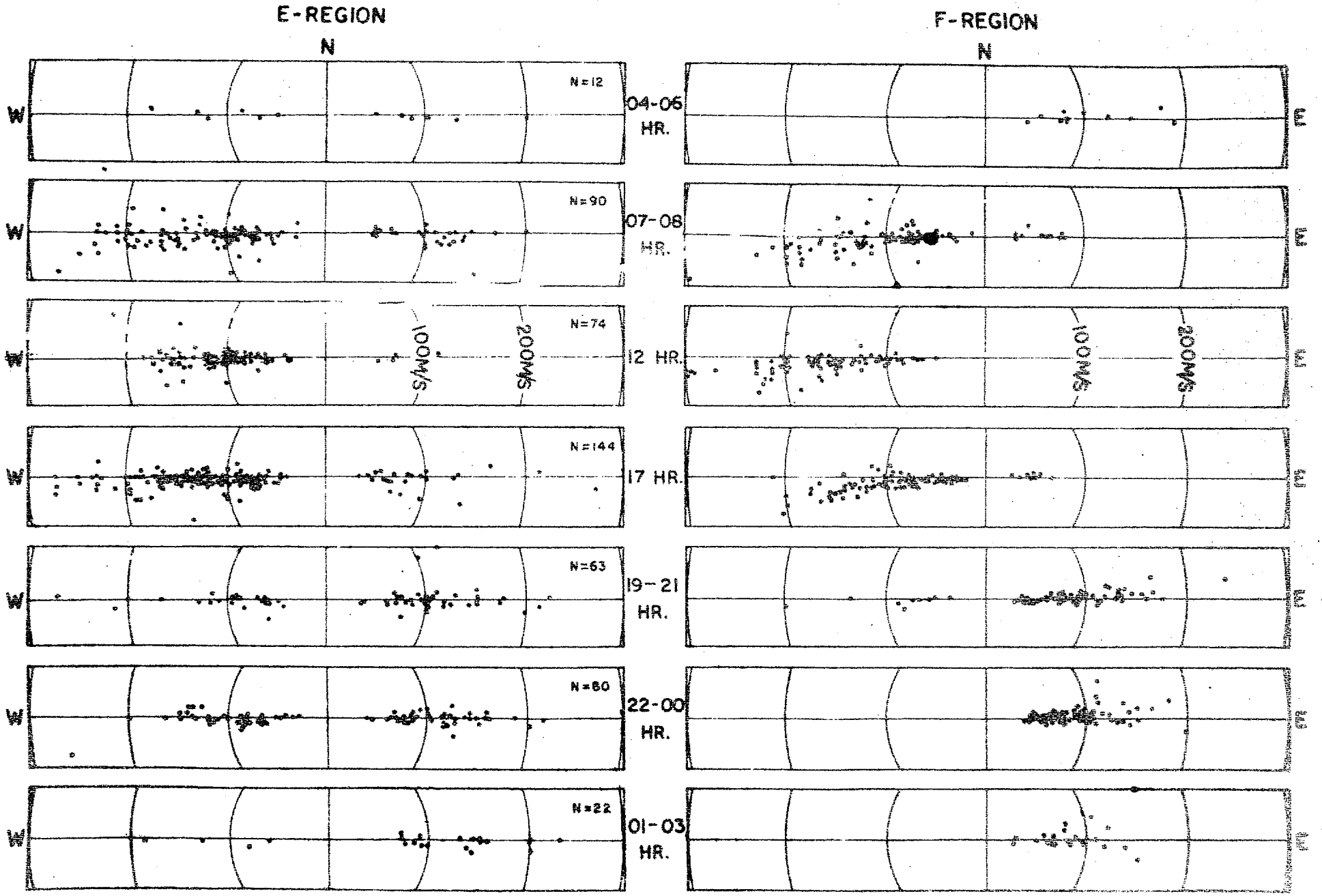
E-REGION
F-REGION
N
W
S
N=12
04-06 HR.
N=90
07-08 HR.
N=74
100M/S
200M/S
12 HR.
N=144
17 HR.
N=63
19-21 HR.
N=60
22-00 HR.
N=22
01-03 HR.

FIG. 2.17

wards for 99% of the cases but in the early night hours (22 - 00 hr), though the F-region drift has reversed completely from west to east the E-region drift still has equal probability for both east and westward directions. As a matter of fact E-region drift has never completely changed over to eastward for all days studied in the whole of the night, while F-region drift is completely eastward from 22 to 06 hr in the night. The night-time drifts in E-region at equator being first-time studied by this method, the above feature is interesting to note.

Fig.2.18 is the mass plot of the East-west component of all the observations at Thumba during 1968-69 for E and F regions for all hours of the day. The scatter of points during night hours for E-region and for the afternoon and evening hours during summer season for F-region is considerable.

Fig.2.19 gives the contour diagram for the magnitude of drift velocity in E and F-regions for the period 1968-69 for each of the three seasons. The innermost contours, shaded by thick black lines are for values more than 30% in occurrence. The next outer one shaded by continuous lines is for values between 20 - 30 % in occurrence and the outer most shaded by dotted lines for values between 10 - 20% of

MASS PLOT OF THE E-W COMPONENT OF APPARENT DRIFT SPEED AT THUMBA DURING ISOS

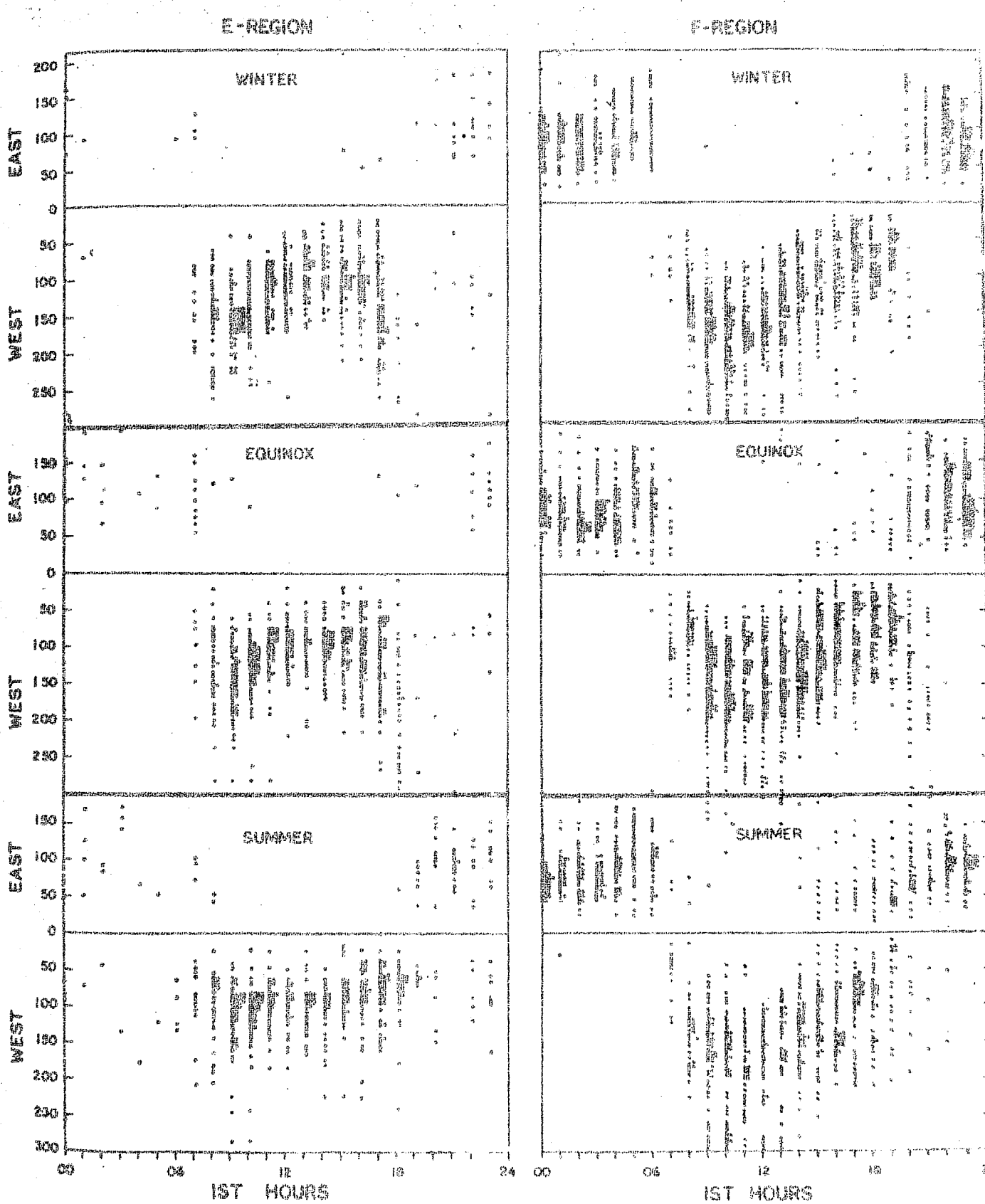

FIGURE 2.10

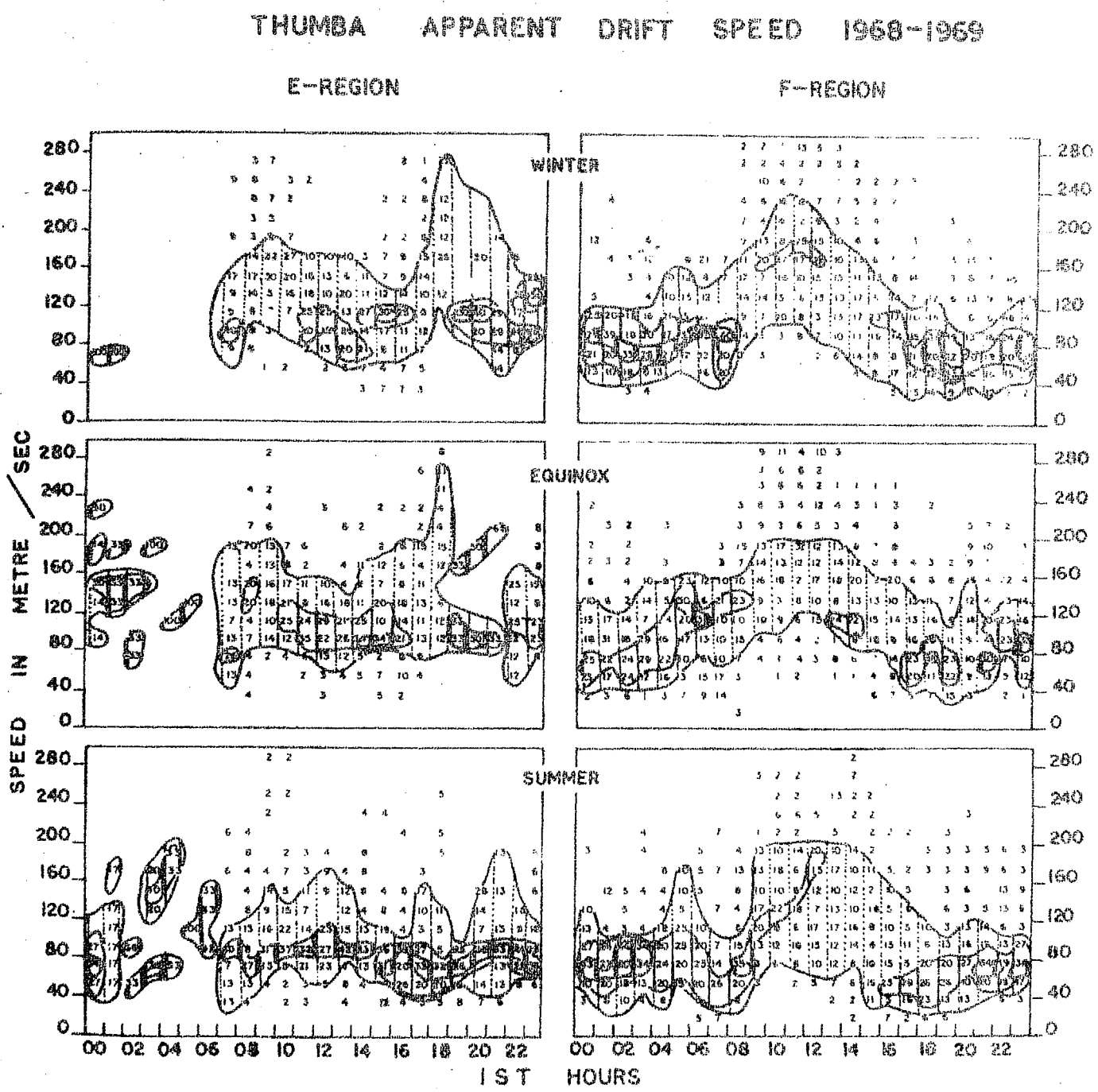
THUMBA APPARENT DRIFT SPEED 1968-1969
E-REGION
F-REGION
WINTER
EQUINOX
SUMMER
SPEED IN METRE / SEC
0
40
80
120
160
200
240
280
00 02 04 06 08 10 12 14 16 18 20 22
I S T HOURS

FIGURE 2.19

occurrences. This method of representation of percentage occurrence has been used extensively by RAWER ET AL.(1968) for Dapango and other West German drift stations.

2.6 Statistical errors in V' and its day-to-day fluctuations at a particular solar hour

In order to establish the significance of the drift velocities determined by the similar fades method (MITRA, 1949) standard errors ' σ ' were estimated at each hour of the day for each of the three seasons of the period 1968-69. These are given in table 3. The diurnal variation of σ for E and F-regions is shown in Fig.2.20. The large errors during the night hours for E-region can be accounted for the smaller number of observations as the appearance of E_s at Thumba during night is very rare. The errors involved for the day-time V' are fairly low (less than 10 m/s) i.e. 5 - 10% and the results are reliable. The evening peak is near to the maximum E-region drift speeds at Thumba and hence the percentage error is not increased much. The observations in the early morning hours (04 and 05 hr) are however scarce.

Coming to the F-region, the errors are less than 5% for whole of the day and the results are quite reliable. ..s the number of observations used at each hour of the day for both E and F regions, in calculating these errors are

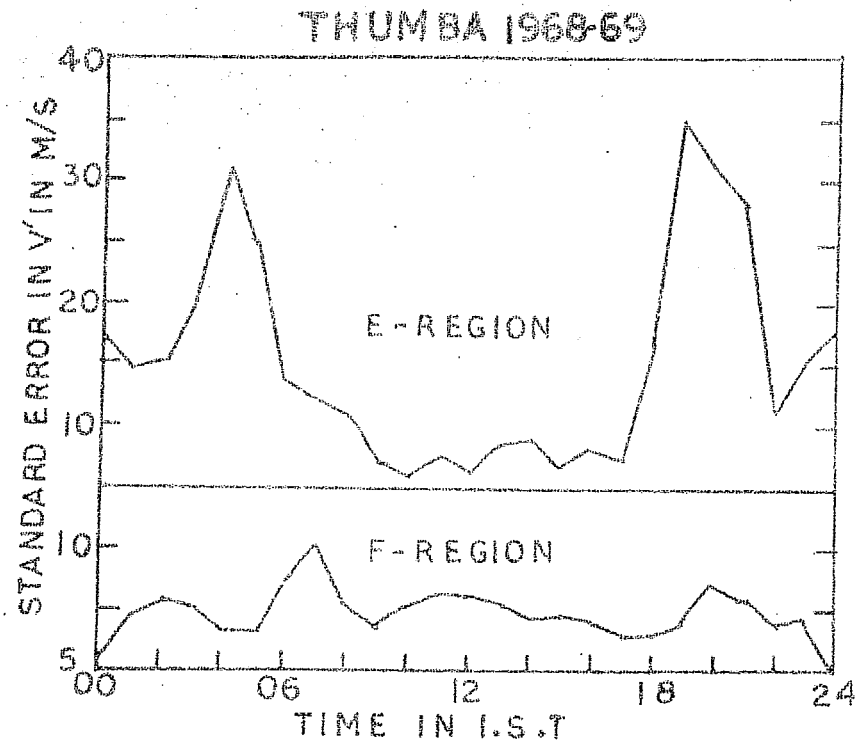
THUMBA 1968-69
STANDARD ERROR IN V IN M/S
E-REGION
F-REGION
TIME IN I.S.T
00
06
12
18
24

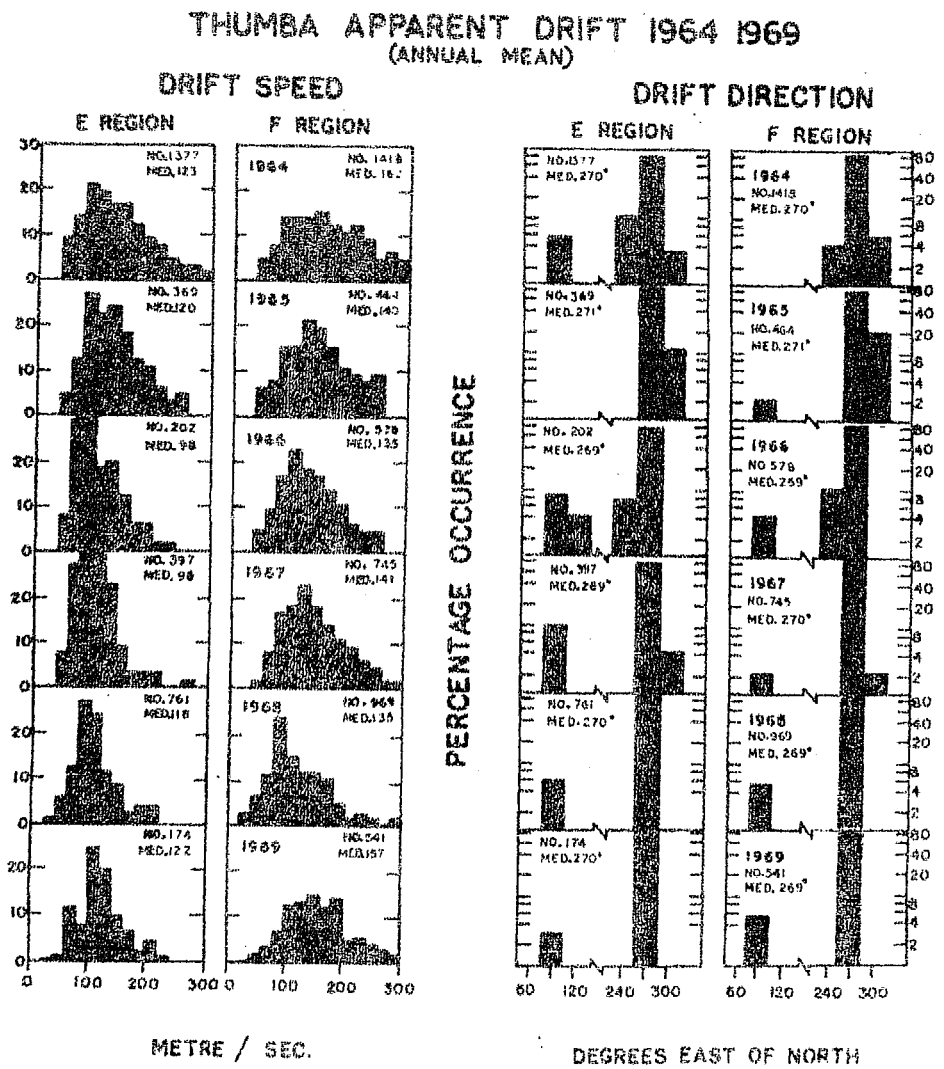
THUMBA APPARENT DRIFT 1964 1969
(ANNUAL MEAN)
DRIFT SPEED
DRIFT DIRECTION
E REGION
F REGION
PERCENTAGE OCCURRENCE
METRE / SEC.
DEGREES EAST OF NORTH

Fig. 2.21

fairly large (about one hundred), the error seems to have been caused by the day to day variability of the drift at the same hour of the day. Such an effect will arise from the day to day fluctuations in E at the given hour of the day. MORRIS (1967) has discussed a similar result for the equatorial station Ibadan.

2.7 Effect of solar cycle on the apparent drift at Thumba

This aspect of the ionospheric drift is discussed in detail in paper . attached here. The Figs.1,2,3,4 and 5 are the Figs.2.21,2.26 , 2.30, 3.20 and 2.31 respectively. The seasonal variation of this effect is shown in Figs. 2.22,2.23, 2.24, 2.25 and Figs.2.27 and 2.28. The variation of night-time apparent drift for E and F-regions from 1967 to 1969 is given in table IV. E-region night-time data was available only for 1968 and 1969. The values are slightly higher for 1969 than 1968. The F-region night-time drift does not show any definite trend from 1967 to 1969.

2.8 Latitudinal variation of apparent drift parameters

(a) Magnitude of apparent drift

The day-time apparent drift speeds for a large number of stations over the world are collected in table IV..

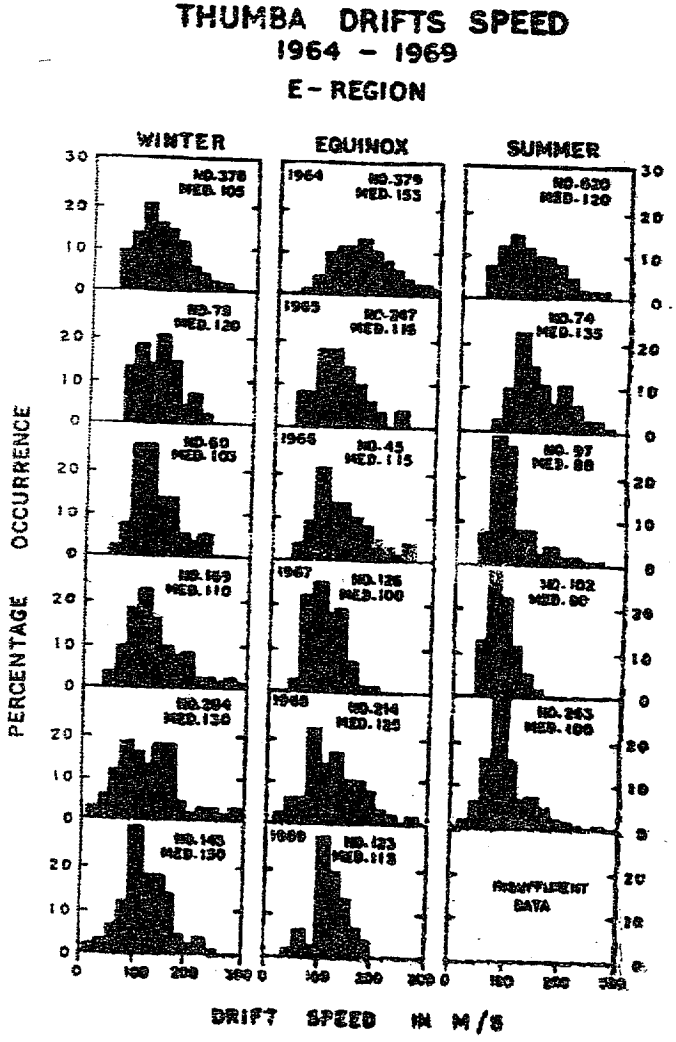

FIGURE 2.22

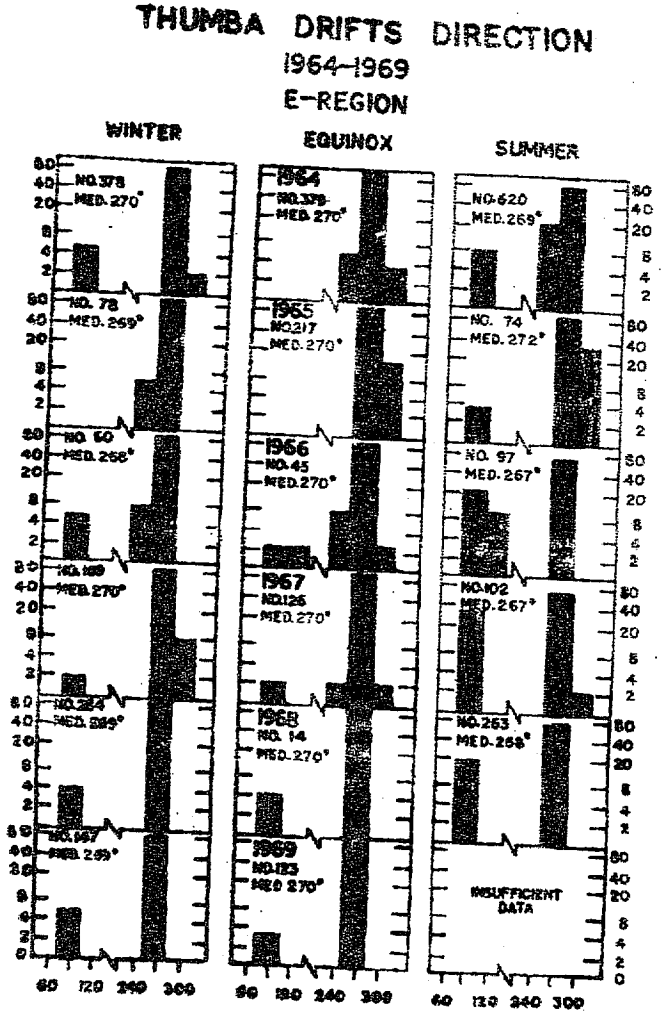

FIGURE 2.23

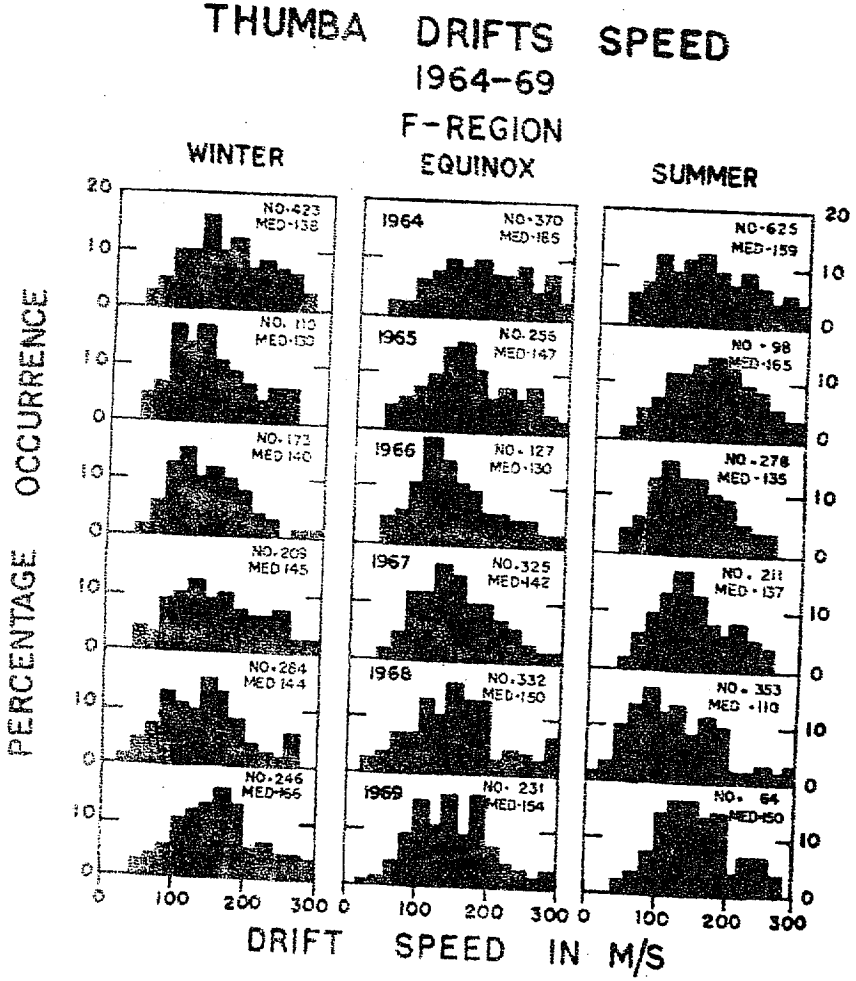
THUMBA DRIFTS SPEED
1964-69
F-REGION
WINTER
EQUINOX
SUMMER
PERCENTAGE OCCURRENCE
1964
1965
1966
1967
1968
1969
NO-423 MED-138
NO. 110 MED-130
NO-173 MED 140
NO-209 MED 145
NO-284 MED 144
NO-246 MED-166
NO-370 MED-185
NO-255 MED-147
NO-127 MED-130
NO-325 MED142
NO-332 MED-150
NO- 231 MED-154
NO-625 MED-159
NO-98 MED-165
NO-278 MED-135
NO- 211 MED-137
NO- 353 MED-110
NO- 64 MED-150
0 100 200 300
DRIFT SPEED IN M/S

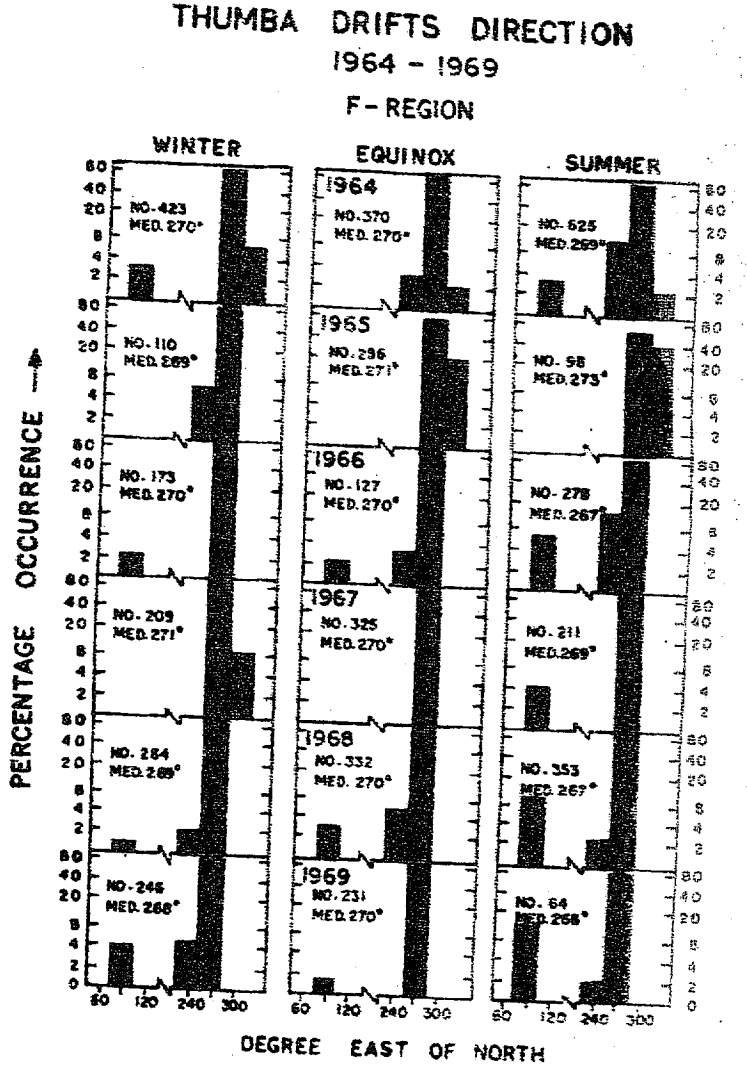
THUMBA DRIFTS DIRECTION
1964 - 1969
F-REGION
WINTER
EQUINOX
SUMMER
PERCENTAGE OCCURRENCE
1964
1965
1966
1967
1968
1969
NO-423 MED. 270°
NO-110 MED. 269°
NO. 173 MED. 270°
NO. 209 MED. 271°
NO. 284 MED. 269°
NO-246 MED. 268°
NO-370 MED. 270°
NO. 296 MED. 271°
NO-127 MED. 270°
NO. 325 MED. 270°
NO. 332 MED. 270°
NO. 231 MED. 270°
NO. 625 MED. 269°
NO. 98 MED. 273°
NO. 278 MED. 267°
NO. 211 MED. 269°
NO. 353 MED. 267°
NO. 64 MED. 268°
60 120 240 300
DEGREE EAST OF NORTH

FIGURE 2.24

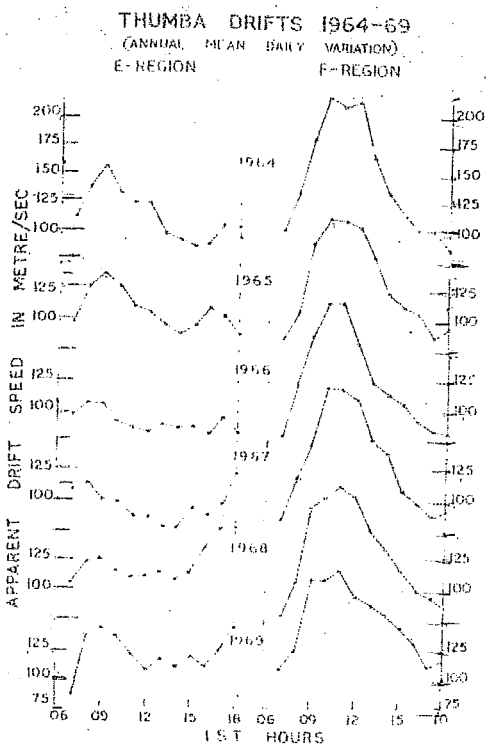

FIGURE.2.26

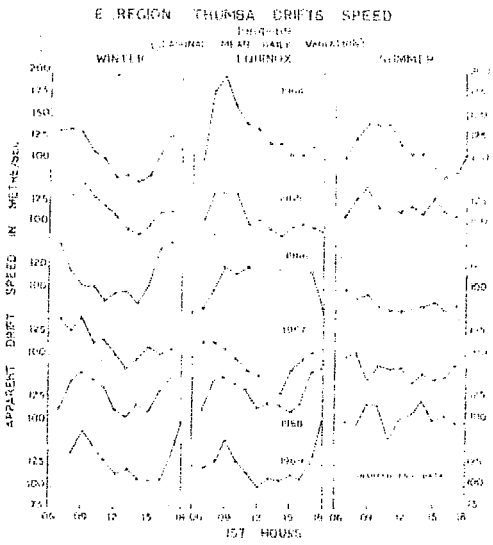

FIGURE.2.27

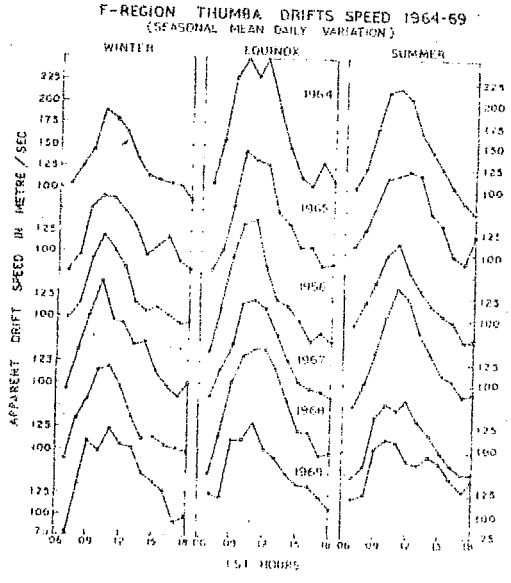

FIGURE.2.28

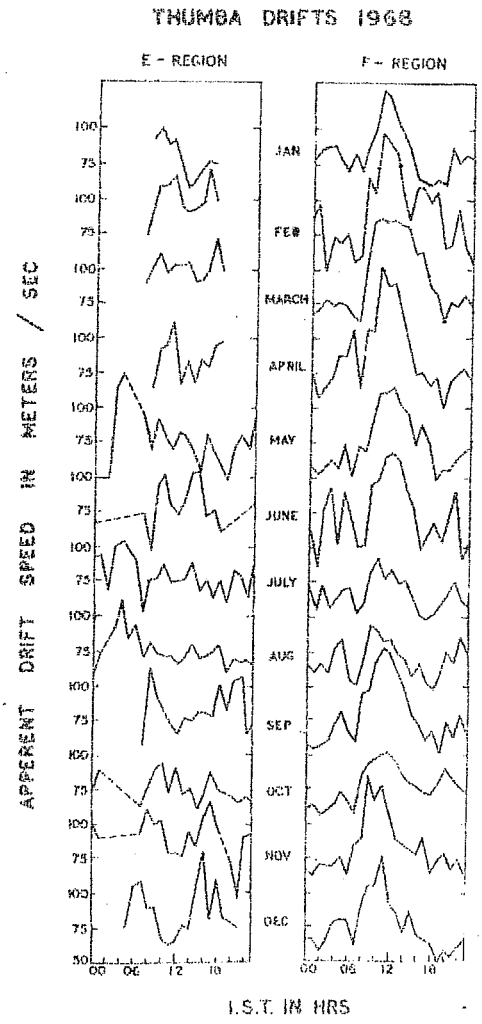

FIGURE.2.29

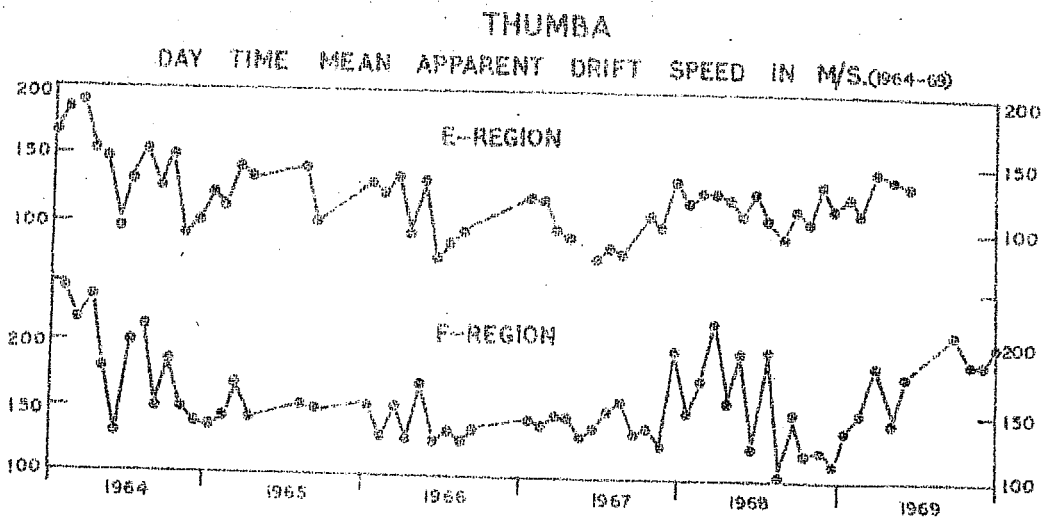

FIGURE 2.30

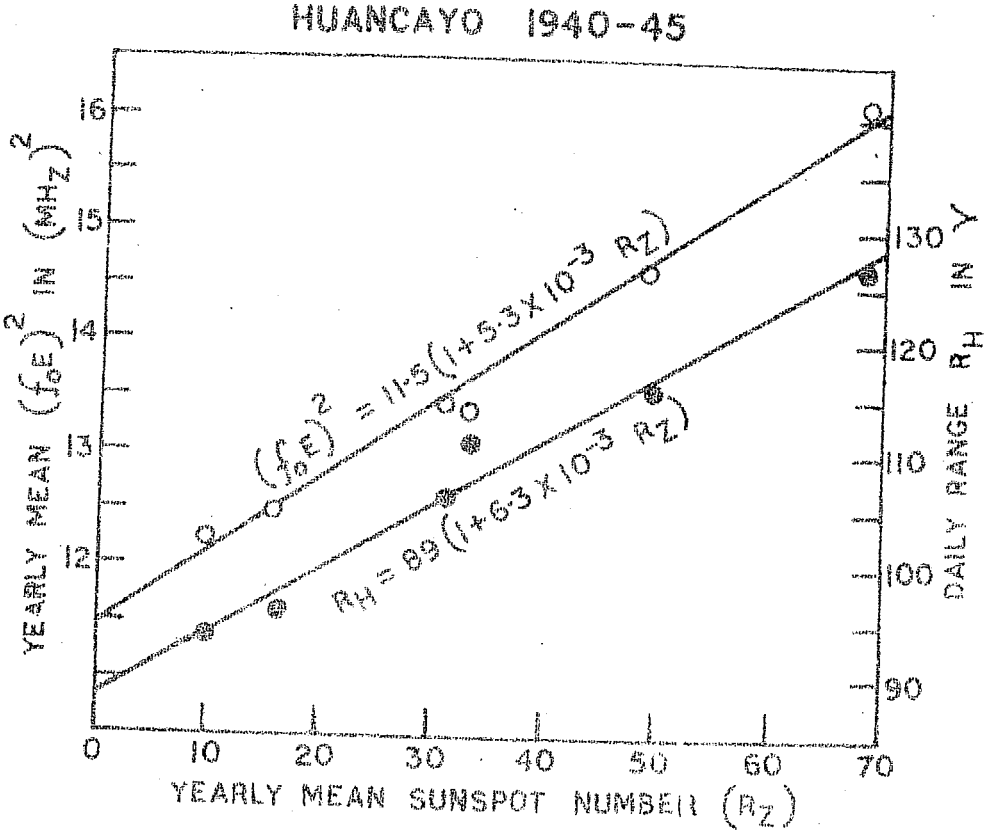

FIGURE 2.31

Their variation with respect to the magnetic latitude is plotted in Fig.2.32 for E and F regions. A strong peak is seen to occur at the equator which decays sharply within ± 5° magnetic latitude after which the drop in V' is slow, attaining a more or less constant value for the mid-latitude stations around S_q focus. There is a slight tendency of increase in V' at very high latitudes, which are near to the auroral electrojet region. The variations of E and F region drifts are fairly similar, excepting a slightly lower drift speed in F-region than E at all the latitudes. This kind of variation is easily explainable from the pattern of the S_q current system (MAEDA, 1955).

(b) Diurnal and semi-diurnal drift vectors:

The latitudinal variation of the daytime steady, diurnal and semi-diurnal components of the apparent drift is shown in Fig.2.33. Starting with Thumba, the steady drift is mainly westward while the diurnal drift vector is westward in day and eastward in night with very little N-S component. Rotation is anti-clockwise. The times of day and night maxima occurring at around 12 and 00 hr. Semi-diurnal component is very small. At a slightly higher latitude i.e. Waltair, steady drift is small and southeast. The diurnal drift vector rotates anit-clockwise like Thumba

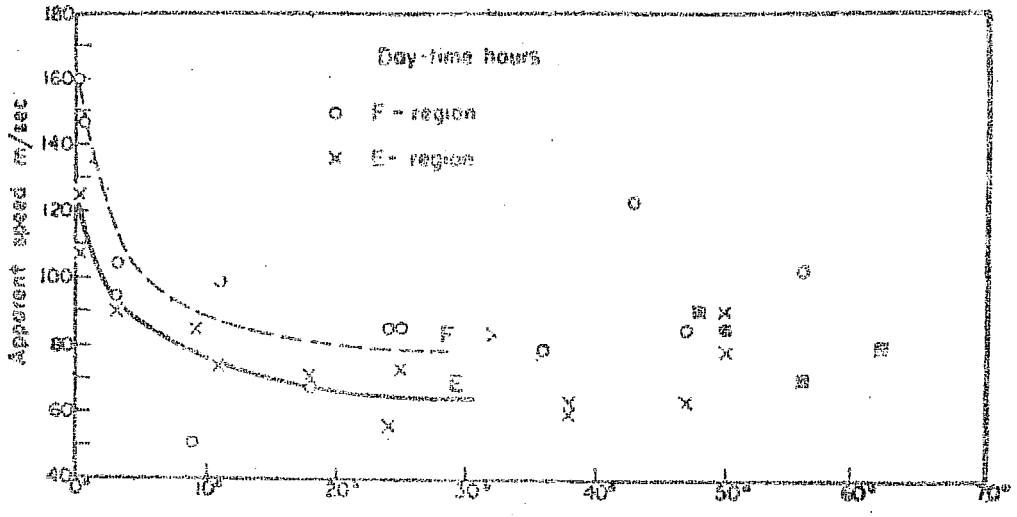

FIGURE 2.32

F-REGION DRIFT VECTORS

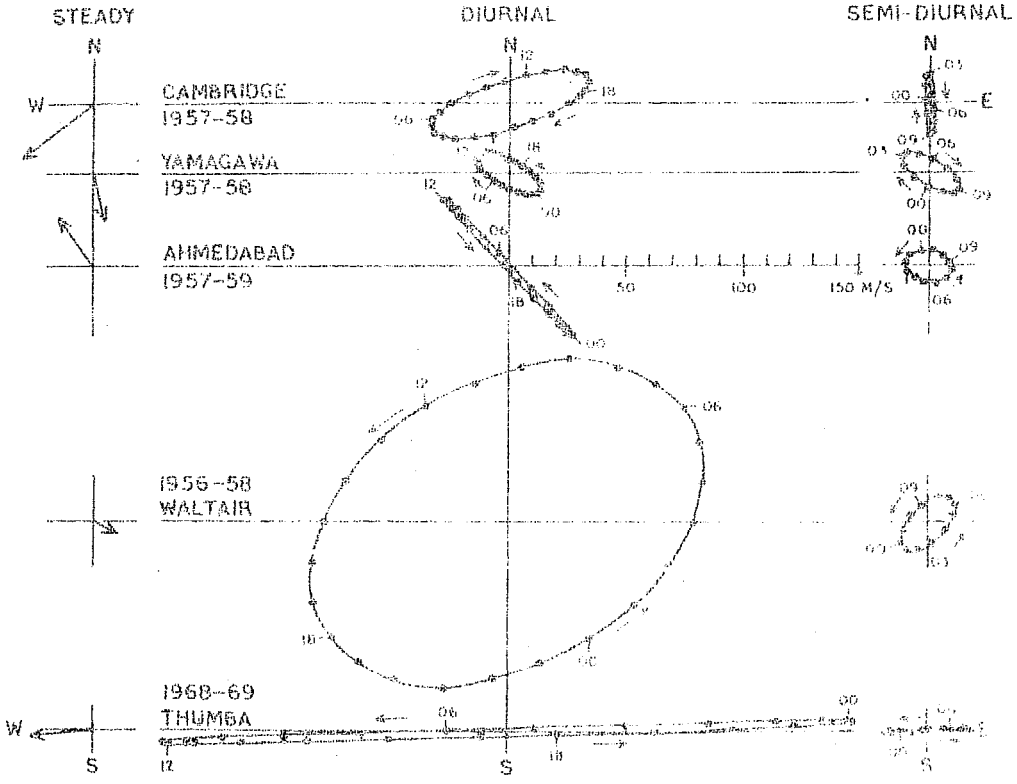

FIGURE 2.33

and both E-W and N-S components are comparable. Semi-diurnal vector also rotates anti-clockwise but is much smaller. Nearer to the S_q focus, Ahmedabad has a diurnal drift vector rotating anti-clockwise but north-west during day and south-east by night. Semi-diurnal vector also rotates anti-clockwise but is very small. The steady drift is northwest. . . . Beyond the S_q focus at Yamagava, the steady drift vector is nearly southward while the diurnal and semi-diurnal components are equally strong. Both the vectors move clockwise which is expected as the direction of S_q current system and is reversed beyond S_q focus. At a much higher magnetic latitude i.e. Cambridge the steady drift is southwest and diurnal as well as semi-diurnal drift vectors describe an ellipse clockwise.

KAZIMIROVSKIY (1962) has derived the pattern of general circulation of ionisation over the globe, using the IGY drift data for various stations.

2.9 Conclusions

In short, the ionospheric drift at Thumba are predominantly westward by day and eastward by night for both E and F-regions. The drifts are maximum during equinoxes. The effect of solar cycle on apparent drift is not very clear. The drifts at equator are highest and fall off sharply within few degrees of equator.

Harmonic coefficients of the daily variation of the E-W component of apparent drift speed for E and F regions during the year 1968-1969 for Thumba upto four harmonics

Period		Amplitudes in M/s					Time of maxima in hours (I.S.T)				Time of morning reversal in I.S.T.	Time of evening reversal in I.S.T.
		a_r	r_1	r_2	r_3	r_4	ϕ_1	ϕ_2	ϕ_3	ϕ_4		
E region	Winter	-27	107	24	50	12	0.4	4.0	4.6	9.1	0615h	1840h
	Equinox	-32	137	62	16	20	2.0	2.0	5.4	4.2	0615h	2130h
	Summer	-29	81	16	15	30	0.0	4.4	3.1	2.6	0420h	1915h
	Annual	-29	105	29	23	9	1.0	2.2	4.3	2.8	0530h	2000h
F region	Winter	-34	148	21	38	14	0.7	3.7	5.5	7.2	0640h	1930h
	Equinox	-36	157	26	45	18	1.0	3.9	6.0	7.2	0650h	2000h
	Summer	-15	136	12	40	15	0.9	4.2	5.5	4.2	0645h	1940h
	Annual	-29	151	18	41	11	0.7	4.2	5.5	4.5	0640h	1940h

Table - I

Harmonic co-efficients of the daily variation of the N-S component of apparent drift speed for E and F regions during the year 1968 - 1969 for Thumba upto four harmonics

	Period	Amplitudes in M/s					Time of maxima in hour in L.T				Time of morning reversal	Time of evening reversal
		a_o	r_1	r_2	r_3	r_4	ϕ_1	ϕ_2	ϕ_3	ϕ_4		
E region	Winter	-0.8	1.7	0.6	0.8	0.4	23.5	11.9	5.7	4.5	0530h	2000h
	Equinox	-0.9	1.6	0.8	0.4	0.7	1.6	9.9	0.7	0.9	0450h	2100h
	Summer	+0.3	3.1	2.3	2.4	1.7	21.5	9.7	5.0	3.6	0500h	1830h
	Annual	-0.5	1.9	1.1	0.8	0.4	23.2	10.1	5.4	3.7	0450h	1900h
F region	Winter	-4.2	7.2	1.9	1.5	0.6	0.0	3.6	6.4	1.2	0430h	2150h
	Equinox	-2.9	5.3	1.1	1.1	0.3	0.1	4.8	5.2	0.1	0550h	2000h
	Summer	-0.7	1.7	0.6	0.8	0.2	2.2	4.1	5.8	5.7	0550h	2050h
	Annual	-2.6	4.5	1.1	1.1	0.3	23.8	4.2	6.0	0.3	0550h	2030h

Table - II

Estimates of the standard error $\sigma / \sqrt{n}$ in Mean E-W Apparent drift speed for 1968-69

Hour	E-region				F-region			
	Winter	Equinox	Summer	Annual	Winter	Equinox	Summer	Annual
0	16.8	18.0	17.1	17.3	5.1	5.3	5.8	5.4
1	7.4	17.0	19.6	15.0	8.0	6.3	6.9	7.1
2	-	19.0	11.3	15.2	5.4	6.1	12.0	7.8
3	-	-	20.4	20.4	8.6	6.2	8.3	7.7
4	-	-	31.3	31.3	5.5	6.2	8.1	6.6
5	-	-	24.7	24.7	6.4	5.6	7.8	6.6
6	-	-	13.6	13.6	8.3	8.5	9.5	8.8
7	14.8	9.9	11.4	12.0	8.7	8.2	13.0	10.0
8	9.5	11.3	11.0	10.6	7.8	8.0	7.1	7.6
9	6.7	6.9	7.0	7.0	6.2	7.0	6.9	6.7
10	5.3	6.3	7.0	6.2	6.9	8.3	7.3	7.5
11	7.1	7.7	6.7	7.5	7.6	8.1	8.8	8.2
12	6.9	7.0	6.0	6.6	7.3	7.7	9.3	8.1
13	8.8	9.5	6.5	8.5	7.6	6.8	8.7	7.7
14	10.6	6.5	9.0	9.0	7.5	5.3	8.0	7.0
15	6.3	6.1	7.1	6.7	7.3	6.0	8.1	7.1
16	7.5	6.3	8.2	7.7	7.6	5.7	7.2	6.8
17	7.5	8.6	6.0	7.5	6.8	5.7	7.4	6.6
18	17.0	16.5	13.8	16.0	4.0	4.2	7.3	5.2
19	-	37.4	4.9	35.0	6.7	5.3	8.8	7.0
20	21.8	38.9	9.8	31.2	9.0	8.1	8.8	8.6
21	17.4	31.4	27.0	28.2	7.4	8.4	8.1	8.0
22	8.9	12.5	9.1	11.0	4.7	6.0	9.9	7.9
23	15.7	14.2	16.6	15.0	4.2	5.5	6.0	5.2

Table - III

E-region drift speed at Thumba during night-time
(2000 - 0400 hr)

Year		Winter	Equinox	Summer	Annual
1968	Count	32	11	80	123
	Median	111	111	100	107
1969	Count	10	30	7	47
	Median	120	158	100	126

F-region drift speed at Thumba during night-time
(2000 - 0400 hr)

Year		Winter	Equinox	Summer	Annual
1967	Count	221	289	199	709
	Median	111	130	100	114
1968	Count	193	225	278	696
	Median	86	80	75	80
1969	Count	97	177	51	325
	Median	91	107	100	99

Table - IV

The mean apparent drift speed in the E and F regions of the Ionosphere during the day time hours at different stations in the world

Station	Mag. Lat.	Layer	Year	Time	Speed	Reference
1.	2.	3.	4.	5.	6.	7.
Thumba	0.3°S	E	1964-69	Day	125	
		F	1964-69	Day	1	
Tenalo	0.6°S	E	1962 Feb.,Mar.	Day	1	Koster (1966)
		F	1962 Feb.,Mar.	Day	14	
Ibadan	3°S	F	1957 Aug.Sep.	Day	105	Skinner et al.(1958)
		E	IGY	Day	90	Skinner et al.(1963)
		F	IGY	Day	95	Skinner et al.(1963)
Bandung	9°S	E	1958	Day	85	Annals IGY, Vol.35,(1965).
Singapore	9°S	F	1953-54	Day	50	Usborne (1965)
Waltair	11°N	E	1954-55	Day	65	Rao et al (1956)
			1957-59	Day	81	Rao and Rao (1961)
			1960-62	All hrs.	75	Rao and Rao (1964)
			Mean		74	
		F	1958		99	Rao and Rao (1964a)
Ahmedabad	18°N	E	1956-66	Day	70	Unpublished.
		F	1956-62	Day	68	
Delhi	24°N	E	1958-59	All hrs.	55	Mitra et al.(1960)
		F	1958-59		85	
Yamagawa	25°N	E	1958	Day	73	Rao and Rao (1965)
		F	1958	Day	85	Rao and Rao (1964a)
Puerto Rico	32°N	E	1958 Mar-Feb 1959	Day	83	Koneshea et al.(1965)
Ashkabad	36°N	F	1958	Day	79	Rao and Rao (1964a)
		E	1958	Day		Mirkotan

Table - V

Table - V (cont'd)

1	2.	3.	4.	5.	6.	7.
Brisbane	38°S	E	1952-53	Day	78	Burke and Jenkinson(1957)
			1953-54	Day	57	
		E	1958	Day	51	Rao and Rao (1965)
			Mean		62	
Seimiz	43°N	F	1958	Day	123	Rao and Rao (1964a)
Halley Bay	47°S	E	1958	All hrs	63	Piggott and Barclay(1963)
		F	1957-58	All hrs	85	Bellchambers and Piggott (1965)
Cologne	43°N	E	Winter(1941-42)	All hrs	90	Krautkramer(1950)
Freiberg	48°N	F			100	Kazimirovskiy(1967)
Wellington	50°S	E	1958	Day	78	Rao and Rao (1964)
De Bilt	50°N	E	1958	Day	90	Rao and Rao (1965)
Cambridge	50°N	E&F	1952	All hrs.	85	Phillips (1952)
Washington	56°N	E&F	1950 Mar,Dec.	Day	70	Salzburg and Greenstone (1951)
Gorky	56°N	F	1958	Day	103	Rao and Rao (1964a)
Ottawa	62°N	E&F	1950 Jun,Oct.	All hrs.	80	Chapman (1953)
Irkutsk	52°N	F	1958		90	Kazimirovskiy (1967)
Moscow	55°N	E&F	1958		80	Kazimirovskiy (1964)
Kharkov	49°N	E	1958		50	
		F	1958		80	Kazimirovskiy (1963)
Tomsk	56°N	E	1958		90	Kazimirovskiy (1965)
		F	1958		130	
Tojhe		E	1958		60	
Rostov--on-the Lon	47°N	F	1958		80	
Kutivik	55°N	F	1963		80	Kazimirovskiy (1963)
Kjellar	60°N	F	1963		80	Kazimirovskiy ( )

(Accepted for publication in J. of Geomag. Geoelect.)

SOLAR CYCLE EFFECTS IN THE ELECTRON DRIFTS OVER THE MAGNETIC EQUATOR

by
R.K.Misra, R.Chandra and R.G.Rastogi
Physical Research Laboratory
Ahmedabad-9
India

ABSTRACT:- The E and F region apparent and true drifts over the equatorial station Thumba are studied for the period 1964-69 in relation to the solar activity. The apparent drift is found to reduce slightly while the true drift is reduced considerably, with the increasing solar activity. This result is interpreted by comparing the sensitivity factors for N_e and the solar daily range R_H of the earth's magnetic field.

INTRODUCTION

With the introduction of the method of measuring the electron drifts in the ionosphere by recording the fading of field strength of the echoes at spaced receivers by Mitra (1949) and Krautkramer (1950), large number of ionospheric drift stations were established in different parts of the world. However, drifts at regions very close to the magnetic equator were measured during IGY at Ibadan by Skinner et. al. (1958) and during IQSY by Morris and

Lyon (1966). Observations have also been made at Tamale (Koster, Karsriku, 1966) and at Dapango (Harnischmacher, Rawer, 1969) for a short period. Regular measurements of ionospheric drifts at the magnetic equator in India were started in January 1964 and were continued systematically upto December 1969 thereby providing a uniform series of data for a period, during which solar activity had considerably changed.

The measurements at Thumba were done only in the daytime hours in years 1964-65, due to the absence of sporadic E in the night hours and also due to the very low value of f_oF_2 in the night hours of a low sunspot year. Since January 1967, 24 hourly observations of F-region were started. In January 1968 with the installation of a powerful transmitter night-time E_s reflections were also recorded on certain occasions. Some of the results of the Thumba have been published earlier (Deshpande and Rastogi, 1966; Chandra and Rastogi, 1970).

Besides the similar fade analysis, quite a large number of records were analysed by full correlation technique (Briggs et. al. 1950; Phillips and Spencer, 1955; Fooks, 1965). The true drifts and other parameters

of the irregularities for the low-sunspot years have been published by Rastogi et. al. (1970).

RESULTS

The present paper describes the effect of solar cycle on the parameters of ionospheric drifts. Firstly the annual average drift speed and direction are discussed. Fig.1 shows the annual average histograms of the drift speed and drift direction for the daytime hours (08 - 16 hr) in the E and F regions. The number of observations and the median value of the parameter are also given in the histograms. It is seen from the diagram that the drift speed continues to decrease from 1964 to 1968, both for the E as well as for the F-region. The drift directions were always predominently towards west. The average drift speed for each of the seasons are given separately in table I. The histograms corresponding to the high sunspot years are much narrower than for the high sunspot years showing that the scatter of the points is reduced on high sunspot activity.

The annual average daily variations of the apparent speed V' for the E and F regions for each of the years in the period 1964-69, are shown in Fig.2. In any

of the years the E region has a maximum drift speed around 09 hr and minimum around 15 hr while the F-region drift speed is maximum around 11 hr. The monthly mean values of V' for the E and F regions are shown in Fig.3. It is seen that both for the E and F region drifts there is slight tendency of drift speed decreasing from 1964 to 1967.

The drift speed and the ratio of random to true component of the drift speed (V_c/V) were computed for the years 1964, 67 and 68, using the full correlation analysis. The percentage occurrence of these parameters are shown in histograms of Fig.4. It is very clearly seen from this diagram (fig.4) that the true drift speed decreases with the increasing sunspot number, the value being 74 m/s for 1964 and 55 m/s for 1968 for the E-region, and the corresponding F-region drift speed for 1964 and 1968 are 99 m/s and 50 m/s respectively.

The histograms of V_c/V do not show any systematic increase of the quantity with increasing sunspot number.

DISCUSSION

The ionospheric currents at the equatorial region are proportional to the conductivity and the electric field in the Eastwest direction of E-region. East-west electric field is proportional to the maximum electron density (N_e) of the E-region.

The solar daily range of H can be taken as an index of the electrojet current. In order to explain rather constant or a decreasing drift velocity with sunspot number, we have plotted in Fig.5 the solar cycle variation of the yearly mean N_e (proportional to f_oE^2) and the solar daily range in H at Huancayo for the period 1940-45. Both f_oE as well as R_H are seen to increase linearly with sunspot number. The sensitivity of these parameters to sunspot number is also of the same order suggesting that both the electron density in the E-region and the daily range i.e. the electrojet current increases with the same proportion with the increase of sunspot number, consequently one would expect the drift speed to be constant. The sunspot sensitivity index for R_H is 6.3×10^{-3} while that for f_oE is 5.3×10^{-3}. This suggests that with the increasing sunspot number, there

Table I

DAY-TIME APPARENT DRIFT SPEED AT THUMBA (0800 - 1600 HR)

Year		E-REGION				F-REGION			
		Winter	Equinox	Summer	Annual	Winter	Equinox	Summer	Annual
1964	Count	378	379	620	1377	423	370	625	1418
	Mean	106	166	129	134	144	219	181	181
	Median	105	153	120	123	138	185	159	162
1965	Count	78	217	74	369	110	256	98	464
	Mean	125	127	142	131	136	158	167	154
	Median	120	116	135	120	130	147	165	140
1966	Count	60	45	97	202	73	127	278	578
	Mean	120	117	98	112	145	140	135	140
	Median	103	115	88	98	140	130	135	135
1967	Count	169	126	102	397	209	325	211	745
	Mean	123	101	82	102	156	143	146	148
	Median	110	100	80	99	145	142	137	141
1968	Count	284	214	263	761	284	332	353	969
	Mean	140	130	105	125	150	160	115	142
	Median	130	125	100	118	144	150	110	135
1969	Count	143	123	10	276	246	231	64	541
	Mean	133	128	122	127	170	167	152	164
	Median	130	115	120	122	166	154	150	157
All the 6 years	Count	1112	1104	1064	3282	1445	1641	1629	4715
	Mean	124	138	112	121	150	167	149	153

REFERENCES

Briggs,B.H., Phillips,G.J. and Shinn,D.H.; The analysis of observations on spaced receivers of the fading of radio signal; Proc. Phys. Soc., B63, 106 (1950).

Chandra,H., and Rastogi,R.G.; Daily variation of F-region drift at Thumba; J.Atmos. & Terr. Phys., 32, 1309 (1970).

Deshpande,M.R., and Rastogi,R.G.; Ionospheric horizontal drifts within the equatorial electrojet region in India; Annls. Geophys., 23, 418 (1966).

Fooks,G.F.; Ionospheric drift measurements using correlation analysis - methods of computations and interpretation of results; J. Atmos. & Terr. Phys., 27, 979 (1965).

Harnischmachar,E., and Rawer,K.; Scientific Report No.AF61(052)-944, Ionosphere Institute, Germany. (1969).

Koster,J.R., and Katsriku,I.K.; Some equatorial ionospheric E and F region drifts measurements at Tamale; Annls.Geophys 22, 440 (1966).

Krautkramer,J.; Uber Wanderererscheinung rascher Feldstarke-Schwankungen von Ionospharen-Echoes, Arch. Elek. Ubertr., No.4, p.133 (1950).

Mitra,S.N.; Statistical analysis of fading of a single down-coming wave from the ionosphere; Proc. IEE.96,Part III, 441 (1949).

Morris,R.W., and Lyon,A.J.: Equatorial Ionospheric Drifts; Nature, 310, 607 (1966).

Olson,W.P., Contribution of nonionospheric currents to the quiet day magnetic variations at the earth's surface; J. Geophys. Res., 75, 7244 (1970).

Phillips,G.J., and Spencer,M.; The effect of anisometric amplitude patterns in the measurement of ionospheric drifts; Proc. Phys. Soc., B68, 106 (1955).

Rastogi,R.G., Chandra,H., and Deshpande,M.R.; Drift and anisotropy parameters of the irregularities in the E and F regions of ionosphere over Thumba during 1964; J. Atmos. & Terr.Phys., 32, 999 (1970).

Skinner,N.J., Hope,J. and Wright,R.W., Horizontal drift measurements in the ionosphere near the equator; Nature,182 1363 (1958).

CHAPTER III

FULL-CORRELATION METHOD OF ANALYSIS OF FADING RECORDS AT SPACED RECEIVERS

Time delay method of MITRA (1949) & KRAUTKRAMER (1950) for analysing the spaced antenna fading records assumes that the fading is produced at the ground entirely due to a uniform movement of the diffraction pattern and that the contours of constant amplitude have circular symmetry i.e. the pattern is isotropic. The method is therefore limited only to those records where the fading patterns at all the three aerials are similar in shape. However, the diffraction pattern itself undergoes some changes in shape during the time it moves between the aerials and hence the time delay between similar fades at the spaced antenna will depend on the steady drift of the pattern past the aerial plus the random changes in the pattern itself (RATCLIFFE, 1948). The fading pattern at two spaced points will therefore depart from being similar with the increasing separation due to the effect of changing pattern, till after some separation the two fadings may be rather independent.

3.1 (A) Method of Briggs, Phillips and Shinn and its extension by Phillips - Spencer and Fooks

BRIGGS, PHILLIPS and SHINN (1950) gave for the first time the method for the separation of the steady

and random components of the drift. The term 'random drift' here stands for the rate at which the pattern changes its shape. The method is based on the computation of auto and cross-correlation functions between the fading records at different set of aerials. It is assumed that:-

(i) the three receivers are separated by a distance so as to give rise to reasonably similar fading patterns; this distance is normally of the order of one wave-length.

(ii) the diffraction pattern is isotropic

(iii) the space and time variations are identical

(iv) the drift speed remains the same during the course of a record.

Definition of velocity parameters

The auto and cross-correlation curves for the fading records are shown in Fig.3.1. BRIGGS et al. (1950) have defined four velocity parameters to describe the movement of a ground diffraction pattern in terms of these correlation coefficients.

(a) Fading velocity V_c'

V_c' is the drift velocity of an unchanging ground pattern that would explain the observed rate of fading at a particular point on the ground. Under the assumption of isotropy, this quantity will be independent of the direction.

V_c' is also defined as the ratio of space shift (ξ_1) to time shift (τ_1') needed to produce on the average the same change in the value of amplitude R. Thus from the correlograms shown in Fig.3.2a:

$$\rho(\xi_1, 0) = \rho(0, \tau_1')$$

and $V_c' = \xi_1 / \tau_1'$ .....(1)

It is assumed as mentioned earlier that the spatial and temporal correlation functions are similar in forms (on the basis of the experimental evidence of BRENNOM, 1960) and that the contours of correlation of the diffraction pattern are Gaussian in shape.

(b) True drift velocity V

V is the velocity of an observer who experiences slowest fading in the received signal. This is also called the steady drift speed as whatever slow fading is now experienced is on account of the random changes in the diffraction pattern. Thus if a distance ξ_1 is moved in time τ_1 by the observer to experience the least fading, then :

$$V = \xi_1 / \tau_1 \qquad .....(2)$$

For a two dimensional ground, V has a direction ϕ and can be represented by two components $V_x = V \cos \phi$ and $V_y = V \sin \phi$.

(c) Characteristic velocity V_c

This is the value of fading velocity V_c' for an observer moving with a uniform velocity V. The slowest

fading experienced by this observer is due to random variations of the diffraction pattern and V_c is a measure of this rate of change. For this observer, V_c (by definition) is the ratio of space shift to time shift needed to produce same change in R

i.e. $V_c = \xi_0 / \tau_1''$ .....(3)

where $\rho'(\xi_0, v) = \rho(\xi_1, \tau_1'')$

(d) Apparent drift velocity V'

This is the velocity of the diffraction pattern experienced by a fixed receiver on the whole, without taking into account any random changes in the pattern. If τ_0 be the time delay for the cross-correlation peak between two receivers at x = 0 and x = ξ_0

then $V' = \xi_0 / \tau_0$ .....(4)

For a two dimensional ground, if t_{ox} and t_{oy} be the timelags in x and y directions, it can be seen geometrically that:

$1/V'^2 = 1/V'_x{}^2 + 1/V'_y{}^2$ .....(5)

where $V'_x = \xi_0 / t_{ox}$

$V'_y = \eta_0 / t_{oy}$

Relationship between V', Vc', V and Vc

BRIGGS et al.(1950) have shown that for an isotropic diffraction pattern:

$$V_c'^2 = V_c^2 + V^2 \qquad \ldots\ldots\ldots(6)$$

$$V_c'^2 = VV' \qquad \ldots\ldots\ldots(7)$$

$$\text{hence } VV' = V_c^2 + V^2 \qquad \ldots\ldots\ldots(8)$$

$$\text{or } V' = V + (V_c^2/V) \qquad \ldots\ldots\ldots(9)$$

Thus $V' > V$ and the contribution due to random variations within the pattern is equivalent to (V_c^2/V), which has a direction same as that of V, as V_c^2 has no particular direction.

Determination of V_c' and V from correlograms

If τ_1 be the time shift on the auto-correlation curve corresponding to $\phi(\tau_1, 0)$ in the X-direction (see Fig.3.2a) then by definition:

$$(V_c')_x = \xi_0/\tau_1$$

$$\text{similarly } (V_c')_y = \eta_0/\tau_2 \qquad \ldots\ldots\ldots(10)$$

$$\text{and } (V_c')_{xy} = (\xi_0^2 + \eta_0^2)^{\frac{1}{2}}/\tau_3$$

V' is calculated from the shift of the maxima of cross-correlograms i.e. from t_x and t_y using the relations

$$V_x' = \xi_0/t_x \; ; \; V_y' = \eta_0/t_y \text{ and}$$

$$1/V'^2 = 1/V_x'^2 + 1/V_y'^2$$

Knowing V_c' and V', one can estimate steady and random drift velocities V and V_c using the relations (6) and (7).

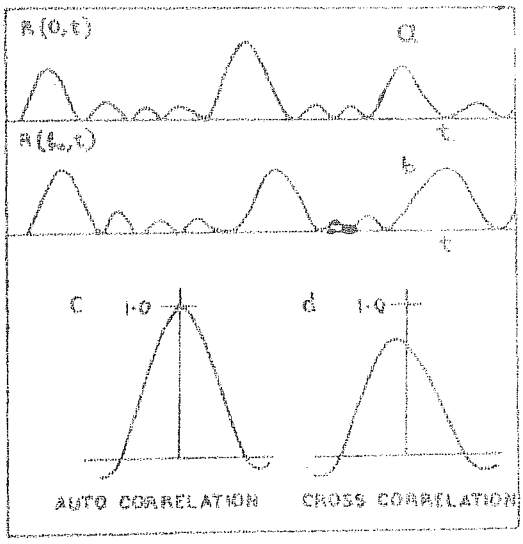

FIGURE 3.1

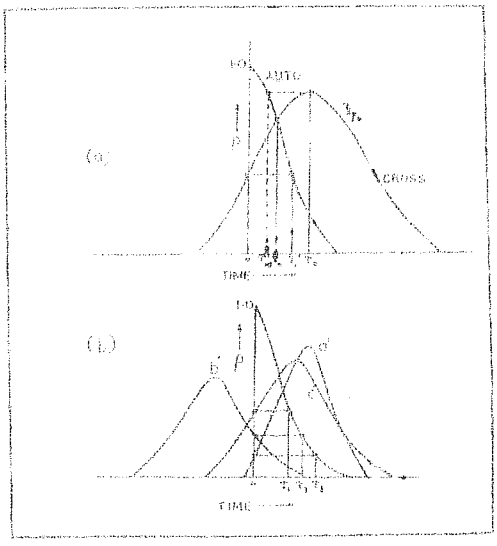

FIGURE 3.2a

METHOD OF BRIGGS, PHILLIPS AND SHINN

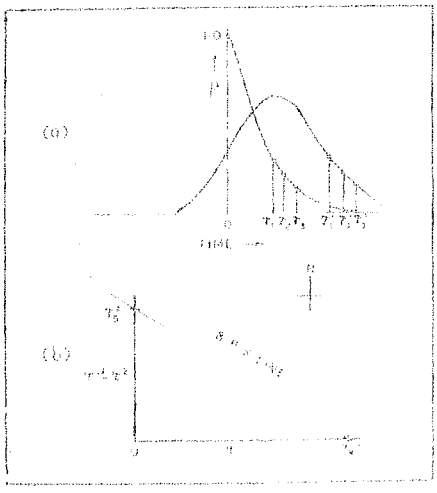

FIGURE 3.2b

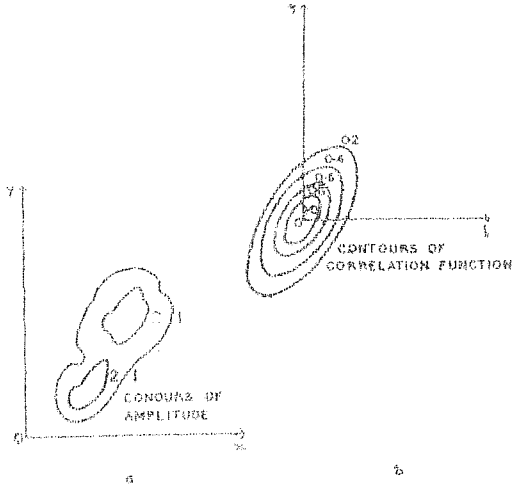

FIGURE 3.3a

Geometrical method: A more accurate method of application consists in finding out time shifts τ and τ' for equal correlation values in time and space. This is done by drawing horizontal lines on the cross and auto-correlograms (see uppr part of Fig.3.2b).

Then ($\tau'^2 - \tau^2$) is plotted against τ . It can be shown from simple geometrical considerations that

$$\tau'^2 - \tau^2 = (\xi_o^2 - 2V \xi_o \tau) / V_c'^2$$

Thus a plot of ($\tau'^2 - \tau^2$) against τ would be a straight line for any pair of aerials and this is called BPS line (see lower part of Fig.3.2b). The intercepts of this line on two axes are given by τ_e and τ_s^2 as follows:

$$\xi_o / 2V = \tau_e \quad , \quad \xi_o / V_c' = \tau_s$$

Thus V and V_c' can be determined.

(B) Extension of BPS method to anisotropic diffraction pattern

The previous technique of estimating V and Vc as given by BRIGGS et al. (1950) assumes that the diffraction pattern on the ground is isometric so that its statistical properties show a circular symmetry. In practice, however, the pattern is statistically anisometric so that the contours of constant auto-correlation are not circular.

Consider, for example, a pattern in which the amplitude contours are so elongated that they appear as a set of parallel lines. It is evident that the motion of the pattern in a direction parallel to these lines can never be detected and only the component of motion perpendicular to them will be measured. When the pattern has a finite structure in all the directions, the situation is not so serious, but the errors may still arise if it is not completely isometric. The pattern near the magnetic equator is highly elongated and calls for a special care while deducing the various parameters. PHILLIPS and SPENCER (1955) extended the work of BRIGGS et al. (1950) to anisotropic diffraction patterns.

The contours of constant amplitude for an anisometric pattern and its two dimensional auto-correlation function which is in the form of concentric ellipses are shown in Fig.3.3a. It will be concentric circles in the case of an isometric pattern. This type of pattern can be produced from a statistically isometric pattern by stretching it in one direction. Distortion of this type may be represented by a 'characteristic ellipse' similar to the contours of constant correlation. The complete information regarding the anisotropy of the pattern can therefore be described in terms of the axial ratio and orientation of the characteristic ellipse.

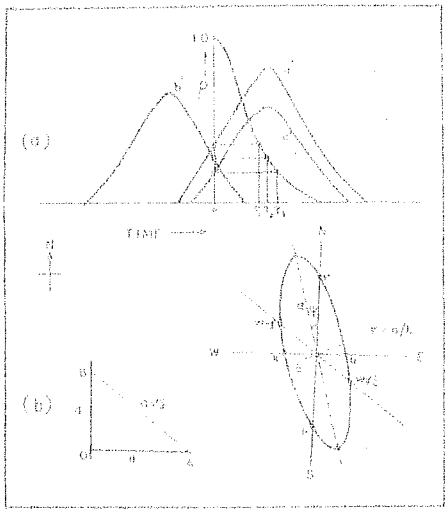

FIGURE 3.3b

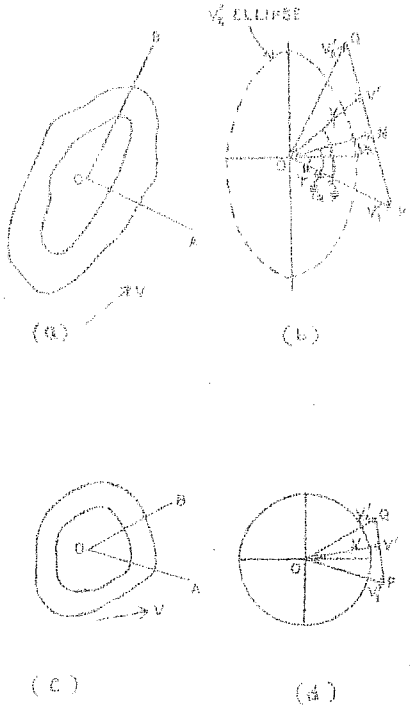

FIGURE 3.4

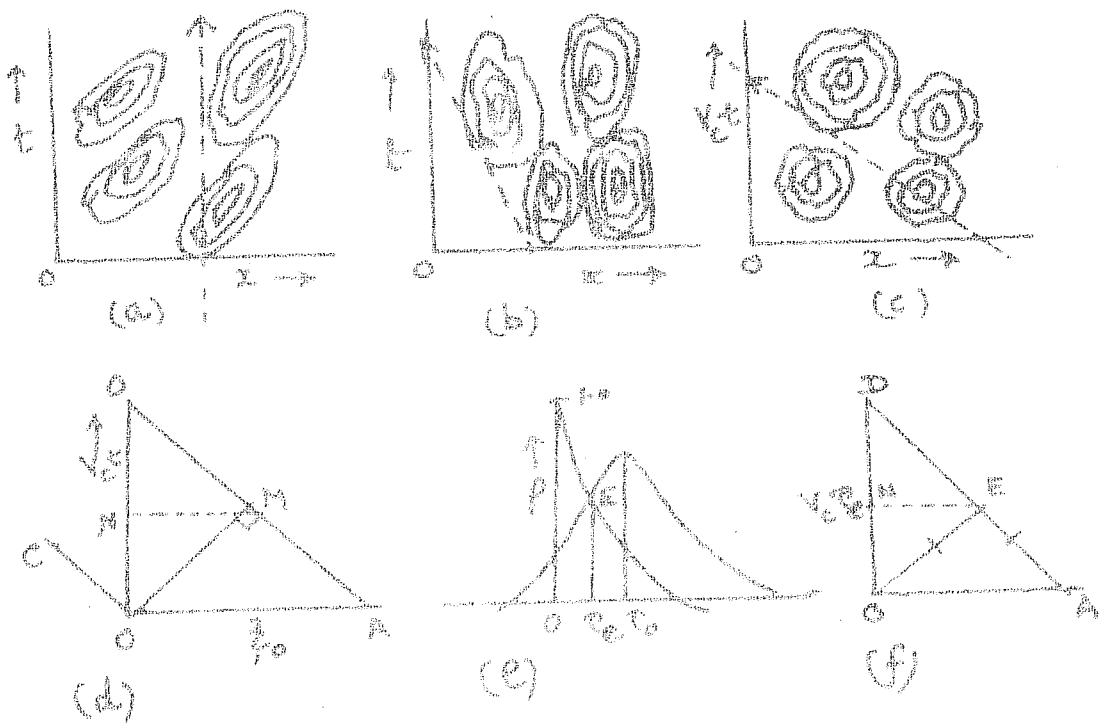

FIGURE 3.5

Determination of characteristic ellipse from auto and cross-correlation

Let $\rho(\xi, \eta, \tau)$ be the correlation coefficient between amplitudes recorded at two points with a relative displacement (ξ, η) in cartesian co-ordinate system and at times separated by τ. Let the curves a', b' and c' in Fig.3.3b give the cross-correlograms between the fading records at aerials O and A, O and B, and A and B respectively, where OA = OB = a and the angle AOB = 90°.

The values $\rho(a, o, o)$, $\rho(o, a, o)$ and $\rho(a-a, o)$ of the cross-correlation coefficients at time $t = o$ are converted to the equivalent time shifts τ_1, τ_2 and τ_3 respectively, on the auto-correlogram for the same value of ρ. Thus by the definition of fading velocity V_c', as given by BRIGGS et al. (1950):

$$(V_c')_{OA} = a/\tau_1 = u$$
$$(V_c')_{OB} = a/\tau_2 = v$$
$$(V_c')_{AB} = a\sqrt{2}/\tau_3 = w\sqrt{2}$$

For $\tau = 1$, u, v and $w\sqrt{2}$ are equal to the three sides of the isosles triangle and the correlation is $\rho(0, 0, 1)$. Thus the polar plot of V_c' would give rise to an ellipse of constant correlation centered at O. The axial ratio γ and the tilt angle ψ for the ellipse can therefore be directly found out geometrically from the polar

plot of V_c' . The method consists in marking the values of u, v and w on the axes x = 0, y = 0 and x = -y on both positive and negative sides. A smooth ellipse is drawn through these six points using the fact that a diameter of ellipse bisecting a chord bisects all chords parallel to it (see Fig.3.3b). The values of semi-major axis and semi-minor axis are read to get the axial ratio ' γ ' and the orientation angle ' ψ ' with respect to a particular axis is also noted. The geometrical method, described above, becomes more handy in cases of unequal antenna spacings when the mathematical relations, to be described below, become complicated.

Mathematical relations for γ and ψ :

PHILLIPS and SPENCER (1955) have shown that the axial ratio and orientation angle ψ of the major axis of the characteristic ellipse is given by the following relations:

$$\gamma = \frac{R + (P^2 + Q^2)^{\frac{1}{2}}}{R - (P^2 + Q^2)^{\frac{1}{2}}} \qquad \text{.....(14)}$$

$$\text{and } \psi = \frac{1}{2} \tan^{-1} (P/Q)$$

$$\text{where } P = \tau_1^2 + \tau_2^2 - \tau_3^2$$

$$Q = \tau_1^2 - \tau_2^2$$

$$R = \tau_1^2 + \tau_2^2$$

These relations hold for an isosles right angled triangle of receivers and can be modified for any other

geometry of the receiving aerials.

In order to correct the drift parameters for the anisotropy of the diffraction pattern PHILLIPS and SPENCER (1955) used the results of BRIGGS et al. (1950) for an 'equivalent isometric pattern' (see Fig.3.4). Their main results are as follows:

$$\tan(\phi - \phi_a) = \frac{(V^2 - 1)\tan(\phi - \psi)}{1 + r^2 \tan^2(\phi_a - \psi)} \quad ..(15)$$

$$\text{also } V_a = V' \cos(\phi - \phi_a) \quad .....(16)$$

$$(V'_c)^2_v = (V_c')^2_1 \frac{1 + (r^2 - 1)\cos^2\psi}{1 + (r^2 - 1)\cos^2(\phi - \psi)} .(17)$$

$$\text{and } V = (V'_c)^2_v / V' \quad ..... (18)$$

Errors in the Estimates of Direction without Anisotropy correction

The difference $(\phi - \phi_a)$ between true and apparent directions of drift is related to the angle $(\phi_a - \psi)$ as shown in Fig.3.7a. It depends on the axial ratio of the ellipse. The error $(\phi - \phi_a)$ may be as large as 55° for $\psi = 3$. Second diagram 3.7b gives the relation between the ratio V_a/V and the angle $(\phi_a - \psi)$. It can be seen that there are no errors in the estimates of the velocity or direction when the minor or major axis of V'_c ellipse is directed along the true direction of drift i.e. when $(\phi - \psi) = 0$, 90° or 180°. In the lower half of the Fig.3.7 is shown the percentage occurrence of the corrections $(\phi_a - \psi)$,

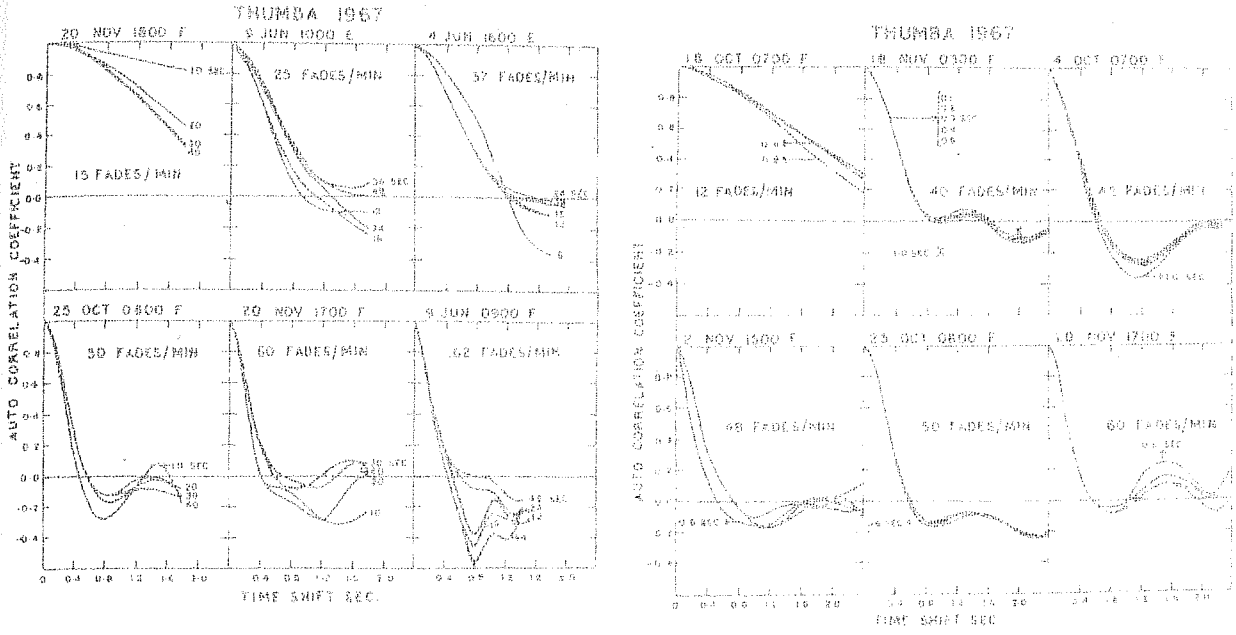

FIGURE 3.6

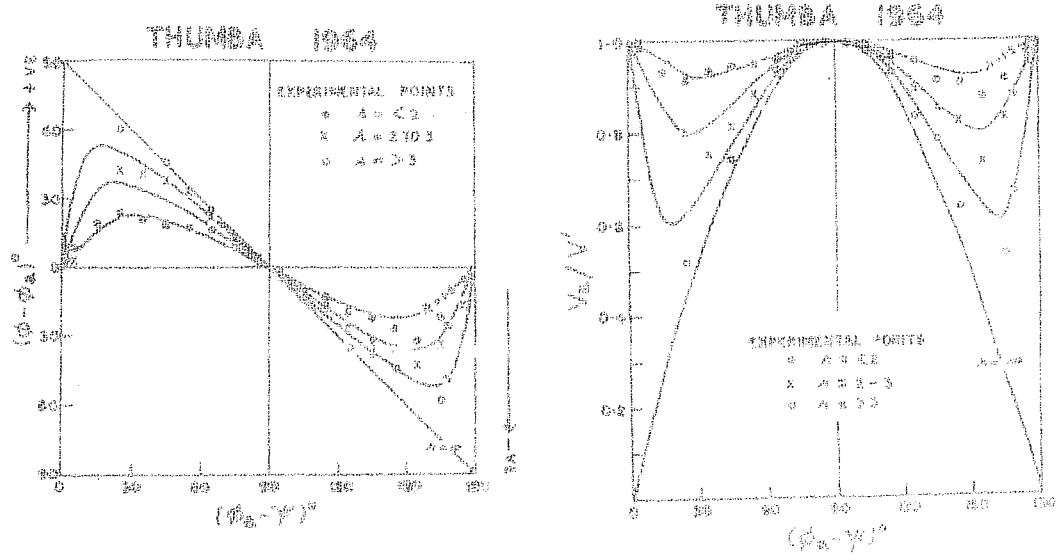

T H U M B A 1 9 5 4

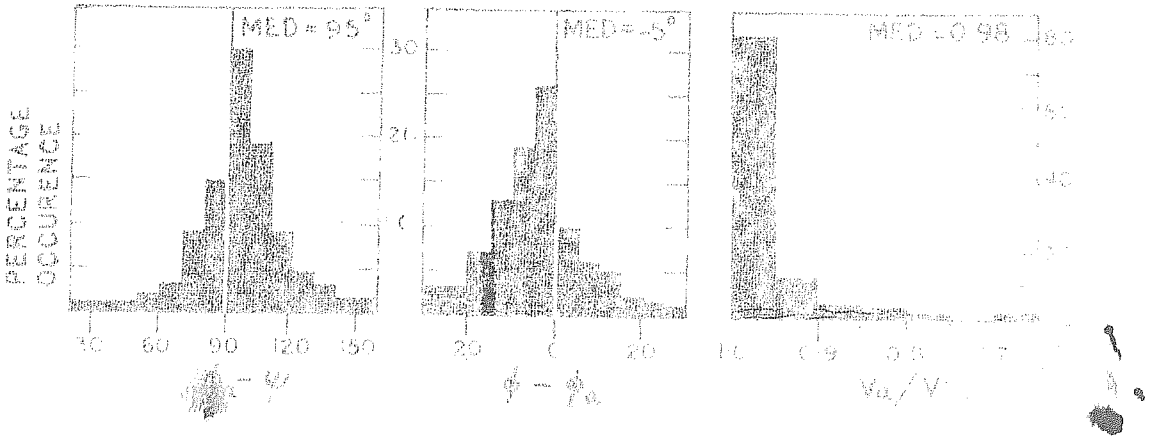

FIGURE 3.7

$(\phi - \phi_a)$ and V_a/V for Thumba (1964). This also shows that $(\phi - \phi_a)$ and V_a/V are least when $\psi = 0$ and increase as ψ increases. Thus for Thumba, where the irregularities are highly elongated along the magnetic north-south, the errors in V and ϕ due to anisotropy of the ground deffraction pattern are least.

Fook's modification of Phillips Spencer's method

FOOKS (1965) suggested two modifications in the use of the correlation techniques over that of BRIGGS et al. (1950) and that of PHILLIPS and SPENCER (1955). They are as follows:

(a) To use of a mean auto-correlogram from the three antenna fading records in order to reduce statistical deviation which produce appreciable difference between them.

(b) To use an alternative method of finding times τ_{12}, τ_{21} and τ_{23} in which only the top portion of cross-correlograms is used, and hence values are less affected by statistical variations. This is given by:

$$\tau_{12}^2 = (\tau_{12}')^2 + (\tau_m)^2 \qquad \ldots\ldots(19)$$

Where τ_{12}' is the displacement of the maximum of the cross-correlogram and (τ_m) is the corresponding

time-shift on mean auto-correlation curve (see Fig.3.2a).

According to (19), $\tau_{12} > \tau'_{12}$

or $V'_c < V$

and hence from (6), $V_c = (V'^2_c - V^2)^{\frac{1}{2}}$

since $V = V'^2_c/V'$ or $V < V'_c$, which is always real.

The main advantage of Fook's modification is therefore to remove the occurrence of negative V_c^2, due to statistical deviations in the lower portion of the correlation curves. If negative V_c^2 still comes, it has been interpreted by HINES (1968) as due to presence of internal gravity waves, affecting the movements of irregularities. This effect is discussed in more details for Thumba in Sec 5.11 of Chapter V, along with the occurrence of negative r^2.

Definition of V_c for an anisometric pattern

BRIGGS et al. (1950) have defined V_c as the value of V'_c found by an observer moving with a uniform velocity V. For such an observer, the entire fading is due to the random changes in the pattern. V'_c is the ratio of the space shift to time shift required to produce, on the average, the same change in the value of ρ. For a stationery pattern, the shift required to reduce the correlation to 0.5 can be defined as the mean life time of the pattern. Thus another

way of defining V_c will be:

$$V_c = \frac{\text{Pattern size}}{\text{Mean life time}}$$

In this case, there is no need to identify V_c with any specific velocity component in the pattern. For an anisometric pattern considered by PHILLIPS and SPENCER (1955), V_c will be a function of direction. Now as the mean life time will be independent of direction, V_c for any particular direction, will be proportional to the corresponding radius of the characteristic ellipse. Neither the pattern size nor the life-time is affected by V, and the above definition of V_c will hold for a moving pattern also. FOOKS and JONES (1961) gave the parameter $(V_c)_v/V$ in order to indicate the effects of random changes in the same direction as that of V. In this definition of V_c no further assumptions are introduced about the statistical behaviour of the pattern.

Average size of irregularities in the pattern

PHILLIPS and SPENCER (1955) derived expressions for axial ratio 'r' and orientation 'ψ' of the characteristic ellipse; size of the ellipse is, however, not mentioned by them. FOOKS (1965) has given a method to derive the values of semi-major and minor axes 'a' and 'b' from the Vc' values. The ellipse has the dimensions of velocity and can be converted to distances to give the average size and shape of the irregularities in the pattern.

This is achieved by multiplying the correlations by 0.5 (i.e. the value of time displacement required to give $\rho = 0.5$ on the mean auto correlograms).

FOOKS (1965) results are:

$$a = \frac{(MN' - M'N)^{\frac{1}{2}}}{(N'-N)^{\frac{1}{2}}} \quad \text{and} \quad b = \frac{(M'N-N'M)^{\frac{1}{2}}}{(M'-M)^{\frac{1}{2}}}$$

where $M = r_1^2 \cos^2(\theta_1 - \psi)$, $M' = r_2^2 \cos^2(\theta - \psi)$

and $N = r_1^2 \sin^2(\theta_1 - \psi)$, $N' = r_2^2 \sin^2(\theta - \psi)$

(r_1, θ_1) and (r_2, θ_2) are two arbitrary points lying on the characteristic ellipse.

3.2 Optimization of the method for the present analysis

(a) Sampling theory

In theory it is assumed that each record is a sample taken from an indefinitely long record with an auto-correlation function $\rho(0,t)$. Due to the finite length of the record, however, the errors will be involved in the calculation of $\rho(o,t)$. SOPER (1915) has shown that the standard deviation of sample correlation coefficients is given by:

$$\sigma(\rho) = \frac{1-\rho^2}{N-1}\left(1 + \frac{1+\rho^2}{4N}\right) \quad \ldots\ldots\ldots,(21)$$

N being the number of sampling points used.

For large values of N

$$\sigma(\rho) = \frac{1-\rho^2}{N-1}$$

Now $\bar{\rho} = \rho\left(1 - \frac{(1-\rho^2)}{2N}\right)$

for large N, $\bar{\rho} = \rho$

Thus for a finite length of record, a good estimate of variance is:

$$\sigma(\bar{\rho}) = (1 - \bar{\rho}^2) / (N-1)^{\frac{1}{2}} \quad \ldots\ldots(22)$$

It can be seen from this equation that the variance increases directly with the number of sampling points on the amplitude record. But there exists an upper limit to this, beyond which the variance does not increase significantly and this number N is called the number of independent points on the fading record. BARTLETT (1956) has shown that the variance of a computed correlation coefficient from a time series is related to its auto-correlation function by the expression:

$$\text{Var}\ (\ \rho(\tau)\ ) \approx \frac{1}{T} \int_{-\infty}^{+\infty} \rho^2(v)\, dv \quad \ldots.(23)$$

Where T is the length of the sample record. Hence, if the amplitudes are scaled at intervals closer than T/N, they are not independent of each other and would not lead to any improvement in the variance. Combining equations (22) and (23):

$$\frac{(1-\rho^2)^2}{N-1} = \frac{1}{T} \int_{-\infty}^{+\infty} \rho^2(v)\, dv$$

$$N = \left(T (1-\rho^2)^2 \ / \int_{-\infty}^{+\infty} \rho^2(v)\, dv \right) + 1$$

Maximum value of N corresponds to $\tau = 0$ or $\rho = 1$

and hence $N = \left(T / \int_{-\infty}^{+\infty} \rho^2(v)\, dv \right) + 1$

For a Gaussian distribution of $\rho(v)$, $N = T / \sqrt{\pi}\, b$

where $\rho(v) = \exp\ (-v^2/2b^2)$

Thus, the maximum number of independent points is given by $N = T / \sqrt{\pi}\, b$. BOWHILL (1956) has shown that the average fading period for a Gaussian auto-correlogram is given by:

T_2 = T / (No. of maxima of amplitude in time T)

= 3.63b

Thus N = 2 (No. of maxima in time T).

(b) Criterion for the sampling interval and length of the record

From the foregoing discussions it follows that the record of amplitude variation must be read at least at two points in one fade. Scaling of the record at closer intervals would not lead to any significant improvement in the accurary in the estimation of ρ . A number of drift records for Thumba have been studies (HARISH, 1969) for the effect of increasing scaled points and the length of the sample on the accuracy of the correlogram. It was concluded that at least three amplitude scalings should be taken within one fade and at least 12-15 fades should be included in one analysis.

The effect of shorter records and wider sampling intervals are felt mostly in the lower portions of the correlogram i.e.around the base line values (see Figs.3.6a and 3.6b).

3.3 Results of steady and random drift components at Thumba

Results of steady and random drift parameters of the ground diffraction pattern at Thumba for the year 1964 have been discussed by RASTOGI et al. (1970). The method of PHILLIPS and SPENCER was used. The ratio of random to steady drift was found to be on the average 0.91 for E-region and 0.81 for F-region (both for the day-time). The median value for the steady drift speed was 74 m/sec and 98 m/sec for E and F regions respectively. The ratio of true to apparent drift speed was about 1/2 for the E and about 2/3 for the F-region. As regards the drifts direction, it was mostly towards west lying in the range of 235° to 315° east of north for about 90% of the occasions. Table I summarises these results for 1964. The daily variation of V and Vc/V during daytime (07-18 hr) for 1964 have been shown to have no systematic variation in Vc/V for both E and F-regions and V varying similarly as the apparent drift speed for E and F-regions.

HARISH CHANDRA (1969) studied these parameters for Thumba for the year 1967 and his results are summarised in the tables IIa and IIb. For E-region, median value of the ratio of random to steady drift was found to be 0.64 for daytime. The F-region results for night-time were also studied. The median values for the ratio V_c/V for day and

night time hours in the F-region for 1967 were found to be 0.54 and 0.43 respectively, and the steady drift speed was 85 m/s and 89 m/s respectively. The diurnal variations of V and V_c/V for E-region showed two peaks, one around 0800 hr and another around 1500 hr. For F-region, the value of V first decreases upto 0400 hr then there is a sudden rise around 0700 hr. Another maximum is observed about noon. There is again a slow decrease till evening with a maxima again at about 200 hr IST. Diurnal variation of V_c/V for F-region showed a more systematic variation with a maximum around noon-time and minimum around midnight. The eastward component of the true drift speed for F-region was also studied and the harmonic coefficients for the same are given in Table III alongwith those for 1968.

Nearly eight hundred records analysed by author using full-correlation method for both E and F-regions for the period 1968-69. The criterion laid down in Sec.3.2(b) of this chapter was followed in choosing the sampling interval and length of the record. The shift of the maxima of cross-correlograms from zero was determined accurately. Each drift record was projected on centimeter graph paper with a suitable magnification and traced for sufficient length. The amplitudes at pre-selected intervals (depending on the rate of fading) were read manually for all the three aerials

and the auto and cross-correlograms were computed using IBM 1620 computer. Various time-lags (see Fig. 3.2a) were read manually from the set of auto and cross-correlograms for each record and used to compute various parameters namely V_a, V', V, V_c, ϕ_a, ϕ, V_c/V, γ, ψ and b for the diffraction pattern, using the relations (14) to (20).

Seasonal study of the percentage occurrence of V_a, V, V_c and V_c/V

Fig.3.8 and Fig.3.9 give the histograms of V_a and V for each season as well as the whole period of two years (1968-69) for E and F-regions respectively. The count and the median values for each of them is also written in the respective blocks. The night time E-region results for Thumba are presented for the first-time and owing to the rare occurrence of E_s layer at Thumba during night huurs, the statistics is comparatively low. The median values of V_a are 148 and 145 m/s and that of V are 55 and 33 m/s during day and night respectively for E-region over the entire period of observation. Similarly from Fig.3.9, one finds the median values of V_a to be 142 and 98 m/s and that of V to be 50 and 60 m/s for day and night-time respectively for F-region over the whole period of observation (1968-69). Regarding the seasonal variation, daytime values of V_a and V for both the regions are least during summer season and maximum during winter season. The night

THUMBA 1968-69

E - REGION

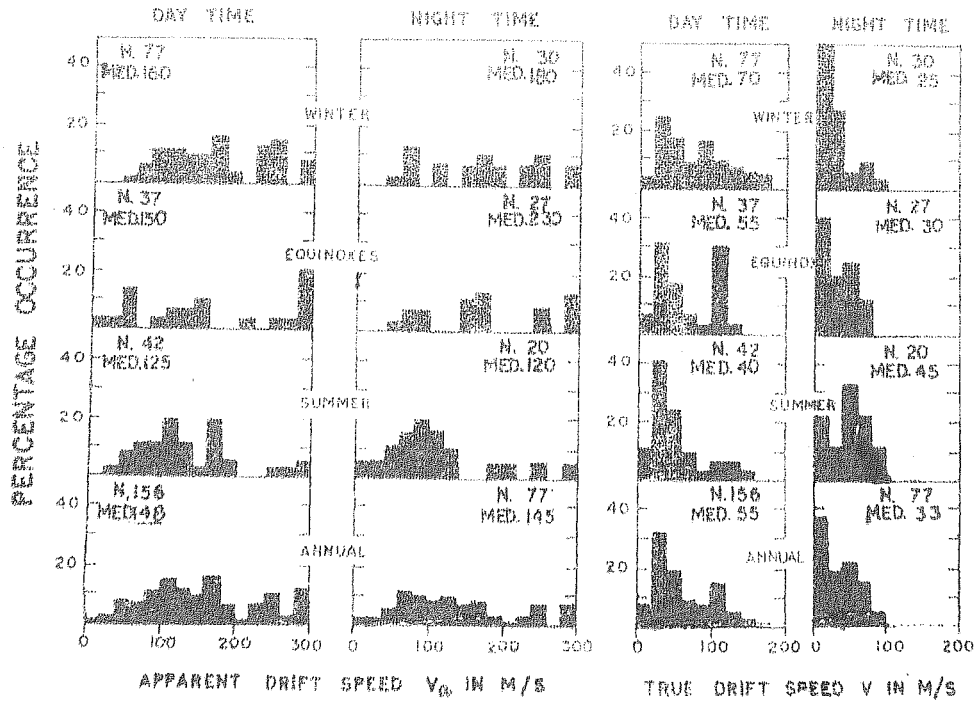

FIGURE 3.8

F - REGION

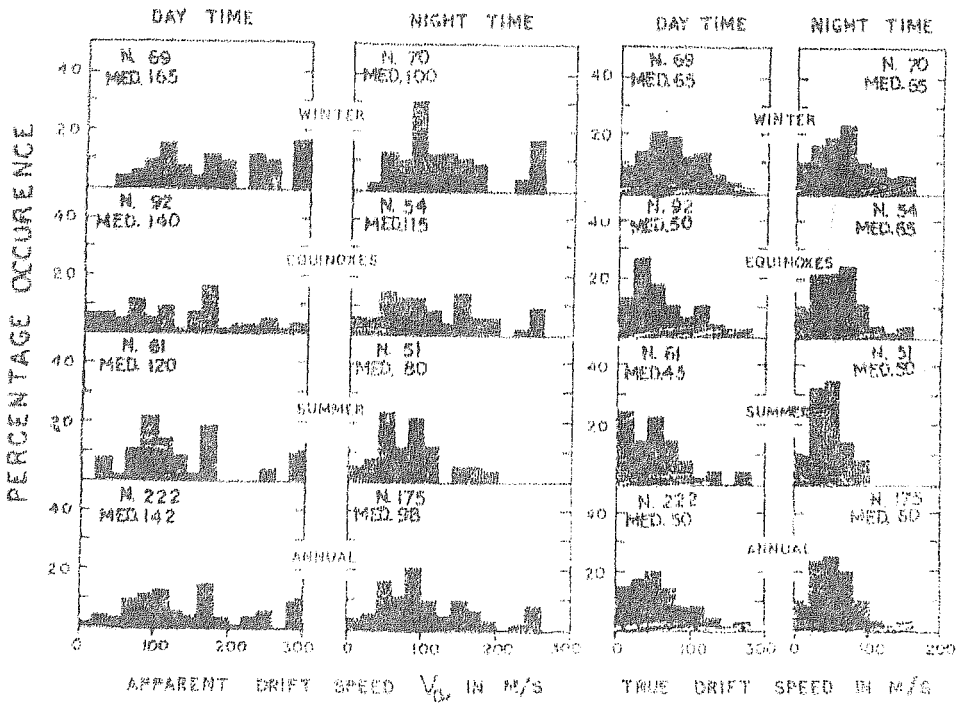

FIGURE 3.9

time values of V_a are maximum during equinox and least during summer for both E and F-regions whereas the values for steady drift speed V show a slightly different trend for E-region than the usual minimum during summer. The median value of V is maximum during summer and minimum during winter for night-time at Thumba in E-region while in F-region it is minimum during summer and equal for winter and equinoxes. The greater scatter of histograms for V_a as compared to V values for any of the seasons is another significant feature to be noted. This suggests that the variability in the measurement of V' is largely due to the variability of V_c rather than V.

Referring the true drift direction $\emptyset$ for E- as well as F-regions during day-time, it is mainly towards west, the median values of $\emptyset$ being 264° and 265°east of north respectively. E-region shows a slight tendency for an eastward drift during day during equinox and summer whereas in F-region there is no seasonal change. During the night time steady drift direction in the F-region has a predominantly eastward drift. The E-region drift direction at Thumba however, behaves in a peculiar way during night. The drift is eastward in 60% cases and westward in the remaining 40% cases. They can be explained from the prevailing effect of electrojet in E-region

till late in the night (MISRA and RASTOGI, 1971). F-region drift direction does not show any striking seasonal behaviour in the night whereas there is an interesting seasonal effect in E-region drift direction. There is the maximum tendency for a westward drift in night during equinoxes and least during summer. This can be attributed to the equinoxial maximum of the electrojet current at Thumba.

The contribution of random variations of the diffraction pattern i.e. the ratio V_c/V is plotted for the percentage occurrence in Fig.3.11 for both E and F-regions for the period 1968-69 . It is seen that median value of the ratio of random to steady drift speed for E and F-regions for the whole two years period during daytime is 1.10 and 1.13 respectively, indicating a slightly higher value for V_c than V. For the night hours however, the contribution of V_c is significantly reduced in the F-region (median $V_c/V = 0.67$) while there is a slight increase for the E-region (Median $V_c/V = 1.20$). The more turbulent conditions prevailing in the E-region throughout the twenty four hours in contrast to the relatively quiet conditions in the F-region seems to be responsible for such an effect. As regards the seasonal changes, E-region shows the least value of V_c/V (median) during summer both for the day and for the night and maximum values during winter months. F-region

THUMBA 1968-69

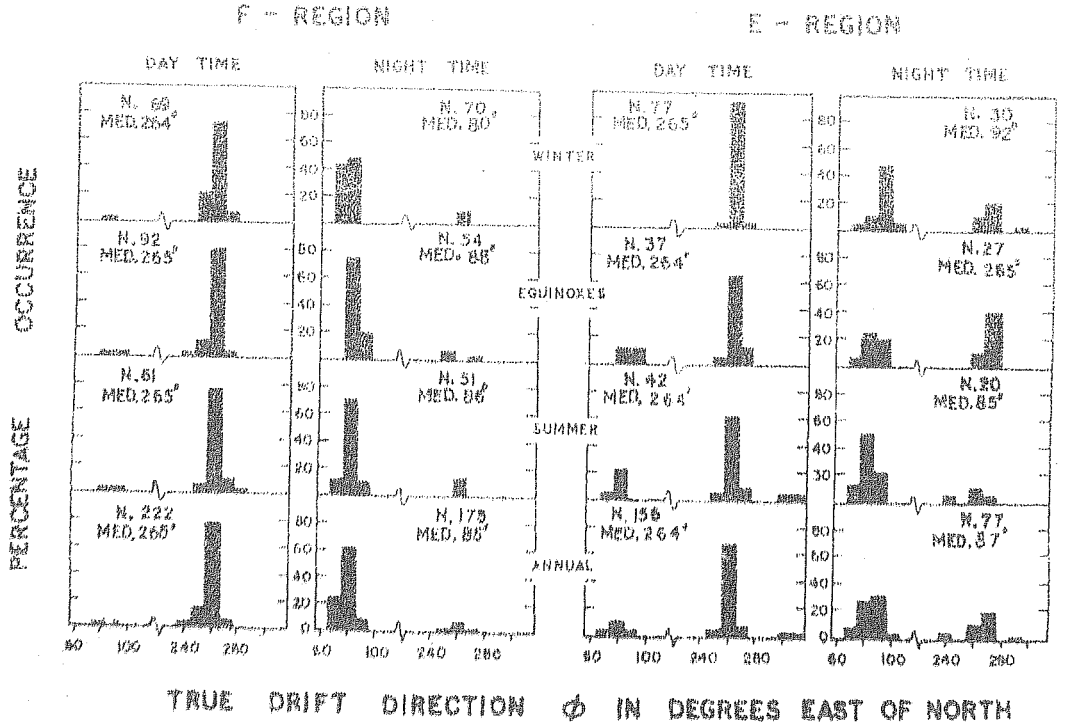

FIGURE 3.10

THUMBA 1968-69

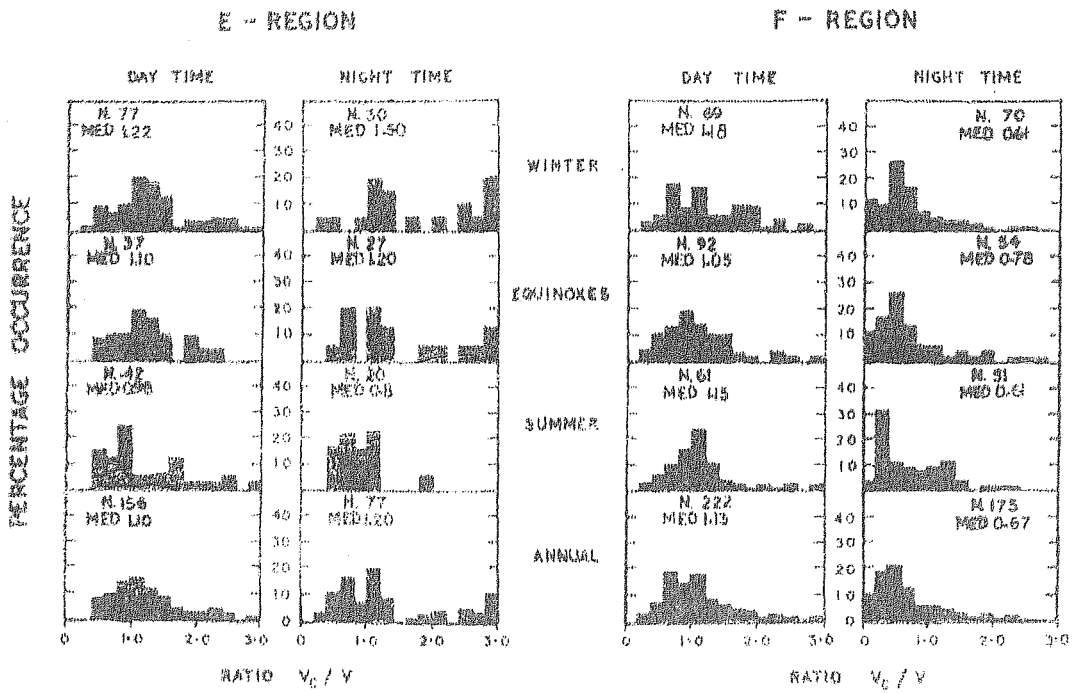

FIGURE 3.11

daytime values are almost uneffected seasonally while the night time V_c/V again shows a minimum during summer and maximum during equinoxes.

Diurnal variation of V, V_c and V_c/V during 1968-69

The daily variation for E-region drift parameters for Thumba is presented in the Fig.3.12. The steady drift speed V shows a double peak, one around 0800 hr and another around 1500 hr IST, in similarity to the apparent drift speed V, described in Chapter II. The morning peak is most pronounced during winter and least during summer, while the evening peak is virtually unaffected seasonally. The depression in the noon-time values of V is maximum during equinoxes and least during winter. The values of V range from 30 m/s to 100 m/s on the average.

The random drift speed 'Vc' which contributes in the same direction as 'V', also shows morning and evening peaks, which is most clear for winter and least for summer season. V_c values also range from nearly 30 m/s to 100 m/s on the average. Lastly the ratio of random to steady drift speed (V_c/V) exhibits a very clearly noon time peak during equinoxes and summer also but not in winter. The contribution of V_c is therefore maximum during noon (around 1200 hr IST) during equinoxes and summer due to rather turbulent conditions of the ionosphere at E-region level. The

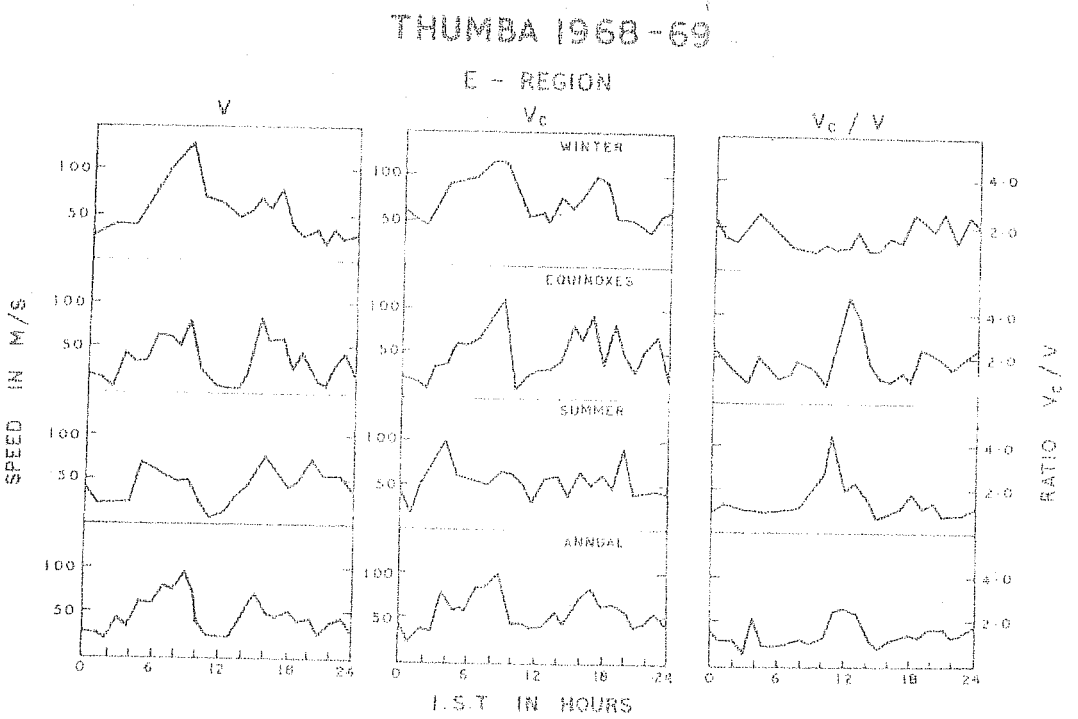

FIGURE 3.12

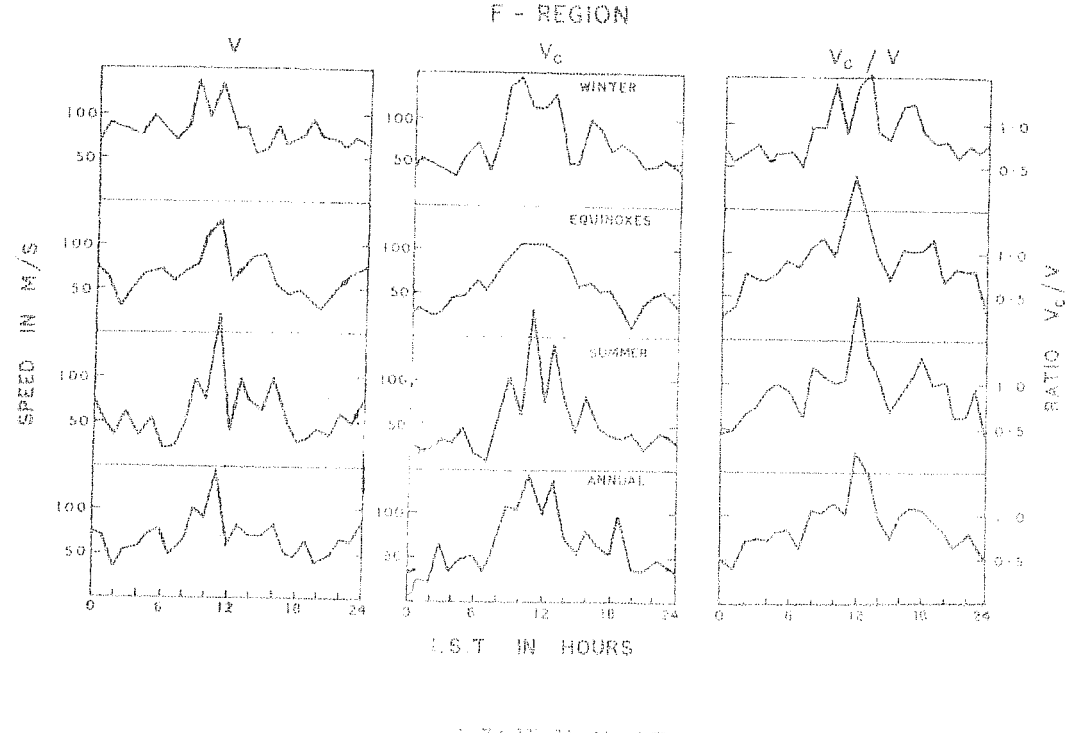

FIGURE 3.13

average range of V_c/V is from 1.0 to 3.0 for E-region. A small peak in the early morning hours is significant.

Referring to the F-region values of V, V_c and V_c/V, Fig.3.13 shows a significant rise in the steady drift around 1100 hr, in similarity to apparent drift speed V', described in Chapter II. The seasonal characteristic is also similar to that for the apparent drift, namely a least during summer season. Random drift contribution is maximum around noon and also in the summer season. The values of V_c range from 40 m/s to 150 m/s on the average. The ratio of random to steady drift speed(V_c/V) also shows a peak centred at 1200 hr IST. The maximum value of V_c/V is least during winter and the average value ranges from 0.5 to 1.7.

Fig.3.14 gives diurnal variations of the east-west component of steady drift speed at Thumba during 1968-69 for E and F regions. Table.III also gives four harmonic coefficients of the daily variation of F-region V, for 1968-69, alongwith that for 1967. The E-region values could not be subjected to harmonic analysis due to a few missing points on the diurnal curve.

E-region steady drift is predominantly westward during day and eastward during night hours. The times of reversal are 0500 hr, 0530 hr and 0415 hr IST during

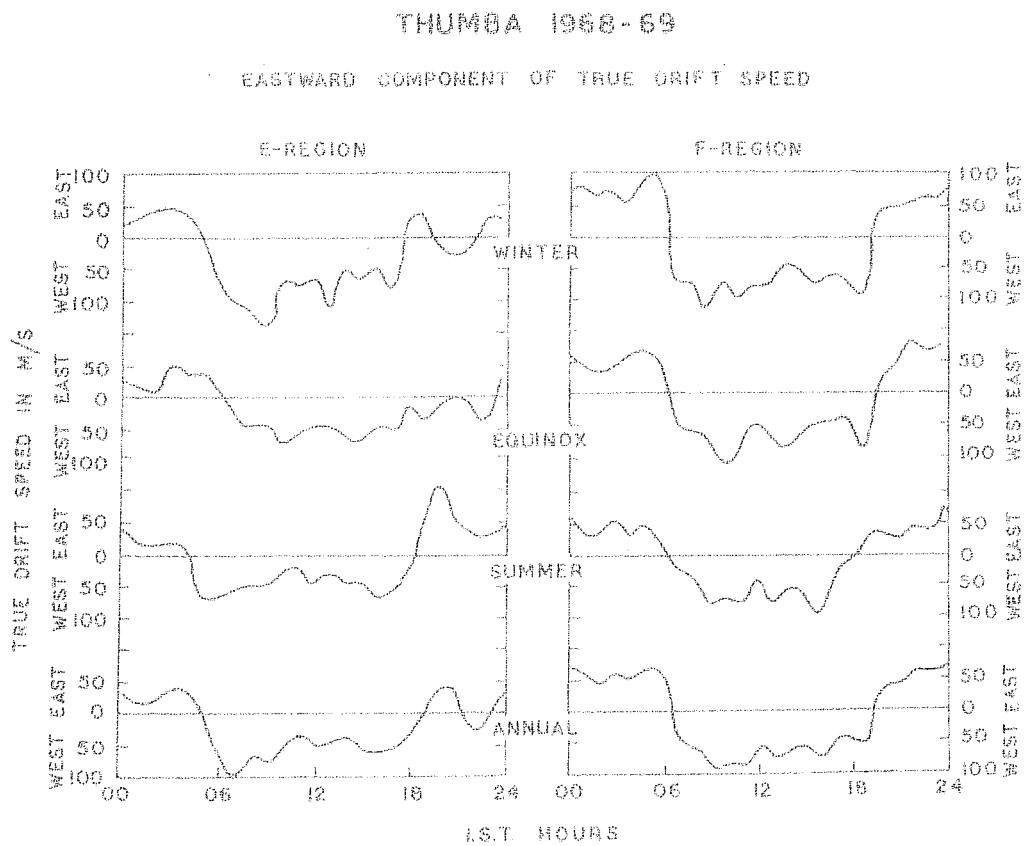
THUMBA 1968-69
EASTWARD COMPONENT OF TRUE DRIFT SPEED
E-REGION
F-REGION
TRUE DRIFT SPEED IN M/S
WEST EAST
WINTER
EQUINOX
SUMMER
ANNUAL
00
06
12
18
24
I.S.T HOURS

FIGURE 3.14

winter, equinox and summer seasons respectively in the morning and 1745 hr, 2330 hr and 1830 hr IST respectively, in the evening. The annual curve shows the reversal timings to be 0445 hr and 1900 hr IST respectively. Thus the morning as well as evening reversals are latest during equinoxes. Unlike F-region, reversal timings are quite uncertain in E-region.

The F-region eastwest component of steady drift speed as shown in the second part of the Fig.3.14, shows the reversal timings to be 0645 hr, 0640 hr and 0700 hr IST during winter, equinoxes and summer seasons in the morning and 2000 hr, 2015 hr and 1845 hr IST respectively in evening. The annual curve shows the reversal to occur at 0645 hr and 1950 hr IST respectively.

3.4 Results of Anisotropy Parameters of Ionospheric Irregularities over Thumba

A study of the anisotropy parameters and b was made for daytime E- and F-regions for the year 1964, using Fook's modification of PHILLIPS - SPENCER's method by DESHPANDE and RASTOGI (1966). The patterns were found to be aligned along the magnetic north south; on about 60% of occasions, the major axis was found to be within 10° from the magnetic north-south for either of the two regions. The mean axial ratio was 3.16 and 3.24 for E- and F-regions respectively, the semi-minor axis 'b' having

a mean value of 105 meters for E-regions and 99 meters for F-region. Seasonal study of the anisotropy parameters for the daytime E and F region reflections in the year 1964 has been described by DESHPANDE (1966). The mean axial ratio was found to be maximum in summer for both E- and F-regions. No significant difference was observed in the mean value of b in different seasons except that the mean value of b for the F-region during winter season was smaller than those of other seasons. Table IV summarizes the results for 1964 for E- and F-regions. The values of b and for E and F-regions both, are higher during summer season. There is no significant seasonal effect on the values of tilt angle . All the results during 1964 were confined to day-time.

The results of anisotropy parameters for the year 1967 were presented by H.CHANDRA (1969) and they are summarized in Table Va and Vb. Here again for E-region, the semi-minor axis was maximum during summer and least during winter whereas the axial ratio showed an opposite trend, i.e. a maximum during winter and a minimum during summer. The tilt angle however showed no seasonal dependence, being within $\pm$ 2° of north.

The F-region shows a maximum of during equinoxes and a minimum during summer while the semi-minor

axis 'b' shows a minimum during equinoxes and nearly equal values for winter and summer. This is in consistency with the fact that the stretching of ellipse along N-S direction causes the reduction in its minor axis. The characteristic ellipse is aligned in the magnetic north-south line within one degree for all the three seasons.

Referring to the nighttime F-region parameters for 1967, it is seen (see table V) that b as well as γ' is minimum in summer and maximum in equinox. Tilt angle ψ is always to the west of north by four to seven degrees. The overall values of 'b' are higher and those of γ' are lower compared to the daytime F-region values.

Daily variations of γ' and b for E-and F-regions for 1964 (for day hours only) shows an increase in γ' around noon and a corresponding decrease in b. The effect is more clear for F region than the E-region. Tilt angle shows very little hour to hour variation for E-region being centred around 5° west of north at all hours. The F-region tilt angle shows a more westward tendency for early morning and evening hours and near north orientation around noon.

For E-regions during 1967, b lies in the range 40-140 m with an annual median of 70 meters, which are considerably smaller than the value 98 m obtained for the

year 1964. The axial ratio γ lines in the range 1-14 with an annual median of 5.3, and the orientation is found to be within $\pm$ 25° of north, with a median orientation along magnetic north south. For the F-region, b ranges upto 300 m with an annual median of 67 m for day and 87 m for night hours. The axial ratio γ, varies from 1 to 30 with an annual median value of 6.7 for day time and 5.6 for night time. The orientation ψ has the range of $\pm$ 20° of north during day and in the range of -25° to + 10° of north in the night. Annual median was 0° for day and -5° for night hours.

Daily variation of b shows morning and evening maxima as in 1964. Evening maximum (around 1800 hr IST) was more pronounced for E-region and morning maximum (around 0600 hr IST) was more pronounced for F-region. Axial ratio showed a clear midday peak for E-region but not for F-region. Orientation angle ψ for E-region showed no clear diurnal variation. It was slightly eastward by day and westward by night.

A new receiving antenna system was installed at Thumba in January 1968 in order to get a better estimate of the north-south elongation of the irregularities in the E-and F-regions over Thumba. The antenna system is shown in the Fig.1.14. A total separation of nearly

one kilometer was then available in the north-south direction and the regular drift-records were taken using the highly elongated triangle E-S4C of aerials in order to get a significant time lag in the north-south direction. This modification was felt necessary in order to avoid the dependence of γ, b and ψ on the dimensions of the smaller receiving antenna triangle, which was in use so far (i.e. γ_1 $W_1 cs_1$). This effect is discussed separately in detail in Chapter VI.

Seasonal Study of the Percentage Occurrence of b, γ and ψ for 1968-69

Referring to Fig.3.16 it is seen that for E-region the annual median values of b, γ and ψ for day hours are 88 m 11.0 and 350° east of north respectively and for the night hours they are 55m 11.0 and 356° respectively. The night time E-region results are presented for the first time for Thumba. Looking at the seasonal effects, one finds lowest value of b during summer for daytime and during equinox for night-time. The axial ratio is not effected significantly with season for day-time. In the night hours, however γ is least in summer and maximum in the winter. There is no significant seasonal effect on b for E-region. The median values for 'b' during winter, equinox and summer are 91, 90 and 83 m

THUMBA 1968-69

ANISOTROPY PARAMETERS FOR E-REGION

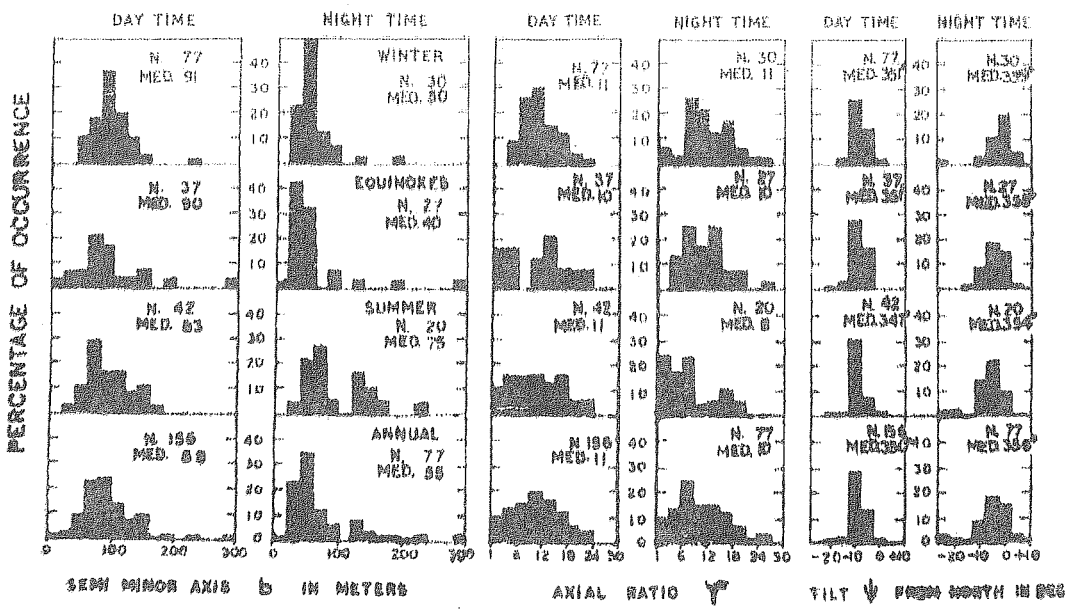

FIGURE 3.16

THUMBA 1968-69

ANISOTROPY PARAMETERS FOR F - REGION

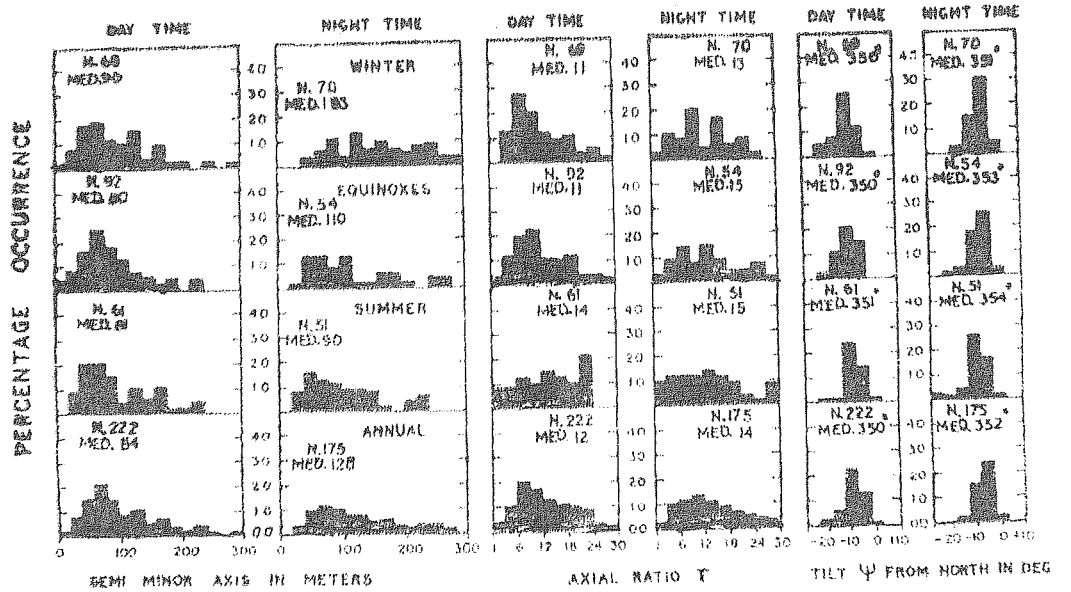

FIGURE 3.17

during day and 50, 40 and 75 m during night time. The median value of γ for three seasons are 11.0, 10.0 and 11.0 during day and 11.0, 10.0 and 8.0 during night. The tilt angle ψ has the median values equal to 351°, 351° and 349° east of north during day and 359°, 355° and 359° during night-time.

Fig.3.17 gives the anisotropy parameters for F-region during 1968-69 and one finds the annual median values of b , γ and ψ to be 84 m 12.0 and 350° east of north during day hours and 128 m 14.0 and 352° east of north during night hours. The value of b is highest in winter and that of γ in summer for day time as well as night-time. The orientation ψ is virtually unaffected by season. The median values for winter, equinox and summer for semi-minor axis are 90, 80 and 81 m during day and 183, 110 and 90 m during night. For axial ratio, the median values during three seasons are 11.0, 11.0 and 14.0 during day and 13.0, 15.0 and 15.0 during night. The median values for ψ during three seasons are 350°, 350° and 351° east of north during day and 351°, 353° and 354° east of north during night hours.

Daily variation of b, γ and ψ for 1968-69

Fig.3.18 gives the complete hour to hour plot of anisotropy parameters for E-region over the period 1968-69.

THUMBA 1968-69

ANISOTROPY PARAMETERS IN E - REGION

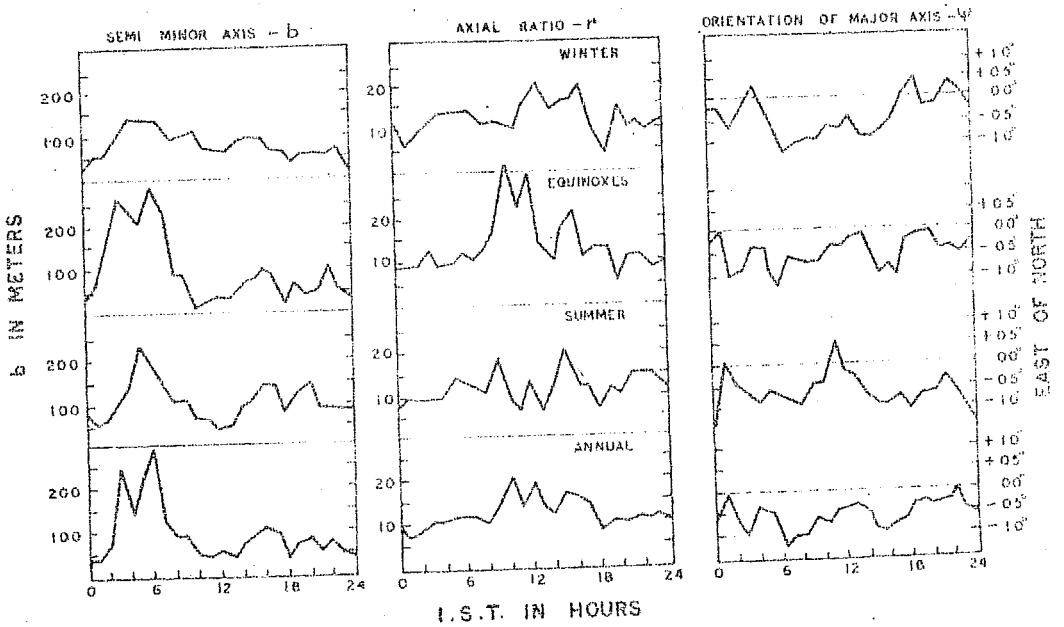

FIGURE 3.18

THUMBA 1968-69

ANISOTROPY PARAMETERS IN F - REGION

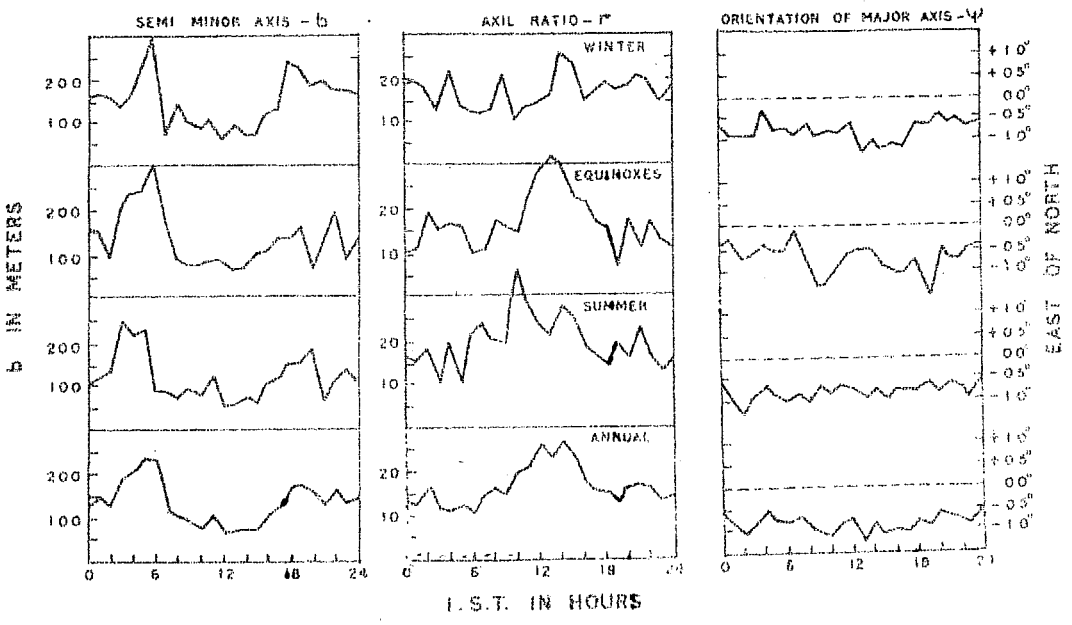

FIGURE 3.19

It is found that 'b' has a prominent rise in the early morning between 0400 and 0600 hr IST. This effect is least in the summer and maximum in equinoxes. There is an indication of slight increase in 'b' around 1800 hr IST also. The value of b ranges from 50 meters to 300 meters. The axial ratio γ is found to rise in the noon around 1200 IST. This tendency is most clear during equinoxes. The increase in is slightly late during the winter. The value of ranges from 5 to 30. The orientation angle ψ is mostly towards the west of north by 5 to 10 degrees and there is no definite seasonal change.

The F-region daily variations of b, r and ψ are shown in Fig.3.19. The semi-minor axis shows two clear maxima, one in the early morning around 05-06 hr and another in the evening between 19-20 hr. These coincide significantly with the times of reversals of the drift in F region in the morning and evening. The morning peak of b is fairly fixed in time while the evening peak is latest, in the equinoxes and earliest in the summer which is in accordance with the drift reversal timings (see table III). This point is taken up in detail in Chapter VI. The morning maximum of b is as high as 250 m. The smallest 'b' occurs during noon and is about 50 m. The axial ratio of characteristic ellipse in F-region

shows a broad peak around 12 hr, which is not very clear in winter, like the E-region. Small secondary peaks early in the morning and late in the evening are similar to those in the diurnal curves for V' and the fading rate N (see Chapter II). The rate of fading and the apparent drift speeds therefore seem to be related to the size of the irregularities in the ionosphere.

The orientation ψ does not show much variation and is all the time to the west of north within 10°.

3.5 Solar Cycle Effect on Drift and Anisotropy Parameters

(a) Steady and Random drift speeds

Day-time results for Thumba during 1964 and E and F-regions were subjected to full correlation analysis and steady and random drift speeds as well as the anisotropy parameters for the ground diffraction pattern were estimated using correlation technique by DESHPANDE (Ph.D thesis 1966) and later by H.CHANDRA (Ph.D thesis 1969). These have been described in section 3.3. of this chapter. Fig.3.20 here gives the comparative idea of V and Vc/V over the three periods of solar activity namely 1964, 1967 and 1968. As is seen, the true drift speed has reduced significantly for both E and F-regions from low to high sunspot years. This fall in V is more pronounced for F-regions. The

THUMBA

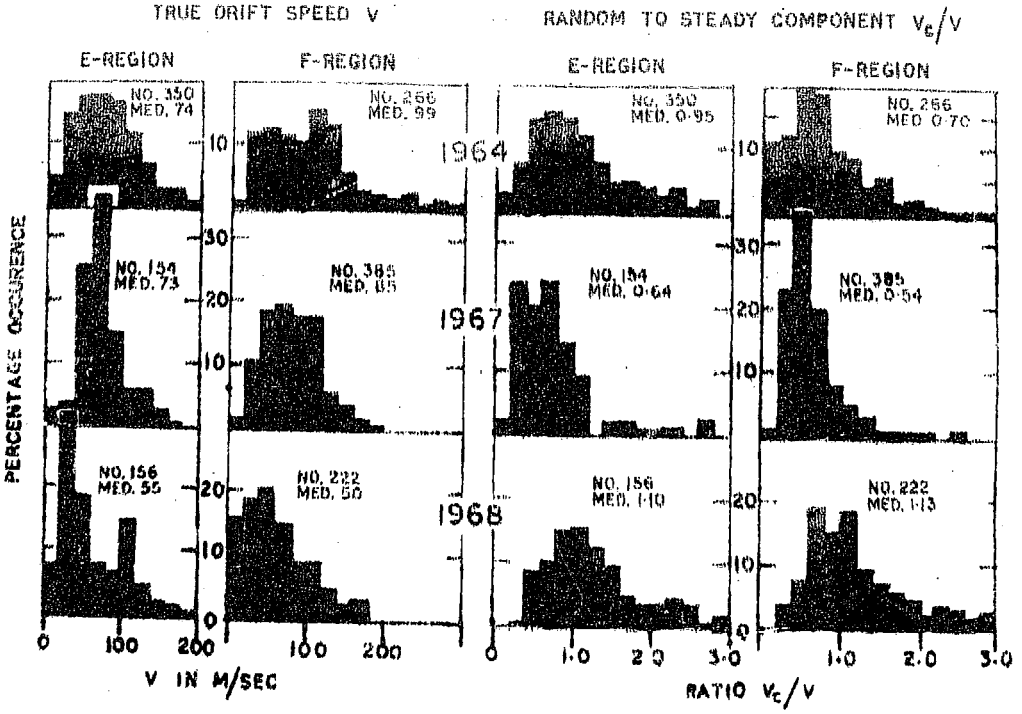

FIGURE 3.20

THUMBA

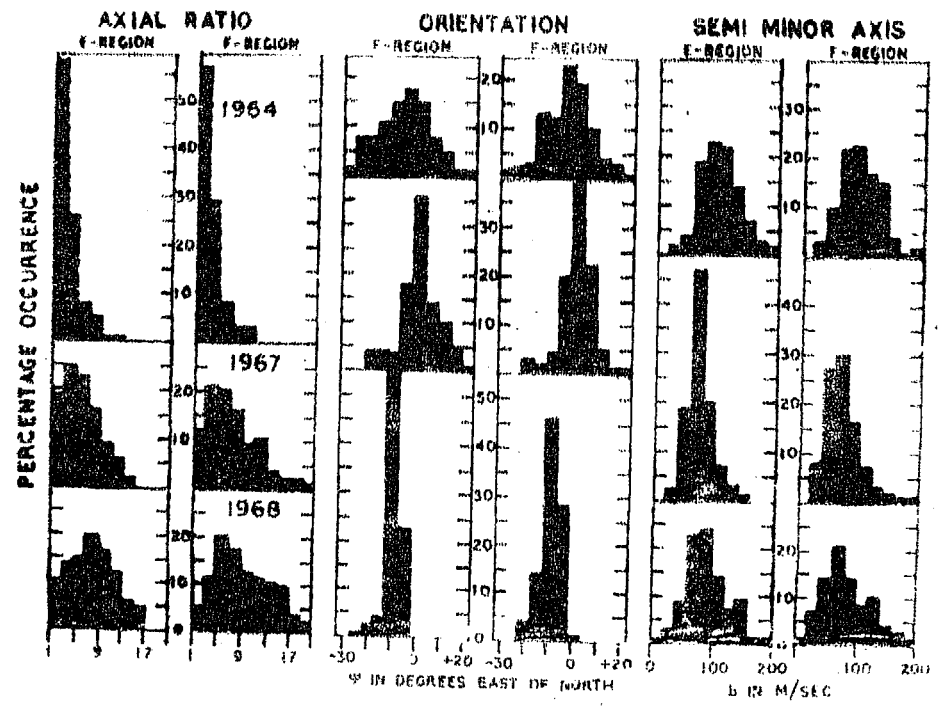

FIGURE 3.21

contribution of random drift, as given by the ratio Vc/V is found to have increased during 1968 compared to the previous year. This suggests a more turbulent ionosphere during the high sunspot activity (1968-69) and hence a lesser value for steady drift speed. The effect of solar cycle on V', V and Vc is discussed by the author in detail (MISRA et al. 1971).

(c) Anisotropy parameters:

Referring to Fig.3.21 which gives the anisotropy parameters over the three different periods of observation at Thumba, namely 1964, 1967 and 1968, one finds a clear cut increase in the axial ratio ' γ ' from low to high sunspot years for both E-and F-regions. This increase is more for E-region as expected due to stronger electrojet effects at that height. The orientation of the characteristic ellipse is more and more close to magnetic north-south with increasing sunspot activity. Nearly 60% times in E-region and 40% times in F-region, the ellipse is aligned within ten degress west of north during 1968, compared to 20% such cases during 1964. The semi-minor axis 'b' does not show a very clear dependence on solar cycle but there is a noticeable reduction in its value with the rising solar cycle.

3.6 Occurrence of negative Vc^2 and r^2 at Thumba

About five hundred drift records analysed by full-correlation method were subjected to both, the Phillips Spencer's method (1955) as well as the modified Fook's method (1965). The results of the later are discussed in detail in sections 3.3 and 3.4. It was noted from the results obtained by using the time-lags, τ_1, τ_2, τ_3 (PHILLIPS and SPENCER, 1955) that for a certain type of drift records r^2 worked out to be negative and other drift parameters could not be calculated (see equations, 14). Occurrence of negative r^2 indicates that the characteristic ellipse degenerates into a hyperbola (see Fig.3.23). There were a larger number of records for which V_c^2 came out negative. The percentage occurrence at each hour of negative r^2 and negative Vc^2 for Thumba during the period 1968-69 are shown in Fig.3.22. It is seen that the negative r^2 as well as Vc^2 occurs more frequently during the day than during the night. The maximum occurrence is somewhere between 1100 hr to 1600 hr. There is also a secondary peak in r^2 curve in the early part of the night and coincides with the maxima of spread-F occurrence at Thumba. Comparing these curves to the diurnal variation of the size 'b' of the irregularities (see Fig.3.18 and 3.19), it is clearly seen that smaller the size of the

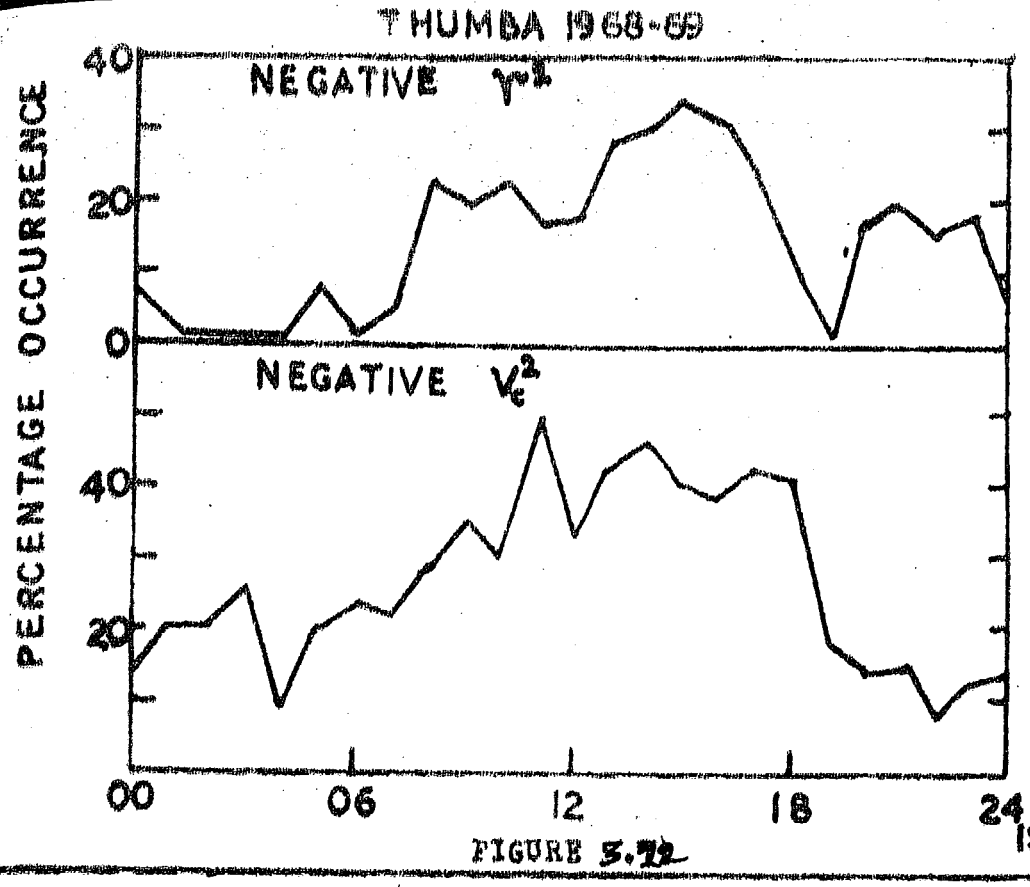

FIGURE 3.22

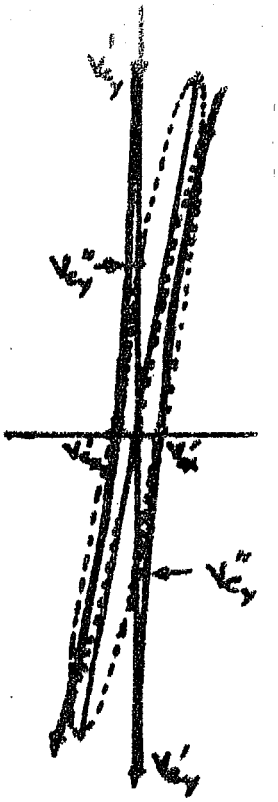

FIGURE 3.23

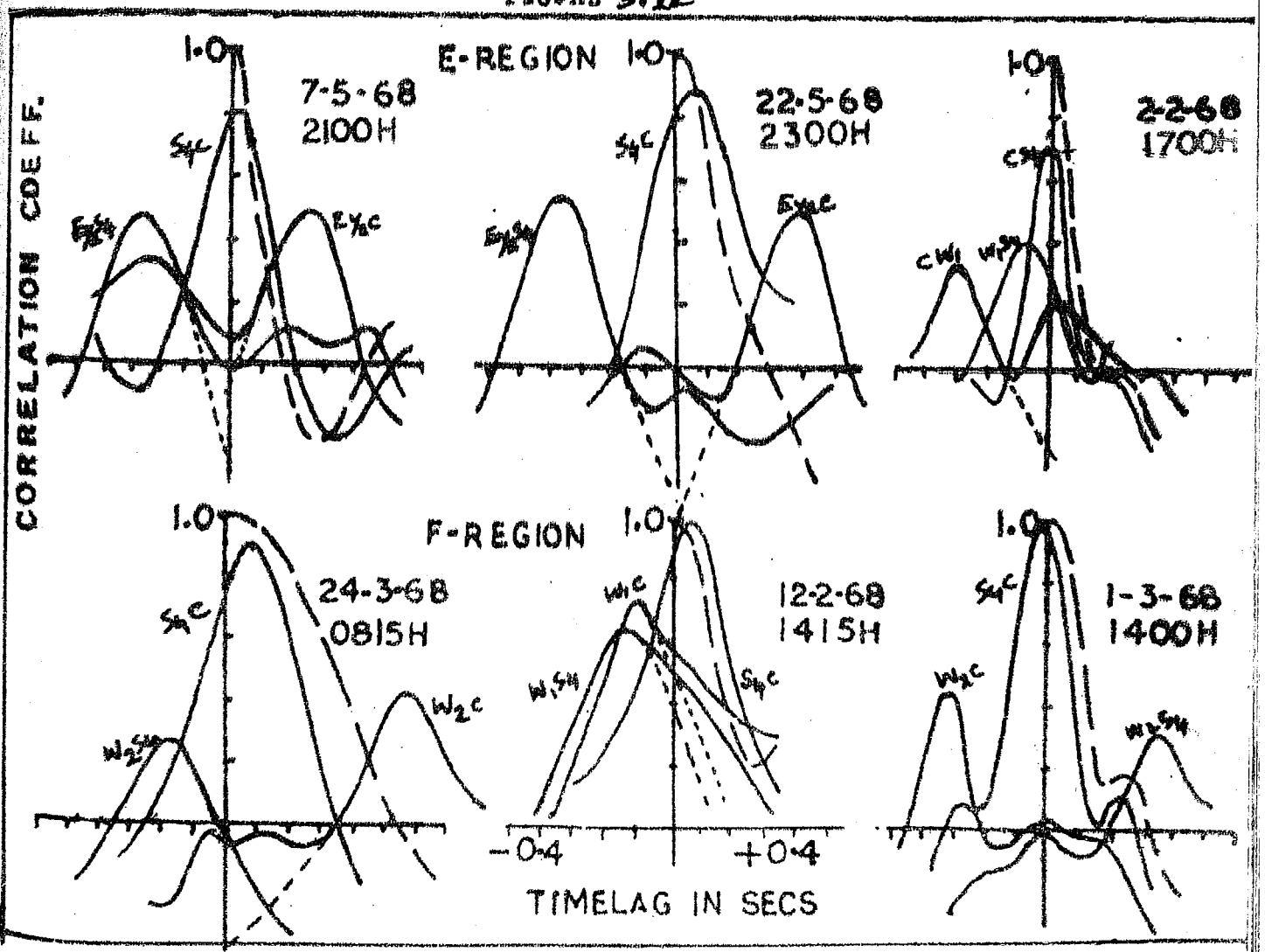

FIGURE 3.24

irregularity, more is the probability of getting negative r^2 and Vc^2. It is least probable both around the morning and evening maximum of b.

Thus when the aerial separation is much larger than the actual size of the irregularities, the possibility of getting negative Vc^2 is more. The presence of smaller scale irregularities in the E and F-regions in the daytime and particularly at those times when negative r^2 and Vc^2 occur, has been confirmed from the increased reflectivity of the layer (i.e. increase of $f_o E_s$ and $f_o F_2$).

As regards the individual cases, it is found that mostly certain symmetric type of cross-correlograms give rise to negative r^2 and Vc^2. Few such examples are given in Fig.3.24. There are two distinct type of correlograms, namely (i) the folded type (ii) skewed type. First one seems to arise due to larger aerial separation than required and the second due to waves in the ionosphere. It is also found that if the correlograms are summetrically extrapolated along the dotted lines, and r^2 and Vc^2 are recalculated from the modified time lags τ_1', τ_2' and τ_3', both r^2 and Vc^2 become positive. The characteristic ellipse corresponding to these valves gives a real value for r (shown dotted in Fig.3.23).

It is thus concluded that the negative r^2 and Vc^2 arise from the asymmetric variations of the lower portions of the correlation curves. Such variations can be caused by:

(1) the use of improper sampling length and sampling interval (see Sec.3.2 (b)).

(2) the use of larger aerial separation than optimum in that particular direction giving rise to folded type of correlograms. This optimum separation seems to be related to the size of the irregularities.

(3) the skewness of the correlograms due to wave-motion (Mc-Gee, 1966)

(4) the shape of the cross-correlograms also goes on varying with the aerial separation in the presence of wave motion in the ionosphere (DOWN and MAUDE, 1968). Thus the folded type of cross-correlograms can also be an indication of dispersion in the ionosphere besides the smaller size of irregularities.

As discussed earlier, FOOKS (1965) suggested the modification of Phillips Spencer's method (1955) in which only the upper portion of the correlograms is used, thereby

eliminating in effect of statistical variations. Use of only the top portion of the correlation curves, however, tends to neglect even the genuine effect of Vc on the lower part of the correlograms, when they are not sun-symmetric or skewed. The extrapolation technique of the correlograms, as suggested here, gets rid of the effect of wave-motions if present in the ionosphere and only the mass-motion would be determined.

It is therefore suggested that the one of the three methods, namely the (i) Phillips-Spencer's methods (ii) the Fook's method and (iii) the method of symmetric extrapolation, should be applied to a particular case after studying the detailed features of the cross-correlograms. Application of Phillips-Spencer or Fook's method to all the recrods may lead to wrong value of V,$\emptyset$, Vc r, b and ψ. Extrapolation method offers a new technique to remove the effect of waves in the ionosphere.

3.7 Latitudinal Dependence of drift and anisotropy Parameters:

Table VI gives, for a number of stations over the world, the results of Va, V and Vc/V alongwith the period of measurements. The plot of these parameters against the magnetic latitude is shown in Fig. 3.25. A decrease in the values of Va and V and also a slow increase

in the value of Vc/V is noticed with the increasing magnetic latitude, both for E and F regions. This picture is consistent with the prediction of Martyn's theory(Chapter I).

Table VII gives the values of γ, b and ψ for many stations over the world along with their periods of observations. A sharp decrease in axial ratio and an increase of the semi-minor axis, with the increasing magnetic latitude are clearly seen from the Fig.2.25. HIBBERD (1971) has shown that the axial ratio of the correlation ellipse on the ground is a function of the magnetic dip according to the relation γ = COSEC I. This equation more or less fits with the observed variation of as given in the figure. The field alignment of the irregularities results in a restriction of the angular spectrum of the reflected wave in the north-south meridian plane and hence produces a ground pattern that is elongated in the north-south direction. However this effect is appreciable only in low latitudes and increases rapidly as the magnetic dip angle aproaches zero, so that highly elongated ground patterns occur only near the magnetic equator. This is in contrast to the highly elongated patterns in all latitudes for waves that have been transmitted through the ionosphere, where the ground pattern is found in a straight forward way by Fresnel diffraction.

LATITUDINAL VARIATION OF DAYTIME DRIFT PARAMETERS

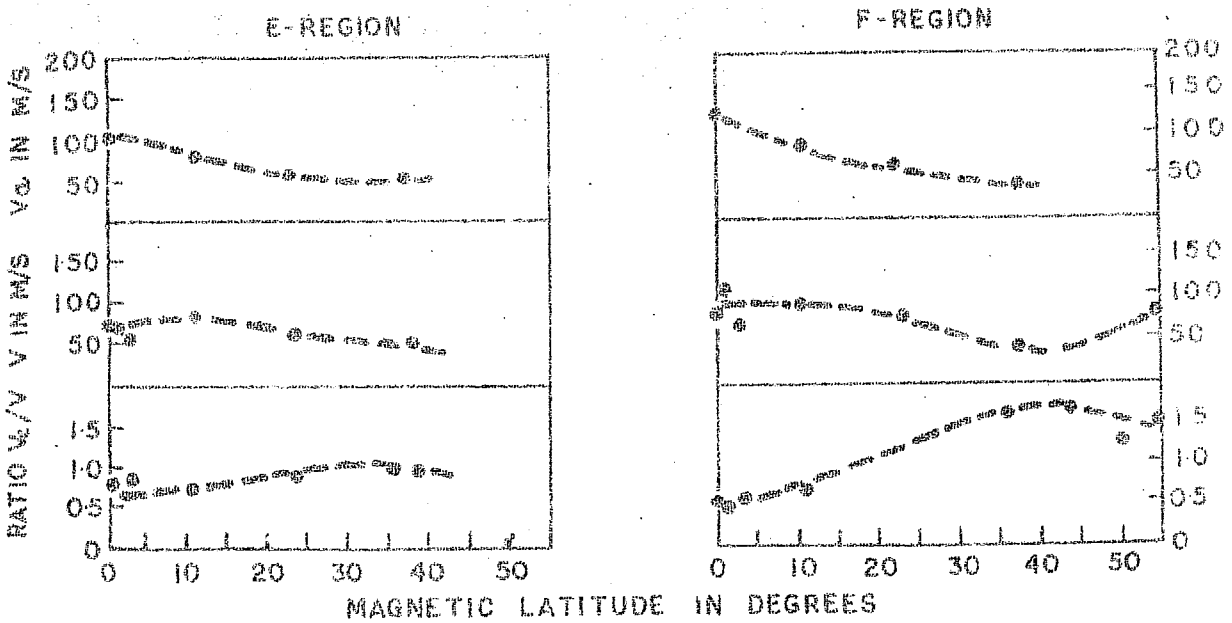

FIGURE 3.25

LATITUDINAL VARIATION OF DAYTIME ANISOTROPY PARAMETERS

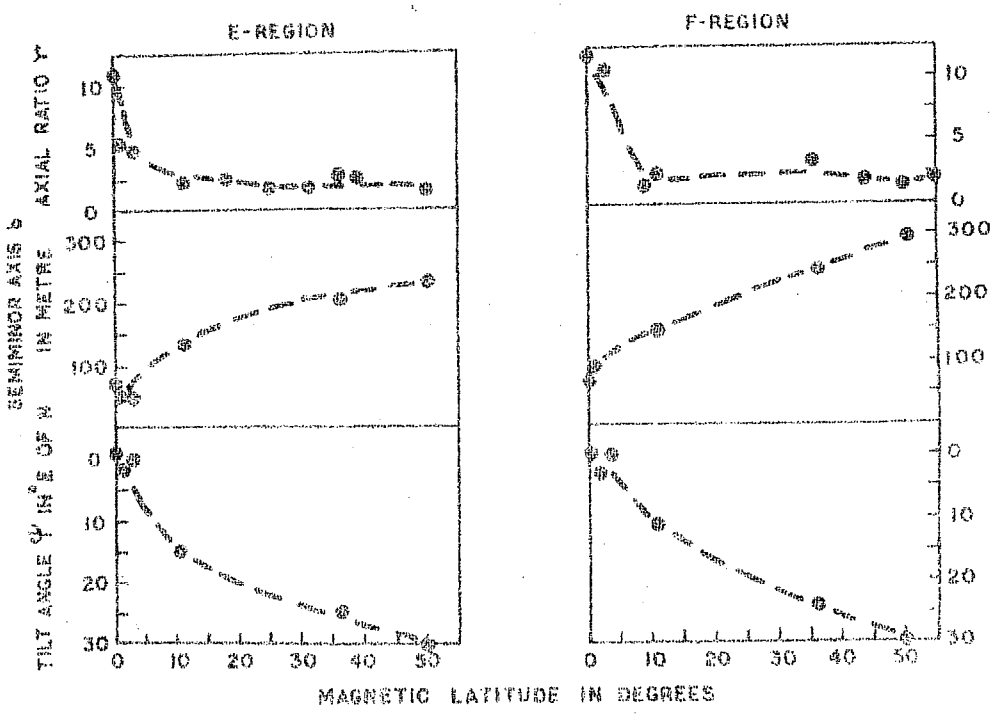

FIGURE 3.26

3.8 Conclusions:

From these results it can be concluded in short that the steady drift speed at Thumba is westward during the day and eastward during night. It is maximum during the equinoxes. The magnitude of the steady drift falls with the increasing solar activity. The random drift speed shows a slight increase with the solar activity. The steady as well as random drift speeds are largest around the equator.

The axial ratio of the characteristic ellipse of the ground diffraction pattern is maximum around noon for both E and F-regions while the transverse size 'b' of the ellipse is least during the noon time. Also during equinoxes, r is large and 'b' is least, for a particular year. The axial ratio increases while the size of the irregularities decreases with the increasing solar activity. The orientation of the characteristic ellipse is nearly magnetic north south and shows very little diurnal, seasonal or solar cycle effect. Axial ratio 'r' is maximum and the size 'b' is minimum at the magnetic equator. The orientation of the irregularities is very nearly magnetic north-south at the equator and departs more and more towards west of north with increasing magnetic latitude.

Daytime drift parameters during 1964

Period	Counts	Apparent drift speed V_a (in m/sec) Mean	Med.	True drift speed V (in m/sec) Mean.	Med.	Ratio random to steady drift V_c/V Mean	Med.
			E-REGION - 2.2 Mc/s				
Winter	144	163 ± 8	149	92 ± 5	83	1.04 ± .04	.81
Equinoxes	86	177 ± 10	149	78 ± 5	75	1.17 ± .07	.97
Summer	120	166 ± 5	120	71 ± 4	63	1.33 ± .09	1.06
Annual	350	169 ± 8	139	80 ± 5	74	1.18 ± .07	.95
			F-REGION - 4.7 Mc/s				
Winter	70	165 ± 8	161	110 ± 5	107	0.59 ± .05	.52
Equinoxes	91	188 ± 11	160	115 ± 9	101	1.08 ± .13	.76
Summer	105	177 ± 10	142	96 ± 6	88	1.10 ± .09	.82
Annual	266	177 ± 10	154	107 ± 7	99	0.92 ± .10	.70

Table - I.

Daytime drift parameters at Thumba during 1967

E - REGION 2.2 Mc/s

Period	Counts	Apparent drift speed V_a (in m/sec)		True drift speed V (in m/sec)		Ratio random to steady drift V_c/V	
		Mean	Med.	Mean	Med	Mean	Med
Winter	36	112 ± 8	100	80 ± 5	78	.58 ± .05	.56
Equinoxes	51	125 ±10	115	77 ± 5	75	.78 ± .08	.70
Summer	67	93 ± 6	83	65 ± 4	65	.76 ± .08	.65
Annual	154	105 ± 8	93	74 ± 5	73	.69 ± .07	.63

Table - II.a

Drift parameters at Thumba during 1967

F - REGION - 4.7 Mc/s

Period	Counts	Apparent drift speed V_a (in m/sec)		The drift speed V (in m/sec)		Ratio random to steady drift V_c/V	
		Mean	Med	Mean	Med	Mean	Med
				DAYTIME			
Winter	121	130 ± 4	119	89 ± 4	85	.63 ± .03	.56
Equinoxes	159	125 ± 5	119	90 ± 3	90	.58 ± .04	.46
Summer	105	126 ± 5	120	82 ± 3	81	.70 ± .05	.59
Annual	385	127 ± 5	120	87 ± 3	85	.60 ± .04	.52
				NIGHTTIME			
Winter	59	130 ± 7	119	103 ± 6	98	.47 ± .05	.38
Equinoxes	119	155 ± 7	130	107 ± 4	102	.55 ± .06	.38
Summer	73	134 ± 9	100	75 ± 5	67	.63 ± .09	.56
Annual	251	140 ± 8	116	95 ± 5	89	.55 ± .07	.44

Table - II.b

Harmonic coefficients of the daily variation of the E-W component of True Drift velocities in F-region at Thumba

Period	Amplitude in M/sec					Time of maxima in hour (I.T)					
	a_0 M/sec	r_1 M/sec	r_2 M/sec	r_3 M/sec	r_4 M/sec	ϕ_1 hour	ϕ_2 hour	ϕ_3 hour	ϕ_4 hour	Time of morning reversal	Time of evening reversal
Winter (1967)	-3	124	15	36	14	1.7	1.0	5.6	4.6		
Equinoxes(1967)	-9	122	27	28	20	1.2	2.4	5.9	5.1		
Summer (1967)	-3	96	24	21	28	1.4	6.0	5.6	3.6		
Annual (1967)	-5	114	11	28	18	1.1	3.2	5.7	5.3		
Winter (1968-69)	8	89	22	32	8	1.1	2.5	5.5	4.4	0645hr	2000hr.
Equinoxes(1968-69)	10	79	10	26	18	0.9	2.2	5.6	4.7	0640hr.	2015hr.
Summer(1968-69)	10	74	10	15	11	0.4	5.3	5.2	1.0	0655hr.	1845hr.
Annual (1968-69)	10	81	11	24	6	0.8	3.0	5.5	5.0	0645hr.	2000hr.

Table - III

Daytime anisotropic parameters at Thumba during 1964

Period	Counts	Semi-minor axis b (in meter)		Axial ratio		Orientation of characteristic ellipse in degrees each of North	
		Mean	Med	Mean	Med	Mean	Med
			E - REGION - 2.2 Mc/s				
Winter	144	99 ± 2	98	3.2 ± .2	2.4	356 ± 2	353
Equinoxes	86	102 ± 5	95	2.9 ± .2	2.4	356 ± 2	354
Summer	120	115 ± 5	102	4.0 ± .1	3.7	355 ± .5	355
Annual	350	105 ± 4	98	3.4 ± .2	2.7	356 ± 1.5	354
			F - REGION - 4.7 Mc/s				
Winter	70	90 ± 3	87	3.0 ± .3	2.9	357 ± 1	356
Equinoxes	91	105 ± 6	91	2.8 ± .2	2.5	358 ± 1	356
Summer	105	105 ± 7	94	3.9 ± .2	3.6	355 ± 1	355
Annual	266	100 ± 5	91	3.2 ± .2	2.8	357 ± 1	356

Table - IV

Daytime anisotropic parameters at Thumba - 1967

E-REGION - 2.2 Mc/s

Period	Counts	Semi-minor axis b (in meter)		Axial ratio		Orientation of characteristic ellipse in degrees East of North	
		Mean	Med.	Mean	Med.	Mean	Med.
Winter	36	70 ± 3	66	6.4 ± .5	5.6	0 ± 1.5	359
Equinoxes	51	71 ± 3	69	6.0 ± .5	5.2	5 ± 0.5	362
Summer	67	85 ± 4	74	5.4 ± .4	5.1	357 ± 1.5	358
Annual	154	75 ± 3	70	5.9 ± .5	5.3	1 ± 1.5	360

Table - V.a

Anisotropic parameters at Thumba during 1967

F-REGION - 4.7 Mc/s

Period	Counts	Semi-minor axis b (in meter)		Axial ratio		Orientation of characteristic ellipse in degrees East of North	
		Mean	Med	Mean	Med	Mean	Med
			DAYTIME				
Winter	121	82 ± 4	68	8.7 ± .6	6.5	1 ± 1	1
Equinoxes	159	71 ± 4	64	13.1 ± .8	8.1	2 ± 2	1
Summer	105	80 ± 6	69	7.0 ± .5	5.6	359 ± 1.5	358
Annual	385	78 ± 5	67	9.6 ± .7	6.7	1 ± 1.5	0
			NIGHTTIME				
Winter	59	135 ± 7	84	8.0 ± .7	6.2	355 ± 1	356
Equinoxes	119	140 ± 4	98	8.6 ± .4	5.9	354 ± 1.5	355
Summer	73	116 ± 8	80	7.0 ± .8	4.6	353 ± 3	353
Annual	251	130 ± 7	87	7.9 ± .7	5.6	354 ± 2	355

Table - V.b

Comparison of the true drift parameters at different stations

Station	Mag.Lat.	Period of study.	Region.	Counts.	V_a	V	V_c/V	Reference
Thumba	0.3°S	1964	E-day	350	169	80	1.18	
			F-day	266	177	107	0.92	
		1967	E-day	154	105	74	0.69	
			F-day	385	127	87	0.60	
		1968-69	F-night	251	140	95	0.55	
Tamale	0.6°S	Feb-Mar 1962	E-day	43		67	0.8	Koster and Katsriku (1966)
			F-day	83		115	0.5	
			F-night	38		70		
Ibadan	3.0°S	IGY	E-day	1000		55	0.8	Skinner et al. (1963)
			F-day			70	0.6	
			F-night					
		IGY	E-day	24				Skinner et al. (1958)
			F	25				
Waltair	11°N	Sum.60	E	75	80	79	0.71	Rao and Rao (1963)
		Win.61	F	95	87	93	0.67	
Cambridge	50°N	Mar-Apr 1955	E-day	39			0.08	Fooks and Jones (1961)
			F-day	37			1.2	
		Feb 1958	F-night	35			0.7	
Ashkhabad	36°N	1960	E_s			50	0.9	Mirkotan (1962)
Moscow	55°N	1959	F_2			40	1.6	Mirkotan (1962)
Murmansk		1958	F_2				0.6	Mirkotan (1962)
Yamagawa	20.3	1960-61	E-day			72	0.80	Rao and Rao
Debilt	58.8°N	1960-61	E-day			36	1.10	Rao and Rao.
Halley Bay	65.7°S	1960-61	E-day			97	1.40	Rao and Rao.
Rustov on the DON		1958					1.00	Mirkotan.

Table - VI

Comparison of the anisotropy parameters at different stations

Station	Mag.lat.	Period of study.	Region.	Counts.	r	ψ^0	b in M	Reference
Thumba	0.3°S	1964	E-day	350	3.4	-4	105	
			F-day	266	3.2	-3	100	
		1967	E-day	154	5.9	1	75	
			F-day	385	9.6	1	67	
		1968-69	F-night	251	7.9	-6	130	
Tamale	0.6°S	Feb-Mar 1962	E-day	43	5.5	-2.4	40-60	Koster and Katsriku (1966)
			F-day	83		-2.7	92	
			F-night	38				
Ibadan	3.0°S	IGY	E-day	100			50	Skinner et al. (1965)
			F-day					
			F-night					
		IGY	E-day	24	5	0.0		Skinner et al. (1958)
			F	25	11	0.0		
Waltair	11°N	Sum.'60	E	75	2.1	-16	135	Rao and Rao (1963)
			F	95	2.3	-11	147	
Singapore	9°S		F		1.7			Harriston (1965)
Cambridge	50°S	Mar-Apr. 1955	E-day	39	1.5	N-W	235	Med values Fooks and Jones (1961)
			F-day	37	1.6	N-W	296	
		Feb.'58	F-night	35	1.8	N-W	140	
Ashkhabad	36°N	1960	E_s		2.7	**		Mirkotan(1962).
Moscow	55°N	1959	F_2		3.3	50@		Mirkotan
Puerto Rico					1.8			Yerg (1956)
Murmansk		1958	F_2		1.9			Mirkotan(1962).
Rostov-on-the-Don		1958	F_2		1.5			
Simez	44°N	1958	F_2		1.7			Patel CM(61-62)
Ahmedabad					2.6E			Kaube(65-66)
Yamagawa					1.6E			

** along the meridian in daytime
@ large scatter

Table - VII

CHAPTER IV

IONOSPHERIC DRIFTS IN RELATION TO THE EQUATORIAL ELECTROJET DURING MAGNETICALLY QUIET AND DISTURBED CONDITIONS

4.1 Equatorial ionospheric drift and the electrojet

This is discussed in detail in the first paper at the end of this chapter. The extra Figs.4.5 and 4.6 show the electrojet control of the drift during low and high sunspot periods, for each of the three seasons and different hour groups.

4.2 Effect of magnetic activity on electron drifts in the equatorial electrojet

The variation of apparent drift speed with Kp index as well as its dependence on quiet and disturbed conditions is dealt in the second paper attached at the end of this chapter. Figs.4.7 and 4.8 show the diurnal variations of E and F-region apparent drift speeds during low and high sunspot years. No solar cycle control is seen.

4.3 Steady and random drift parameters during magnetically quiet and disturbed days

Various drift parameters, namely Va, V, Vc and Vc/V as derived from full-correlation analysis are

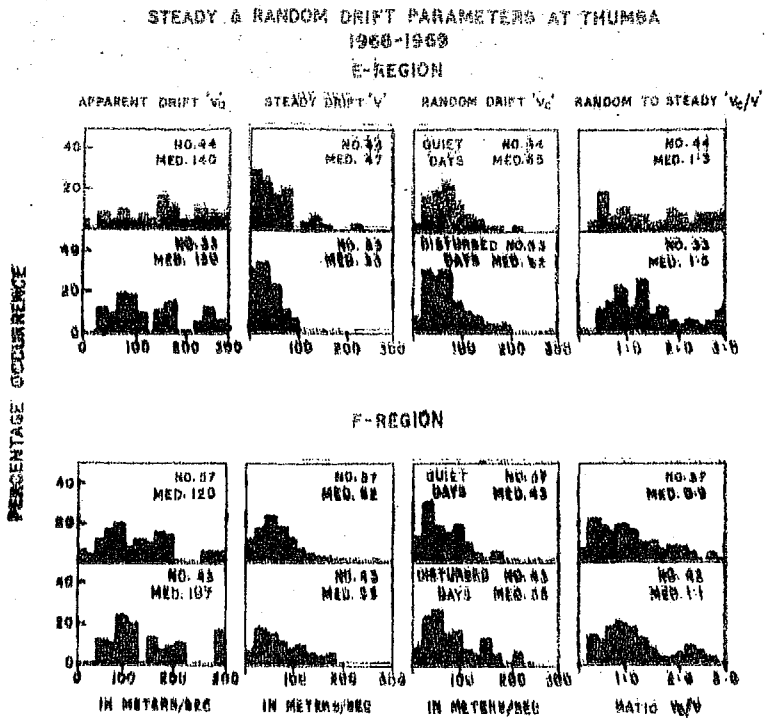

FIGURE 4.9

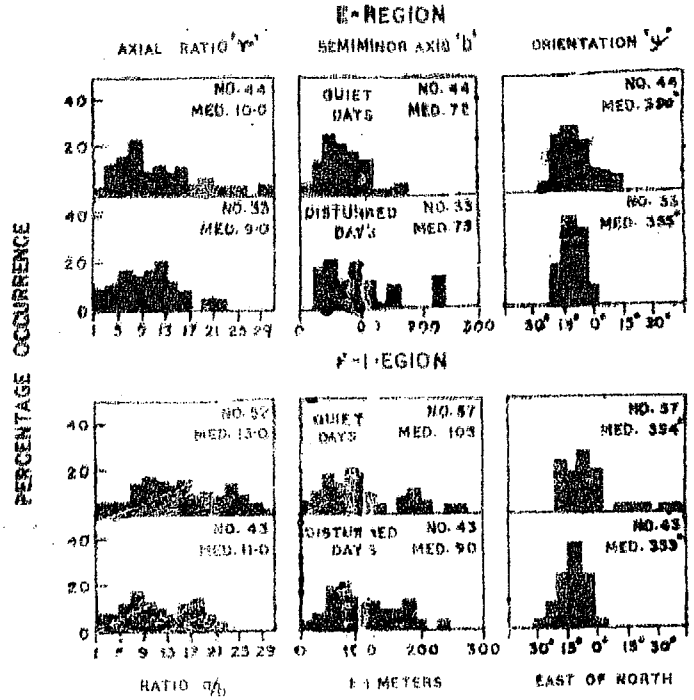

FIGURE 4.10

divided into five internationally quiet and disturbed days for both E and F regions for the period 1968-69. The percentage occurrence of these parameters for quiet and disturbed conditions are shown in Fig.4.9. The count and median values are also shown in respective blocks. It is seen that for both E and F regions Va and V are smaller on the disturbed days i.e. the days of weaker electrojet. This has been discussed in detail in Sec.4.2. The random drift Vc does not change much for E-region but for F region Vc increases on the disturbed days. The random to steady drift Vc/V increases for both E and F regions. The increase in Vc on magnetically disturbed days results from the higher collision rates, causing more turbulent movement of the ionization. The latitudinal variation of V, Vc and Vc/V (See Fig.3.25) provides an obvious explanation for reduced value of V and increased value of Vc on weak electrojet days.

4.4 Anisotropy parameters of the ground diffraction pattern during magnetically quiet and disturbed days

The axial ratio, semi-minor axis and the orientation of the characteristic ellipse of the ground diffraction pattern at Thumba for the echoes returning from E and F regions are also studied with respect to the

magnetic activity. The five internationally quiet and disturbed days are used and the percentage occurrences are shown in Fig.4.10. It is clearly seen from the median values mentioned in the figure that the axial ratio 'r' is slower while the semi-minor axis 'b' is higher on the magnetically disturbed days. The orientation angle shows almost no change. The latitudinal variation of r and b (see Fig.3.26) also shows a sharp fall in r and an increase in b with the increasing magnetic latitude. On the magnetically disturbed days when an electrojet is comparatively weak, the conditions at Thumba are similar to that of a slightly higher latitude station and hence the values of r and b change accordingly. The near north-south orientation of irregularities at Thumba results from the N-S direction of the magnetic lines of force of earth's magnetic field and hence does not change with disturbance.

4.5 Reversal of drift and disappearnce of sporadic-E during the short-term depressions in H

E and F region drift data for the period 1964-69 was studied in the light of the finer details of the magnetograms for each day. It was observed on certain occasions that the drift speed had reversed from west to east even in the day-time. This was found to coincide

very well with the depression in H for that period of the day, below a certain threshold level. Two such cases for E and F region respectively, are shown in Fig.4.11 and 4.12. The sporadic E ionization was also found to have disappeared for this period (RASTOGI et al. 1971) as is seen from the figures. The reversal of drift during the periods of very low H values are in verification of the fact that the currents in the ionosphere flow in the opposite direction during night-time. The disappearance of Es is associated with the reversal of drift through the cross-field instability mechanism (suggested by FARLEY 1962) according to which irregularities are produced only when the gradient of electron density $\Delta n/n$ and the electric field are in the same direction. As the $\Delta n/n$ is always positive at E-region height and the electric field is upwards during day and downward during night, the Es irregularities would appear only in the day at Thumba. However when the drift is reversed to eastward even during day, the electric field will be downward (see 6.2) and hence this mechanism will not work. The ionization would therefore disappear. On the other hand the appearance of Es on certain night at Thumba may be caused by a downward gradient of n, at certain heights, besides the ionization produced by the upward discharge of thunder cloud charge (MISRA and RASTOGI, 1971).

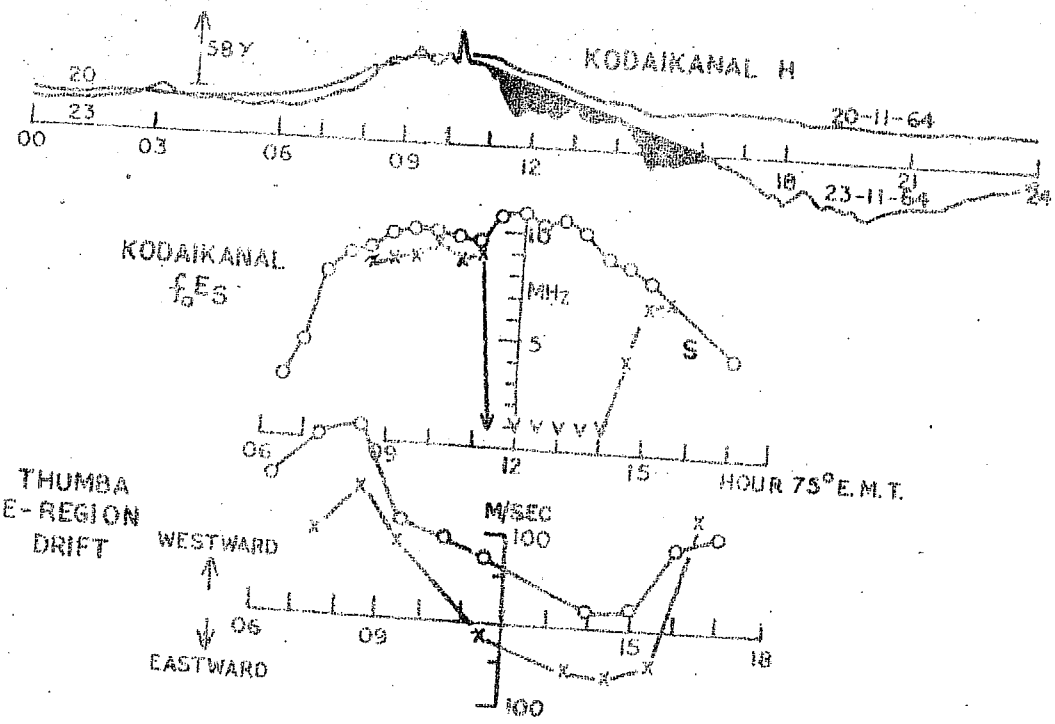

FIGURE 4.11

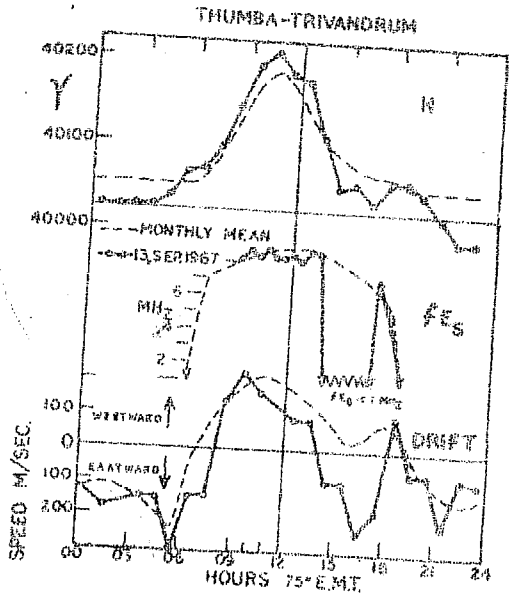

FIGURE 4.12

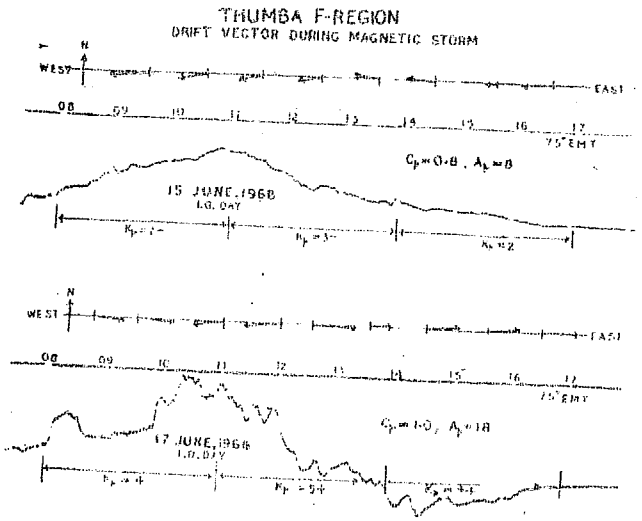

FIGURE 4.13

4.6 Drifts during magnetic storms

On reviewing the drift results at Thumba during individual magnetic storms, it was felt in general that the drift direction shows a slightly anomalous behaviour during these days. Figure 4.13 gives the orientation of drift vector at different hours of the day, on a magnetically quiet day (15 June, 1968) as well as a storm day (17 June, 1968). The Cp and Ap values on these two days were 0.8, 1.0 and 8, 18 respectively. The Kp values in the morning, noon and evening hrs are also indicated on the figure. There was a sudden commencement on 17th June at about 10 hr, 75° EMT and the H values were subsequently very high for 11 and 12 hr after which there was a sharp fall in the value of H. It had gone below the normal night level around 1230 hr and remained so far the rest of the day. Comparing the orientation of the drift vector in two days, it is seen that though the drift vector was throughout westward on 15th June, it was mostly eastward on 17th June, excepting at 1030 and 1130 hrs when H was very high.

The variation of drift vector in 15 June represents the typical result for Thumba whereas on 17th June,

the H values have remained below the night level and hence resulting from an opposite current system. The drift is therefore eastward even during the day time. WOOKS (1961) has also studied the changes in drift during magnetic storms and found a reduction in their values.

4.7 Conclusions:

These results show that the ionospheric drifts at Thumba are closely associated with the equatorial electrojet. The magnetically disturbed days result in the weakening of the electrojet thereby causing the reduction in the drift values, as well as the anisotropy of the irregularities.

(Accepted for publication in Planetary and Space Science)

EQUATORIAL IONOSPHERIC DRIFT AND THE ELECTROJET

by
H.Chandra, R.K.Misra, and R.G.Rastogi
Physical Research Laboratory,
Ahmedabad-9
India

ABSTRACT:- The results of the horizontal drift measurements at Thumba (0.6°S dip), a station situated at magnetic equator, are studied in relation to the equatorial electrojet currents estimated from the variations of H component of the geomagnetic field. The daily, seasonal, and latitudinal variations of drift show a close similarity between the drift and electrojet. Even the short-time variations like day to day differences or temporary changes lasting only a few hours in the magnetic field have corresponding effects on the drift parameters. It is concluded that the drift measurements near equator indicate the electron movements and are good index of the ionospheric currents.

INTRODUCTION

The variation of the geomagnetic field during the course of a day observed at ground has been attributed to the currents flowing in the conducting regions of the upper atmosphere. These currents are driven by the dynamo fields set up due to the tidal winds carrying the ionisation with its across the vertical component of the earth's magnetic field.

The height of the ionosphere most suitable for sustaining these currents were suggested to be in the E region of the ionosphere. Recent rocket measurements have indicated the height of the peak current intensity somewhere between 105 to 110 Km (Cahill 1959; Maynard and Cahill 1965; Sastry 1968). On the basis of the dynamo theory world-wide current systems as well as the wind systems at dynamo level have been mapped out from the observations of the magnetic field variations at ground stations (Chapman and Bartels 1940; Maeda 1955). The electrostatic field at the E-region heights are communicated to the F-region heights along the highly conducting magnetic field lines where they cause E x B drift. The world-wide pattern of drift in the F-region heights have been calculated by Maeda (1962). At the E-region heights the electrons are more mobile than the ions while the F-region heights the mobility of the ions as well as the electrons are the same and they move together. Thus the movements of electrons at F-region do not contribute to the magnetic field variations at the ground level.

The amplitude of the daily variation of the horizontal component of geomagnetic field (H) is enhanced abnormally within a narrow zone centred on the magnetic

equator (Egedal 1947; Pramanik and Narayanan 1952; Pramanik and Hariharan 1953; Chwuneehilli and Alexander 1959; Forbush and Casevardo 1961). Martyn (1949) has shown the enhanced daily range to be due to the enhanced east-west electric conductivity near the magnetic equator during the day-time hours, because of the inhibition of the vertical Hall currents due to the polarization of the medium. This narrow belt of currents was named by Chapman (1951) as equatorial electrojet.

Maeda (1955) has found that the E-region winds at equator are Eastward during night and Westward during day the change in direction occurring around 03 hr and 15 hr. The computations by Matsushita (1967) indicated that the currents in the dynamo region are eastward during the day and westward during the night. The reversal near the equatorial region occurs at 08 hr in the morning and around 16 hr in the evening. Balsley (1966) has shown evidence of currents flowing in the night-time hours from VHF radar scattering from the equatorial electrojet irregularities. These currents are too small in magnitude due to decreased conductivity hence are not conventional in the magnetograms.

DRIFT MEASUREMENTS AT THUMBA

Ionospheric drift measurements in E and F regions

over the magnetic equator at Thumba were started in January 1964 employing Mitra's technique (1949). The drift values at Thumba were found to be higher than the values reported earlier for any other station. Further it showed drift during day-time entirely westward for either of E or F region measurements (Rastogi et al. 1966). The night-time drift in F-region were found towards East (Deshpande and Rastogi 1968; Chandra and Rastogi 1970).

Another noteworthy feature at Thumba was that practically no time shift could be obtained between the fading of the radio waves at the north-south pair of aerials, indicating either the drift have no north-south component or the irregularities are elongated in north-south direction. It was found that the correlation along the north-south direction decreases very slightly with the increase of antenna separation while along East-west direction the correlation decrease very rapidly with the antenna separation suggesting that the irregularities are highly field aligned along the magnetic lines of forces (Rastogi et al. 1968). Observations were taken for the period 1968-69 with much larger antenna separation in north-south direction (480 metres) and it was found that the drifts are really along East-west direction. At the beginning of 1968 a new high-power transmitter was

installed at Thumba and night-time E-region drift observations were tried whenever possible.

DRIFT RESULTS AT THUMBA

The annual average histograms of the drift speed and the drift direction for the E and F regions separately for the day-time hours (8 - 16) and night-time hours (20-04) are shown in Fig.1. During the day-time hours both the E as well as F-region drifts are predominently westward; during the night-time F-region drifts are entirely Eastward while the E region drift is Eastward on about 65 percent of occasions and Westward around 35 percent occasions. It may be noted that night-time observations of E-region drift are comparatively few due to the absence of equatorial sporadic-E during the night-time. It is also to be noted that the histograms shown here do not have been minor side-lobs either in East or West direction indicating the absence of the Meridional drift. The drift speed in the E region is about 120 m/sec either during the day or during the night. The F-region drift is about 146 m/sec during the day-time and 90 m/sec during the night-time. The drift speed for the year 1964 were found to be 132 m/sec and 161 m/sec respectively for E and F region for day-time (Deshpande and Rastogi, 1966).

THE DAILY VARIATION OF DRIFT AND H

In order to study the relation in the drift and the equatorial electrojet the daily variations of the horizontal components of the magnetic field H are compared with East-west component of the F-region drift speed for each of the seasons for the year 1967-69 (Fig.2). The characteristics of daily variation of H at Trivandrum are the increase of H from sun-rise, peak around 1130 hr and comparatively slow decrease of H till late evening hours. The daily variation of the East-west drift in general have a good correspondence with that of H. The drift direction changes from West to East at around 20 hr and again from East to West around 0630 hr. Seasonally the time of morning reversal does not change with season while the evening reversal occurs about an hour earlier during the summer months. The east-ward drift speed reaches a maximum value about an hour before the morning reversal. Similarly before the evening reversal there are indications of a minor hump in the drift speed. These features are very similar to the drift speed obtained at Jicamarca using the VHF radar signal technique (Balsley 1969).

SEASONAL VARIATION

The mean drift speed averaged for each of the month of the year for the entire period of observation (1964-69)

are compared with the corresponding values of the solar daily range of H, the RS_q (Chapman and Rajarao, 1965). If it is assumed that the magnetic field at an equatorial station during the night-time hours is the base value of the magnetic field, then the value of RS_q would be proportional to the equatorial electrojet current. It is seen from the diagram that the seasonal variation of both the Drift and the RS_q are fairly similar indicating maximum during the equinoctial months. The drift speed during the summer months are significantly lower than in winter solstices.

LATITUDINAL VARIATION OF THE DRIFT PARAMETERS

The different parameters of the ionospheric irregularities collected from the published or otherwise available observations are grouped in Fig.4. The latitudinal variation in terms of magnetic latitude refers to the day-time hours only. The parameters used are the apparent speed (V') of the irregularities, the axial ratio (r) of the characteristic ellipse qualifying the shape of the irregularity, orientation (ψ) of the major axis of the ellipse and the semi-minor axis (b) of the ellipse. The results for the E and F-region have been plotted separately but the mean curves have been drawn from combined E and F region results. The salient features observed are:

(1) The apparent drift speed V' shows a sharp maximum close to the magnetic equator (within ± 5° magnetic latitude). Speeds averaged for day-time are about 150 m/sec at equator and about 80 m/sec at other latitudes.

(2) Similar sharp change is seen in the axial ratio indicating the irregularities are highly elongated near the equator where they attain axial ratio of the order of ten. Away from equator axial ratio is of the order of two.

(3) The irregularities are aligned along the magnetic lines of forces near the equator and they start departing from the magnetic meridian towards the west as they go away from the equator till at mid-latitudes the irregularities are roughly aligned in north-west and south-east direction.

(4) The semi-minor axis 'b' representing the transverse size of the irregularities is about 50 - 100 meter at equator and gradually increases to about 250 meter at high latitudes.

DAY TO DAY VARIATION OF THE DRIFT SPEED AND THE ELECTROJET

The results indicate that the ionospheric drift measurements at Thumba are closely associated with the equatorial electrojet currents. To investigate the relation between these two parameters an attempt was made to study

the relations between the day-to-day variation of the drift speed and the equatorial electrojet current as evidenced by the H variation. Nair et al. (1970) had suggested that the daily variation of the H at non-equatorial station is greatly affected by the magnetospheric currents. They argued that the daily range of H at Alibag (ΔH_A), a station outside the influence of the equatorial electrojet is largely caused by weakening of the ambient field on the night-side. The effect may be caused by magnetospheric currents which flow at a distance of more than 3000 Km above the surface of the earth, and would produce identical effects at Alibag and Trivandrum situated on the dip equator, 1,100 Km south of Alibag. On the otherhand the daily range of H at Trivandrum (ΔH_T) is predominently caused by the equatorial electrojet. Secondly they suggested that ($\Delta H_T - \Delta H_A$) would be a proper indication of the ionospheric currents. It was also shown that linear relationship exists between the drift speeds in the E or the F regions and the electrojet intensity as deduced by ($\Delta H_T - \Delta H_A$). In Fig.5 are plotted the mean values of the midday E-region drift speeds at Thumba for the year 1964 averaged for different groups of ($\Delta H_T - \Delta H_A$) as well as similar relationship between the drift speed and ΔH_T alone. It is seen that the correlation between V' and ($\Delta H_T - \Delta H_A$) is 0.91 $\pm$ 0.05 while that between the V' and ΔH_T is only .78 $\pm$ .09. This indicates

that the difference ($\Delta H_T - \Delta H_A$) is more correct representative of the ionospheric currents than ΔH_T alone.

IONOSPHERIC DRIFTS AND THE DISAPPEARANCE OF E_s

It has been recently shown (Rastogi et al. 1971) that at stations close to the dip equator within the electrojet region on quiet days as well as on disturbed days, whenever there is abnormally large decrease in H during the day-time, there is a simultaneous disappearance of E_s and reversal of the drift from westward to eastward. This has been suggested due to the reversal of the equatorial electrojet currents.

CONCLUSION

These observations have indicated that the drift measurements at equatorial station Thumba are closely related to the equatorial electrojet currents and the variation of the two can be identified with each other on a long term as well as on short term basis.

ACKNOWLEDGEMENT

Thanks are due to Professor V.A.Sarabhai, Chairman Indian National Committee for Space Research and Professor K.R.Ramanathan for their keen interest towards the installation of ionospheric drift station at Thumba.

REFERENCES

Balsley,B.B. (1966) An. Geophys., 22,460.

Balsley,B.B. (1969) J. Atmosph. Terr. Phys., 31,475.

Cahill,L.J. Jr. (1959) J. Geophys. Res.,64,489.

Chandra,H., and Rastogi,R.G. (1970) J. Atmosph. Terr. Phys., 32,1309.

Chapman,S. (1951) Proc.Phys. Soc., London, B64,833.

Chapman,S., and Bartels,J. (1940) Geomagnetism Vol.I,2, Oxford University Press.

Chapman,S., and Raja Rao,K.S. (1965) J. Atmosph. Terr. Phys., 27, 559.

Deshpande,M.R.,and Rastogi,R.G. (1966) An. Geophys., 22,418.

Deshpande,M.R.,and Rastogi,R.G. (1968) J. Atmosph. Terr. Phys., 30,293.

Egedal,J. (1947) Terr. Magn.Atmosph. Elect.,52,449.

Forbush,S.E., and Casaverde,M. (1961) Carnegie Inst. Wash. Publ.620.

Maeda,H. (1955) J. Geomagn. Geoelect., VII No.4, p.121.

Maeda,H. (1962) Proc. Intern. Conf. on Ionosphere, London, edited by A.C.Stickland,p.187.

Maynard,N.C., and Cohill,L.J . Jr. (1965) J. Geophys. Res., 70,5923.

Martyn,D.F. (1949) Nature, London. 163,685.

Matsushita,S. (1967) Physics of Geomagnetic phenomena, part I, edited by S.Matsushita and W.H.Campbell.

पुस्तकालय THE LIBRARY
भौतिक अनुसंधान प्रयोगशाला
PHYSICAL RESEARCH LABORATORY
नवरंगपुरा, अहमदाबाद-380009.
NAVRANGPURA, AHMEDABAD-380009.
भारत/INDIA

Mitra,S.N. (1949) Proc. IEE 96, Part III, 441

Nair,K.N., Rastogi,R.G., and Sarabhai,V. (1970) Nature, 226, 740.

Onwumechilli,C.A.,and Alexander,N.S. (1959) J. Atmosph. Terr. Phys., 16,115.

Pramanik,S.K., and Narayan,S.Y. (1952) Ind. J. Met. Geophys., 3,212.

Pramanik,S.K., and Harinaran,P.S. (1953) Ind. J. Met. Geophys.,4,353.

Rastogi,R.G., Deshpande,M.R., and Kaushika,N.D. (1966) J. Atmosph. Terr.Phys., 28,137.

Rastogi,R.G., Deshpande M.R., and H.Chandra (1968) J. Atmosph. Terr.Phys., 30,597.

Rastogi,R.G., Chandra H., and Chakravarty,S.C. (1971) Proc.Ind.Acad.Sci.

Sastry,T.S.G. (1968) J. Geophys.Res., 73,1789.

FIGURE CAPTIONS

Fig.1 - Annual average histograms of the apparent drift speed and direction for daytime and nighttime in the E and F regions of ionosphere over Thumba during the period 1968-69.

Fig.2 - Diurnal variations of the F-region drift speed at Thumba and horizontal component of magnetic field (H) at Trivandrum during different seasons averaged for the period 1967-69.

Fig.3 - Month to month variations of peak day-time E-region drift speed and range in H (rSq) averaged for the entire period 1964-69.

Fig.4 - Latitudinal variation of the apparent drift speed (V'), axial ratio (r), orientation ( ) and transverse size (b) of the irregularities.

Fig.5 - Relation between the midday drift speed in the E-region with the range in H at Trivandrum (H_T) and the difference of ranges at Trivandrum and Alibag ($H_T - H_A$).

THUMBA 1968-69

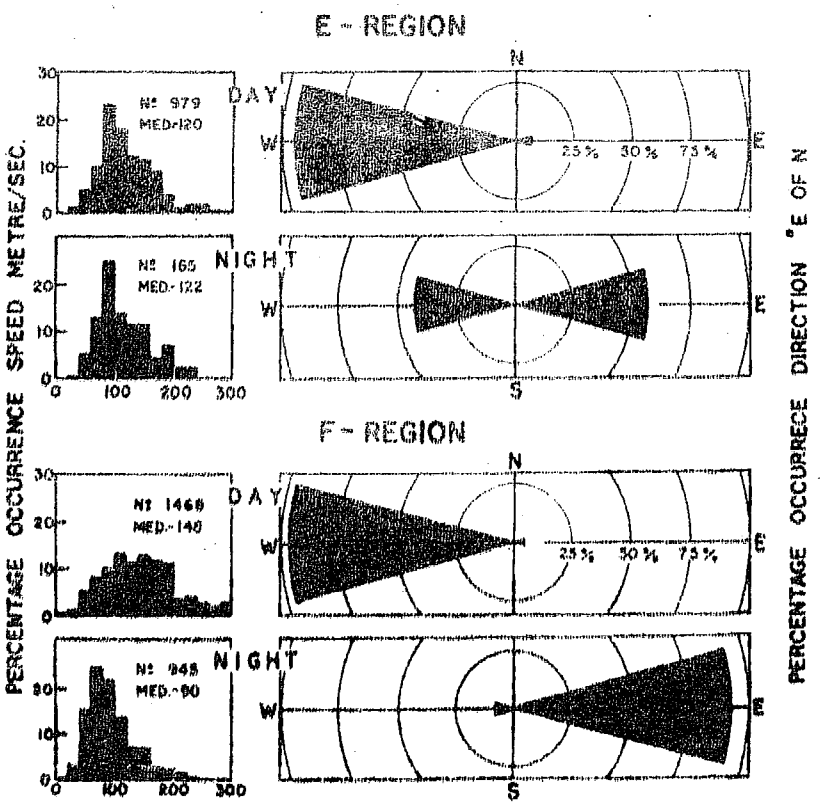

FIGURE 1

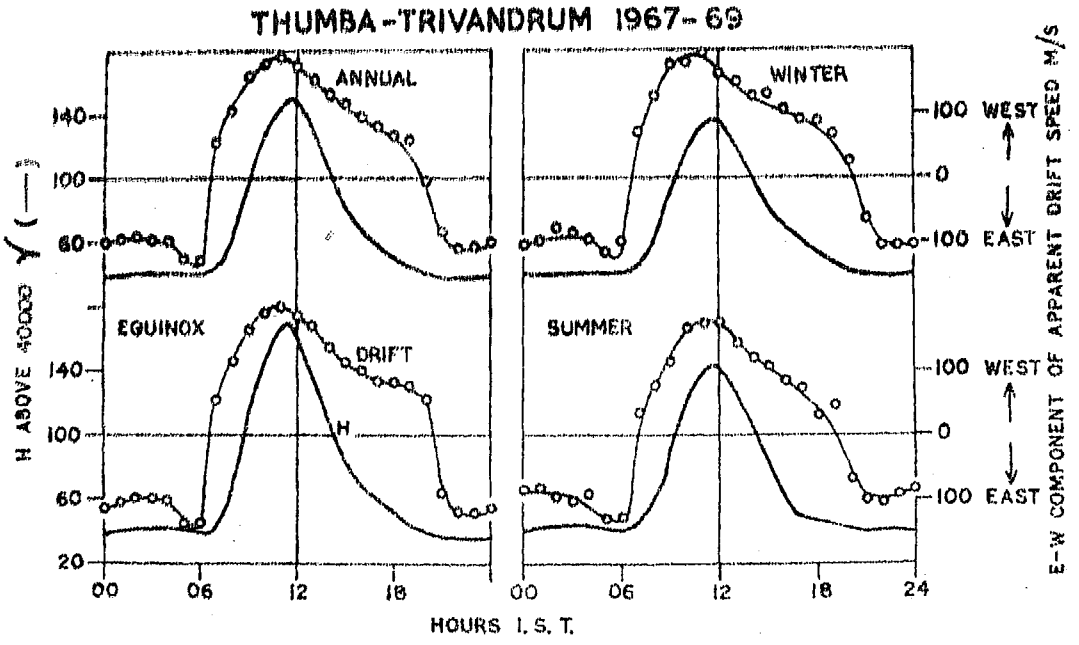

FIGURE 2

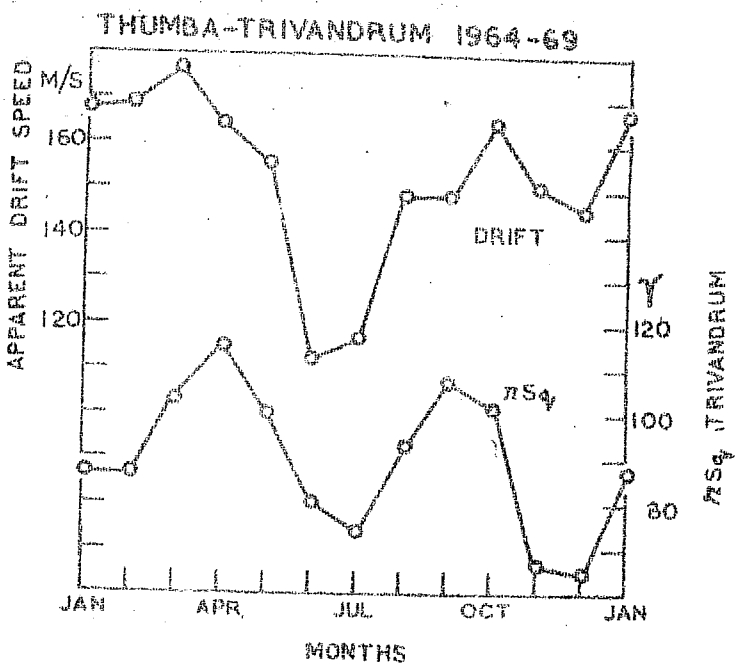

FIGURE 3

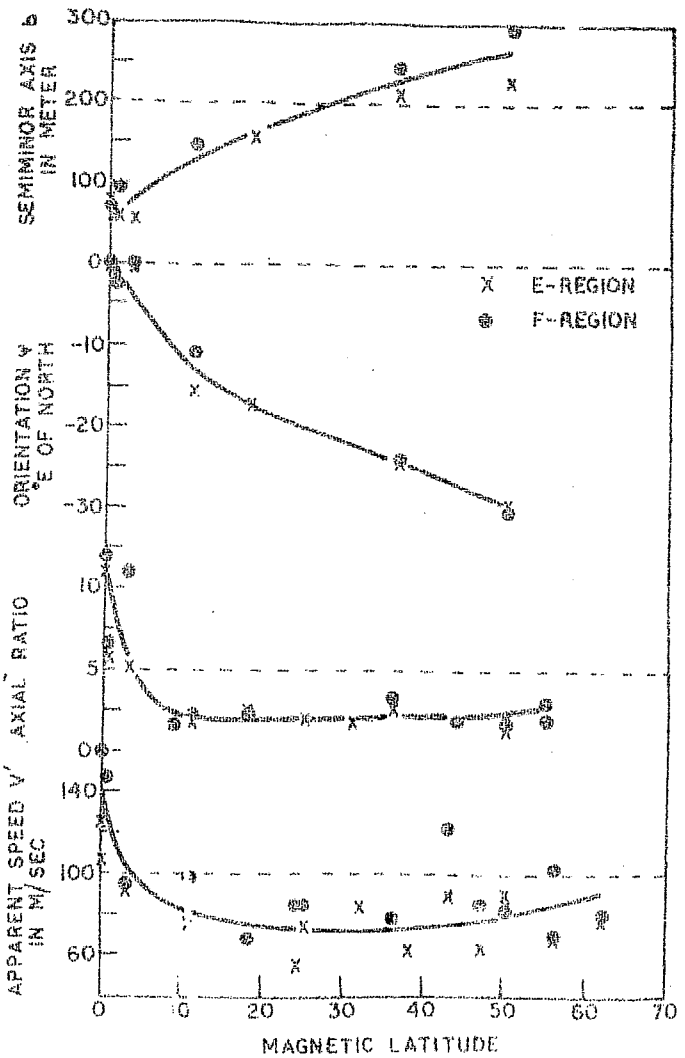

FIGURE 4

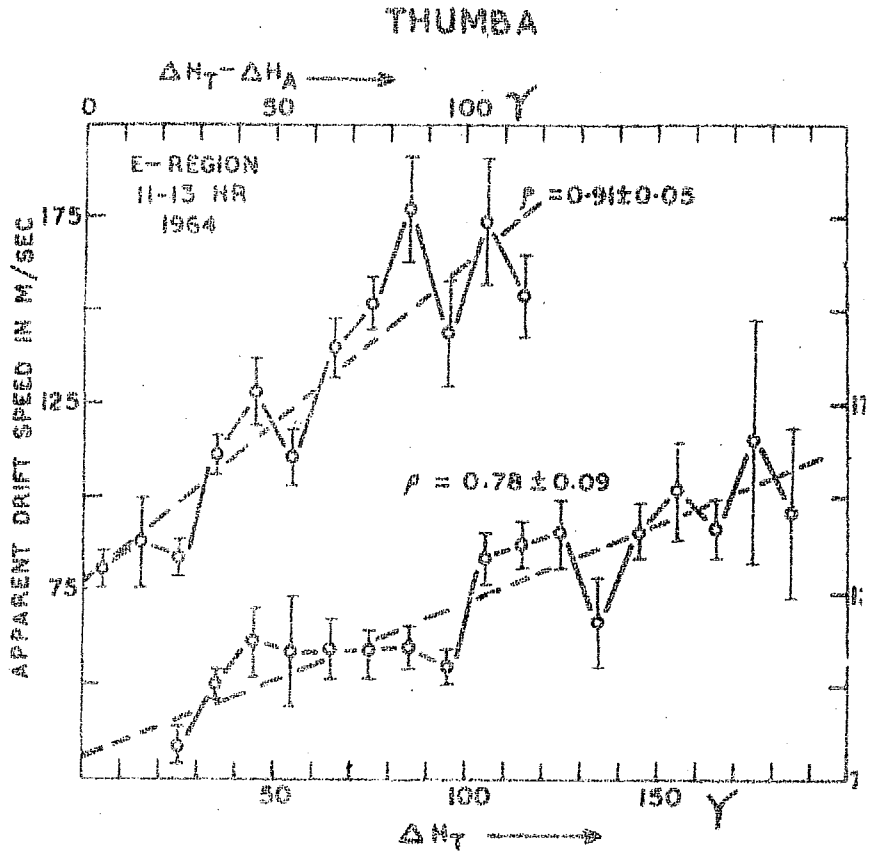
THUMBA
$\Delta N_T - \Delta H_A$
0
50
100 γ
E-REGION
11-13 HR
1964
ρ = 0·91±0·05
ρ = 0.78 ± 0.09
APPARENT DRIFT SPEED IN M/SEC
175
125
75
50
100
150 γ
ΔN_T

FIGURE 5

(Accepted for publication in Nature)

EFFECT OF MAGNETIC ACTIVITY ON ELECTRON DRIFTS IN EQUATORIAL ELECTROJET REGION

by

R.G.Rastogi, H.Chandra & R.K.Misra
Physical Research Laboratory
Ahmedabad-9
India

Electron drift measurements by spaced receiver technique[1] that were initiated in January 1964 at Thumba, near the magnetic equator have shown close association of drifts with the equatorial electrojet currents as regards the diurnal, seasonal and latitudinal variations[2,3]. Even on day to day basis E or F region drift speeds are proportional to the difference in the daily ranges of H at Trivandrum and Alibag[4], suggesting drift near the magnetic equator closely linked with the magnitude and direction of the electrojet currents. The E or F region drifts at Thumba are predominantly westward during daytime (07 - 18 hours) and eastward during night-time (19 - 07 hours). At low latitudes the pattern of electric field variations at the E-region are reproduced into the F-region through the conducting magnetic lines of forces and thereby the variations in the ionospheric drifts at E and F regions

are similar to each other.

The effects of magnetic activity on horizontal drifts in the ionosphere have been reported by several authors. At high latitudes drift speeds were found to increase with 'K' index[6,7]. But results were not consistent at low latitudes. At Waltair, results showed an increase in E-region drift and decrease in F-region drift with 'K' index[8,9]. Recently Sastry and Rao[10] have reported true drift speed at Waltair decreasing with increased magnetic activity. At Ibadan night-time F-region drift was shown to be reduced considerably on disturbed days[11].

In this article the variations of drift speed at Thumba with magnetic activity are presented. First the apparent drift speeds in the E and F-regions are studied in relation to the three hour 'K_p' index nearest to the time of observations and results are shown in Fig.1, alongwith the number of observations and standard deviations. Both the E and F region drifts are reduced with increasing 'K_p' index. Second the drift speeds were studied averaged for five international quiet and five international disturbed days. Fig.2(a) shows histograms of E-region drift speeds averaged for midday (11 - 13 hrs) during a low sunspot year (1964) and high sunspot years

(1967 - 68). Similar histograms for F-region drift speeds are shown in Fig.2(b) which also includes histograms for midnight (23 - 01 hrs) during the years 1967 - 68. Very rare occurrence of night-time sporadic-E at Thumba does not allow such comparison for night-time E-region. It is clearly seen that in all cases shown here the histograms are shifted towards lower drift values for disturbed days as compared to those for quiet days.

Thus it is evident that the ionospheric drifts over the magnetic equator decrease with increased magnetic activity both for day and night hours. The E-region electron density being larger by a factor of about 100 during day than during night[12,13], the changes in drift speed would affect the electrojet currents and thereby in H field at ground level mainly during the daytime hours.

The equatorial electrojet current is given by the product of E-W conductivity and E-W electrostatic field. The recent models of magnetosphere[14] have shown (1) Electrons are more dense on the dawn side of the magnetosphere than the dusk side while for protons the reverse is true (2) for protons and electrons of same energy in tail, protons drift closer to the earth than the electrons and hence become more energized. (3) At the onset of a

storm there is increase in the plasma density in the tail. Thus a space charge would be produced opposite to that of the normal S_q field at the equator. With increased magnetic activity, the electrostatic field of the magnetospheric origin would increase while the normal S_q field seems to be unaffected. Thus the total electrostatic field at the low latitudes would decrease with increasing magnetic activity. This explains the decrease of electron drifts with magnetic activity at low latitudes.

At high latitudes both the normal S_q and the magnetospheric electric fields are in the same direction. This would cause increase of drift speed with increasing K_p at high latitudes. This is in confirmity with the observed results[6,7].

ACKNOWLEDGEMENT

Thanks are due to Profs. K.R.Ramanathan and V.A. Sarabhai for their keen interest and encouragements towards the installation of ionospheric research station at Thumba and to Dr.M.R.Deshpande for supervising the station during the initial stages.

REFERENCES

1.	Mitra,S.N.	Proc. Instn. Elec.Engrs., 96, Part III, 441.	(1949)
2.	Deshpande,M.R., and R.G.Rastogi	Ann. de Geophys.,22,418	(1966)
3.	Rastogi,R.G., H.Chandra, and R.K.Misra	Proc. Symposium on problems of the Equatorial Electrojet, 8th August 1970, PRL, Ahmedabad.	(1970)
4.	Nair,K.N., Rastogi,R.G., and Sarabhai,V.A.	Nature (London), 226,740	(1970)
5.	Chandra,H., and R.G.Rastogi	J. Atmosph. & Terr. Phys., 32, 1309.	(1970)
6.	Chapman,J.H.	Canad. J. Phys.,31,120.	(1953)
7.	Briggs,B.H., and Spencer,M.	Rep. Prog. Phys.,17,245.	(1954)
8.	Rao,R.R.,and Rao,B.R.	Proc. IGY Symp. CSIR, New Delhi, p.202.	(1961)
9.	Rao,B.R., Rao,E.B., and Murthy,Y.V.R.	Proc, IGY Symp. CSIR, New Delhi, p.205.	(1961)
10.	Sastry,J.H., and Rao,B.R.	In Ionosphere-Magnetosphere Interactions, at NPL, New Delhi, Feb. 1971.	(1971)
11.	Skinner,N.J., Lyon,A.J.,and Wright,R.W.H.	Proc. Int. Conf. on the ionosphere, edited by Stickland,A.C., p.301, Physical Society,London.	(1963)
12.	Satya Prakash, S.P.Gupta, and B.H.Subbaraya.	Planet. Space Sci., 18, 1307.	(1970)

13. Satya Prakash; B.H.Subbaraya, and S.P.Gupta — J. Atmosph. & Terr. Phys., (1971) 33, 128.

13. Kavanagh,L.D.; Freeman,J.W.; and Chen,A.J. — J. Geophy. Res., 73, 5511. (1968)

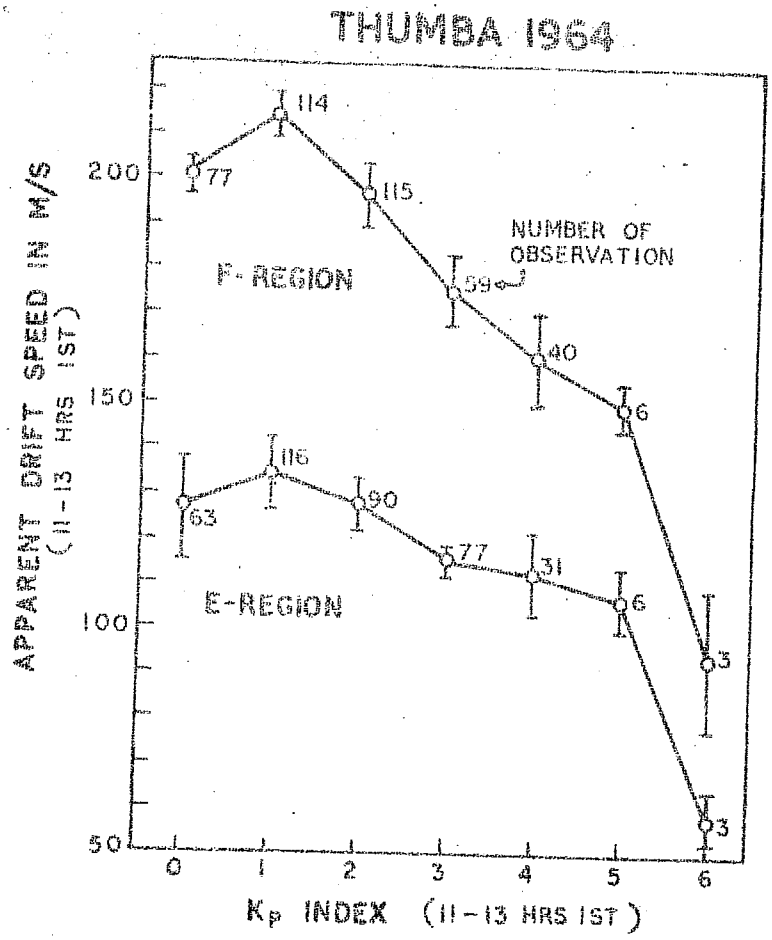

FIGURE 1

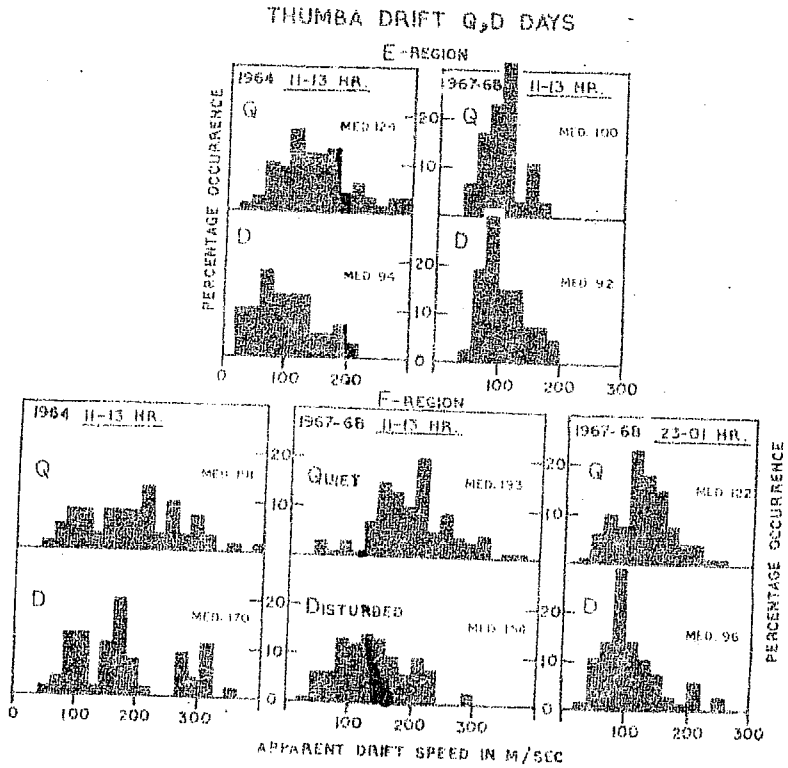

FIGURE 2

THUMBA E-REGION

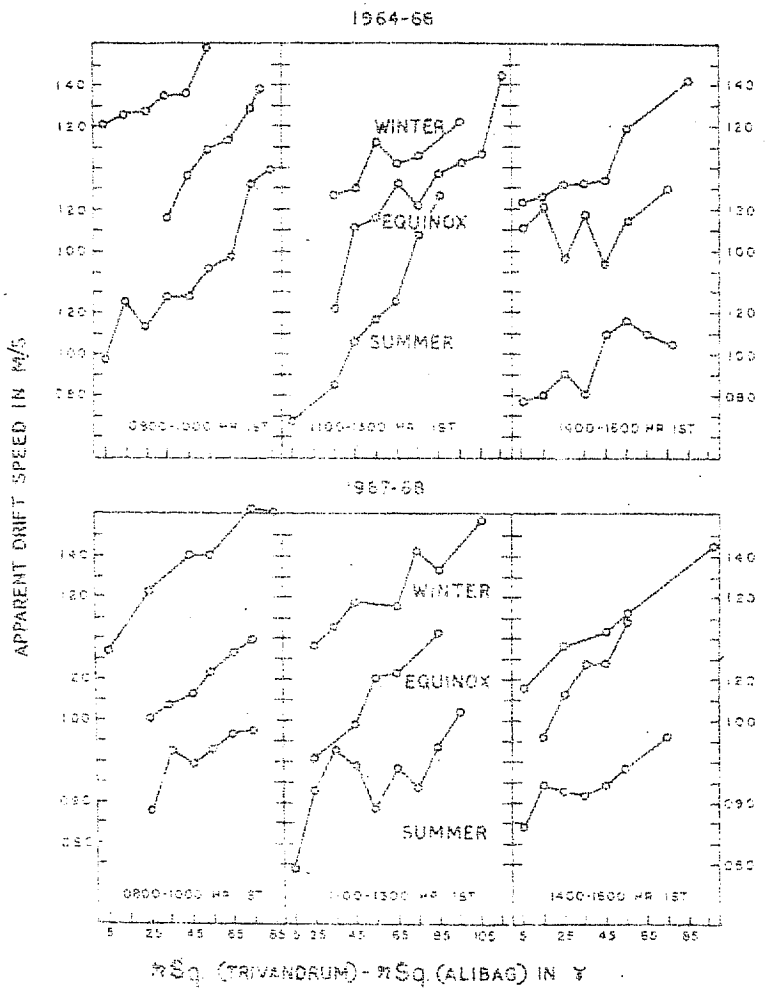

FIG — 4.5

THUMBA F — REGION

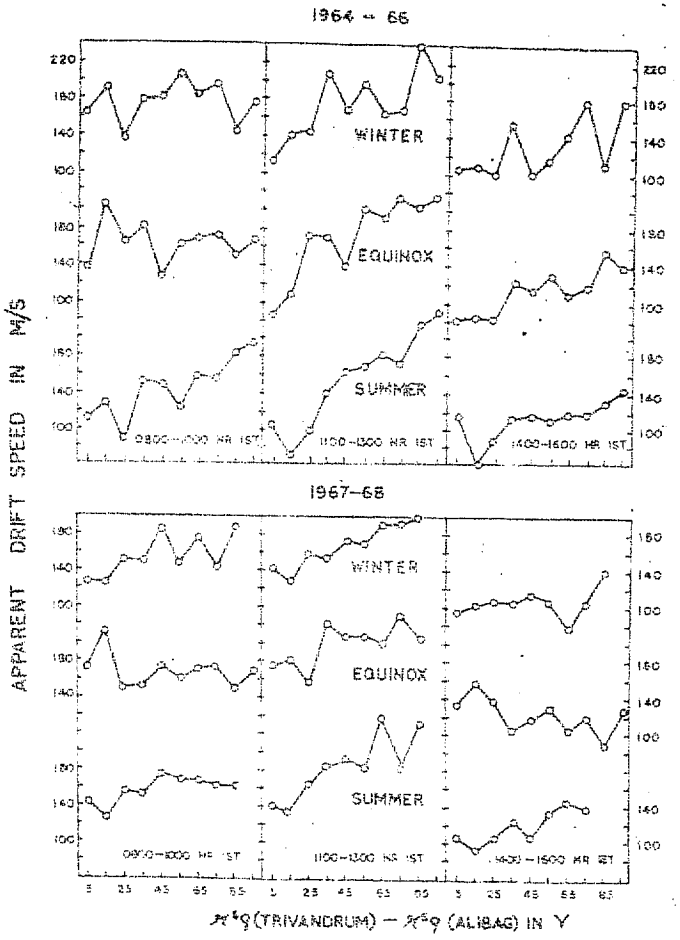

FIGURE 4.6

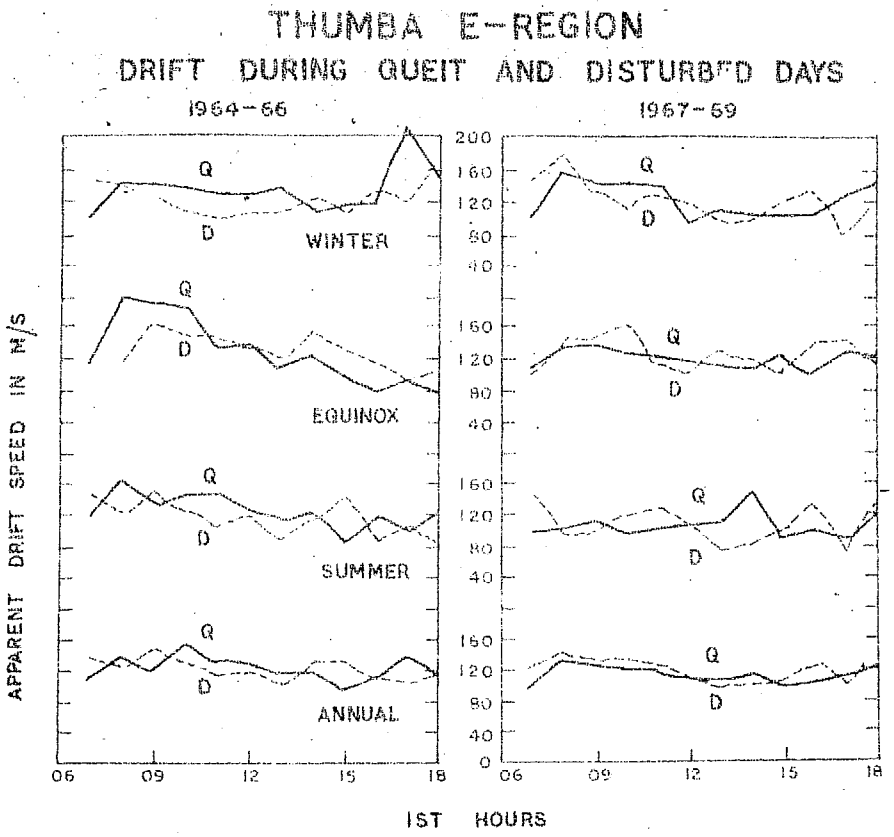
THUMBA E-REGION
DRIFT DURING QUEIT AND DISTURBED DAYS
1964-66
1967-69
APPARENT DRIFT SPEED IN M/S
Q
D
WINTER
EQUINOX
SUMMER
ANNUAL
200
160
120
80
40
0
06
09
12
15
18
IST HOURS

FIGURE 4.7

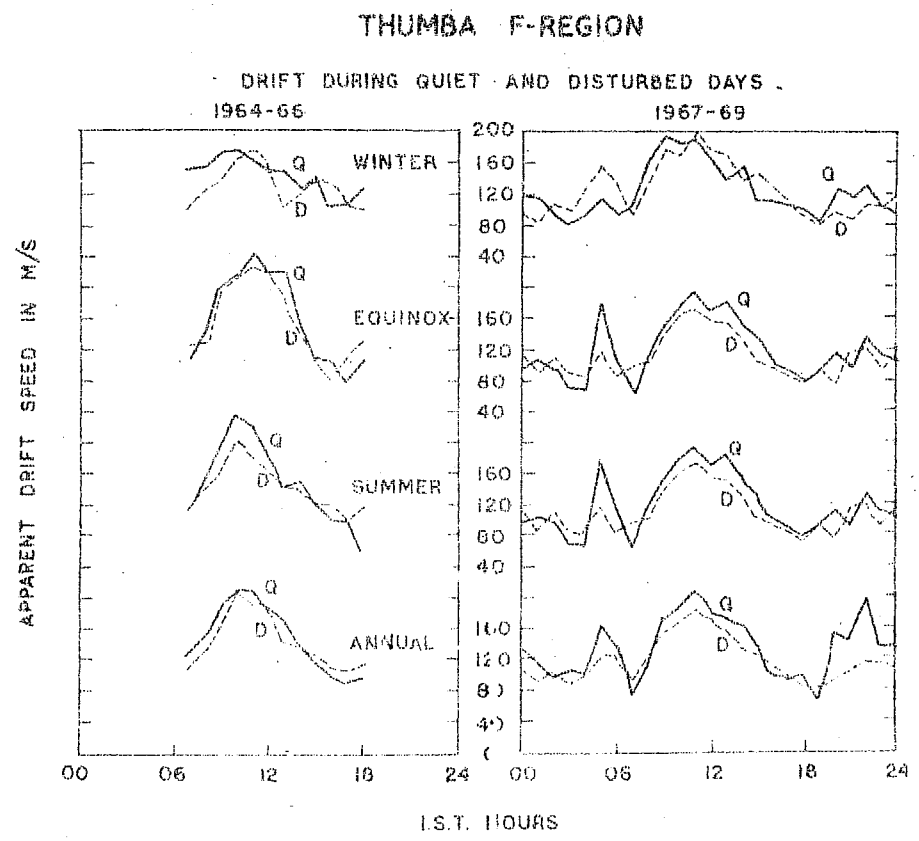
THUMBA F-REGION
DRIFT DURING QUIET AND DISTURBED DAYS
1964-66
1967-69
APPARENT DRIFT SPEED IN M/S
Q
D
WINTER
EQUINOX
SUMMER
ANNUAL
200
160
120
80
40
00
06
12
18
24
I.S.T. HOURS

CHAPTER V

THE COMPARISION OF VARIOUS METHODS OF ANALYSIS AND THEIR VALIDITY

The drift records obtained by the closely spaced receiver technique are most commonly analysed by the Mitra's similar fades method (1949). It was however shown by Phillips at Cavendish Laboratory in 1953 using a special time shift recorder, that the time shifts between any of the two pairs of fading records was considerably variable in magnitude and sometimes even with opposite sign, over a short period. This variability of time shifts was explained by RATCLIFFE (1954) in terms of the curvature of the line of maximum amplitude. For a given set of the contours of constant amplitude, the line of maximum amplitude for a given direction of movement of the diffraction pattern is the locus of the points of contacts of the tangents on each contour drawn parallel to the direction of movement. This line of maximum amplitude is generally curved and its curvature changes in magnitude and direction with the passage of time as the ground diffraction pattern changes its shape. It was shown by RATCLIFFE (1954) that if χ be the angle of this line to the direction of propagation, the time

shifts along X and Y direction of the aerial systems will be given by:

$$tx = \frac{\lambda_{10}}{V} \frac{\cos(\chi + \phi)}{\cos\chi}$$

$$ty = \frac{\lambda_{10}}{V} \frac{\sin(\chi + \phi)}{\cos\chi} \qquad \ldots\ldots(1)$$

Where V and ϕ are the speed and direction of the movement of the diffraction pattern. As is evident from these equations, depending upon the value of χ , tx and ty can assume any value and the sign.

MITRA (1949) and KRAUTKRAMER (1950) based their analysis on the tacit assumption that $\chi = 0$, (that is the line of maximum is always perpendicular to the direction of motion) and obtained somewhat wimpler relations, as given in Chapter II. This method of analysis would however lead to different values of velocity for different set of fades depending upon the value of at that instant. The effect of χ would however be more or less eliminated if a fairly large number of samples of tx and ty are averaged, as χ is symmetrically distributed about zero for an isotropic ground diffraction pattern.

5.1 Pütter's method

PÜTTER (1955) pointed out that in the absence of random velocities (that is when the pattern is fixed in shape), all the time shifts obtained would be related to one another by a simple straight line - called Pütter's line.

This can be seen from the equation (1) by eliminating χ that;

$$\frac{tx}{\xi_0} \cos \phi + \frac{ty}{\eta_0} \sin \phi = 1/V \qquad \ldots\ldots(2)$$

Thus for a fixed pattern, the plot of t_x and t_y against each other would be a straight line given by equation (2), which has a slope angle λ, given by

$$\tan \lambda = \frac{\xi_0}{\eta_0} \tan \phi \qquad \ldots\ldots(3)$$

Solving the equations (2) and (3), one can determine the values of V and ϕ uneffected by the curvature of the line of maximum amplitude. Geometrically, a line from origin and perpendicular to Pütter's line would give the velocity of the drift of the pattern both in magnitude and direction.

The above treatment does not in any way depend on the statistical distribution of the points corresponding to different maxima and it is the relative orientation of

the points rather than their actual positions which is important. Putter's method therefore applies even to an anisotropic diffraction pattern, which does not change its shape as it moves. Another advantage of this method lies in the fact that far less number of maxima are needed and hence it is quicker to apply.

BANERJI(1960) has modified this technique to the case of a turbulant anisotropic pattern. This is discussed separately later in Sec.5.3.

5.2 Method of Briggs - Page and Spencer (Probability distribution of time lags)

BRIGGS and SPENCER (1955) showed how to deduce the poperties of the changing diffraction pattern from the statistical observations of time lags alone. If the pattern is anisotropic the problem is shown to be insoluble if only two sets of time lag t_x and t_y are available. The availability of a time shift t_z in a third direction only enables the determination of all the involved parameters.

The distribution $P(t_x)$ and $P(t_y)$ for t_x and t_y is shown by BRIGGS et al. (1955) to be:

$$P(t_x) = \Phi\left(\frac{t_x - \bar{t}_x}{(\text{数}/(V^2 + V_c^2) - \bar{t}_x^2)} \right) \ldots\ldots(4)$$

Similarly for $P(t_y)$

When the above theoretical distribution is compared with the experimental distribution of t_x and t_y, it is found that the two curves give a best fit only for a particular value of V_c.

5.3 Banerji's statistical method for anisometric and turbulent patterns

BANERJI (1958) demonstrated, that even in the presence of random variations of the pattern as it moves, the value of $\emptyset$ can be obtained equally easily by drawing a mean straight line through the plot of t_x against t_y, if the ground pattern is isotropic. The magnitude of V obtained by the mean straight line has, however, to be corrected by using the correlation coefficient ' ρ ' between t_x and t_y valves.

(a) Isometric Turbulent Pattern

In the presence of turbulence for an isotropic pattern, the plot of t_x against t_y will have some spread instead of a straight line. The lines of equal probability on this diagram would be ellipses, the major axis of which will be perpendicular to the direction λ, given by equation (3). Hence the major axis lies in the same direction as the Pütter's line in the absence of turbulence

and hence ϕ is same. However the intersection of this line with $t_y/t_x = \eta_0/\xi_0 \tan\theta$ does not yield the magnitude of the velocity but leads to a new parameter $V(1 + Vc^2/V^2)$. The spread of the points about the major axis is an independent indication of the magnitude of V_c. It can be shown that V and V_c are related by the following equation:

$$\frac{2}{V^2 + Vc^2} = \left(\frac{\bar{t}_x^2}{\xi_0^2} + \frac{\bar{t}_y^2}{\eta_0^2}\right) + \left[\left(\frac{\bar{t}_x^2}{\xi_0^2} + \frac{\bar{t}_y^2}{\eta_0^2}\right)^2 + 4\,\frac{\bar{t}_x \bar{t}_y}{\xi_0 \eta_0}\,\frac{1}{\rho^2}\right] \quad \ldots(5)$$

where ρ is the correlation coefficient between t_x and t_y values. Hence V and V_c can be determined unambiguously.

(b) Anisometric Turbulent pattern

When the pattern is anisotropic as well as turbulent, two additional unknowns appear in the equations, namely the axial ratio 'r' and the orientation 'φ' of the auto-correlation ellipse. This necessiates the evaluation of another statistical parameter. BANERJI (1960) used the results of BRIGGS and SPENCER (1955) for an anisotropic pattern by a suitable transformation of the coordinate system, in which the pattern appears to be isotropic and the results of BRIGGS and SPENCER could be used. Standard deviation of t_x and t_y was the additional parameter.

Following scheme of calculations is given by Banerji to determine various parameters of drift and anisotropy by this method.

(i) Calculate $\bar{t}_x$, $\bar{t}_y$, $\sigma_{t_x}^2$, $\sigma_{t_y}^2$ and ρ

(ii) Calculate $A = \bar{t}_x / \lambda_x$, $B = \bar{t}_y / \lambda_y$, $C = \frac{2}{n}\left(\frac{\sigma_{t_x}}{\lambda_x}\right)^2$

$D = \frac{2}{n}\left(\frac{\sigma_{t_y}}{\lambda_y}\right)^2$

(iii) Calculate $\psi = \frac{1}{2}\left[\frac{\rho\sqrt{CD} + AB}{D - C}\right]$ ....(6)

(iv) Calculate $P = \cos 2\psi \left[\frac{C + D}{C - D}\right]$

(v) Calculate $r = \left(\frac{P+1}{P-1}\right)^{\frac{1}{2}}$ ....(7)

(vi) Calculate $\phi = \psi + \tan^{-1}\left[\frac{1}{r^2}\left(\frac{\cos\psi - (A/B)\sin\psi}{\sin\psi - (A/B)\cos\psi}\right)\right]$

(vii) Calculate .....(8)

$$L = \frac{1}{r^2}\cos\psi\cos(\phi - \psi) - \sin\psi\sin(\phi - \psi)$$

$$M = \frac{1}{r^2}\sin^2\psi + \cos^2\psi$$

$$N = \frac{1}{r^2}\cos^2(\phi - \psi) + \sin^2(\phi - \psi)$$

(viii) Calculate $V_x = (A/C - M/L)$

$V_y = (B/D - M/L)$

$V = V_x V_y / (V_x^2 + V_y^2)^{\frac{1}{2}}$ .. (9)

(ix) Calculate $V_c = (VL/A - NV^2)^{\frac{1}{2}}$ .....(10)

5.4 Method of Lyon, Morris and Bamgboye using Standard deviation of time lags

As shown earlier, the method of BRIGGS and SPENCER (1955) requires a large number of time lags

t_x and t_y in order to get a good fit of the actual distribution (BRIGGS and PAGE, 1955). Briggs and Spencer used about an hour long record. It is however doubtful that the conditions remain stationary over such a long period. Since the experience shows that the distribution of time lags is approximately Gaussian in majority of the cases, it was proposed by LYON, MORRIS and BAMGBOYE (1969) that the standard deviation of a series of time shifts i.e. t_x and t_y, should be used as an adequate means of fitting the distribution and it is then possible, to use Briggs- Page -Spencer's method for a relatively short drift records of a few minute duration, which are normally used in the drift measurements.

If t_x has the distribution given by equation (4) of Briggs and Spencer, then the variance of the quantity $(tx - \bar{t}x)/ (x - \bar{t}x^2)^{\frac{1}{2}}$ where $X = \sigma_v^2 / (V^2 + Vc^2)$ will be 0.37 (for a normal distribution).

As t_x is mean and X is a constant,

$$t_x^2 / (x - \bar{t}x^2) = 0.37$$

$$\text{or } X = \bar{t}_x^2 + 2.70 \; t_x^2 \qquad \ldots\ldots(11)$$

Similarly for Y and Z

If a better value of variance of the function Ø is σt^2 instead of 0.37,

$$\text{then } X = \bar{t}x^2 + t_x^2 / \sigma t^2 \qquad \ldots\ldots(12)$$

This modified time delay method yields unambiguous values for the parameters of the characteristic ellipse, exactly in the same way as the correlation technique. The two methods are related by the equation:

$$X = (\xi_0 / V'_{cx})^2 = \tau_1^2$$

$$Y = (\eta_0 / V'_{cy})^2 = \tau_2^2 \qquad \ldots\ldots\ldots(13)$$

$$Z = (\sqrt{\xi_0^2 + \eta_0^2} / V'_{cz})^2 = \tau_3^2$$

Having obtained V'_c and τ_1, τ_2, and τ_3 from this, all the relations of PHILLIPS and SPENCER (1955) can be applied to obtain r and ψ and also V_c and V_{co} (V_c along the minor axis of ellipse).

The mean distance Lo between the irregularities can be deduced from the mean time ' To ' between the maxima of the pattern.

$$L_o = V_{co}' \; T_o$$

where Vco' is the value of fading velocity Vc' along the minor axis of the ellipse.

Following relations are given LYON et al. 1969) for the drift speed and direction as well as the anisotropy parameters of the pattern for an equatorial station where the irregularities are field aligned (i.e. $\psi = 0$) by substituting the values of τ_1, τ_2 and τ_3 and Vc'

from equation (13), in the Phillips-Spencer's relations for full-correlation analysis, as given in the Chapter III. These equations hold for an isosceles right angled triangle with the diagonal 'd' and two sides along the north-south and east-west directions.

$$V_E = d\ \bar{t}_x / \sqrt{2}\ x$$

$$V_N = d\ \bar{t}_y / \sqrt{2}\ y \qquad \ldots\ldots(14)$$

$$r = (X/Y)^{\frac{1}{2}} \qquad \ldots\ldots(15)$$

$$V_{co}' = d / (2x)^{\frac{1}{2}}$$

$$V_{co} = d/(2X)^{\frac{1}{2}}\ (1 - \bar{t}_x^{\,2}/X - \bar{t}_y^{\,2}/Y)^{\frac{1}{2}} \ldots\ldots(16)$$

$$\text{and } Lo = To\ d / (2X)^{\frac{1}{2}} \qquad \ldots\ldots(17)$$

Comparision of Lyon-Morris method with the Phillips-Spencer's method

(1) The shift of the maxima of cross-correlograms corresponds to the mean time lag t_x or t_y.

(2) The time lag τ_1, τ_2 and τ_3 correspond to the quantities $X^{\frac{1}{2}}$, $Y^{\frac{1}{2}}$ and $Z^{\frac{1}{2}}$.

(3) Comparing the equation (16) with the one derived by BRIGGS, PHILLIPS and SHINN (1950), according to which:

$$\tau_c^{\,2} = \tau^{\,2} + \tau_m^{\,2}$$

$$\text{or } \tau_{mx} = 1.64\ \tau_{tx} \qquad \ldots\ldots(18)$$

Similarily for τ_{my} and τ_{mz}

Here τ_c stands for τ_1, τ_2 and τ_3 and for the shift of maxima of cross-correlogram 'τ_m' is the time lag on auto-correlogram corresponding to the maximum cross-correlation coefficient. LYON et al. (1969) have also discussed the condition for the real values of r and V_{co} and the possible causes of errors.

5.5 Sprenger and Schminder's method (Variant-2)

SPRENGER and SCHMINDER (1969) have shown that there are atleast two different ways of making similar fades analysis, which may possibly yield considerably different drift velocity.

Variant-1 is the conventional Mitra's method described in Chapter II and consists of measuring the individual time delays between similar fading maximum or minimum and averaging them separately for any two pairs of records. The mean drift vector V_1' is deduced from these two mean time delays $\bar{t}_x$ and $\bar{t}_y$. Variant-2 (SPRENGER and SCHMINDER, 1969) consists in measuring the individual pair of time lags for each fading maximum or minimum which occurs similarly at all the three traces and determining the drift vector for individual pairs of t_x and t_y. The mean drift vector V_2' is found out by averaging all these individual drift vectors. In short, Variant-1 is the

method of averaging the time delays and variant-2 is the method of averaging drift vectors. Instead of using the means, median values of this may be used with advantages as recommended by the URSI-C19 working Committee on Ionospheric Drift analysis (WRIGHT and KENT, 1968).

Variant-1 gives the apparent drift velocity, where the effect of the curvature of line of maxima is eliminated by averaging a large number of t_x and t_y but the Variant-2 takes into account of the different values of drift velocity at different set of similar fades within the same record and the vector sum of these will result into a velocity slightly lower than V_2'. Fade to fade variation of the drift vector can also be due to genuine variation of drift during the course of an observation.

5.7 Six point correlation method of Yerg and its modification by Keneshea and by Fedor for 3.D case

(a) YERG (1955) developed a slightly different method of analysis for determining V, Vc and Vc', which requires only six values of correlation coefficients rather than the whole curve (as in Phillips and Spencer's method) and therefore offers much saving of time. These six correlation coefficient are: $\rho(\xi_0, 0, 0)$, $\rho(0, \eta_0, 0)$, $\rho(\xi_0, \eta_0, 0)$ $\rho(\xi_0, 0, \tau_0)$, $\rho(0, \eta_0, \tau_0)$ and $\rho(0, 0, \tau_0)$

The first three are cross-correlation coefficients between three pairs of aerials at zero time. Next three at an arbitrary time .

The correlation coefficient (ρ)is a function of space and time. It is assumed that:

(1) this function may be represented as a Taylor's series in three variables (i.e. it has a parabolic form) and

(2) near the origin, only first and second order terms are retained.

Thus we have:

$$\rho(\xi, \eta, \tau) = 1 + (A\xi^2 + B\eta^2 + C\zeta^2 + 2H\xi\tau + 2M\eta\zeta + 2N\xi\eta) \quad \ldots\ldots(20)$$

The six coefficients A,B,C,H,M and N are evaluated of the pattern, then it can be shown that:

$$Vx = (MN/AC - H/A) / (1 - N^2/AC)$$

$$Vy \quad (HN/AC - M/C) / 1 - N^2/AC) \quad \ldots\ldots(21)$$

Hence $V = (V_x^2 + V_y^2)^{\frac{1}{2}}$

and $\phi = \tan^{-1} (Vx/Vy)$

and $Vc' = B (1 + \tan^2 \phi) / (A + C \tan^2 \phi + 2N \tan \phi)$ ....(22)

and so, $Vc = (V_c'^2 - V^2)^{\frac{1}{2}}$

This method is simple as it needs only six values of . Also it includes the effect of random motion as well as anisotropy of the pattern.

WIEWALL (1962) modified Yerg's six-point method by using a triangular shape of the correlation function than a parabolic shape. According to him:

$$\rho = 1 - f\left(A\xi^2 + B\eta^2 + C\tau^2 + 2H\xi\tau + 2M\eta\tau + 2N\xi\eta \right)^{\frac{1}{2}} \quad \ldots\ldots(23)$$

The main defects of Yerg's method are:

(1) the arbitrary choice of time lag τ_1 and

(2) the assumed parabolic-shape of the correlation function near the peak of the curve.

(b) Best fit correlation method

The basic assumption of the BRIGGS et al.(1950) in their full correlation analysis of the drift records was that the contours of the constant correlation are similar concentric ellipsoids of the same orientation in the ground plane and time coordinate system. Since the actual data deviates more or less from this assumption, KENESHEA et al. (1965) proposed a new method in which first the correlation ellipsoids are computed which give the best overall fit to the measurements.

The generalized equation of the correlation ellipsoids is:

$$\rho(\xi, \eta, \tau) = 1 - f\left(A\xi^2 + B\tau^2 + C\eta^2 + 2H\xi\tau + 2M\eta\tau + 2N\xi\eta \right) \quad \ldots\ldots(24)$$

Using six points on the correlogram, one can find out the values for the constants A,B,C, H,M and N as in case of Yerg's method as well as the time lags τ_1, τ_2, τ_3, τ_4, τ_5, and τ_6. The slopes (τ_1^2/τ_2), (τ_3^2/τ_4) and (τ_5^2/τ_6) of these three BPS lines are made to satisfy the following equation for an ellipsoid by rotating the straight lines about their best-determined points.

$$\frac{\tau_1^2}{\tau_2} + \frac{\tau_3^2}{\tau_4} - \frac{\tau_5^2}{\tau_6} = 0 \qquad \ldots\ldots,(25)$$

The six resulting intercepts are then used to determine the parameters V, $\emptyset$, Vc, r and ψ as the Yerg's method described earlier in Sec.6. This method uses all available values of cross-correlation down to some arbitrary minimum to determine the best straight lines, but treats each receiver pair separately; even the 'best fitting' straight lines so achieved are then abandoned to satisfy the relation (25) amongst their slopes. FEDOR (1967) extended this method to 3-dimensional case and a larger number of aerials.

(c) Statistical determination of the three dimentional Ionsopheric drifts

A general method of analysis, based upon the concepts introduced by BRIGGS et al. (1950) and

KENESHEA et al. (1965) has been developed by FEDOR (1967). From any adequate combination of the cross-correlation functions among spaced measurements of the random fading of a pulsed radio echo from the ionosphere, the method extracts the best-fitting value of average drift, velocity of random changes and parameters describing the average size, life-time, spatial orientation and characteristic shape of the irregularities in the echo amplitude. The analysis was developed in three spatial dimensions plus time and is useful when the fadings at two closely spaced frequencies are also available. The method offers three distinct advantages over previous treatments of this problem:

(i) it provides a best fit to the available data in accord with the principle of least squares,

(ii) it places no upper limit on the quantity of the data that may be so fitted and in particular permits the mathematical over determination of the problem, which is desirable from its inherently statistical nature,

(iii) the method permits a complete description of the average three dimensional space and time structure of the measured quantity.

It is shown that the horizontal velocity components are not given correctly by the two dimensional

methods if vertical movements of anisometric irregularities occur. The main results of this method are as follows:

Expending 3-dimensional correlation function upto first order even terms of a taylor's series, we have

$$\rho(x, y, z, t) = \exp\left(-\tfrac{1}{2} f(x,y,z,t)\right) \text{ where}$$

$$f(x,y,z,t) = (a_{11} x^2 + a_{22} y^2 + a_{33} z^2 + a_{44} t^2 + a_{12} xy + a_{13} xz + a_{14} xt + a_{23} yz + a_{24} yt + a_{34} zt)$$

The coefficients a_{11}, a_{12} et. can be determined by using ten known values of $\rho(x,y,z,t)$.

Thus one gets V_x (eastward) $= (a_{12} a_{24} - 2a_{22} a_{44}) / \Delta_1$

$$- V_z (2a_{22} a_{13} - a_{12} a_{23}) / \Delta_1$$

V_y (northward) $= (a_{12} a_{14} - 2a_{11} a_{24}) / \Delta_1$

$$- V_z (2a_{11} a_{23} - a_{12} a_{13}) / \Delta_1.$$

$$V_z \text{ (vertical)} = (\Delta_2 \Delta_3 - \Delta_1 \Delta_4) / (\Delta_1 \Delta_5 - \Delta_2 \Delta_2)$$

where $\Delta_1 = (4a_{11} a_{22} - a_{12}^2)$, $\Delta_2 = (2a_{11} a_{23} - a_{12} a_{13})$

$\Delta_3 = (2a_{11} a_{24} - a_{12} a_{14})$, $\Delta_4 = (2a_{11} a_{34} - a_{14} a_{13})$

and $\Delta_5 = (4a_{11} a_{33} - a_{13}^2)$

Also $a_{11} = (l_{11}/d_1)^2 + (l_{12}/d_2)^2 + (l_{13}/d_3)^2$

$a_{22} = (l_{21}/d_1)^2 + (l_{22}/d_2)^2 + (l_{23}/d_3)^2$

$a_{33} = (l_{31}/d_1)^2 + (l_{32}/d_2)^2 + (l_{33}/d_3)^2$

$a_{12} = 2 (l_{11} l_{13}/d_1^2 + l_{12} l_{22}/d_2^2 + l_{13} l_{23}/d_3^2)$

$$a_{13} = 2\,(l_{11}l_{21}/d_1^{\,2} + l_{12}\,l_{32}/d_2^{\,2} + l_{13}l_{33}/d_3^{\,2})$$

$$a_{23} = 2\,(l_{21}l_{32}/d_1^{\,2} + l_{22}\,l_{32}/d_2^{\,2} + l_{23}\,l_{33}/d_3^{\,2})$$

where d_1, d_2 and d_3 are the semi-axes of the spatial characteristic ellipsoid and l_{ij} are their direction cosines. Solving these equations, one gets the size ie d_1, d_2, d_3 and orientation l_{ij} for the characteristic ellipsoid.

Horizontal drift velocity, $V_H = (V_x^{\,2} + V_y^{\,2})^{\frac{1}{2}}$ ...(27)

$$\phi_H = \tan^{-1}(V_y/V_x)$$

and the drift velocity $V = (V_H^{\,2} + V_z^{\,2})^{\frac{1}{2}}$ .....(28)

$$V_c = \frac{d'^{\,2}}{b^2} \qquad .....(29)$$

where d' is the spatial separation at which the correlation drops to $1/e^{\frac{1}{2}}$ and b is the lifetime of the irregularities.

This technique of analysis has been applied to a few spaced antenna closed frequency simultaneous fading records taken at Thumba to determine 3-dimensional drift. Results are discussed sec.5.12. Following ten correlation coefficients are used to determine the values of the ten coefficients a_{11} a_{12} etc.

$\rho(\xi,0,0,0)$, $\rho(0,\eta,0,0)$, $\rho(0,0,h,0)$, $\rho(0,0,0,\tau)$, $\rho(\xi,0,0,\tau)$, $\rho(0,\eta,0,\tau)$, $\rho(0,0,h,\tau)$, $\rho(\xi,\eta,0,0)$, $\rho(\xi,0,h,0)$ and $\rho(0,\eta,h,0)$

5.7 Briggs spatial correlation method of analysis

The analysis of a moving random diffraction pattern where the whole pattern can be recorded, was given by BRIGGS (1968). The pattern is assumed to have a certain mean velocity and also to change randomly in shape, as it moves. It is shown how the parameters used in the standard correlation analysis, namely V, Vc r, b and γ can be determined from two records of a two dimentional moving pattern obtained at a known time interval. The velocity of motion can be obtained without making the assumption that the spatial and temporal correlation functions have the same shape. If any successive records of the pattern are available separated by different time intervals, then the form of the temporal correlation function of the random changes alone can be determined.

The details of this method are not discussed here as it was not applicable to Thumba drift records, due to limited number of receiving aerials. Using the Buckland Park array of 89 receiving aerials at Adelaide, GOLLEY and ROSSITER (1970), have used this technique to calculate each spatial Fouiner component of drift velocity. This is a useful method of analysis when it is suspected that the dispersive wave motions play a part in the movements of the pattern and the effect of the variability of drift

speed during the course of a record is to be eliminated (see 7.5c).

5.8 Validity of correlation analysis

WRIGHT (1968) and WRIGHT and FEDOR (1969) compared the results of the radio spaced antenna experiment with those of the rocket and gun launched visible trial measurements of neutral winds and found a good agreement between the two for the total reflection (while the standard theory requires the echo pattern from a point source transmitter to move at twice the ionospheric speed) and a poor agreement when the partial reflections were involved. As it does not seem likely that the ionospheric irregularities themselves move at half the neutral wind speed throughout the height range (90 - 140 km) of observations (KATO et al. 1970), one can doubt the simple scattering models from which the doubled velocities are deduced for a pattern from a point source transmitter.

A few workers have however pointed out that such a disagreement can result from the obscure defects in the much involved correlation analysis. BRIGGS (1969) found an increasing true drift speed with the increasing aerial separation and doubted this to be the results of the assumption of the similarity of space and time variations of the pattern. HINES (1964) has questioned the

validity of correlation analysis in the presence of the wavelike motions in the ionosphere.

It has however been recently shown(PITTEWAY et. al. 1971) using a computer simulated fading records, that the correlation analysis introduced by BRIGGS et al.(1950) and PHILLIPS and SPENCER (1955) and developed in an optimal form by FEDOR (1967) detects the mean direction and speed of the diffraction pattern and estimates random velocity fluctuations directly related to the random changes in the model.

5.9 Results and comparison of various methods of analysis for Thumba (0.6°S dip)

Fig.5.1 gives the plot of tx and ty values for a few records at Thumba, in an attempt to apply the Putter's method of analysis. It is found that owing to extreme anisotropy of the ground diffraction pattern, the values are invariably low and the plot of t_x and t_y does not produce a straight line as shown theoretically by PUTTER (1955). The points are clustered at one place and it is not possible to estimate the drift velocity.

Fig.2a compares the results of similar fades method of Mitra (Variant-1) with those of the similar fades methods of Sprenger and Schminder (Variant-2) for F-region.

PÜTTERS METHOD

PLOT OF $T_x - T_y$ FOR THUMBA DRIFT

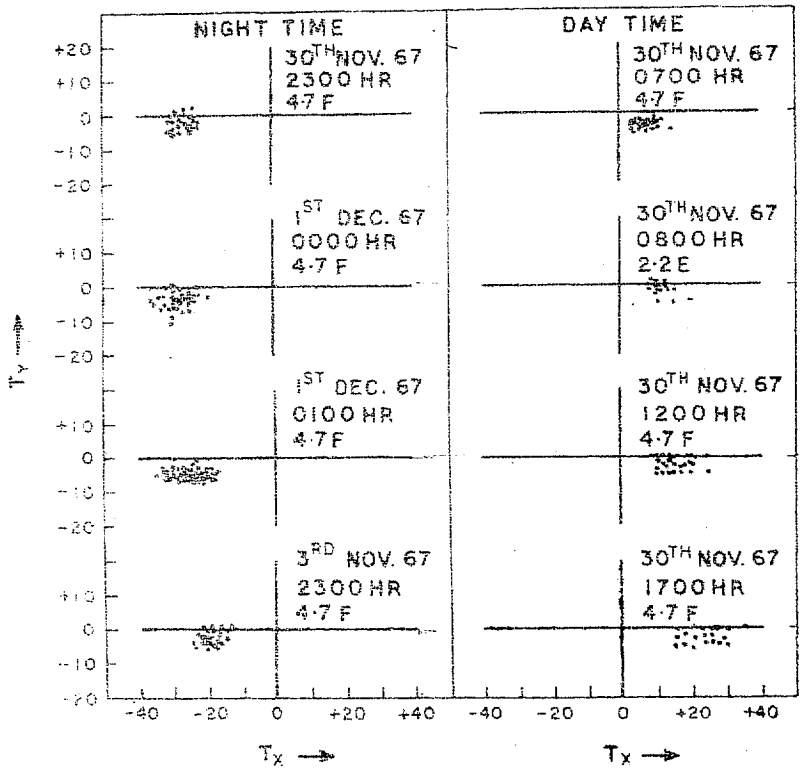

FIGURE 5.1

THUMBA F-REGION 1968-69

APPARENT DRIFT

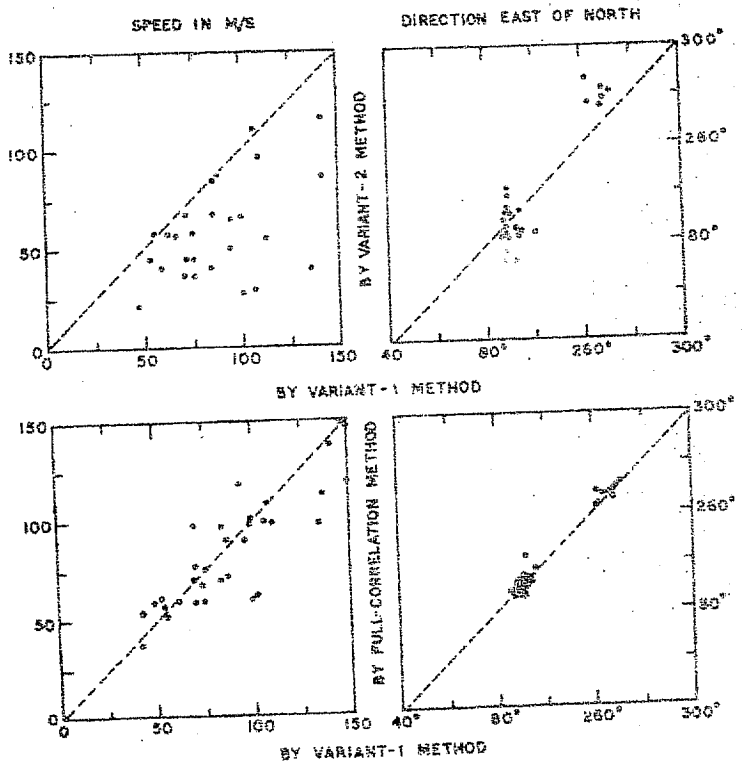

FIGURE 5.2

The dotted lines represent the equal values of the two parameters. It is however found that V_2' is always lower than V_1'. As the drift direction is predominantly east-west at Thumba, the points in Ø2 V_s Ø1 plot are clustered either around 90° or 270° east of north. Comparison of variant-2 results with the true drift velocity of full correlation analysis is shown in Fig.3b. This shows a close correspondence in the values of speed and the direction. This is in accordance with the results of SPRENGER and SCHEMINDER (1969) and shows that Variant-2 leads to the values close to the true velocity.

SPRENGER and SCHEMINDER (1969) analysed drift records for Central Europe by the two variants of similar fades method and also full-correlation method and compared the velocities and found a one to one correspondence between the velocities by similar fades and the full-correlogram method. The correlation was 0.91. The slight deviation of values between V_1' and V' (by full correlation taking anisotropy into account) was accounted for the anisotropy which is not taken into account by the similar fades method.

As already mentioned V_2' is always smaller than V_1' and the difference increases with increasing spread of the individual time delays. Just the same tendency can be

found from the equation $V' = V\left(1 + (Vc/V)^2\right)^{\frac{1}{2}}$ of BRIGGS et al. (1950) between V' and V, where V is always smaller than V' and the difference increases with increasing magnitude of V_c. Thus V_2' may be comparable to the true drift velocity V, assuming that there is some relationship between the spread of the individual time shifts and the magnitude of V_c.

SPRENGER and SCHMINDER (1969) also compared V_2' and V and found a good correlation. The close correspondence of V_2' with V on one hand and V_1' and V' on the other hand, leads us to substitute V_1' and V_2' instead of V' and V respectively into the equation of BRIGGS et al. (1950) for the random drift prameter V_c.

Hence $Vc_s = V_2'\left(V_1'/V_2'\right)^2 - 1)^{\frac{1}{2}}$ .....(30)

SPRENGER and SCHMINDER (1969) also compared the Vc_s with Vc (by full-correlation method) and found a close correspondence in the two values.

Drift speed and directions were also calculated for each fade of a number of drift records for Thumba F-region and the results are given in the table I and II. It is noticed that the drift speed is rarely consistent and this variability of the drift of the pattern from one fade to another can arise either from the actual changes in the ionospheric drift or from the continuously changing

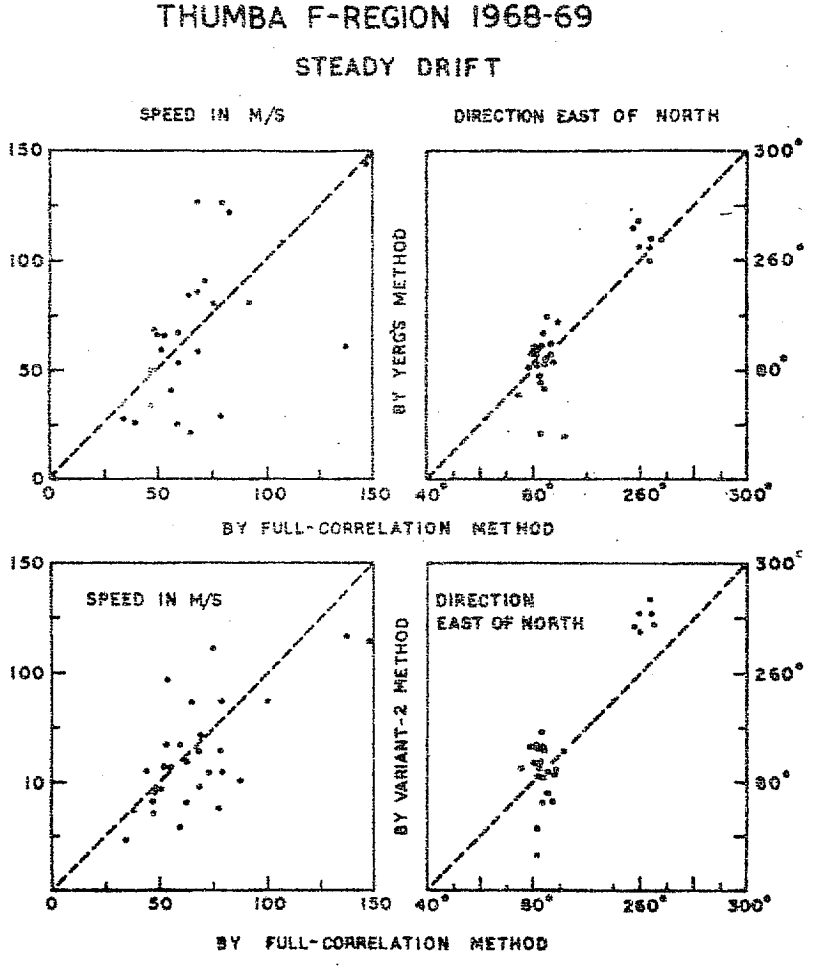

FIGURE 5.3

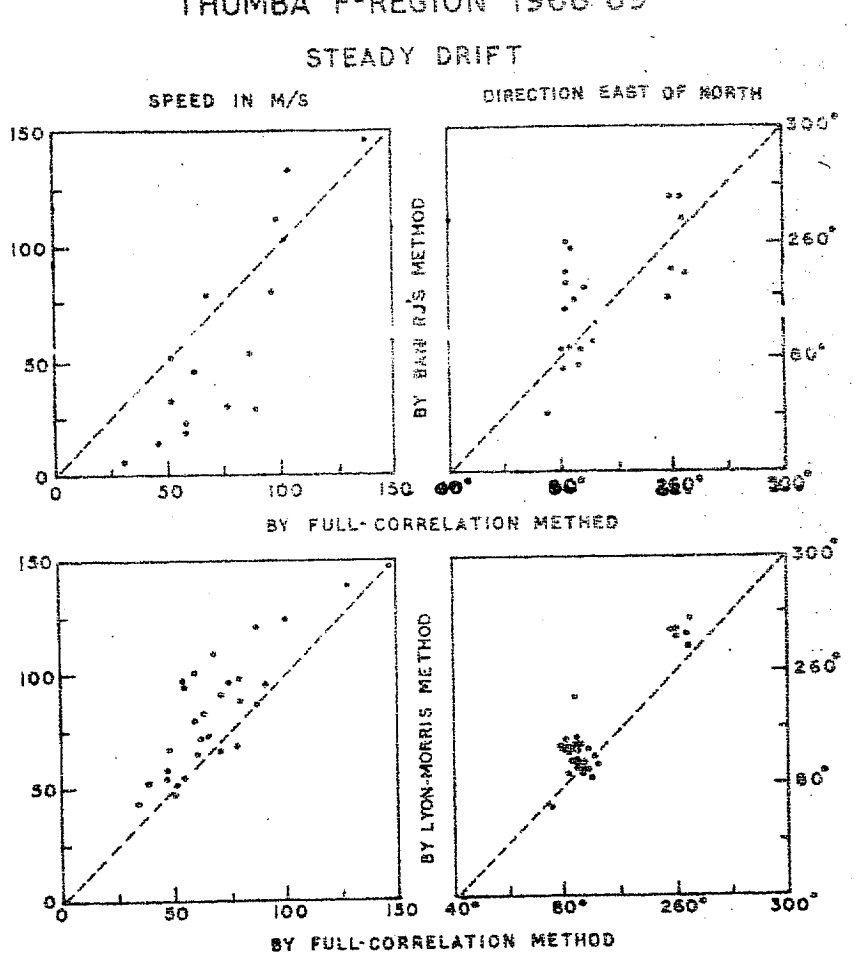

FIGURE 5.4

shape of the pattern. The direction Ø however does not vary much. The variant-2 method of determining average drift during the course of a record is therefore more accurate as it takes care of the changing drift directions also. KASHIN et al. (1970) have given the modified similar fades method when drift changes during the period of observation.

Fig.5.2b shows the comparision of the apparent drift calculated from the Mitra's method (Var-1) and the correlation peak method. The results are very smaller excepting some scatter of the points which can be accounted for by the presence of dispersion in the drift as discussed in Chapter VII (see 7).

Fig.5.3a compares the results for true drift speed V as determined by the full-correlation method and that by Yerg's six point correlation method. The correspondence is fairly good for the direction of drift while for the speed there is slight deviaton for the higher values of the drift speed. The main defects of Yerg's six point method lie in the choice of an arbitrary time lag $_i$. The method yields correct results (equal to those obtained by full-correlation analysis) for smaller values of $_i$, which corresponds to the near peak of the correlogram and hence is subject to less statistical variation.

Yerg's method also assumes a parabolic shape of the correlation function whereas the full correlation analysis of BRIGGS et al.(1950) assumes the contours of constant correlation to be similar concentric ellipsoids. This could result in a slight difference in the values estimated by two methods.

Fig.5.4 compares the V and Ø results of Banerji's method and the method of Lyon et al. to those of the full-correlation method. Though the statistical method of Lyon et al. yields fairly close values, the Banerji's method does not seem to be fully applicable for the equator as the values of both speed and direction are widely distributed around the 45° line. There is a tendency of getting slightly lower values for V. Lyon et al have modified their method for the case of equator by assuming that the characteristic ellipse is oriented along the magnetic lines of force. and then determined V and Ø. Banerji's method on the other hand first estimates the value of the tilt angle and then the value of V and Ø with the suitable corrections. A slight error in the estimation of can result in large change in the value of Ø and hence V. For Thumba, the ty values (along magnetic north-south) are negligibly small compared to tx and the value of B as well as C worked out to be nearly zero and the estimates of various parameters are not accurate.

Fig.5.5 compares the random drift parameter Vc as evaluated by four different methods, namely variant-2, Banerji's, Lyon-Morris and Yerg's with that from the full-correlation analysis. The variant-2 yields nearly the same values as full-correlation method and this has been discussed earlier in this Chapter alongwith the results of SPRENGER and SCHMINDER (1969). The values of Vc by Yerg's six point method deviate slightly for the high magnitudes and the limitations applicable to V also hold for Vc. The results of Banerji's method for Vc like those for V, are not in very good correlation with full-correlation analysis results. The effect of anisotropy does not seem to be removed completely from these values for a station like Thumba, where the pattern is highly anisotropic. The method of Lyon et al gives values of Vc closely agreeing with those of full-correlation values.

Fig.5.6 compares the anisotropy parameters of the ground diffraction pattern as derived by the Banerji's method and Lyon-Morris method, with those from the full-correlation method. Banerji's method yields mostly a lower value of axial ratio 'r' than the complete correlation analysis. The tilt angle ψ of the correlation ellipse is also fairly large in case of Banerji's method compared to full-correlation method. The Lyon-Morris method gives the 'r' values distributed equally on both sides of 45° line.

THUMBA F-REGION 1968-69

RANDOM DRIFT SPEED IN M/S

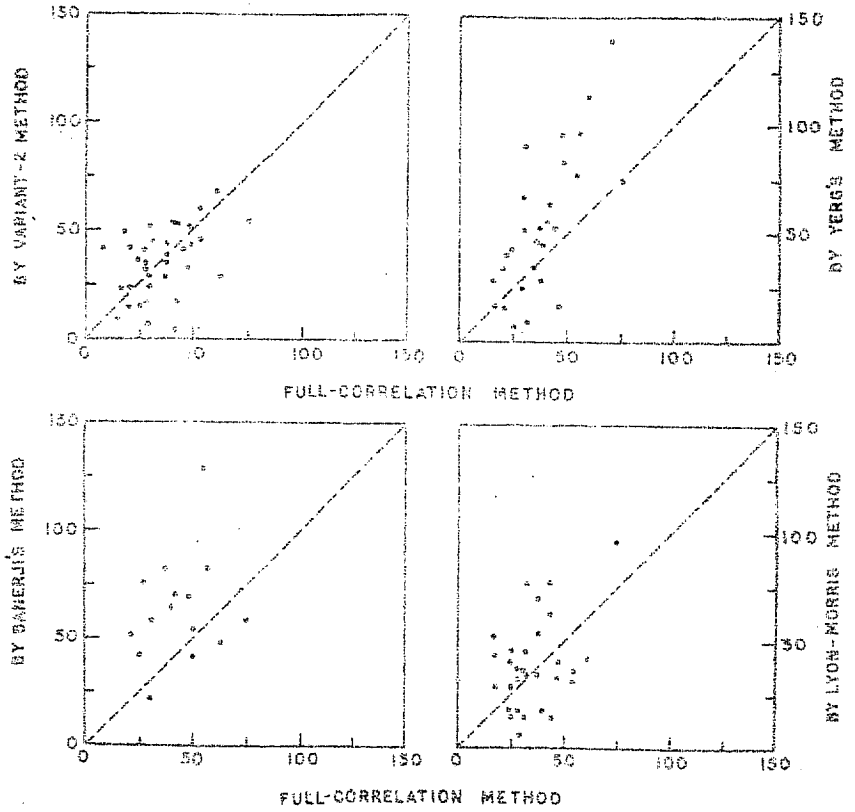

FIGURE 5.5

THUMBA F-REGION 1968-69

ANISOTROPY PARAMETERS

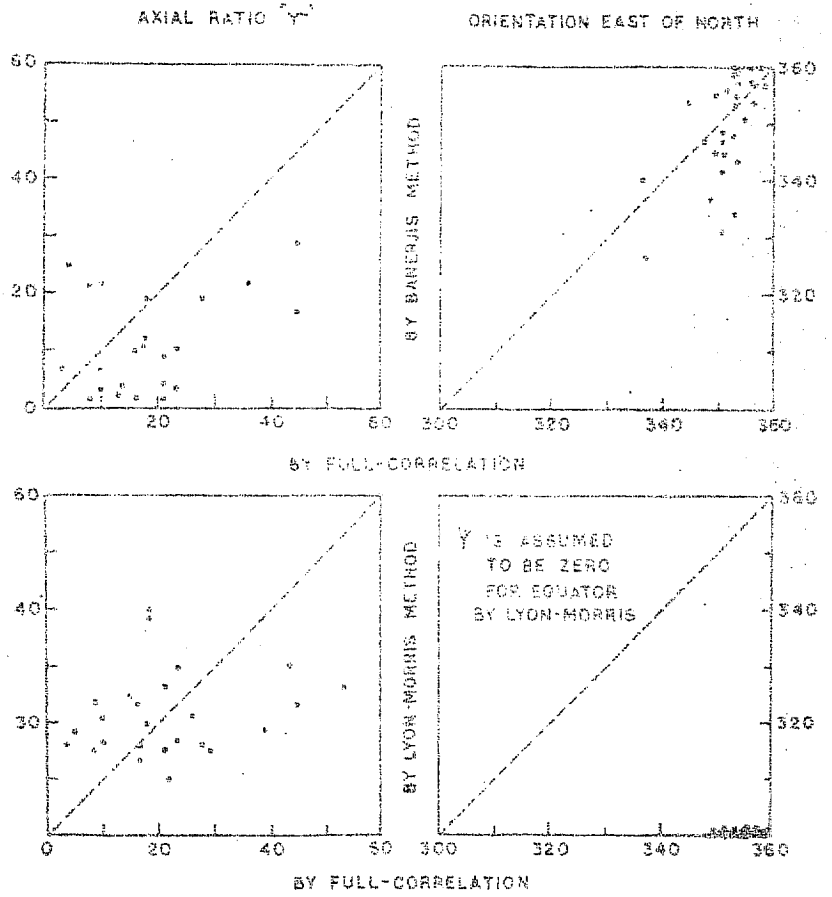

FIGURE 5.6

The tilt angle ψ is assumed to be zero for the equator in this method, which is more or less the case for Thumba.

The results of the three dimensional statistical correlation method suggested by FEDOR (1967) for a few cases at Thumba are summarized in the table No.III.

Conclusions:

The modified time delay method of LYON et al.(1969) offers a good substitute for full-correlation analysis for an equatorial station like Thumba when a complete knowledge of the ground diffraction pattern is to be obtained from the time shift values alone. The methods proposed by PUTTER (1955) and BANERJI (1958) fail completely for the equator due to extreme elongation of irregularities in magnetic N-S direction. Variant-2 offers a good substitute for full-correlation method when only the true drift parameters and the random drift is to be determined but not the anisotropy parameters. Both these methods, namely the Variant-2 and the Lyon-Morris method result in great saving of time and can be applied even in the absence of electronic computer. The method of Yerg, though simpler as far as the computations are concerned, does not result in any special reduction of labour as the fading records have still to be read completely for their amplitudes, as in

the full-correlation method. The values obtained by Yerg's method are however closest to those of the full -correlation technique. On the whole, full-correlation technique of drift analysis is the most accurate and should be used for regular reduction of drift data if the electronic computer is available.

Fedor's three dimensional correlation method is the most ideal and accurate method of analysis provided close frequency spaced antenna simultaneous records are available, as it takes into account the effect of the vertical drift component also.

Fade to fade variation of the drift velocity at Thumba during 1968-69
Drift speed in M/cs

Fade No.	8-1-69 21h	21-11-68 00h	16-11-68 00h	14-11-68 00h	19-12-68 00h	9-1-69 00h	26-11-68 04h	7-11-68 04h	20-2-68 04h	25-11-68 05h
1	300	200	150	240	200	120	200	299	120	240
2	300	200	143	200	239	86	200	239	120	300
3	300	200	135	200	239	86	300	240	299	240
4	240	300	107	200	200	100	240	200	100	400
5	240	199	107	171	200	100	300	200	200	240
6	240	200	150	200	171	86	240	200	150	300
7	300	300	115	199	200	75	240	-	200	300
8	240	200	150	200	171	86	200	240	150	240

Fade No.	7-11-68 06h.	19-2-68 09h.	8-1-69 16h	3-1-69 18h	18-11-68 21h	18-12-68 22h	25-11-68 23h	23-7-68 00h	24-8-68 00h	23-5-68 01h
1	150	300	170	171	200	171	120	200	171	199
2	240	300	240	240	200	200	150	200	150	150
3	299	300	299	150	150	200	171	171	171	100
4	200	300	200	200	171	206	133	199	150	148
5	240	300	200	240	171	200	133	171	133	150
6	300	300	299	150	150	240	120	199	133	100
7	200	300	171	200	200	200	133	200	150	100
8	239	300	239	200	171	200	133	200	150	120

Fade No.	14-5-68 02h	28-5-68 03h	6-7-68 09h.	21-6-68 10h	24-6-68 16h	26-8-68 22h	22-7-68 23h	6-4-68 00h	10-10-68 00h	16-10-68 01h
1	120	120	120	299	200	120	92	299	171	200
2	120	120	150	299	200	100	133	298	133	149
3	100	300	150	300	240	120	133	299	133	171
4	120	200	200	300	150	86	120	300	120	171
5	100	150	150	299	150	100	120	300	150	171
6	100	171	120	298	120	120	120	300	150	200
7	120	200	150	239	150	120	100	300	120	171
8	120	239	150	300	171	86	133	259	133	171

Table - I

Fade to fade variation of the drift direction at Thumba during 1968-69
Drift direction in degrees East of North

Fade No.	9-1-69 21h	21-11-68 00h	16-11-68 00h	14-11-68 00h	19-12-68 00h	9-1-69 00h	26-11-68 04h	7-11-68 04h	20-2-68 04h	25-11-68 05h
1	90	90	90	90	90	90	272	86	274	90
2	90	90	287	90	273	90	90	86	90	90
3	90	90	295	90	273	90	90	90	274	90
4	90	90	296	90	271	90	272	86	271	96
5	87	88	296	90	90	89	90	89	90	90
6	89	90	90	90	90	90	90	86	90	90
7	90	96	289	271	90	89	272	97	90	90
8	90	90	90	90	272	89	90	89	90	90

Fade No.	7-11-68 06h	19-2-68 09h	8-1-69 16h	3-1-69 18h	18-11-69 21h	18-12-68 22h	25-11-68 23h	23-7-68 00h	24-8-68 00h	23-5-68 01h
1	90	90	94	90	271	90	89	90	87	85
2	89	90	90	269	273	90	273	274	90	90
3	86	90	94	268	274	90	273	272	89	86
4	90	90	94	90	273	90	272	275	87	81
5	90	90	92	90	271	90	272	90	88	272
6	90	90	92	269	274	90	272	275	87	272
7	90	90	93	269	271	90	272	272	88	86
8	86	96	94	90	274	90	273	90	90	271

Fade No.	14-5-68 02h	28-5-68 03h	6-7-68 09h	21-6-68 10h	24-6-68 16h	26-8-68 22h	22-7-68 23h.	6-4-68 00h.	10-10-68 00h	16-10-68 01h
1	274	90	91	94	90	271	272	86	272	274
2	274	87	94	94	90	272	272	83	90	275
3	279	90	93	92	90	273	90	86	271	275
4	274	90	90	90	92	272	271	88	271	274
5	274	86	90	94	92	273	271	88	274	273
6	274	86	91	95	91	273	90	90	273	272
7	274	86	93	93	93	271	90	90	271	273
8	274	86	90	90	90	90	273	86	90	272

Table - II

Three dimensional drift and anisotropy parameters for Thumba E-region

Date & time	V_H	ϕ_H	V_z	ϕ_Z	V	V_c	d_1	d_2	d_3	α	ψ
13-5-68 2200hr	66.2	90°	15.0	178°	66.3	48.0	124	330	224	5.0°	8°
7-5-68 2200hr	80.0	89°	17.0	190°	73.0	39.5	130	500	203	5.0°	-4°
18-4-68 1815hr	76.3	268°	17.5	2°	67.8	30.2	90	350	150	-2.5°	5°
7-5-68 1800hr	71.5	271°	16.3	3°	61.8	25.4	155	700	120	-6.0°	7°
13-5-68 2100hr	60.8	92°	19.2	180°	50.7	29.0	98	450	143	0.0°	-2°
21-4-68 2000hr	79.5	88°	17.0	185°	70.6	40.3	132	350	110	7.0°	-6°
16-4-68 2000hr	135.0°	270°	15.0	5°	128.0	52.0	150	620	135	-4.0°	-5°

where V_H = Horizontal drift in M/s

ϕ_H = horizontal drift direction measured east of north.

V_z = Vertical drift in M/s

ϕ_Z = Vertical drift direction measured clockwise from vertical

V = total drift speed in M/s

V_c = Random drift speed

d_1 = semi-minor axis of characteristic ellipsoid in metres

d_2 = semi-major axis of characteristic ellipsoid in metres

d_3 = semi-vertical axis of characteristic ellipsoid in metres

α = tilt angle of third axis to the vertical

ψ = tilt angle of major axis to the magnetic N-S

Table - III

CHAPTER VI

ON THE SPECIAL FEATURES OF THE IONOSPHERIC DRIFTS

6.1 Height gradient of the horizontal drift and anisotropy parameters in E and F regions of the Ionosphere at Thumba

The height gradient of the apparent drift speed during day and night times for the F-region are described in paper attached at the end of this section. Some of these records were also subjected to full correlation analysis and these results are shown in table I. All the drift speed parameters, namely V_a, V', V and V_c are seen to decrease significantly with height. The drift directions ϕ_a and ϕ do not show any change with height. The axial ratio 'r' and size of irregularities 'b' are found to reduce at higher heights. The orientation of the characteristic ellipse 'ψ' is more perfectly aligned to magnetic north-south at lower heights.

As regards E-region, simultaneous spaced aerial fading records were taken at very close frequencies. Frequency of one transmitter was kept fixed at 2.4 Mc/s while that of the other was varied by 0.1 Mc/s for each set of records. A few such records are reproduced in Fig.6.1a. The apparent drift speed and direction for these cases are shown in Table II. No systematic variation of drift

Journal of Atmospheric and Terrestrial Physics, 1970, Vol. 32, pp. 967–969. Pergamon Press. Printed in Northern Ireland

SHORT PAPER

Height variation of F-region horizontal drifts

R. K. Misra and R. G. Rastogi
Physical Research Laboratory, Ahmedabad-9, India

(*Received* 3 *September* 1969)

Abstract—The speed of horizontal drifts in the F-region of the ionosphere over Thumba decreases with height; the gradient being larger during night-time than during the daytime.

F-region horizontal drifts on 4·7 MHz over Thumba have been measured since January 1964. With the addition of another transmitter in January 1968, it became possible to measure drifts on a number of frequencies. Observations were taken on F-region reflections of 2·3, 4·7 and 6·0 MHz, whenever conditions were favourable. The present note describes the variation of the apparent drift velocity with the height of the ionosphere. The true heights of reflection of the echoes on the three frequencies were calculated from the ionograms, obtained at the same time using matrix inversion method (Budden, 1954). The receiving system consisted of the antenna $E_{1/2}$, situated 60 m ($\frac{1}{2}\lambda$ for 2·5 MHz) east of the central antenna (C) and another antenna S_4, situated 480 m (4λ for 2·5 MHz) south of 'C'. The observations were taken at three frequencies in quick succession.

Figure 1 shows an example of fading records separately on three different frequencies. It was generally noticed that the fading was faster on higher frequencies, but the characteristic of high correlation between the fadings at the three aerials was maintained on any of the frequencies. It is seen from the fading records that the time shift between the aerials 'C' and '$E_{1/2}$' is significantly larger for 6·0 MHz than for 2·3 MHz.

Figure 2 shows the variation of the apparent drift speed with height for some observations during July 1968. It is clearly seen that during the night-time, drift decreased significantly with height. The gradient seems to be sharper at 250 km than at higher heights. The mean gradient was found to be 3·0 m/sec/km, during the night-time. During the daytime, the observations were confined between 150 and 250 km and the mean gradient was found to be much less, being 0·3 m/sec/km.

It is to be noticed that the F-region drifts at Thumba are invariably higher than the drifts in the E-region. Thus, there must be a region of maximum horizontal drift velocity somewhere in the lower part of the F-region.

Observations of ionospheric drift have been made by other workers on two or more frequencies. Yerg (1956) found that the average drift speed at Puerto Rico was 73 m/sec on 4·57 MHz and 92 m/sec at 2·33 MHz, which indicates a decrease of speed with height. Rao and Rao (1961) observed F-region drifts on 4·2–4·8 MHz and 6·0 MHz at Waltair and found the most frequent drift speed to be 75 m/sec for $F1$-region and 85 m/sec for $F2$-region. They found the $F2$-region drift speeds to be generally higher than the $F1$-region drift speed, when measured simultaneously.

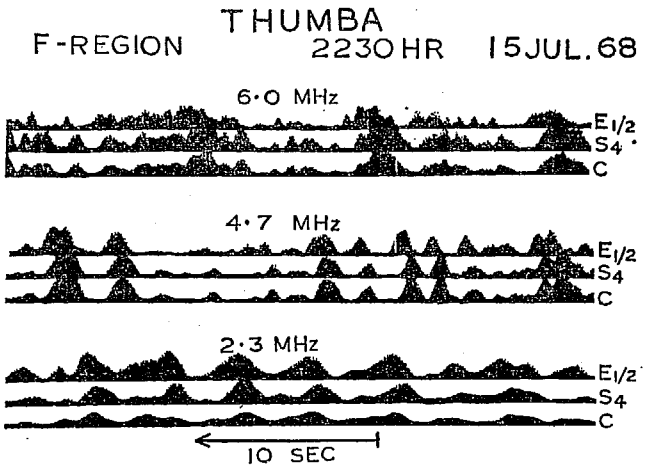

Fig. 1. Fading records on three different aerials of echoes on 2·3, 4·7 and 6·0 MHz at Thumba.

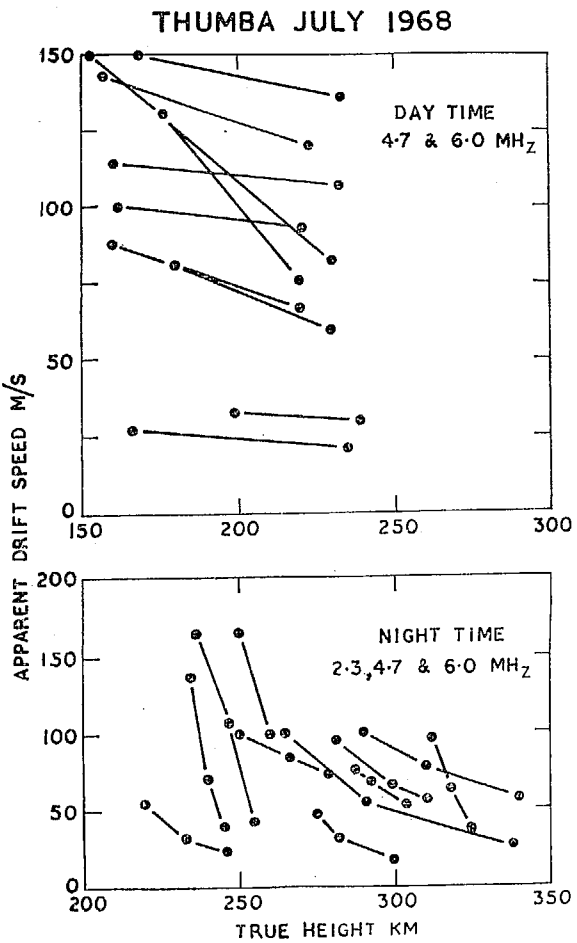

Fig. 2. Apparent drift speeds at different heights of reflection on individual observations.

Rao and Ramana (1961) discussed the drift at different heights taken during the daytime from 0800 to 1100 hr (for heights between 105 and 360 km). They found that the drift speed at first decreases with height, suddenly increases at a height of about 280 km and then fluctuates; the height gradient being about 0·7 m/sec/km. The present observations indicate that at the equatorial stations, the drift speed decreases with height during the day as well as during night-time. Observations are being continued to study the variation of drift characteristics with height.

Acknowledgements—Thanks are due to Indian National Committee of Space Research for the facilities of the experiment at Thumba Equatorial Rocket Launching Station and to the other colleagues at Thumba Equatorial Rocket Launching Station and Space Science and Technology Centre, Trivandrum, for their cooperation.

References

Budden K.G. 1954 *Rep. Camb. Conf. Ionosph. Phys.*, p. 332 *Phys. Soc. Lond.*

Rao B. R. and Ramana K. V. V. 1961 *Proc. IGY-Symp., New Delhi*, Vol. 1, p. 80 CSIR, New Delhi.

Rao Bhagirath and Rao B. R. 1961 *J. Br. Instn. Radio Engrs* **22**, 507.

Yerg D. G. 1956 *J. Atmosph. Terr. Phys.* **8**, 247.

Height variation of drift and the anisotropy parameters for Thumba, 1968

Date & Time	V_a M/s	V' M/s	V M/s	V_c M/s	V_c/V	ϕ_a East of North	ϕ East of North.	r	ψ East of North.	b in M	Frequency used IN Mc/s
13th Aug	85	86	13	31	2.34	267	252	7.07	342	92	6.0F
0800 hr.	149	149	44	68	1.53	265	259	19.71	349	81	4.7F
3rd May	128	129	70	64	0.91	266	258	19.16	348	101	6.0F
1700 hr	180	182	149	80	1.64	270	261	18.01	351	170	4.7F
17th July	49	50	38	21	0.56	85	78	15.95	348	236	4.7F
2000 hr.	291	291	30	89	2.92	82	82	7.13	352	385	6.0F
15th July	178	178	78	65	2.29	81	82	26.24	352	97	2.3F
2200 hr.	78	78	64	30	0.47	88	81	18.58	351	161	4.7F
5th July	85	88	24	39	1.61	86	71	10.05	341	83	4.7F
2300 hr	99	99	36	47	1.32	85	89	18.35	359	119	2.3F

Table - I

Time 5 AUG 68	V' in M/s		Ø' in degree east of north	
	Fixed freq.	Variable freq.	Fixed freq.	Variable freq.
1700 hr.	160 (2.4 MHz)	100 (2.3 MHz)	240°(2.4 MHz)	270°(2.3 MHz)
1702 hr.	120 (2.4 MHz)	85 (2.2 MHz)	270° (2.4 MHz)	269°(2.2 MHz)
1704 hr	135 (2.4 MHz)	60 (2.1 MHz)	269° (2.4 MHz)	290°(2.1 MHz)
1706 hr.	140 (2.4 MHz)	100 (2.0 MHz)	250°(2.4 MHz)	269 (2.0 MHz)

Table - II

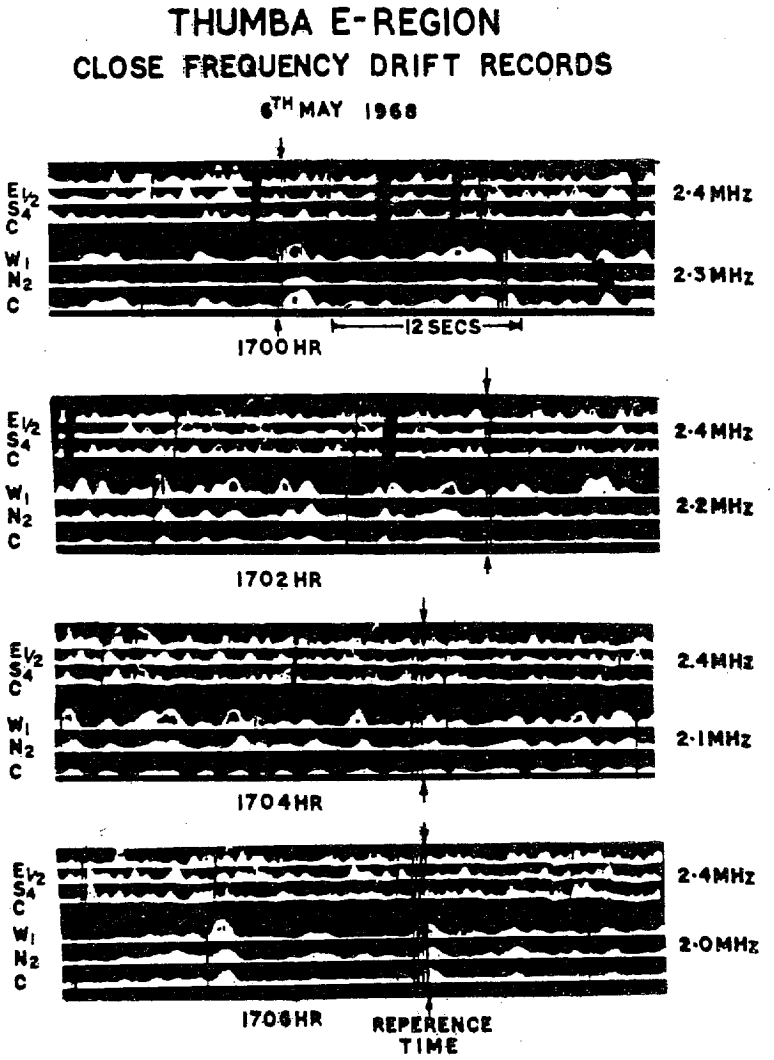

Figure 6.1a

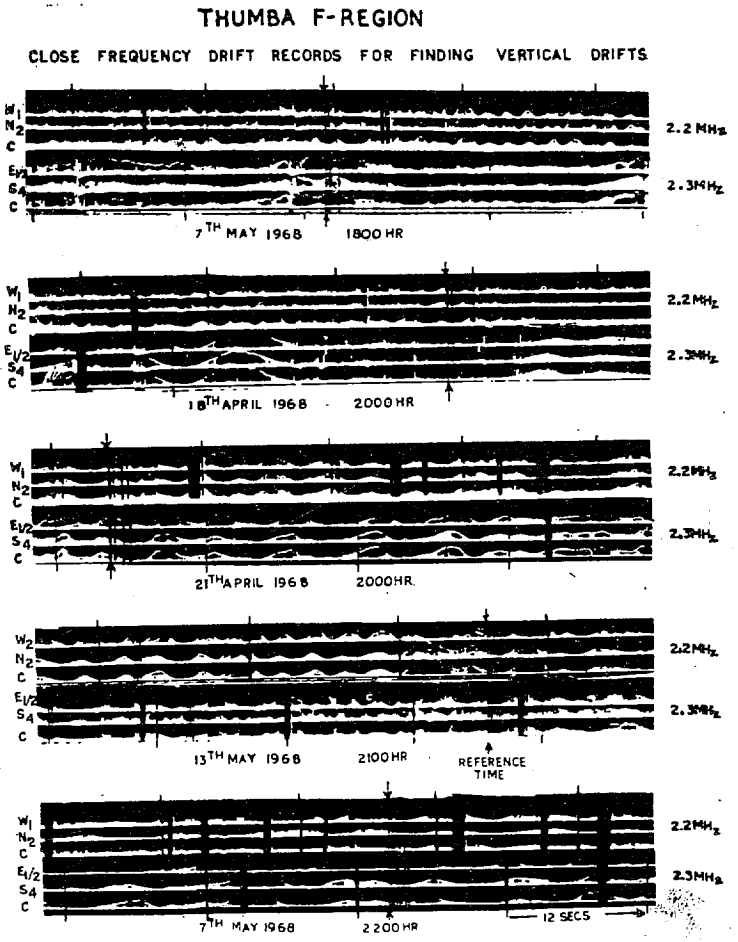

Figure 6.1b

is seen with the increasing frequency separation. RAO and RAMANNA (1961) have shown for Waltair that both r and V_c/V decrease with height from 100 km to 180 km after which there is a sudden increase around 280 km in their values. Between 280 km to 380 km, the values of 'r' and V_c/V fall off sharply.

6.2 Vertical ionospheric drift in E and F regions at Thumba

(a) Introduction

Existence of vertical movement of ionization in the F-region at the equator have been known indirectly for many years. The first direct measurement of vertical drift of ionization in F-region was reported by WOODMAN and HAGFORS (1968) for Jicamarca (2°N dip). RASTOGI (1970) reported the upward drift of the order of 17 m/sec in F-region over Thumba, using the upward moving kinks on the ionograms during daytime.

Based on the close frequency technique suggested by WRIGHT and FEDOR (1969), direct measurement of vertical drift in F-region over Thumba was made in 1968. The basic idea lies in correlating the fading records obtained at two closely spaced frequencies. So long as the vertical separation of the points of reflection of the two closely spaced frequencies is of the order of a wavelength used,

one expects to get a significant correlation between two fading records, for a certain time-lag Δt which is a measure of the vertical drift velocity.

(b) Experimental technique

After the installation of a new drift equipment at Thumba in January 1968, two independent sets of horizontal drift measuring units were available each of which consisted of three channel recording units and transmitters in the range of 2 to 6 MHz. The regular drift observations at Thumba have been made using one of the systems, operated at 2.3 MHz for E-region echoes in the day and F-region echoes in the night. The receiving aerial system for Thumba is shown in Fig.1.14. The triangle E_1S_4C was used for these observations. The other drift unit was operated at a closely spaced frequency of 2.2 MHz and the aerial system W_1N_2C was used. Two independent central aerials 'C' were erected at the same place to be used for the two frequencies in order to avoid the cross-modulation of the two signals at closely spaced frequencies. The recording of the horizontal drifts was then possible at both 2.3 MHz and 2.2 MHz. By running both the equipments simultaneously, it was possible to record the horizontal drifts at two reflection levels at exactly the same instant of time.

CORRELOGRAMS FOR HORIZONTAL AND VERTICAL DRIFTS AT THUMBA

F - REGION

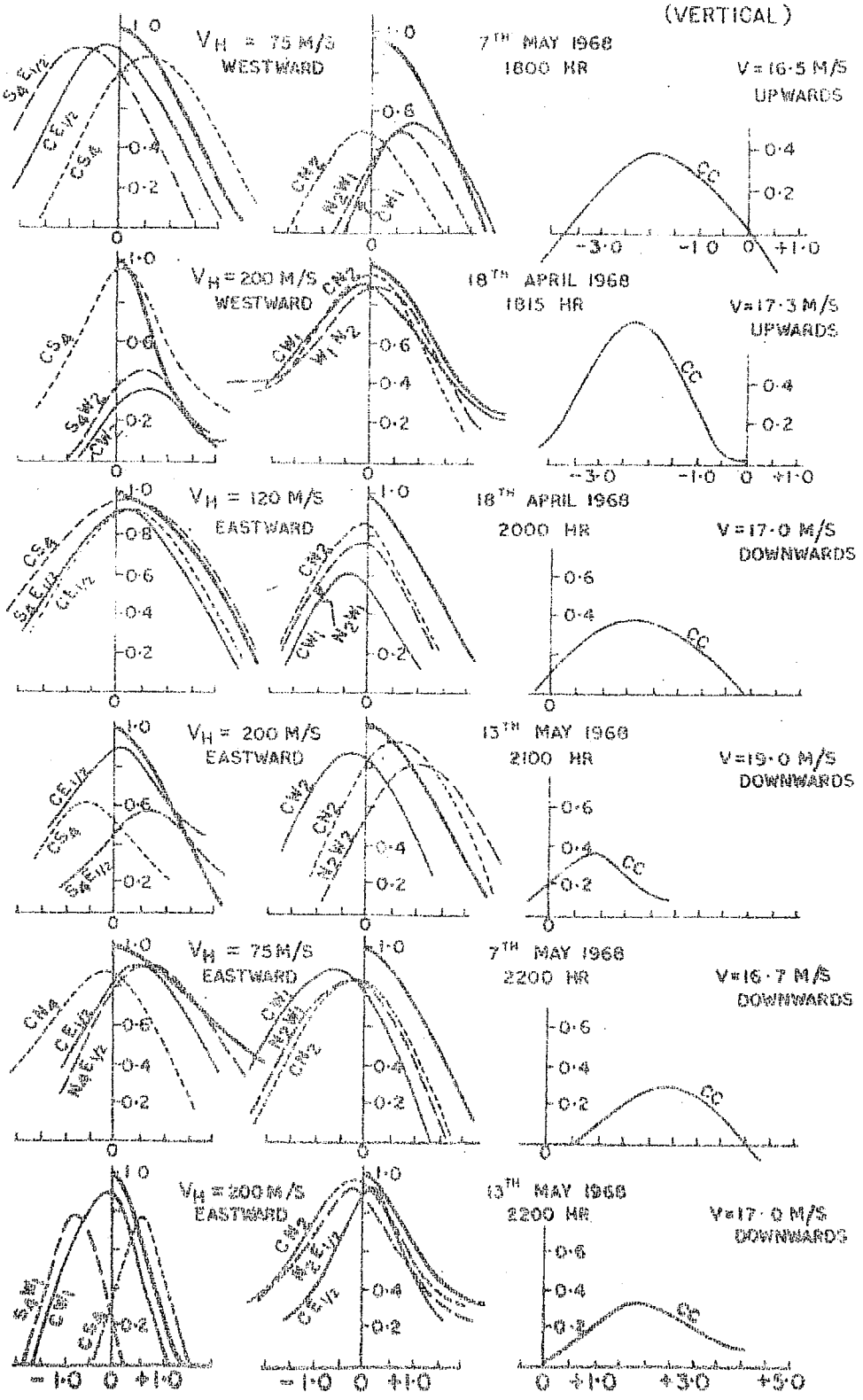

FIGURE . 6.2a

The two recording cameras were similar and their film speeds were matched to the nearest possible by suitable gear adjustment. Common time marking circuit was linked to both the recording oscilloscopes and reference time signals were given at the beginning of the records apart from the usual 12 secs time marks. The records were finally projected and traced on the same scale side by side. A few such records are shown in Fig.6.1a and 6.1b for E and F-regions alongwith their specifications.

(c) Method of analysis

These records were analysed for determining the horizontal drifts at 2.2 MHz and 2.3 MHz from the shift of the maxima of the cross-correlograms. The mean apparent horizontal drift V_H at the mean height of reflection for 2.2 and 2.3 MHz was then determined. These correlograms and the mean V_H values along with their directions for the F-region are shown on the left hand side of Fig.6.2a. The fading records at the two central aerials were also correlated for the vertical drifts. These correlograms are shown on the right-hand side of the same figure. Ionograms corresponding to these times of observation were obtained from the vertical ionosonde operating at the same location (Thumba). These were subjected to true height reduction and the change of true height ' $\triangle$ h' corresponding to

THUMBA E-REGION

MULTI FREQUENCY CORRELOGRAM

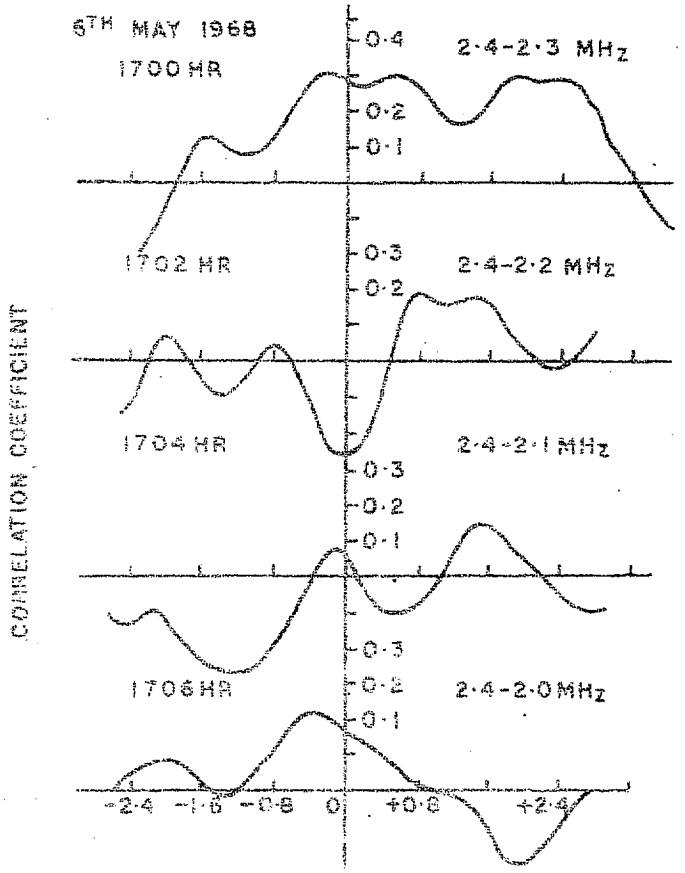

FIGURE . 6.2b

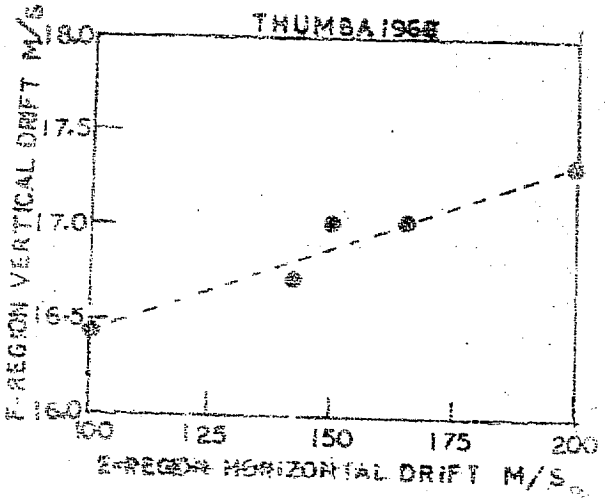

FIGURE 6.3

a frequency difference Δf = 0.1 MHz was determined from the slope true N-h profile. This difference of height Δh was divided by the time-lag Δt corresponding to the maxima of the cross-correlograms between two frequency fading records, to obtain the vertical drift in the F-region between 250 - 300 Km. Similar experiment was also performed for the E-region at Thumba. The close frequency cross-correlograms for this are shown in Fig.6.2b. It was noticed that the maximum correlation was not significant showing that the change in the height of reflection is much more than a wavelength. This technique therefore could not be applied to E-region at Thumba.

(d) Results

Table III gives vertical drift in F-region along with the simultaneous E and F region horizontal drift. The interrelation of F-region vertical drift speed and E-region horizontal drift speed is shown in Fig.6.3. It is seen from these results that the F-region vertical drift is downward when the F-region horizontal drift is eastward and upwards when the horizontal drift is westward. It is also seen that the F-region vertical drift is proportional to the E-region horizontal drift. These results are in verification to the predictions of Martyn's theory of electromagnetic drift (see Chapter I).

S.No.	Date and time.	F-region vertical drift		F-region horizontal drift		E-region horizontal drift	
		speed m/s	Direction	Speed m/s	Direction east of north.	Speed m/s	Direction east of north.
1	7 May 1968, 1800 hr.	16.5	Up.	75	270°	100	270°
2	18 April 1968, 1815 hr.	17.3	Up.	200	270°	200	270°
3	18 April 1968, 2000 hr.	17.0	Down	120	90°	-	-
4	21 April 1968, 2000 hr.	19.0	Down	-	90°	-	-
5	13 May 1968, 2100 hr.	19.0	Down	200	90°	-	-
6	7 May 1968, 2200 hr.	16.7	Down	75	90°	142	90°
7	13 May 1968, 2200 hr.	17.0	Down	200	90°	150	90°

Table - III

6.3 Reversal of drift direction at Thumba

(a) Introduction and observations schedule

The diurnal behaviour of estward and northward horizontal drifts in E and F regions at Thumba has been discussed in detail in Chapter II and III. It is noticed from these results that ionospheric drifts are predominently westward during day and eastward during night hours. The morning and evening changeover timings seem to lie between 0600 - 0730 hrs IST and 1930 - 2100 hrs IST respectively. The routine F-region drift observations at Thumba have been made at hourly intervals over the entire period of the day for every alternative day since 1967. This was however not possible for E-region owing to its rare appearance at Thumba in the night hours. This schedule of observation however was found to be insufficient to get an exact picture as to how does the drift vector changes over from east to west in the morning and from west to east in the evening. The hourly observations showed a complete reversal from one hour to another and it was not definite whether it is truely so or the drift vector swears around slowly with time, going through north or south before coming back to east-west line. With this in view, an extensive series of drift observations at fifteen minutes interval were conducted in 1968 around

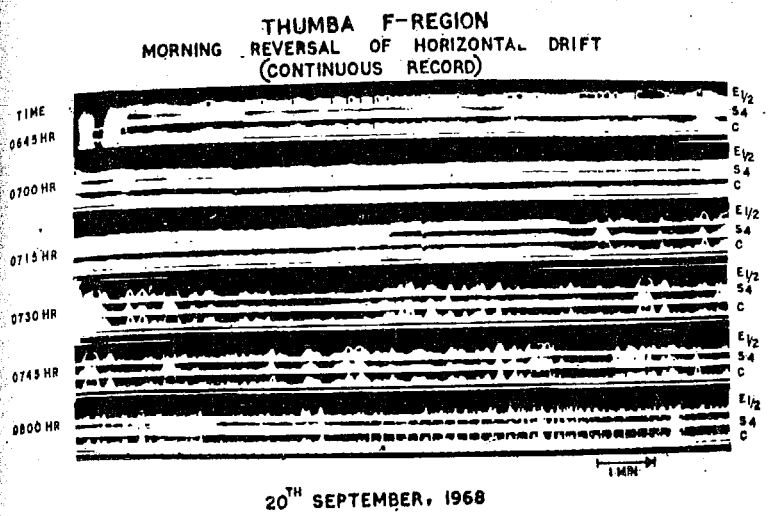

20TH SEPTEMBER, 1968

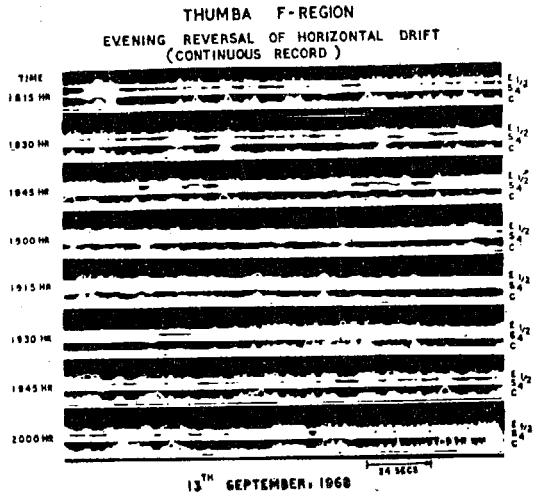

13TH SEPTEMBER, 1968

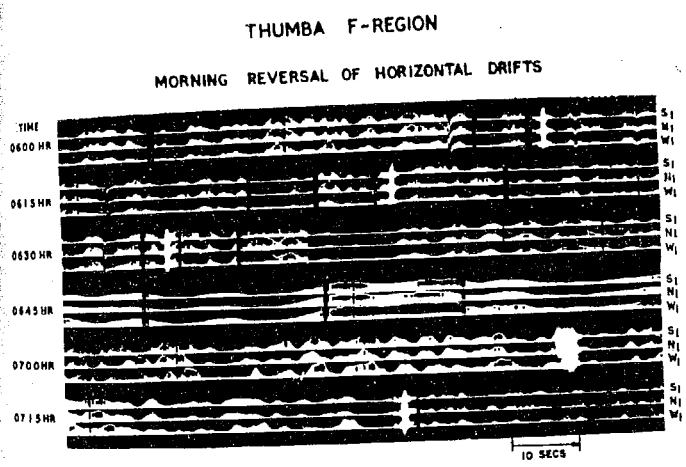

13TH JANUARY, 1968

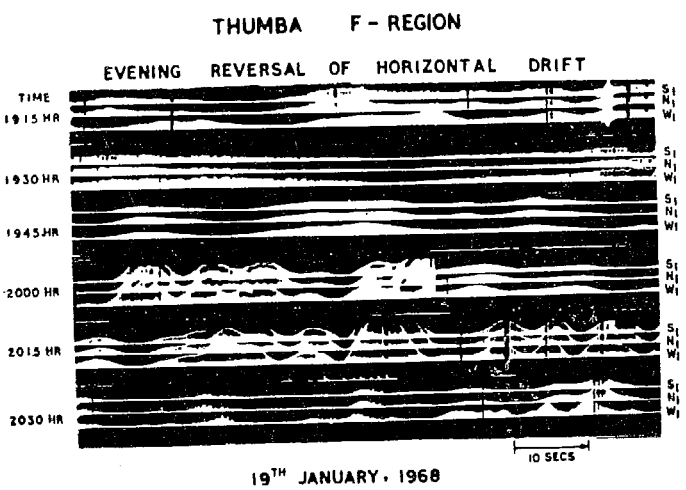

19TH JANUARY, 1968

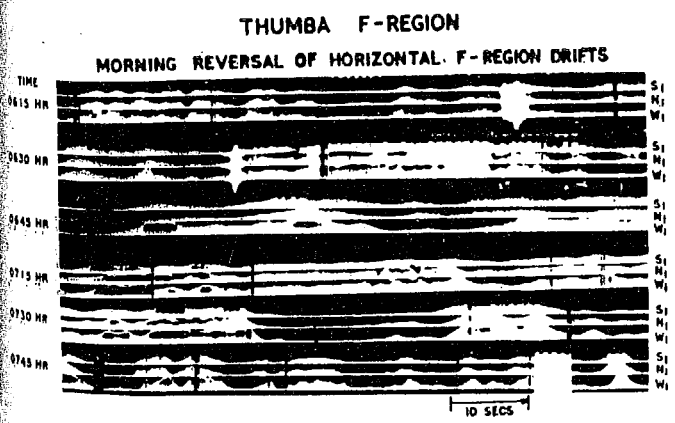

11TH JANUARY, 1968

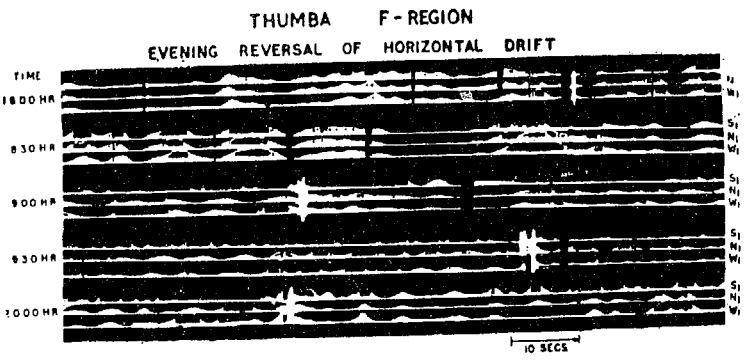

18TH JANUARY, 1968

Figure 6.5

the morning and evening reversal timings. These were spread over a period of one hour before to one hour after the reversal. A few records were also taken continuously for two hours or more around the reversal times, so that a fade to fade variation of drift vector could be obtained for the whole period. A set of few such records for F-region are reproduced in Fig.6.5. The top two are the continuously run records. Such a study was not possible for E-region owing to its rare appearance in the early morning and late in the evening. A few such cases were however available and are under study.

(b) Rate of fading and drift vector around reversal

The rate of fading 'N' and the apparent drift speed and direction were computed (MITRA, 1949) for all these [illegible] records at the short intervals of time. These results are listed in Table IVa and IVb. The symbol S stands for a very slow fading, during which the method of similar fades fails and drift parameters cannot be determined. The variation of N around the morning and evening reversal times is shown in Fig.6.6, and the vector plot for the drift speed is shown in Fig.6.7. It is seen that the fading of the echo becomes very slow around the time of the reversal of direction. The drift vector changes over from east to west or vice versa, more or less suddenly.

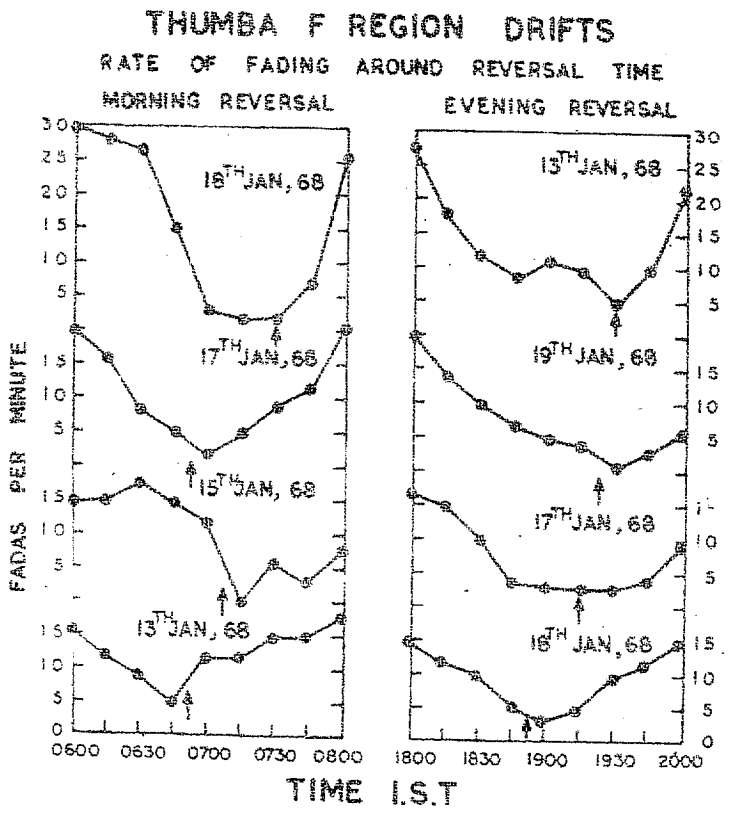

FIGURE 6.6

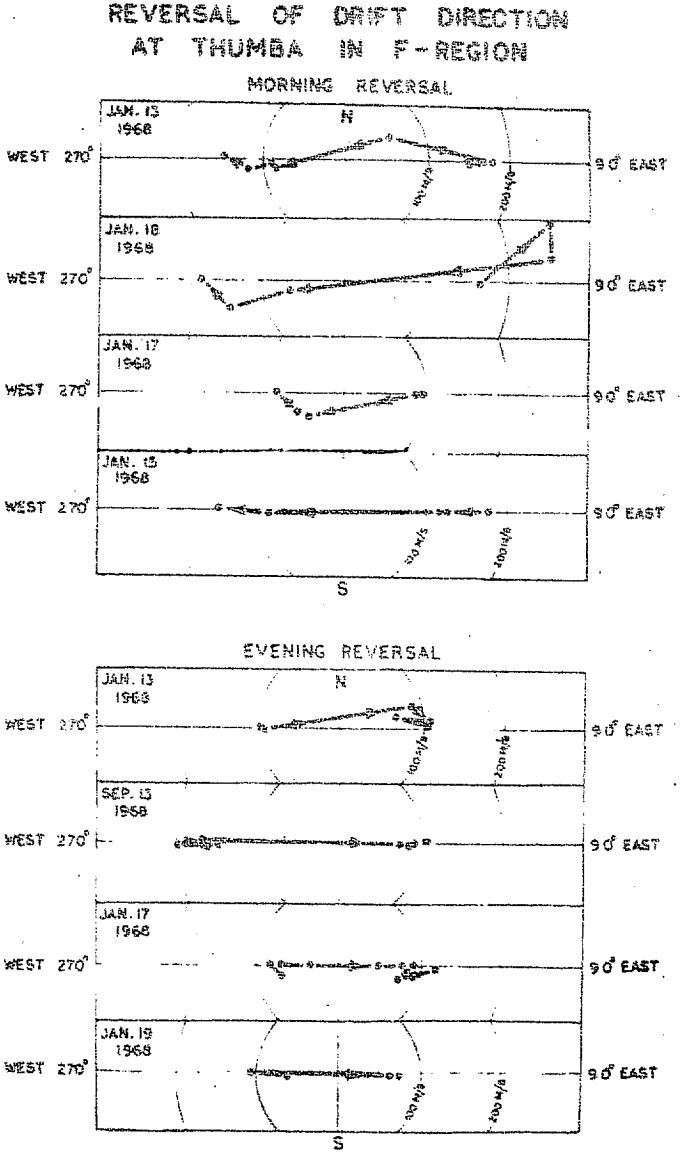

FIGURE 6.7

Apparent drift speed and direction

MORNING REVERSAL

Date/hour (IST)		0600hr	0615hr	0630hr	0645hr	0700hr	0715hr	0730hr	0745hr	0800hr
13th Jan.68	V'	150M/s	150 M/s	180M/s	60M/s	S	86M/s	86M/s	120M/s	150M/s
	Ø'	90°	90°	90°	64°	S	261°	263°	262°	270°
15th Jan.68	V'	180M/s	S	S	130M/s	S	120M/s	90M/s	150M/s	180M/s
	Ø'	90°	S	S	90°	S	90°	268°	269°	255°
17th Jan.68	V'	95M/s	90M/s	S	S	50M/s	60M/s	82M/s	75M/s	82M/s
	Ø'	90°	90°	S	S	235°	248°	270°	251°	268°
18th Jan.68	V'	162M/s		200M/s	200M/s	S	S	70M/s	S	144M/s
	Ø'	90°		73°	83°	S	S	60°	270°	256°

EVENING REVERSAL

Date/hour (IST)		1800hr	1815hr	1830hr	1845hr	1900hr	1915hr	1930hr	1945hr	2000hr
13th Sept.68	V'		150M/s	200M/s		170M/s		90M/s	85M/s	75M/s
	Ø'		268°	268°		269°		92°	93°	91°
17th Jan.68	V'	73M/s	72M/s	85M/s	36M/s	38M/s	S	50M/s	S	78M/s
	Ø'	259°	270°	270°	270°	270°	S	90°	S	90°
19th Jan.68	V'	60M/s	106M/s	S	S	S	S	66M/s	48M/s	78M/s
	Ø'	269°	270°	S	270°	S	270°	90°	90°	90°
13th Jan.68	V'	97M/s		95M/s		90M/s	106M/s	65M/s	106M/s	
	Ø'	269		268°		74°	90°	76°	88°	

Table -IV.a

Rate of fading

(Morning Reversal)

Date/Hour(IST)	0600hr	0615hr	0630hr	0645hr	0700hr	0715hr	0730hr	0745hr	0800 hr
13th Jan. 68	16	12	9	5	12	12	15	15	18
15th Jan.68	15	15	18	15	12	0	6	3	8
17th Jan.68	20	16	8	5	2	5	9	12	21
18th Jan.68	30	28	27	15	3	2	2	7	26

(Evening Reversal)

Date/hour(IST)	1800hr	1815hr	1830hr	1845hr	1900hr	1915hr	1930hr	1945hr	2000hr
13th Jan.68	30	15	10	12	14	12	5	12	22
17th Jan.68	17	15	10	4	3	3	3	4	2
19th Jan.68	20	14	10	7	5	4	1	3	6
13th Jan.68	15	12	10	5	3	5	10	12	15

Table - IV.b

(c) Morning reversal and the size of irregularities

Both E and F-region morning reversal timings are well correlated with the maxima of the semi-minor axis of the characteristic ellipse at Thumba (see Fig.3.18 and 3,19). As the axial ratio in the early morning is very small, the irregularities are very much isometric at this time. The orientation of the irregularities being magnetic north-south, the morning reversal of the drift coincides with the maximum east-west dimension of the irregularities.

(d) Evening reversal and height of the E-layer

It was noticed from the day to day observations that the time of evening reversal usually occurs when the F-layer is at maximum height. The relationshipbetween h'F and the E-W drift speed in F-region at Thumba is shown in Fig.6.8 for each season of the year 1967 separately. The dotted line shows the time of evening reversal. The layer height h'F is maximum at this time both in winter and equinoxes. During summer season the reversal of drift occurs earlier and the h'F peak is not very pronounced.

(e) Reversal of drift in F-region and the appearance and disappearance of sporadic E-layer

Fig.6.9 shows the appearance and disappearance times for E_s at Thumba in relation to the times of morning and evening reversals of the F-region horizontal drift.

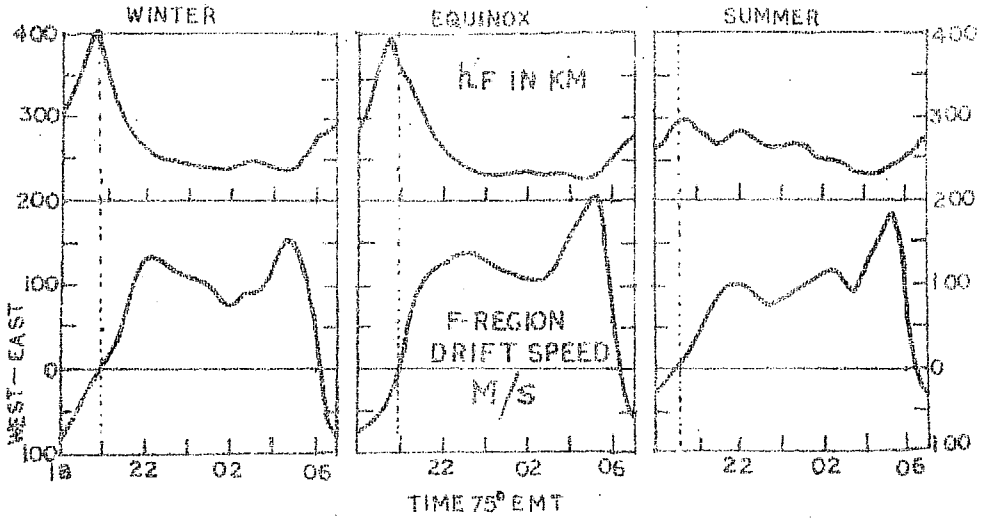

FIGURE 6.8

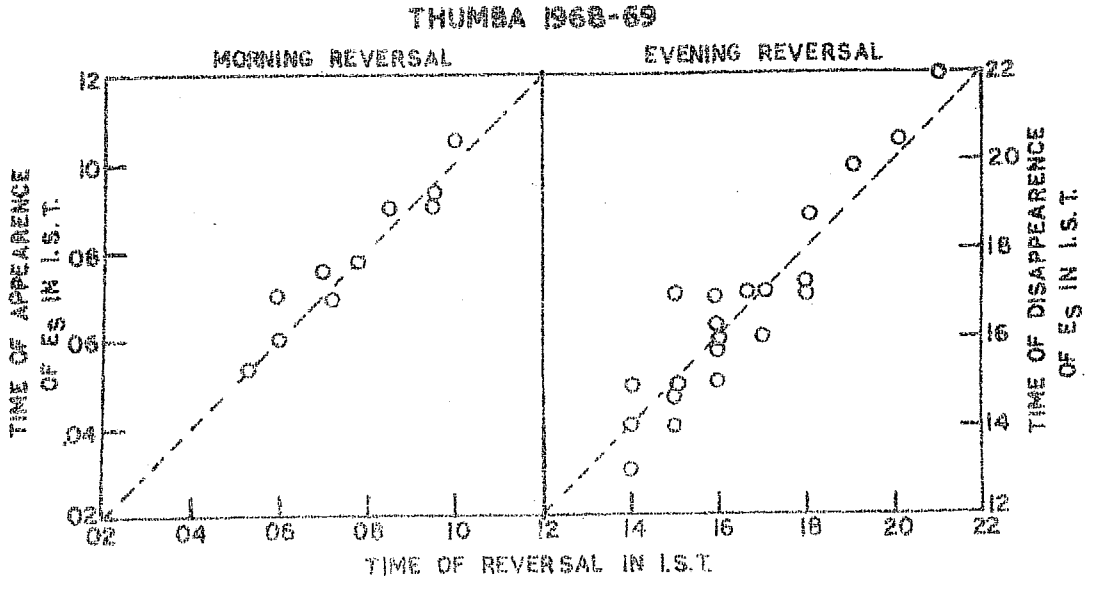

FIGURE 6.9

It is seen that the E_s is present only when the drift is westward. On the days of late morning reversal of the drift in F-region, E_s also appears late while on the days when F-region drift is westward till late hours in the evening, the E_s ionization is seen to exist. The electrojet control of drift in F-region is already discussed in paper No.7 of Chapter IV. On the other hand the occurrence of the equatorial sporadic-E has also been shown to be controlled by the equatorial electrojet (MATSUSHITA, 1962, KNECHT and MCDUFFIE, 1962). The relationship between the direction of the F-region horizontal drift and the occurrence of E_s is therefore linked through the electrojet.

(f) Reversal of drift and short-term fluctuations in H

As discussed in Sec. 4.6 of Chapter IV and shown in Figs. 4.11 and 4.12, the horizontal drift in both E and F regions is found to be reversed when the H value falls down below the normal expected level. The sporadic E ionization is also found to disappear during this period (RASTOGI et al. 1971).

(g) Conclusions

It can be concluded from the foregoing results that the drifts are mainly controlled by the electric fields, resulting in a sudden reversal of drift vector. Also, at the time of morning reversal, the transverse

size of irregularities is largest and at the time of evening reversal the height of the F-layer is highest. The relationship between E_s and drift direction further confirms that electric fields are responsible for the drift.

6.4 Drift and anisotropy parameters at Thumba during spread-F conditions

(a) Introduction

SPREAD-F at Thumba (0.6°S) is predominently a night-time phenomenon and increases with increasing solar activity (HARISH, 1971). The year 1968-69 was therefore specially suited for the study of the characteristics of the fading of the signal reflected from the F-region of the disturbed ionosphere i.e. the spread-F. The drift and anisotropy parameters of the ground diffraction pattern can also be studied at the same-time by using closely spaced fading records on the ground. A special series of observations was therefore planned during 1968-69 so that a sufficient number of records at the onset and during the existence of spread-F could be collected. Spread-F at Thumba usually started at 1900 hr and the rise of the F-lyer on these days was unusually large. This was one indication of the likely occurrence of spread-F on a particular night and the drift observations on such nights were conducted till the spread-F lasted. Mostly it died out by 22 to 23 hr but there were a few days on which it continued for the

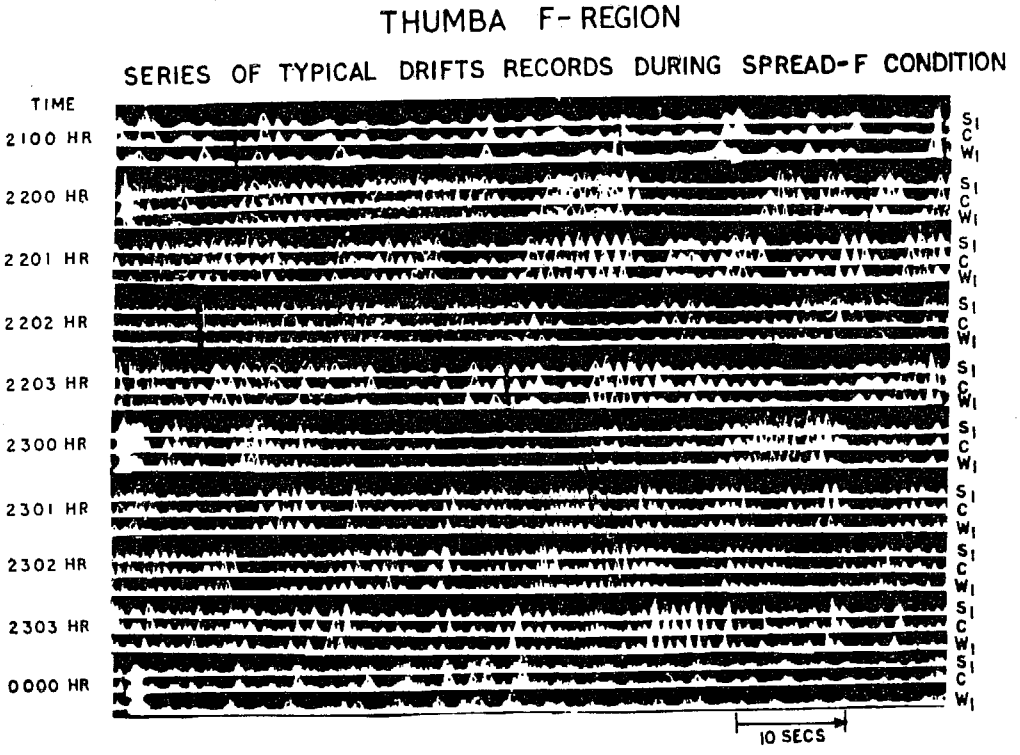
THUMBA F- REGION
SERIES OF TYPICAL DRIFTS RECORDS DURING SPREAD-F CONDITION
TIME
2100 HR
2200 HR
2201 HR
2202 HR
2203 HR
2300 HR
2301 HR
2302 HR
2303 HR
0000 HR
S
C
W
10 SECS
25TH NOVEMBER, 1967, 4·7 MHz

Figure 6.10

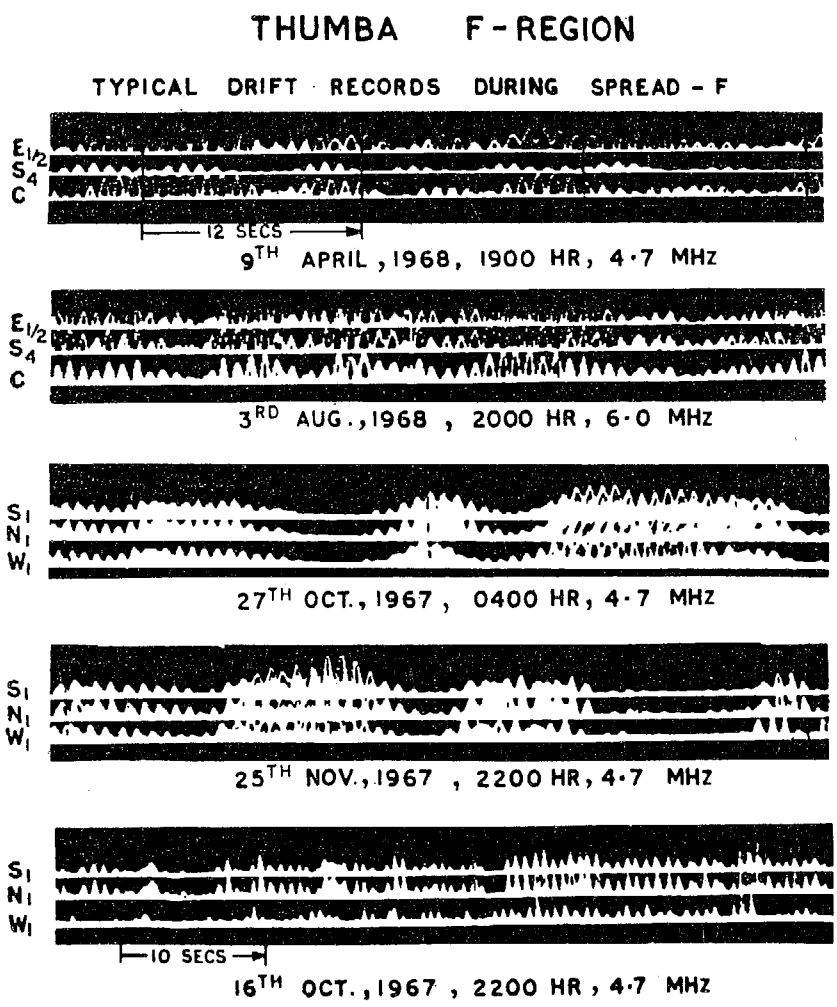
THUMBA F-REGION
TYPICAL DRIFT RECORDS DURING SPREAD - F
E1/2
S4
C
12 SECS
9TH APRIL, 1968, 1900 HR, 4·7 MHz
E1/2
S4
C
3RD AUG., 1968, 2000 HR, 6·0 MHz
S1
N1
W1
27TH OCT., 1967, 0400 HR, 4·7 MHz
S1
N1
W1
25TH NOV., 1967, 2200 HR, 4·7 MHz
S1
N1
W1
10 SECS
16TH OCT., 1967, 2200 HR, 4·7 MHz

Figure 6.11

whole night till 06 hr. All recordings were performed on the leading edge of the spread-F echo by reducing the width of the gating pulse to as small as possible. The slant echoes are thus avoided as far as possible.

(b) Fading characteristics during spread-F

A few continuous drift records were taken from the onset to disappearance of spread-F. One such record is reproduced in Fig.6.10. A number of isolated drift records during Spread-F conditions are shown in Fig.6.11. The very prominent and important feature of these fading records was the presence of a super-imposed fast fading over the normal slow fading of the signal, appropriate to the evening time on no-spread days. A few such records were analysed for the cross-power spectrum and the drift spectrum using JONES and MAUDE (1968) relations. The results for one such case are shown in Fig.6.12. Presence of two distinct fading frequencies centred at about 0.5 c/s (i.e. 38 fades/minute) and 1.4 c/s (i.e. 84 fades/minute) is prominent. The first peak corresponds to normal fading rate at 1900 hr at this time of the day while the second peak corresponds to ripples of fast fading, the special feature of spread-F echoes.

The variation of the apparent drift speed with fading frequency is shown by the thick line. The dotted

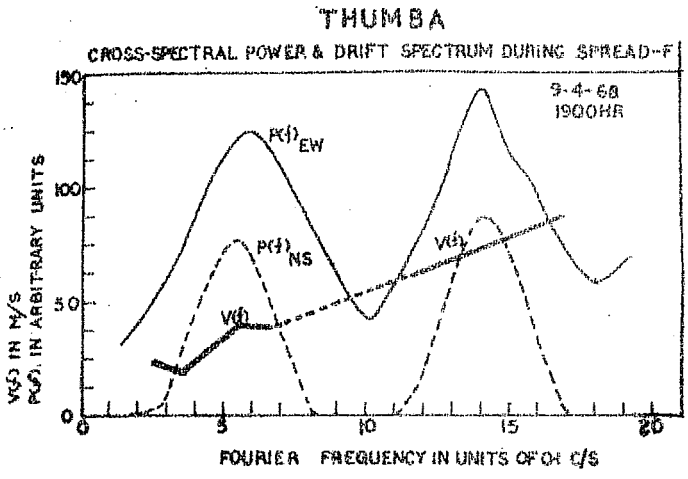

FIGURE 6.12

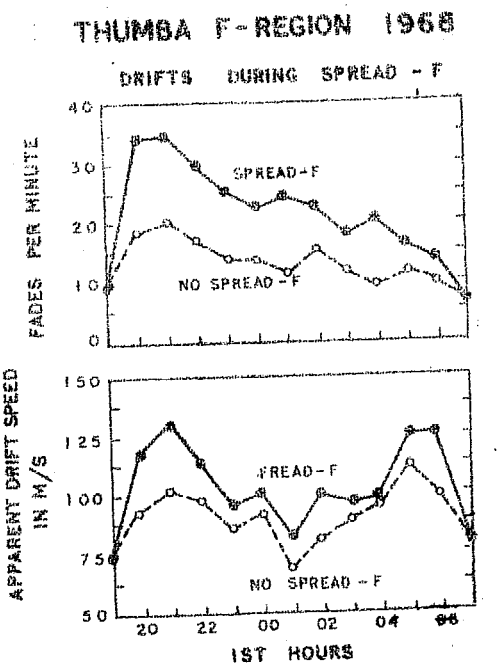

FIGURE 6.13

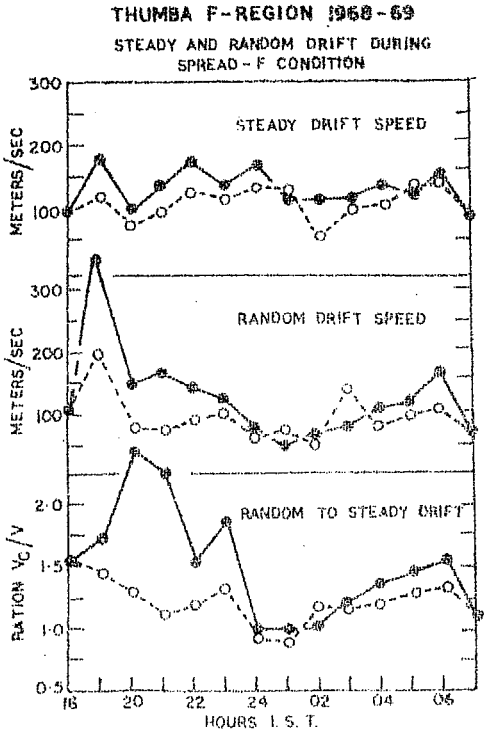

FIGURE 6.14

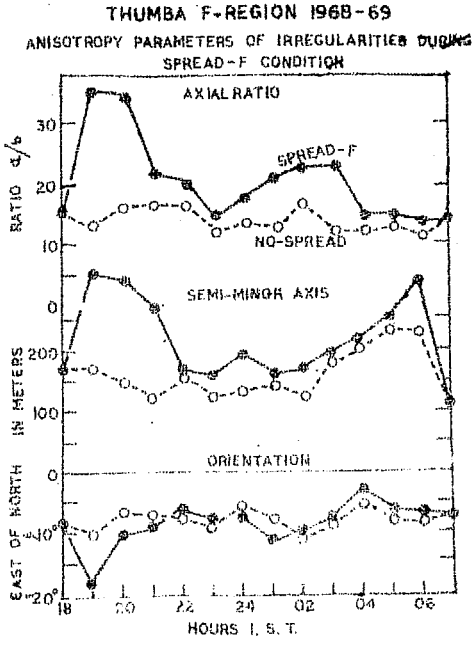

FIGURE 6.15

portion corresponds to the low power region of the record and the results are not significant. The drift speed is seen to be clearly higher (almost double) for the higher fading frequency region than the normal fading frequency region, which would be the actual drift of the ionization on a no spread-F day. The drift direction however shows no significant variation with frequency and is not shown here. A higher value of drift speed at higher fading frequency can also arise due to a positive dispersion of drift in the ionosphere. The various causes of the origin of such a dispersion are discussed at length in Chapter 7.

(c) Results for V', ϕ, V, ϕ, V_o, V, b, r and ψ

All these records were also analysed for V' and ϕ' by the similar fades method and the results are shown in Fig.6.13 in comparison to the normal no spread-F days. The variation of the rate of fading N is also shown. The increase in N as well as V' is maximum in the early part of the night, when the spread-F is usually very strong. The direction ϕ' does not show any significant change over the normal eastward drift in the night.

Steady and random drift parameters, V, Vc and Vc/V were also computed using the full-correlation method of analysis are shown in Fig.6.14 alongwith the normal

day variation. The increase in steady drift V is comparatively less than that in the apparent drift. The increase in the random drift V_c however accounts from this discrepancy as the apparent drift includes the effect of both. The ratio V_c/V shows a fairly large increase in the early part of the night, during which N and V' also increase to a larger extent. Thus the high fading rate during spread-F adds to a higher random component of drift.

The anisotropy parameters of the ground diffraction pattern during spread-F are shown in Fig.6.15 in comparison to the normal day variation. Both axial ratio and the semi-minor axis increase and this increase is much larger in the early part of the night, same as that for N, V' and V_c/V. The orientation ψ of the characteristic ellipse however does not change significantly excepting in the earlier part of night, when the ellipse tilts more towards the west of north. The increase in r and b alongwith that of N, V and V_c is consistent. The Fig.6.16 finally gives variations of the spread-F index, the height of F-layer and the eastwest component of the apparent drift speed at Thumba during 1967. There is a close correspondence between the time of the onset of the spread-F, the peak of h'F and the evening reversal of the east-west drift.

(d) Discussion

The super-imposed fast fading during the spread-F condition can be interpreted in terms of the presence of smaller scale irregularities within the bigger lumps of ionization. The spread-F at an equatorial station is more pronounced during the quiet days (CHANDRA and RASTOGI, 1971) (see Fig.6.17) and hence the present results namely the increase in V' , V, V_c and r and b are consistent with those of Chapter IV where drift and anisotropy parameters are shown to have reduced during the magnetically disturbed days. SIVRAM (1960) has however shown a reduction in V' but an increase in r during the magnetic disturbances for Waltair. FOOKS (1961) has discussed the result of drift parameters for Cambridge during the magnetically disturbed conditions and the spread-F. The appearance of the large values of V_c is explained in terms of the different drifting velocities at different parts of the spread-F echo, due to the finite height range of the gating pulse in the drift recording equipment. He has also shown that the irregularities during the magnetic disturbance are more nearly aligned to the magnetic north-south and are smaller in size. Hence the larger size of irregularities tilted slightly away from the magnetic N-S during the spread-F conditions at Thumba are the representative of a relatively quiet conditions. CLEMSHAE (1964) has

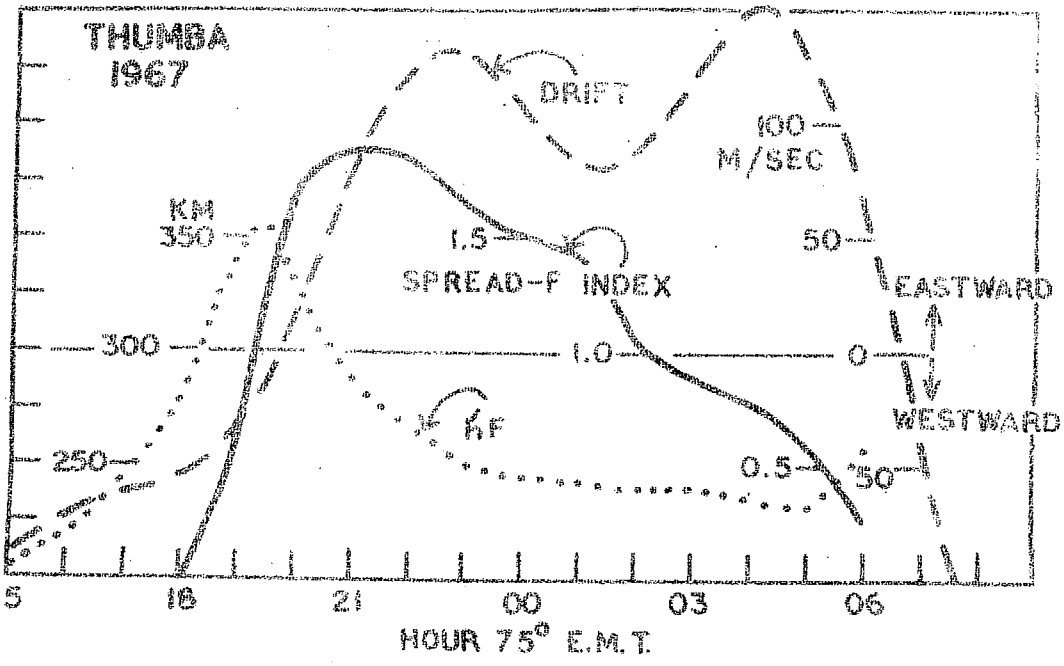

FIGURE 6.16

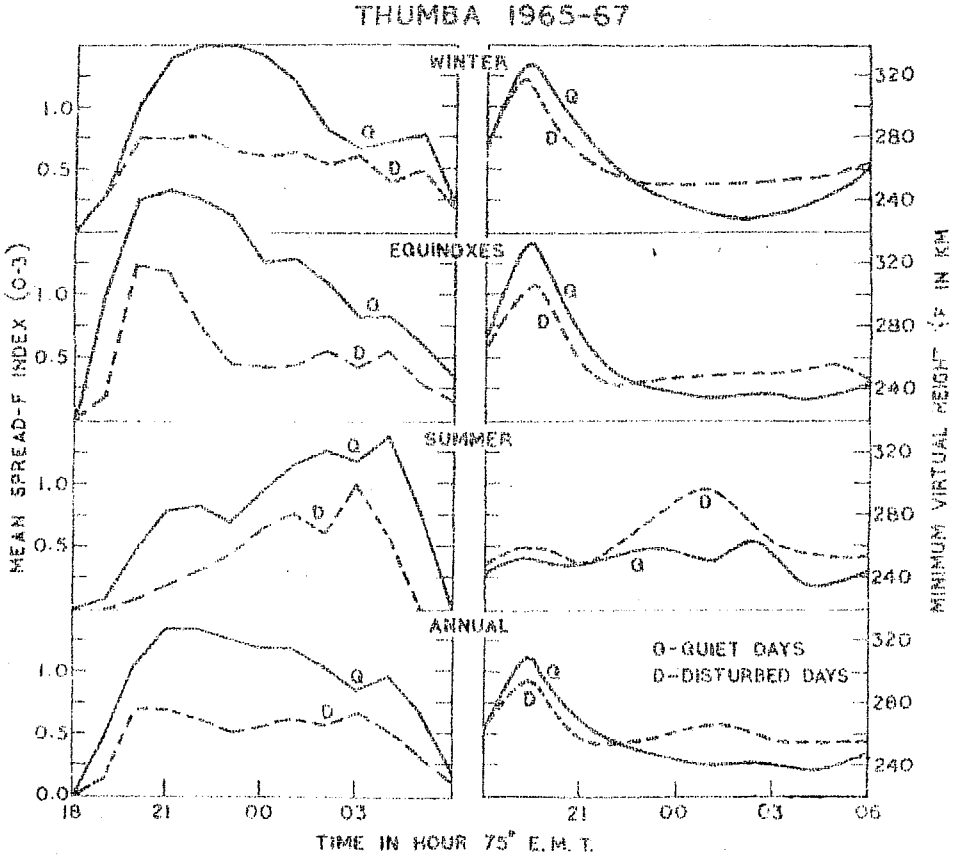

FIGURE 6.17

also studied the drift of spread-F type of the irregularities and found it to be of the order of 100 m/s towards east. He also showed using Doppler shift measurements, that the irregularities sometimes exhibit large vertical velocities. The irregularities are shown to be anisotropic, in the E-W vertical plane.

6.5 Occurrence of opposite drifts in E and F-regions at Thumba

It has been shown earlier (Chapter II and III) that the E and F region drifts at Thumba are predominently westward during day and eastward during night hours. A detailed study of individual records of drift for the year 1968-69 showed that out of nearly two thousand sets of successive E and F region records, nearly one hundred showed opposite drifts. This did not include the periods around the normal morning and evening reversals of the drift.

A few simultaneous E and F-region drift records at the same frequency were also taken by using the two drift recording units and a common transmitter. Two such sets of records are reproduced in Fig.6.18. A number of successive E and F region records in the day and night time, when the drifts are found to be in opposite directions are reproduced in Fig.6.19.

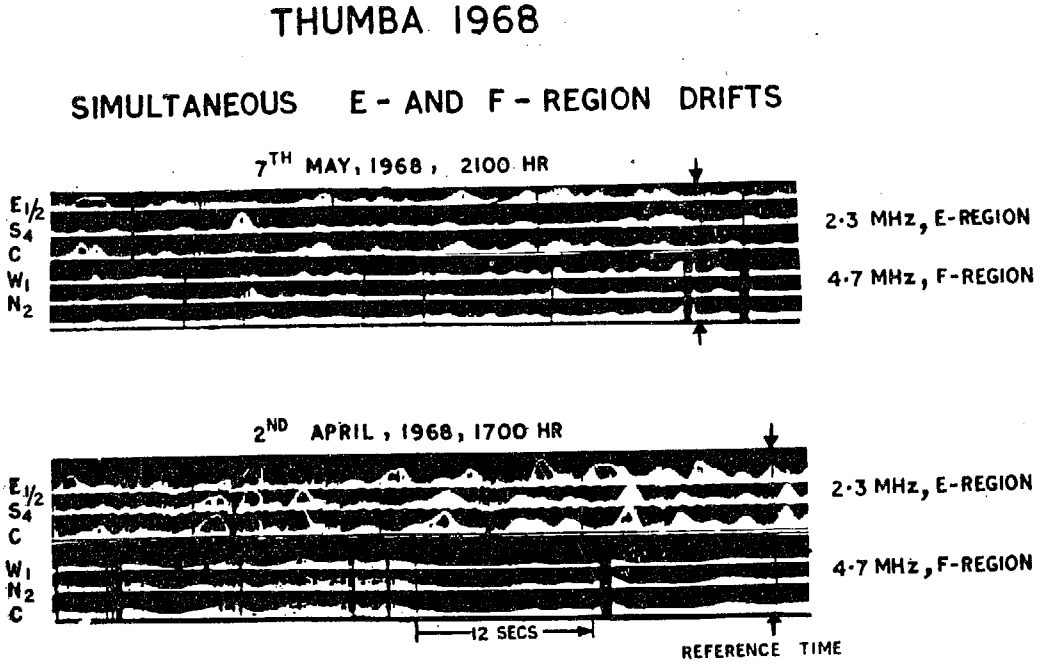

Figure 6.18

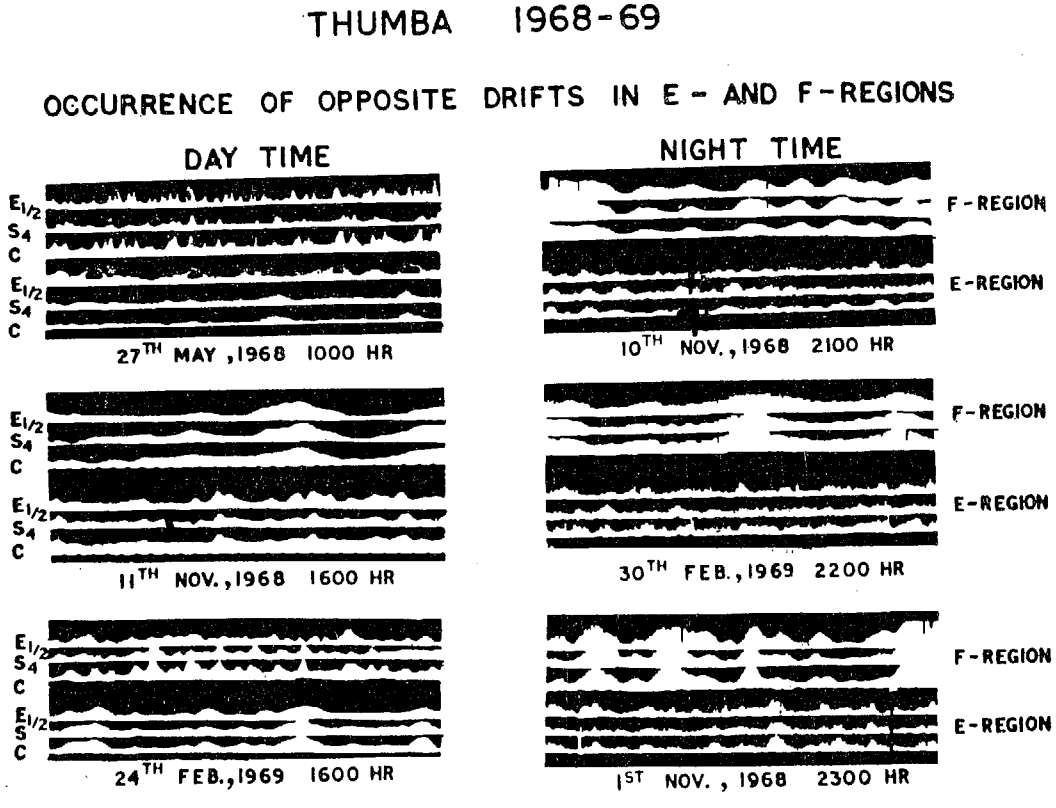

Figure 6.19

Opposite drift in E and F regions show that the E and F region reflections refer to two well separated height ranges and the fading is introduced near the level of reflection. There is however some integration of drift velocities over a finite height range.

6.6 Dependence of the drift and anisotropy parameters of the ground diffraction pattern at the equator on the E-W and N-S extent of antenna separation

(a) Introduction

The D_1-method of drift measurements is based on the tacit assumption that the aerial separation in any direction is much that all the tree antennae see the same irregularity at any time. This separation is normally taken as one wavelength, so that the similarity of the variation patterns at the three spaced receivers is not lost and it is thus possible to estimate the drift of the diffraction pattern on the ground in a particular direction from the time lag between the similar features on the variation patterns at two points in that direction. It is also assumed here that the ground pattern is more or less isometric so that the use of equal north-south and east-west separation of receiving aerials yields equal sensitivity in both the directions.

For equatorial stations however, where the diffraction pattern on the ground is highly elongated in the magnetic north-south direction, same irregularity traverses past the two north-south aerials C and N for a long-time, leading to extremely high correlation between the two records of fading at central and north aerials, whereas the predominant eastwest drift and lesser extent of the irregularity in this direction causes a relatively much sharper fall of the correlation.

(b) Special observations

The routine measurements at Thumba for the ionospheric drifts were conducted from Jan 1964 through Aug 1966 using a right angled isosles triangle of receiving aerials, namely W_1CS_1 ($W_1C = CS_1 = 120$ meters). There was almost a complete absence of the time-lag in N-S direction so that the N-S drift could not be determined. The E-W true drift speed V was found to be on the average 100 m/s and the axial ratio and orientations of the characteristic ellipse of the ground diffraction pattern was found to be on the average 5.0 and $\pm$ 2° of the magnetic north respctively. The north-south separation of receiving aerials was however increased to twice the wave-length in Sept 1966, in order to get an appreciable time-lag in this direction. Though it made no appreciable change in the sensitivity as per

the time-lag is concerned, the axial ratio of the characteristic ellipe was noticed to have on the average increased slightly for the year 1967 for both E and F regions.

In the year 1968, alongwith the installation of a new drift recording unit at Thumba, a much extended north-south aerial system was erected, which is shown in the Fig.1.14. A total separation of four wavelengths corresponding to 2.5 MHz (i.e. 480 meters) was used in the north-south direction for the routine observations. The east-west separation on the other hand was reduced from one to half wavelength. The values of axial ratio 'r' were once again found to have gone up slightly for both E and F regions over the 1967 values though the true velocities were found to be slightly less. The effect of solar activity on the drift and anisotropy parameters at Thumba is discussed in Sec.2.7 of Chapter II and 3.5 of Chapter III. The apparent drift speed does not show any significant variation from 1964 to 1969 whereas the true drift speed decreases. The axial ratio is found to increase and b is found to decrease from 1964 to 1969. The orientation angle ψ is not affected much. The decrease in the values of V from 1967 to 1968 was however much pronounced and appears to be caused by a reduced E-W separation of the aerials. The increase in 'r' was much

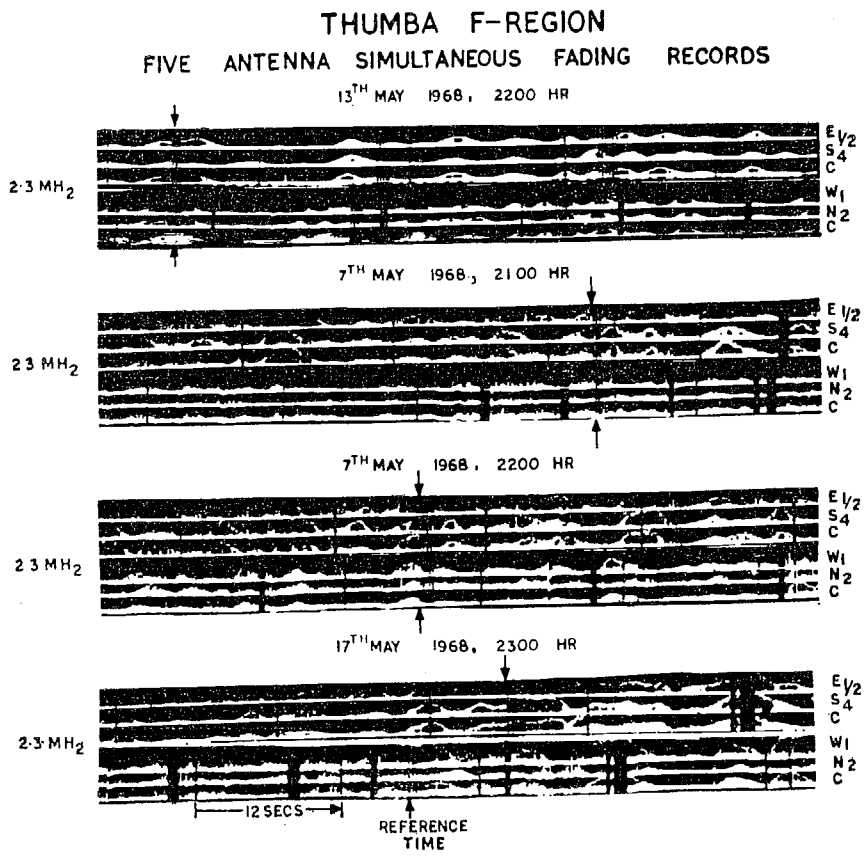
THUMBA F-REGION
FIVE ANTENNA SIMULTANEOUS FADING RECORDS
13TH MAY 1968, 2200 HR
2·3 MH2
E 1/2
S 4
C
W 1
N 2
C
7TH MAY 1968, 2100 HR
2·3 MH2
E 1/2
S 4
C
W 1
N 2
C
7TH MAY 1968, 2200 HR
2·3 MH2
E 1/2
S 4
C
W 1
N 2
C
17TH MAY 1968, 2300 HR
2·3 MH2
E 1/2
S 4
C
W 1
N 2
C
12 SECS
REFERENCE TIME

Figure 6.22

sharper with the change over of antenna system and this lead to a series of special observations by the author in 1968 which were aimed at determining the dependence of drift and anisotropy parameters of the ground diffraction pattern on the east-west and north-south extent of aerial separation at the equator.

Simultaneous drift records were taken at the same frequency for E and F regions using two different drift recording units operating for two different adjacent triangles of receiving aerials. One aerial system was kept to be W_1 N_2C and the other one was having much more N-S separation and lesser E-W separation, namely $E_{\frac{1}{2}}$ S_4C. The common central aerial C was used, by installing two central aerials at the same place. This was necessiated by the need of a reference aerial, so as to get a common auto-correlation function for both the sets of drift records, while subjecting it to full correlation analysis of PHILLIPS and SPENCER (1955). A set of four such simultaneous drift records are reproduced in Fig.6.22. The arrow indicates the same instant of time on the two records.

(c) Results

Auto and cross-correlation functions were computed for the two sets of records and the Vc' ellipses

THUMBA F-REGION DRIFT

CORRELOGRAMS FOR THE SIMULTANEOUS DRIFT RECORDS ON TWO DIFFERENT ANTENNA SYSTEMS

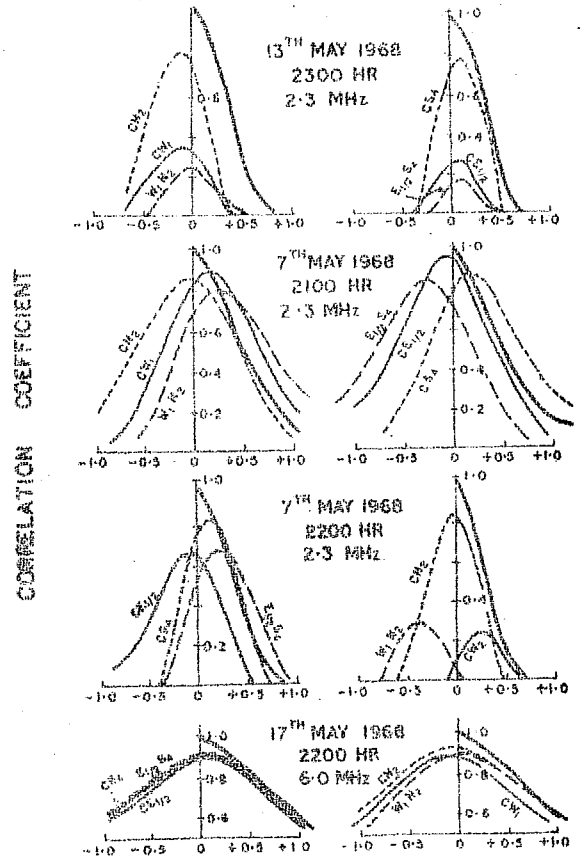

FIGURE . 6.23a

THUMBA F-REGION DRIFT

DEPENDENCE OF ANISOTROPY PARAMETERS ON AERIAL SEPARATION

(SIMULTANEOUS CHARECTERISTIC ELLIPSES)

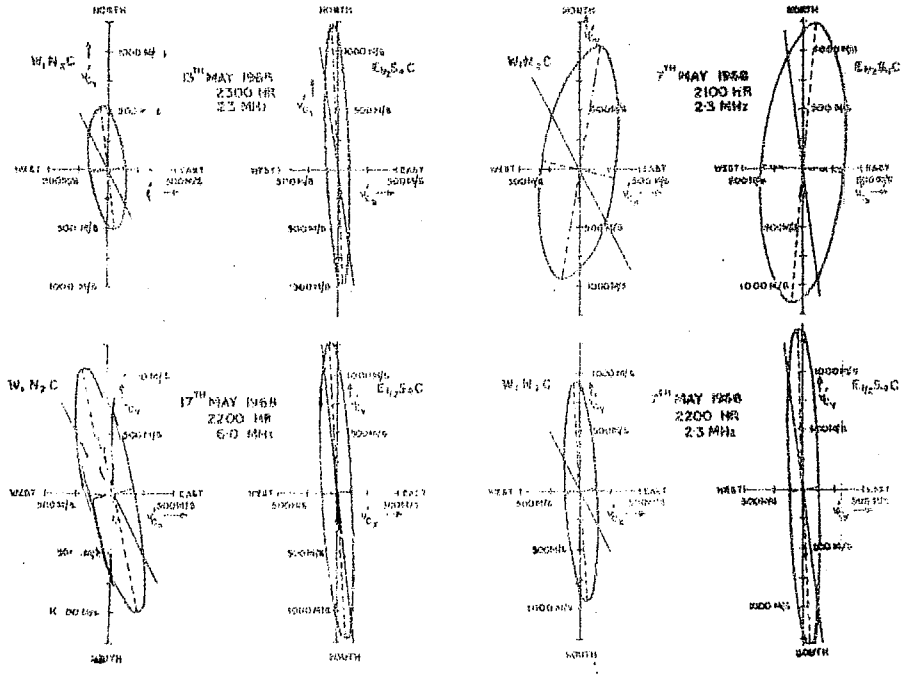

FIGURE . 6.23b

were drawn following PHILLIPS and SPENCER (1955). These are shown in Fig.6.23a and Fig.6.23b respectively. The various drift and anisotropy parameters, namely apparent and true drift speed and direction, the random drift speed, the axial ratio, orientation and the semi-minor axis of the Vc' ellipse were computed and these are given in Table V.

Following points are noteworthy from these results:

(1) The apparent drift speed and direction (Va and Øa) do not show much dependence on the E-W and N-S aerial separation.

(2) The true drift speed V increases with increasing E-W separation while Ø shows no significant change.

(3) Random drift Vc is slightly higher for the smaller E-W separation.

(4) The axial ratio 'r' of the characteristic ellipse increases significantly with the increase in N-S separation.

(5) Semi-minor axis 'b' also shows a very slight increase with increasing E-W separation.

(6) The orientation angle ' ' tends to be more N-S with increasing N-S separation.

A few more records for the year 1967 were looked for this effect. The results for two of such successive

Date	Time	V_a in M/s	ϕ_a E of N	V M/s	ϕ E of N	V_c M/s	r	b in Metre	ψ E of N.	Triangle used for calculation.
13-5-68	2300 hr	210	116°	150	110°	55	3.5	120	354°	W1N2C
		220	92°	128	95°	67	19.5	115	359°	E½S4C
7-5-68	2100 hr	200	83°	180	86°	86	3.3	300	10°	W1N2C
		203	76°	160	80°	102	3.7	290	5°	E½S4C
7-5-68	2200 hr	150	90°	102	90°	42	7.5	120	356°	W1N2C
		170	80°	85	86°	50	10.7	107	358°	E½S4C
17-3-68	2200 hr	250	108°	205	103°	109	6.5	170	349°	W1N2C
		230	84°	183	87°	115	8.4	150	357°	E½S4C

Table - V

Date	Time	V_a	ϕ_a	V	ϕ	V_c	r	b	ψ	Triangle used for calculation
8-8-67	0800 hr	300	86°	250	88°	136	5.2	240	10°	a' = 120M b' = 480M
		250	87°	233	90°	150	3.3	170	22°	a' = 60M b' = 120M
23-10-67	1500 hr	152	269°	130	270°	150	11.5	250	5°	a' = 120M b' = 480M
		150	268	125	266°	168	5.5	240	7°	a' = 60M b' = 120M

Table - VI

records, taken within few minutes of each other, are shown in the Fig.6.24a and 6.24b. The values of various parameters are listed in Table VI. Assuming that the drift and the size of the irregularities remained constant during the period of these successive recordings, once again the dependence of V,Vc, r and ψ on the aerial separation is clear. The semi-minor axis '**b**' is also slightly lower with a lower E-W separation.

(d) Interpretation of results

BENYNON and WRIGHT (1969a) have also discussed the effects of the aerial separation on the drift parameters for higher latitudes namely Aberystwyth and Halley Bay. The variation in the values of V' and $\emptyset$' are accounted for the curvature of line of maximum. The case of an equatorial station is however studied for the first time here in regard to the effect of the size of aerial system. The fact that there is no change in the apparent drift speed with the increasing E-W aerial separation at Thumba while the true drift V increases, indicates towards the non-uniform variation of the shape of the correlograms with the aerial separation. This can arise due to various reasons, particularly the curvature of the line of maximum amplitude. As the drifts at Thumba are predominantly E-W, the effect of N-S aerial separation on Vc and V will

THUMBA F-REGION DRIFT

CORRELOGRAMS FOR SUCCESIVE DRIFT RECORDS WITH DIFFERENT ANTENNA SEPARATIONS

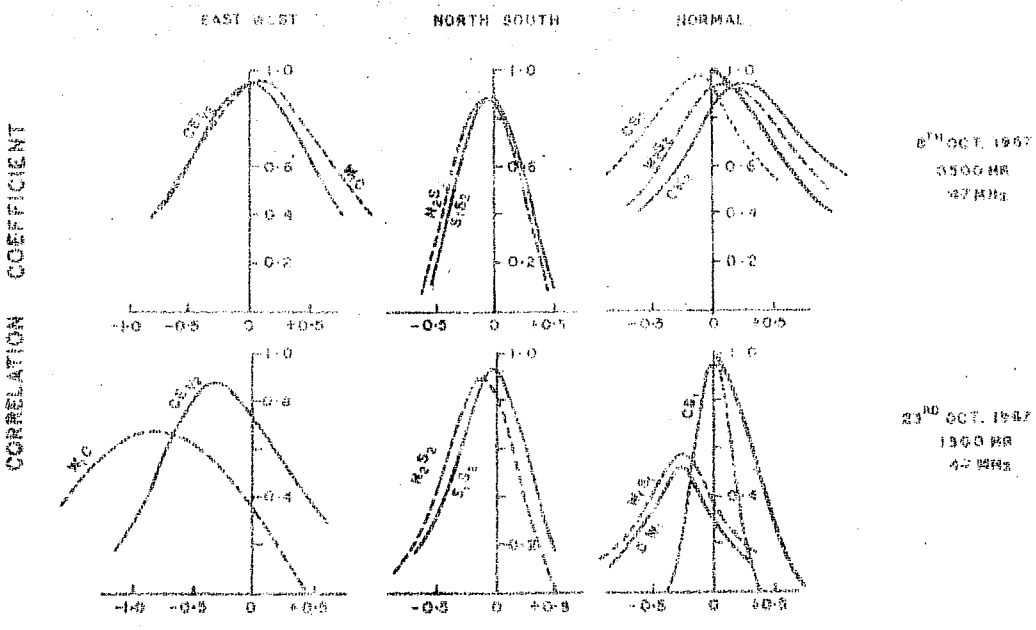

TIME LAG IN SECONDS

FIGURE 6.24a

THUMBA F-REGION

DEPENDENCE OF THE ANISOTROPY PARAMETERS ON AERIAL SEPERATION (CHARECTERISTIC ELLIPSES FOR SUCCESIVE DRIFT RECORDS)

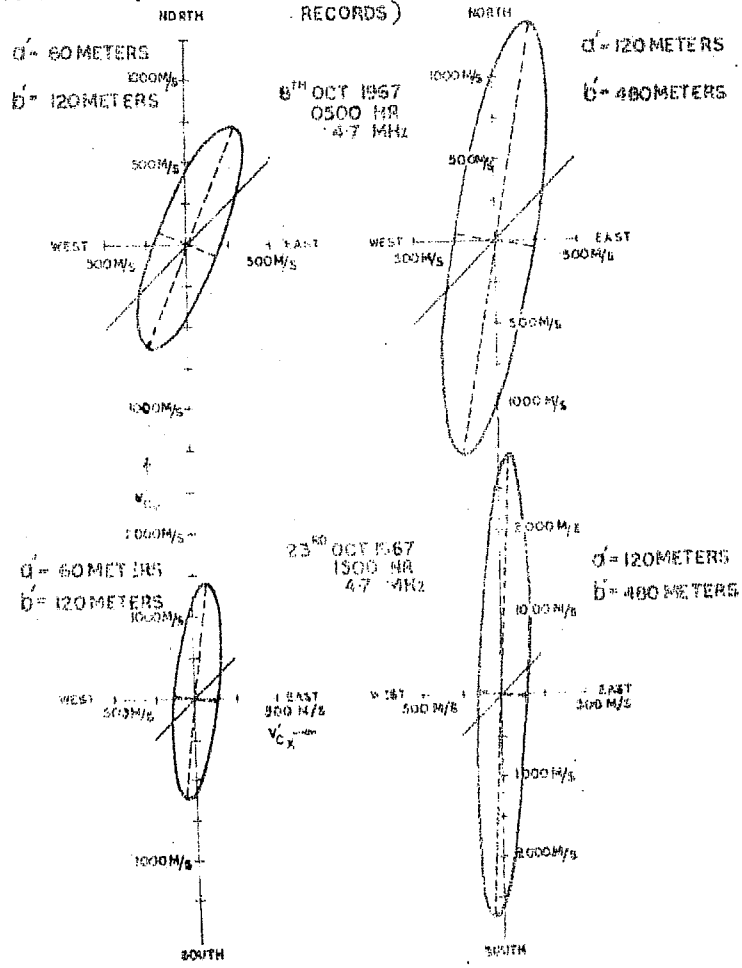

FIGURE 6.24b

be negligible. The presence of waves in the ionosphere can also cause the increase or decrease of the drift velocity with the increase or aerial separation (see 7.9) The increase in random drift Vc with a smaller E- W separation shows the existence of larger number of smaller scale irregularities which are undergoing changes in their shape than the bigger ones. The increase in 'r' with increasing N-S separation indicates towards a highly elongated N-S irregularities in the ionosphere over Thumba, the size of which could be even bigger than 'r' determined by the maximum available 480 meters separation in N-S direction. No further increase in the value of 'r' with the increase in the N-S aerial separation should be observed once this separation is of the order of the size of irregularity in N-S direction.

The semi-minor axis 'b' increases only slightly with E-W separation, indicating that the separation of the order of a wavelength in this direction is optimum as the irregularities are nearly of the same size in their E-W extent. Orientation angle 'ψ' tends to be more and more N-S with increasing N-S separation which shows that the irregularities are highly elongated and almost oriented in magnetic N-S directions. BENYON and WRIGHT (1969b) have shown for Halley Bay and a few other stations that

there is a distinct tendency of the correlation ellipse to be oriented with its major axis along the longest side of the antenna system. They have shown that this dependence can be explained in terms of the distortion of the ground pattern from an exact ellipse wich is the basic assumption of the BRIGGS, PHILLIPS and SHINN(1950). All these results point towards the necessity of optimization of the size and geometry of the receiving aerial system for all the drift stations over the world. It is suggested that for a station like Thumba, the N-S aerial separation be further increased keeping the east-west separation between λ and $\frac{1}{2}\lambda$.

(e) Discussion

KELLEHER (1966) found that the magnitude of true drift velocity increases with triangle size, but did not indicate any upper limit. GOLLEY and ROSSITER (1969) have made an extensive study of this effect using an array of 89 dipoles (at Buckland Park, Adelaide) and found that though Va, ϕa and ϕ are independent of triangle size, V,r, b and ψ show a strong dependence till the optimum size is reached (about 300 m for E-region). Equatorial triangle avoides the dependence of ψ on the diagonal of the triangle.

GOLLEY and ROSSITER (1970) have studied the effect of the triangle size on the drift parameter for the partial reflections for D-region at Adelaide. Little dependence was found as the pattern size was comparable with the smaller triangle size of 140 metre (a side of an equilateral triangle) for Adelaide. SASTRI and RAO (1971) have recently reported for Waltair the results similar to Thumba.

Advantage of the equilateral triangle has been pointed out by BIBL, HARNISCHMACHER and RAYER (1955) and BARBER (1957). SPRENGER and SCHMINDER (1969) considered the effects on drift parameters of filtering the fading records. They substracted the running mean from each record which had the effect of removing low frequency component and by varying the width of the running mean, the filter cut off frequency was varied. Full correlation analysis was applied to the original and filtered records. They found that the true and apparent drift directions and the apparent drift velocities were unaffected by the filtering but the true velocity increased as the cut off frequency is increased. By filtering the low frequency components, the scale size of the pattern is effectively reduced. Thus SPRENGER and SCHMINDER (1969) effectively varied the pattern size relative to a fixed triangle size. The result is therefore consistent

with those quoted here as well as by KELLEHER (1966) and GOLLEY and ROSSITER (1969), that the true velocity increases with the ratio of the triangle size to pattern scale size.

6.7 Effect of solar flares on the drifts at Thumba

E and F region drifts at Thumba during solar flares of period 1968-69 were studied and their variation around the time of maximum of the flare is depicted in the accompanying Fig.6.26. Flare data of Kodaikanal observatory was used for this study. It was observed consistently that both E and F-regions apparent drifts were reduced considerably over their normal values. During some of the very severe flares, there was a complete black-out of the signal and no drift record could be taken.

RAO and RAO (1961) have however shown an increase in the E region drifts on two solar flare days, at Waltair. An interesting feature of their result was a large phase difference of about three hours between the drift vector on solar flare days and the quiet days, the former being ahead. This indicates that the drift systems for these two cases are situated at different levels. In view of the fact that the drift measurements made at E-region reflections might be considerably affected by the enhanced ionization in the lower levels during the solar flares,

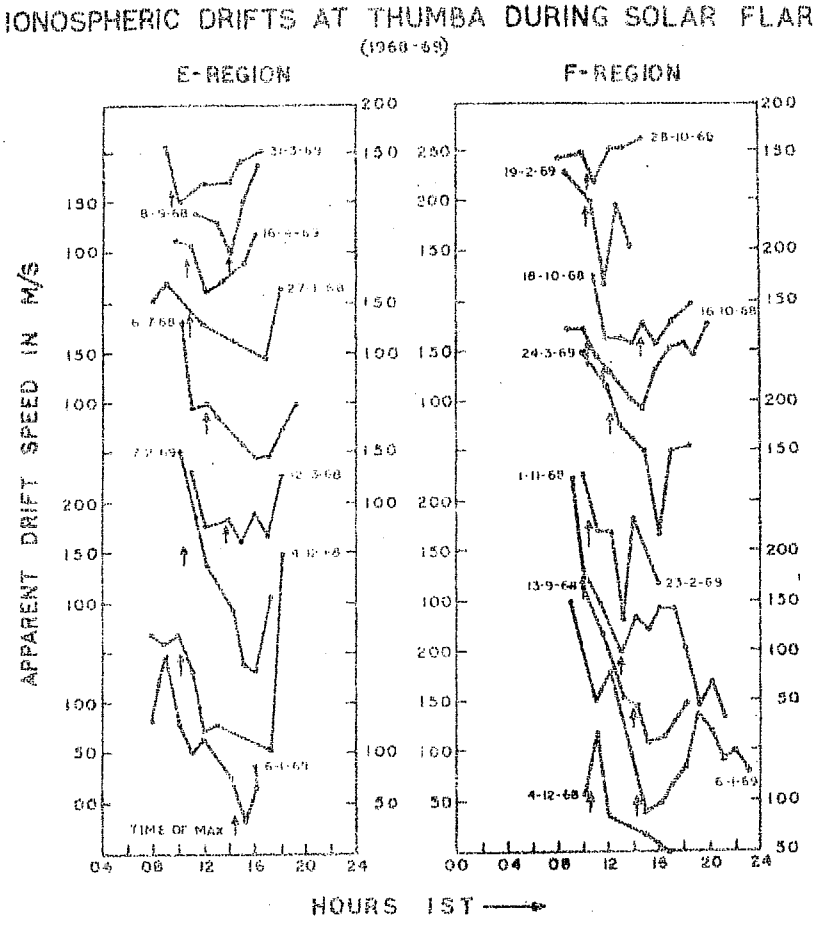
IONOSPHERIC DRIFTS AT THUMBA DURING SOLAR FLARES
(1968-69)
E-REGION
F-REGION
APPARENT DRIFT SPEED IN M/S
TIME OF MAX
HOURS IST
00
04
08
12
16
20
24

FIGURE 6.26

it may be possible that the drift velocities during flares refer to a lower levels in E-region or higher levels in D-region. VOLLARD and TAUBENHEIM (1958) have shown that the disturbed current system may also extend down to the D-region.

6.8 Drift and anisotropy parameters from first and second order reflections recorded at spaced aerials

(a) Introduction

The closely spaced aerial technique of measuring ionospheric drift (MITRA, 1949) assumes that the diffraction pattern on the ground moves with twice the velocity of the ionospheric irregularities. WRIGHT (1968) suggested that the point source effect is valid for the waves reflected totally from the ionosphere at normal incidence. He found discrepancy between the neutral atmospheric winds and the ionospheric drifts determined simultaneously. It has been suggested that the computed ionospheric drift depnds on the antenna spacing used to observe it (KELLEHER, 1966) and for small spacing is less than true velocity by a factor of the order of two. FELGATE (1970) using multiple antenna showed that a classical interpretation is true for waves both totally and partially reflected. BOOKER et al. (1950) have shown that the auto-correlation function $\rho_2(t)$ of the amplitude of a doubly reflected

echo is equal to the square of the auto-correlation function ($\rho_1(t)$) of the amplitude of a singly reflected echo i.e.

$$\rho_2(t) = \left(\rho_1(t)\right)^2 \qquad \ldots\ldots(1)$$

SEN (1964) generalized this result for the n^{th} order reflection from the ionosphere:

$$\rho_n(t) = \left(\rho_1(t)\right)^n \qquad \ldots\ldots(2)$$

The experimental observations by SEN (1964) indicated that the above relation holds only approximately. ESSEX and HIBBERD (1967) have shown that the equation number(2) is valid experimentally when the signal amplitude has a Rayleigh type of distribution. HARANG and PEDERSON (1956) have measured the fading records on eastwest base on the first and second order echoes simultaneously and have found that the relative displacement of fading maxima was same in the first and the second order reflections.

This paper describes the results of closely spaced drift records from the first and second order echoes from the ionosphere at an equatorial station Thumba.

(b) Specular and diffusive reflection mechanisms

The reflection of the radio waves from the ionosphere can be treated as the reflection from the plane

mirror or from a completely diffused layer. The geometry of the two modes of reflections are shown in Fig.6.29. In the specular reflection case,a series of plane mirrors moving with a velocity V at the height of the reflection are reflecting the wave and we obtain the first order reflection pattern on the ground moving with a velocity 2V. When the radio wave from this moving pattern is again reflected from a suitable mirror which now will have only half of the velocity relative to the beam from the pattern, the ground diffraction pattern for the second order reflection will be stationery. The second model of diffusive reflection could be somewhat similar to the model of the diffractive reflection outlined by RATCLIFFE (1947). According to this model the fadings are produced by the doppler effect of the moving diffraction centres which are distributed at random and the diffractive reflection process, the prehistory of the primary waves falling on the radiating centres will be of minor importance and the drift effects will be the same in the first and second order reflection ground patterns. It is assumed so far that the ground is not rough and acts as a plane mirror so as to produce a specular reflection of radio-waves. This condition more or less holds when the soil conductivity is high. Thumba is one such station. In the case of rough ground however, the reflection of radio

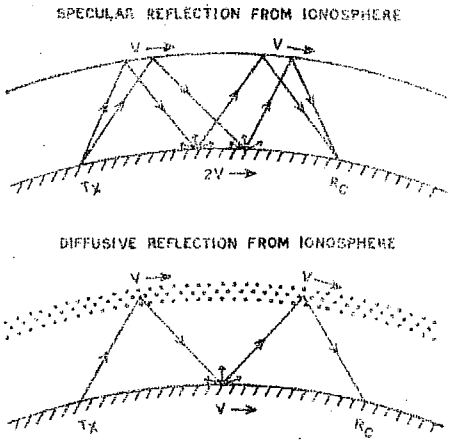

FIGURE 6.29

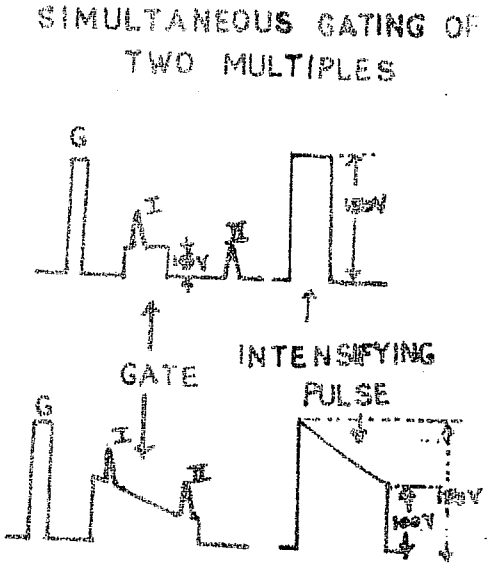

FIGURE 6.30

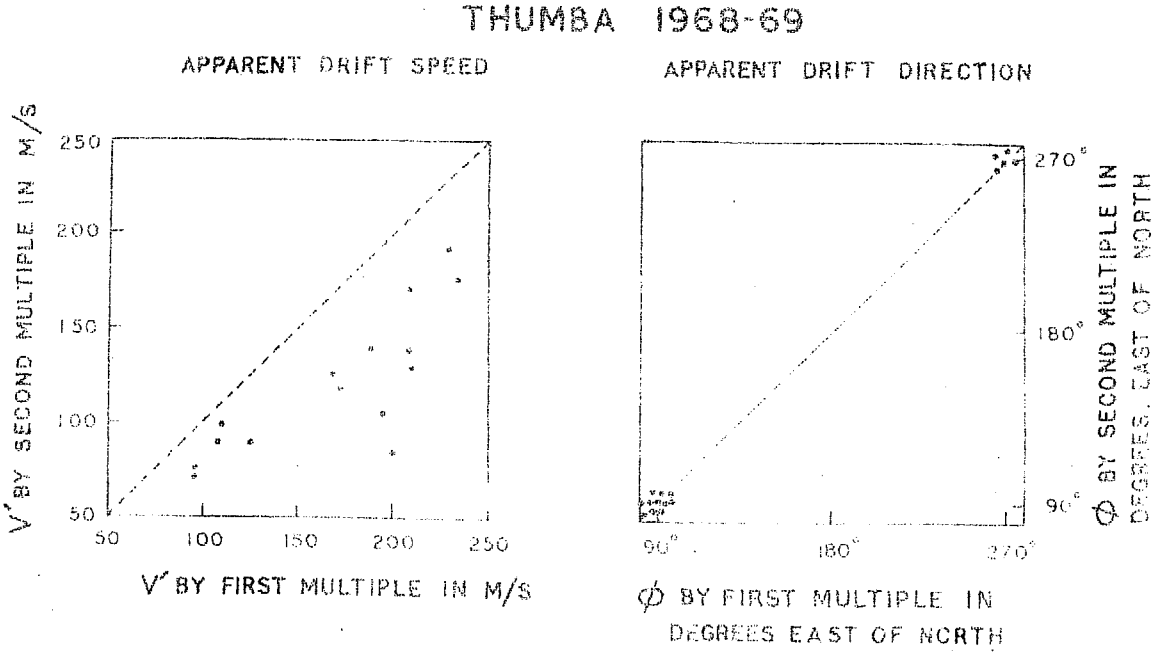

FIGURE 6.31

waves from the ground is diffusive. It can be seen geometrically that if the ionospheric reflection is specular and the ground reflection is diffusive, the drift velocity of the ground pttern as derived from various higher multiples will be same and it will be double of the actual drift velocity of the ionization. In the other case, when both ionospheric and ground reflections are diffusive in nature the drift velocities derived from different order echoes will be same and equal to the actual drift velocity of the ionization.

(c) Experimental arrangements

Regular drift observations at Thumba were started in 1964. With the installation of another drift equipment in 1968, two independent closely spaced drift recording units were available for observations other than the routine drift measurements. It was also possible to obtain higher order multiple echoes with the high power transmiter installed in 1968. The drift measurements on the first and the second order echoes were made both for E and F regions by the three different techniques. Firstly the fading records could be obtained by a single unit on first order echo for a few minute and immediately later on the second order echo, so that the aerial syster remains the same. This method assumes that the ionosphere

has not changed within this interval of few minutes. Two sets of such records are reproduced in Fig.6.28 for E and F regions respectively. In the other method, single transmitter and two independent receiving and recording system were used. Thus drift records could be obtained simultaneously on the first and second order echoes but using two different aerial systems. Third method was based on the use of the very broad gating pulse of the width sufficient to gate both the first and second echoes but the envelope being trapezeum rather than square (see Fig.6.30). It was thus possible to record on the same film, fading of the first and second multiples. The intensity modulation of the two multiples is unequal and hence the second multiple fading appears as a less intense trace on the film than the first one and the two can be followed independently. A few such records are reproduced in Fig.6.27. The advantage of this system is the use of the same receiver and the aerial system used to record the fadings of two multiples and at exactly the same time. The records were analysed by similar fades (MITRA, 1949).method as well as full-correlation technique (BRIGGS et al. 1950; PHILLIPS and SPENCER, 1955) and the results are discussed below.

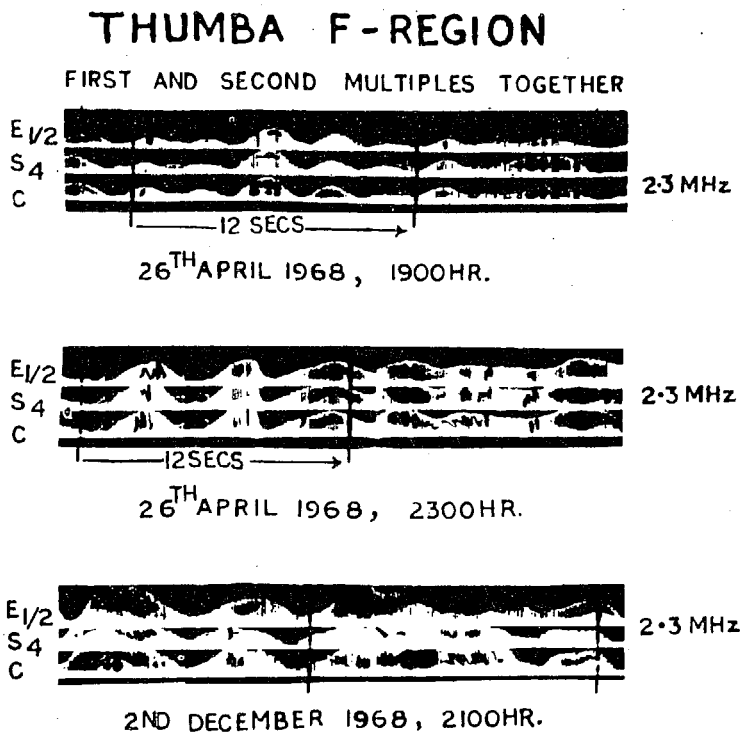

Figure 6.27

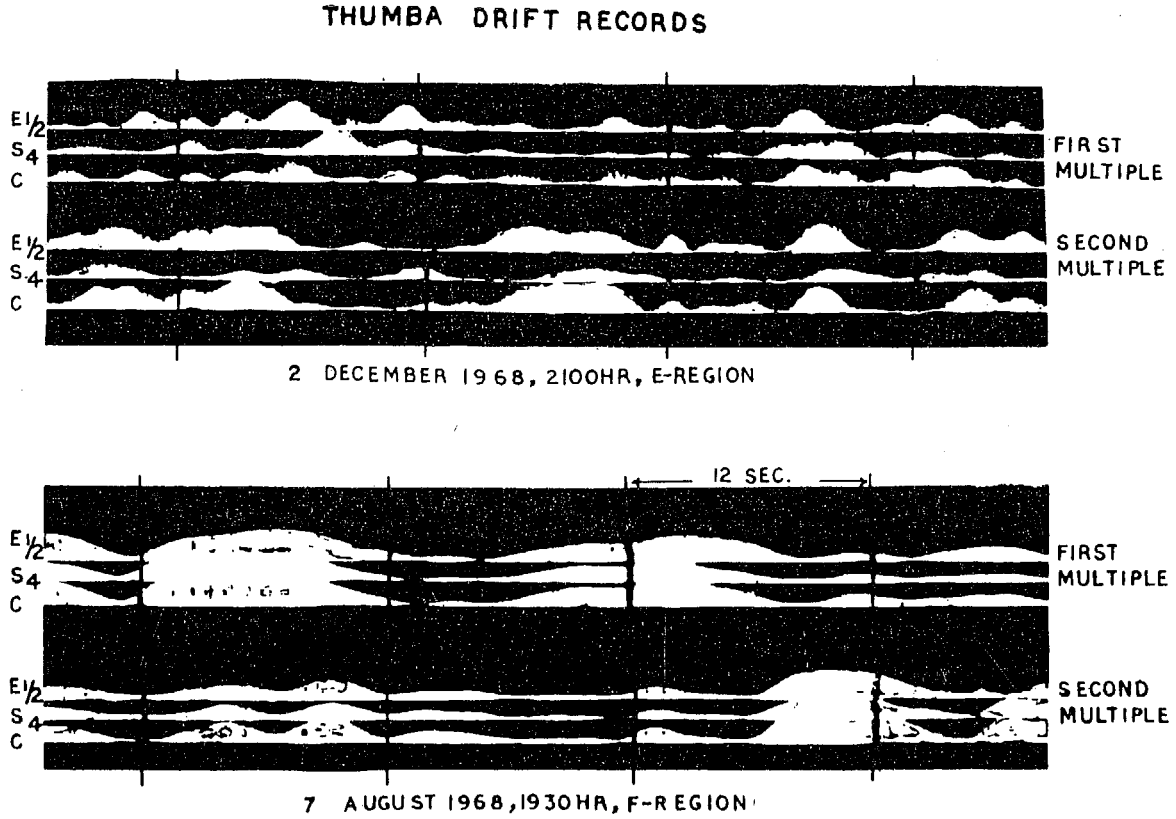

Figure 6.28

(d) Apparent Drifts

The results, both for the first and second multiple echoes are given in Fig.31 It is seen from the diagram that the drift direction is invariably the same for the first and the second order echoes. In no case, the direction were found to be opposite. Regarding drift speed the second multiple drifts are always lower than those derived from the first multiple. The dotted line in the Fig. shows when the two would be equal.

According to the specular reflection mechanism, the drift speed of the second multiple should be zero irrespective of the first multiple speed while according to diffusive mechanism they should be equal. In general, the V' by second multiple is roughly two third of the V' derived from the first.

(e) Steady and random drift

In Fig.6.32 are shown the following parameters derived from both the first and the second multiple: (1) apparent drift speed V_a derived from the shift of the optimum cross-correlation coefficient (2) the true drift speed V (3) the characteristic drift speed V_c and (4) the ratio of random to true drift, V_c/V. The apparent speeds are only slightly less for the second multiple as compared to the first while the true drifts are only slightly more for the second than for the first multiple. Seeing to the scatter of

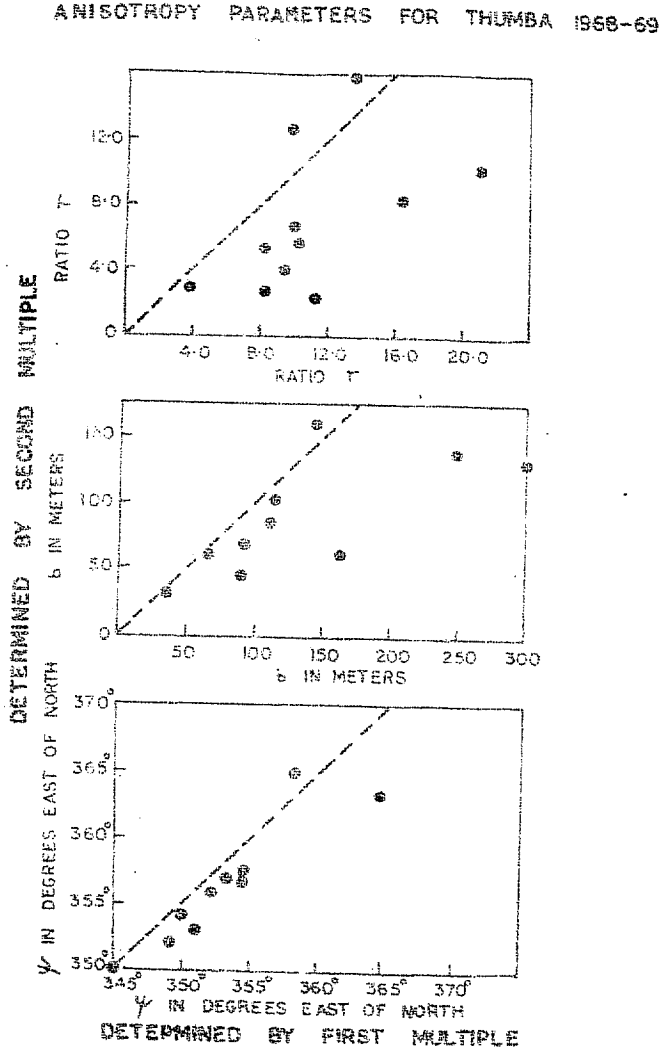

FIGURE 6.33

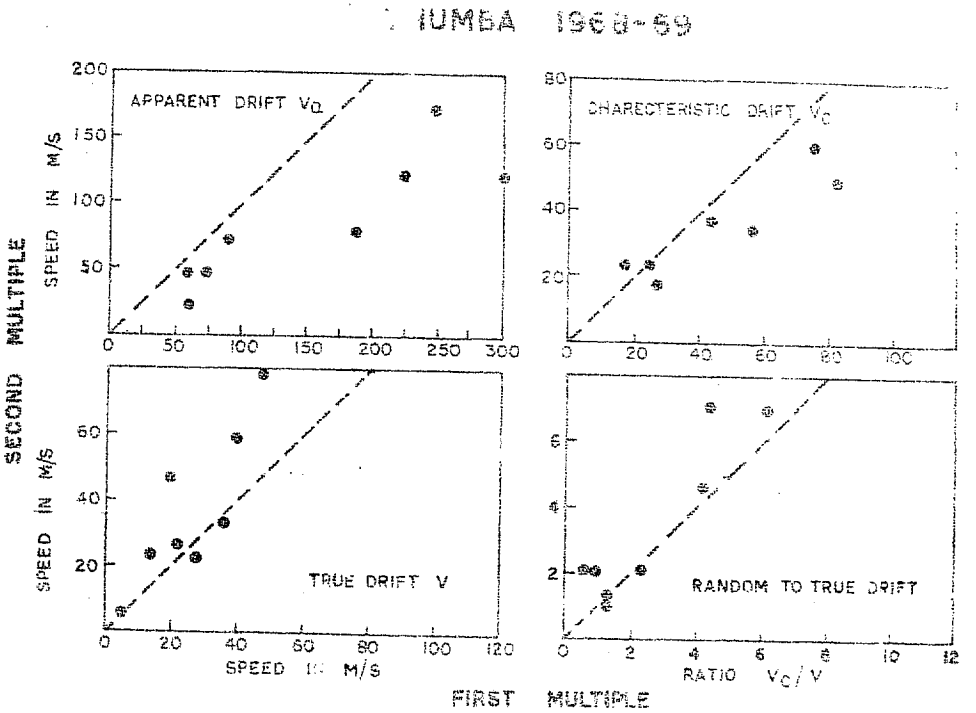

FIGURE 6.32

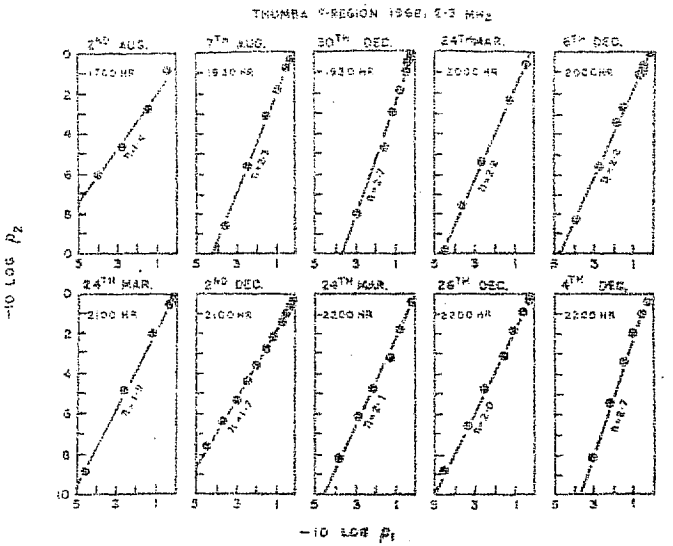

FIGURE 6.34

points it is rather more proper to assign the true drift to be of the same order. The slight difference between the relation of V_a and V between the first and the second multiple is due to the V_c/V being slightly higher in the second multiples. On the average one may suggest that the true drift speed derived from the second and the first multiple suggest that the mechanism which is operative at least at the magnetic equator is predominently diffusive where the factor of two is not valid.

(f) Anisotropy parameters of the diffraction pattern

In Fig.6.33 are shown the arameters of the characteristic ellipse fitted to the diffraction pattern on the ground, namely the axial ratio (γ) the semi-minor axis (B) and the orientation (ψ) of the major axis of the ellipse with respect to the magnetic north-south. The axial ratio (γ) seems to reduce for the second multiple. This would be understandable by the increasing scattering component of the radio wave in the second multiple than in the first. The semi-minor axis (b) and the orientation (ψ) of the characteristic ellipse are nearly the same for the two multiples.

(g) Autocorrelation functions

The mean autocorrelation functions for both first and second multiples were calculated and Fig.6.34 shows the variations of the auto-correlation function of the

first and second multiple (ρ_1 and ρ_2) for corresponding time lags. As the logarithm of the correlation function are plotted, the slope of the straight line will give the coefficient 'n' of the equation (2). It is seen from the diagram that although the 'n' lies between 1.5 - 2.7, but still the validity of the equation (2) is more or less verified.

Discussion

The comparison of drift speeds derived from the first and second multiple echoes from E and F region reflections at Thumba indicate that the process of reflection of the radio waves in the ionosphere are neither completely specular nor completely diffusive but the tendency is more towards diffusive than towards a specular process. The drift speed derived from the second multiple is never zero nor insignificantly low but nearly of the same order as the drift speed of the first, suggesting that the division by two of the drift speed of the ground pattern to obtain the drift speed at the ionospheric level is not valid in most of the cases. The change in the autocorrelation coefficients with the order of multiple is found to be approximately as expected on the theory of diffraction grating suggested by BOOKER et al. (1950)

It is suggested that the routine drift observations should be taken by the Ionospheric stations whenever possible both by first and second multiple echoes, in order to ascertain the mechanism of reflection operative for the individual cases. The dividing factor of two should accordingly be modified.

CHAPTER - VII

DISPERSIVE PROPERTIES OF THE IONOSPHERIC DRIFTS

7.1 Power spectrum analysis of fading records at Thumba

A fading record may be considered to be the sum of a number of sinusoids of different frequency with some phases difference relative to each other. A fourier analysis of such a curve would resolve it into the sine waves, of which it is composed of, giving the amplitude and phase of each component present. One can therefore find out the amplitudes and relative phases of the various fourier components present in a fading records at the three receivers. From the phase lags between any pair of the records for each of these frequencies, the drift speed and direction at that particular fading frequency can be estimated knowing the relative separations of the receivers. If the irregularities in the ionosphere are moving under the influence of a steady wind, and there are no turbulent movements, the diffraction pattern on the ground would move steadily and all the fourier components derived by the above analysis would have same speed and direction. Any dispersion in the values of drift speed and direction is therefore an indicator of the randomness in the diffraction pattern. The random variations of signal strength or noise might also occur and it is a limitation of a single fourier

analysis as described above, as it would not distinguish between the required signal and unwanted noise.

If such an analysis is attempted in practice, it is found that the spectrum is not smooth. The technique of fourier analysis has however been considerably developed to avoid this difficulty. Much improvement in the spectrum analysis have been made to obtain the genuine power of the waves within the desired limits namely the hamming, hanning and other techniques. JONES and MAUDA (1968) have given a working scheme for the cross-spectral analysis of the three receiver fading records.

The ionosphere can be compared to an amplifier of unit amplification, one fading curve being the input and the second as the output. If this amplifier has the linear characteristic the whole operation is known if the phase change and amplification are known for all the frequencies.

Thus if the input is $x(t) = a \sin (2 \pi ft + \emptyset)$ ....(1)

The output will be $Y(t) = a\, G(f) \sin (2 \pi ft + \emptyset + P(f))$ and the operation is defined by the functions $G(f)$ and $P(f)$, which are related by the following equation:

$$H(f) = G(f) \exp (2\, P(f)) \qquad \ldots.(2)$$

The difficulties arise if the relationship of Y and X is contaminated by a noise 'n'. The measured response then must be subjected to a filtering procedure in order to find estimates of gain and phase i.e. G(f) and Φ (f). GOODMAN (1957) examined such a system on the assumption that X, Y and n are stationary Gaussian noises, with X and n statistically uncorrelated with each other. His analysis showed that from the input spectrum $S_x(f)$ and input-output cross-spectrum $S_{xy}(f)$, with suitable smoothing, one can recover the frequency response function in the form.

$$H(f) = S_{xy}(f) \; / \; S_x(f) \qquad \ldots\ldots(3)$$

as though there was no noise 'n'.

Following TUKEY (1949), Goodman established a method of estimating spectra S_x, S_y and S_{xy} from finite sample records of x and y and estimating the frequency response function H(f). In case of ionospheric drift there are three fading records. Three independent estimates of phase differences P_{12}, P_{13} and P_{23} can therefore be obtained for each pair of records, unlike the simple fourier analysis, which will give only two independent phase differences.

(a) Method of analysis

Given amplitudes x (t), y(t) and z (t) for the three fading records obtained at closely spaced receivers

of the D_1 method, the cross spectral analysis involves following steps:

(1) Calculation of co-variance functions.

(2) Correlation of co-variance functions for means and trends.

(3) Calculation of 'raw' spectral estimates.

(4) Smoothing to give the final spectral estimates.

(5) Computation of the estimated gain G(f) and phase P(f) of the frequency response function.

(6) Calculation of velocity and direction from the phase differences e.g. $V_{xy} = x_{12}/P_{12}$, etc.

(7) Rejection of those values in which 'noise' has obscured the true values(significance of the results).

The three fading records are read at a particular sampling interval of time $\Delta t = h$ (say) for amplitudes. Then following BLACKMAN and TUKEY (1958), the 'Nyquist frequency' is given by $f_o = h/2$.

GOODMAN ET AL. (1961) has shown that Δt should not be chosen so small that the whole spectral weight is crowded down to the bottom one or two points. Further, to minimize the distortion due to aliasing, Δt must be small enough to ensure that the continuous data have no appreciable power above f_o. A value of Δt between 0.1 - 0.2 secs was found suitable for the drift records taken at Thumba (0.6°S dip).

The cross-spectral estimates at a given frequency 'f' is given by $S_{jk}(f) = C_{jk}(f) - i Q_{jk}(f)$ ....(1)

and the phase $P(f) = - Q_{jk}(f) / C_{jk}(f)$ ....(2)

From the values of P(f), we can calculate the velocity and direction of each Fourier component as follows:

The phase differences can be converted to time shifts as : $\tau_{jk}(f) = P_{jk}(f) / 2\pi f$ .....(3)

Any pair of time lags for one frequency 'f' can be converted into the velocity and direction of drift in the same way as in similar fades method (MITRA, 1949). However as the present treatment is concerned with the oscillations and waves, it is easier to consider wave fronts rather than the line of maxima. In a plane wave, the wave numbers add vectorially, so that the wave number along the line between the aerials j and R separated by a distance x_{jk} will be $K_{jk} = P_{jk} / x_{jk}$ and the vector addition of two such values will give the vector wave number K in the direction of motion, which has a velocity $V = 2\pi f / |K|$

Hence if x_{12} and x_{13} are at right angles to each other $V = 2\pi f / \left[(P_{12}/X_{12})^2 + (P_{13}/X_{13})^2 \right]^{\frac{1}{2}}$

and angle ϕ with respect to x_{12} is given by:

$\phi = \tan^{-1} (P_{12}/X_{12}) \cdot (X_{13}/P_{13})$

V should be divided by a factor of 2 in order to get the velocity in the ionosphere.

Significance criteria

In order to reject the values of V and ϕ for which the power is negligible, the following criteria is found to work satisfactorily:

Values of V and ϕ are not reliable when $\alpha - \alpha' > \alpha''$

where $\alpha' = \tan^{-1} (P_{12} X_{23} / X_{12} (P_{12} - P_{23}))$

and $\alpha'' = 0.17$ radious or 10°

Coherence (γ) of cross-spectra criteria given by GOODMAN et al. (1961) is found to fail in this case as when γ is low, its estimates are not accurate. Other criteria which may be tried are the extent to which G(f) differs from the value of G averaged over all frequencies.

Also those records for which the equality $P_{12}(f) + P_{13}(f) = P_{23}(f)$ does not hold good, are rejected.

(b) Application to Thumba drift records

Nearly one hundred drift records of Thumba for E and F regions were subjected to the cross-spectral analysis. The amplitudes at each of the three aerials were read at suitable intervals, depending on the fading frequency (see Chapter III for the criterion) and two hundred or more values were used. Nearly 10% lags of the total number of values were given. All the computations were done with the help of IBM 1620 machine.

The cross-power spectrum P(f) for each pair of aerials consists of one broad peak around the most predominant frequency of fading. Secondary peaks whenever present correspond to the higher frequencies, superimposed over the main fading frequency. The cross-power P(f) spectra for a few typical day and night-time drift records of Thumba for both E and F regions are drawn in Fig.7.1, 7.2, 7.3, 7.4 and 7.5. The shape of the cross-power is essentially the same between any pair of the three receiving aerials.

The corresponding drift speed V(f) as a function of fourier frequency is also shown on the same daigrams. The drift direction $\phi(f)$ remains unchanged within a few degrees over the entire frequency range in all the cases studied and hence not shown in figures. The significance of the drift speed and direction over spectral range is ascertained by applying the criteria mentioned in the last section.

The cross-power specturm for Thumba drift records can be broadly classified into three groups. Firstly where the peak power occurring at low frequency (upto 30 fades/min) and a slowly decaying tail. Secondly those showing peak power at medium frequency (30- 60 fades/min) and thirdly those with a double distribution. The first one is common in

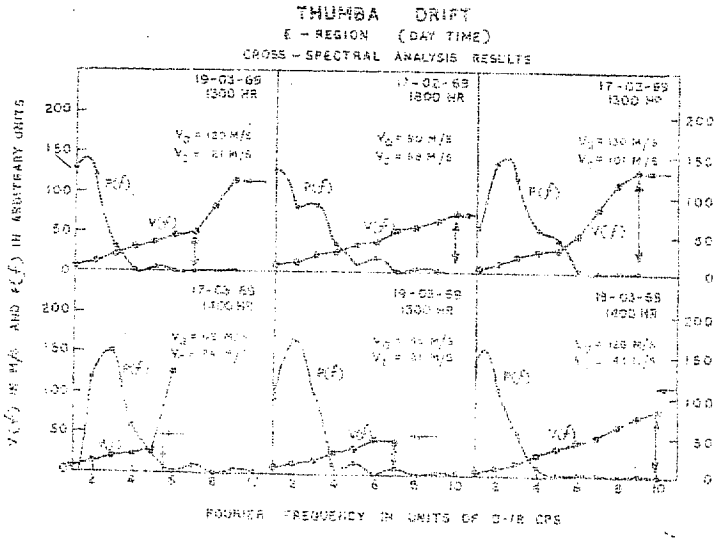

FIGURE 7.1

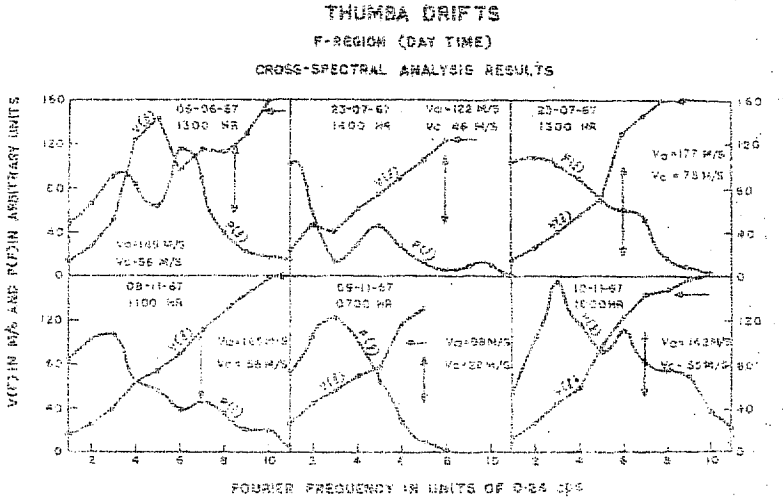

FIGURE 7.2

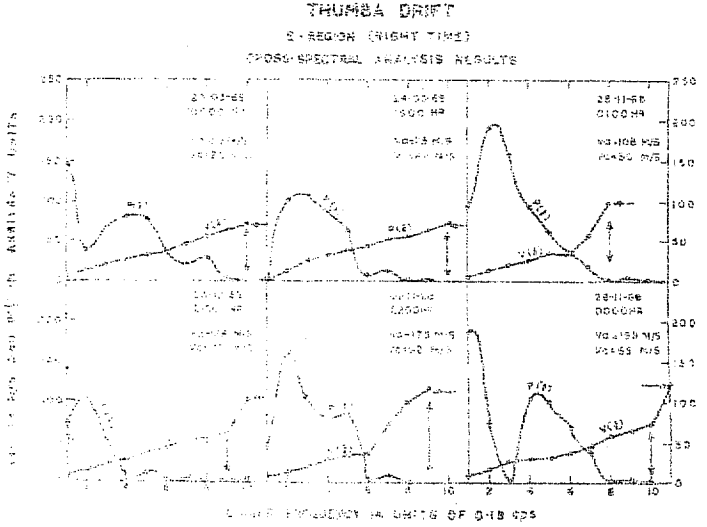

FIGURE 7.3

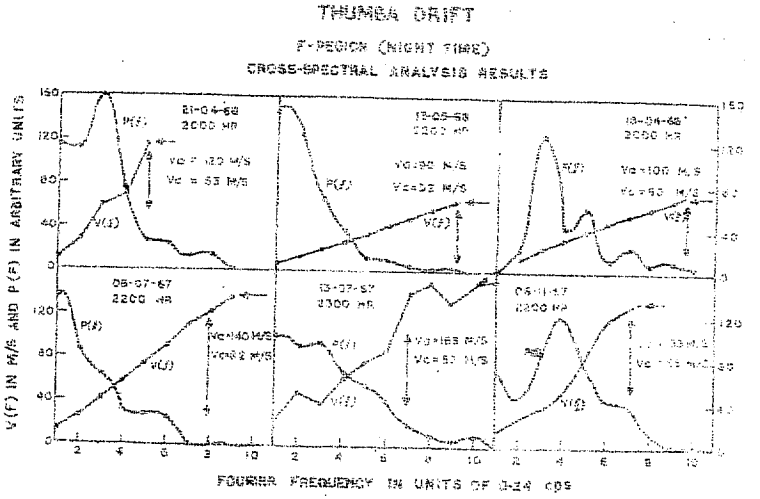

FIGURE 7.4

the daytime records while the last one in the night-time records. The normal distribution seems to be frequent for both the regions as well as day and night hours. The double peak of P(f) in F-region night-time corresponds to the drift records taken during the onset of spread-F where a fast fading is superimposed over a normal slow fading in the night.

The drift speed is found to increase slightly with the fading frequency in most of the cases studied. The drift direction showed no significant change with the fading frequency. The total range of variation of V(f) was higher during day and smaller during night. The values of V(f) varied systematically overthe significant power range after which there was found to be sudden increase in V(f). These values were not used.

The magnitudes of V_a (apparent drift speed as derived from the shift of the peak of cross-correlogram) and the characteristic drift speed V_c (as derived by full-correlation method of BRIGGS et al. 1950) are also mentioned in the corresponding blocks. The horizontal and vertical arrows represent the magnitudes of V_a and V_c respectively on the same scale as V(f). It is noticed that V_a represents in most of the cases the value of V(f) at the highest significant fading frequency and V_c is nearly equal to total frequency spread of V(f).

THUMBA DRIFTS

F-REGION (DAY TIME)

CROSS-SPECTRAL ANALYSIS RESULTS

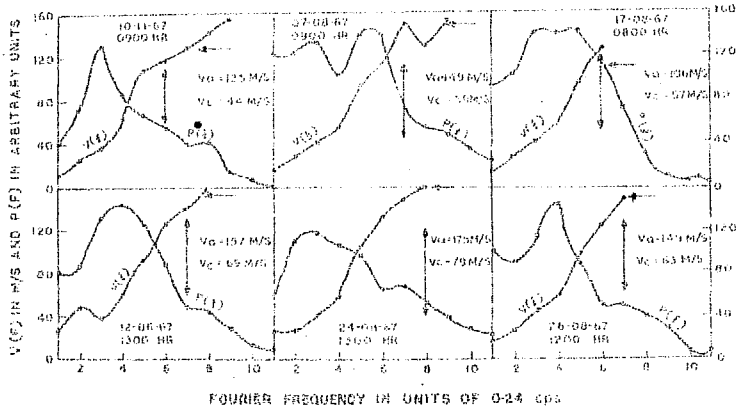

FIGURE 7.5

THUMBA DRIFT 1967-68

COMPARISON OF CROSS-SPECTRAL RESULTS WITH CORRELATION RESULTS

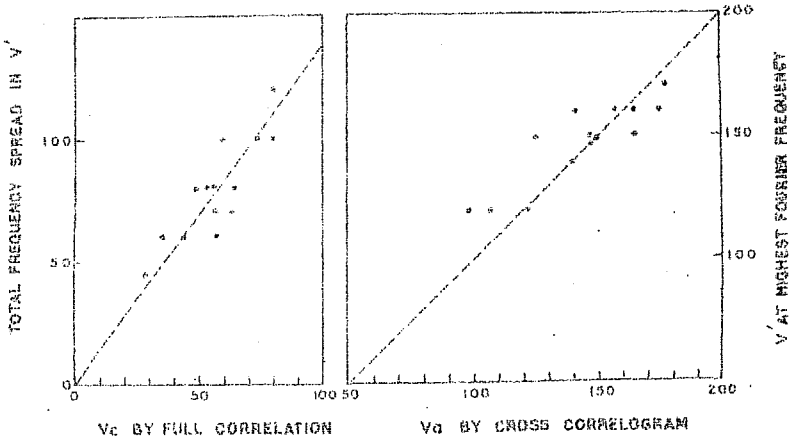

FIGURE 7.6

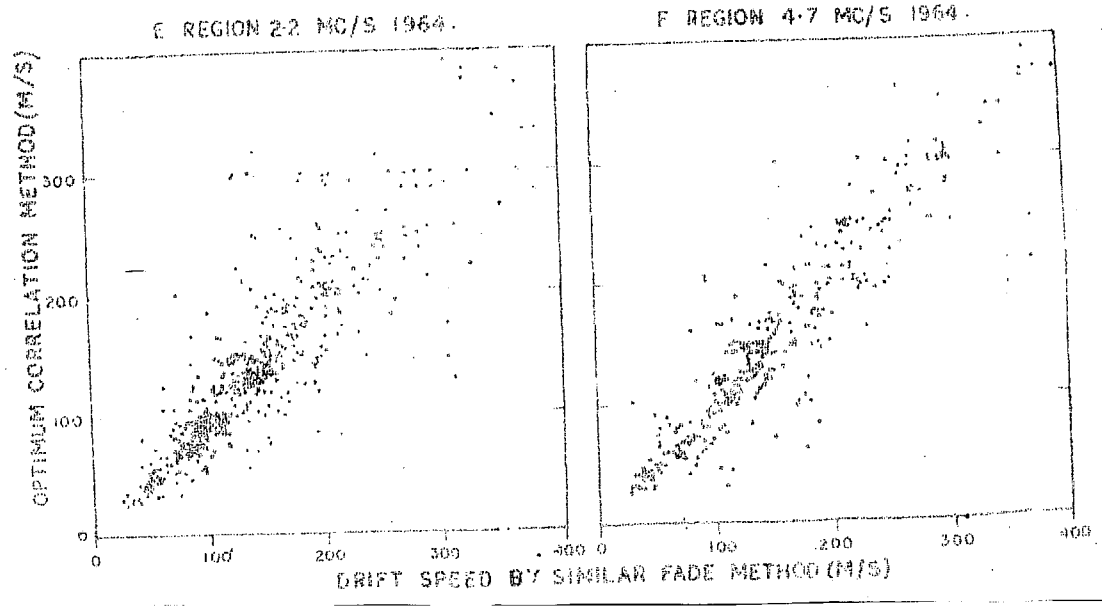

The Fig.7.6 gives the plot of the V_c against the frequency spread in V(f) as well as the plot of V_a against the highest frequency value of V(f). Both the plots show a linear relationship.

The results for Thumba also show that the drift speed (V) determined by the similar fades method agree very well with the drift speed of the major wave component determined from the power spectrum analysis, showing that in most of the cases, except those during spread-F, the similar fades method (MITRA, 1949) yields reliable results.

The present method of analysis yields full information in regard to the dispersive movement of the ionospheric irregularities. Whenever there is a consistent variation of speed with frequency, even after rejecting those values for which power is not significant implies that none of the traditional methods of analysis described in the Chapter II, III and V, yield a meaningful result for V and Ø. The results for Thumba show a positive dispersion of apparent drift speed for both E and F regions. The total extent of this dispersion is more in the day than the night. One explanation of such a result would therefore be that a system of waves exists in the ionosphere, each of these moving with different velocity. This has been shown mathematically by JONES and MAUDE (1965). This

involves an assumption concerning the shallowness of the disturbances and other interpretations are also possible.

7.2 Power spectrum results for drifts at other stations

Dispersion analysis has been applied to a number of different types of drift records from the ionosphere and the interplanetary medium. YERG (1956), JONES and MAUDE (1965), MCGEE (1966), GOSSARD (1967), JONES and MAUDE (1968), GOLLEY and ROSSITER (1970), PFISTER (1970) and HAUG and PATTERSEN (1970) analysed records of ionospherically reflected waves. The analysis has also been applied to records of ionospheric scintillations of radio stars and satellites, by BRIGGS and GOLLEY (1968), PAPAGIANNIS and ELKINS (1970) and to the records of interplenatory scintillations of small diameter radio sources by GOLLEY and DENNISON (1970). The results of some of these workers are discussed below.

GOSSARD (1967) has analysed fading records for 90 Km height by cross-spectral method after removing the Doppler spectral components resulting from the interference of the off-vertical reflections. Significant variations are observed both in $V(f)$ and $\sigma(f)$.

JONES and MAUDE (1968) have applied the above method to a few E-region records for Aberysweth (51°N) and found that the drift speed increases steadily with the fading frequency while the direction is not affected much. BRIGGS and GOLLEY (1968) have also noticed the presence of a positive dispersion of drift speed in the F-region, by the cross-spectral analysis of the scintillation records taken at three spaced interferometers (38 MHz) at Cambridge (52°N). The drift direction however remained more or less unaffected by the fading frequency. They also compared the values of $V(f)$ and $\phi(f)$ with those of Va and ϕa as well as Vc, determined from the cross-correlograms, (BRIGGS, PHILLIPS and SHINN, 1950). They found that Va is nearly equal to the $V(f)$ at the highest significant frequency of the fading in the record and ϕa agreed closely with $\phi(f)$, which did not change much. It was also found by them that Vc is nearly equal to the total range of variation of $V(f)$.

SPRENGER and SCHMINDER (1969) have shown using the high pass mathematical filters of variable cut off frequency f_c for low frequency drift records taken in central Europe, that V_a is independent of fading frequency. They concluded from this that in the lower ionosphere, the drift of the ionization results from a bodily movement of the irregularities, blown by the wind.

GOLLEY and ROSSITER (1970) have studied the frequency dependence of the drift velocity at Adelaide for the E -region and found that a significant number of drift records showed a positive dispersion in the drift. It occurred more frequently for the partially reflected echoes than for the total reflection from the E-region. On comparison with Va and Øa as well as Vc, similar results were obtained as BRIGGS and GOLLEY (1968) have obtained for Cambridge.

An independent confirmation of these findings has been recently reported by PFISTER (1970), using modified experiment with three or more receivers, where phase and amplitude variations are measured, simultaneously in order to dispense with long array of aerials as used by BRIGGS et al. at Adelaide. Pfister has shown that for E-region at Billerica, Massachusetts, V(f) increases with fading velocity and Ø (f) agrees with in 30° to the Øa values.

HAUG and PATTERSEN (1970) have observed a positive dispersion of drift velocity at Tromso (Norway).

7.3 Interpretation of results

Little variation of ϕ (f) and its close agreement with ϕa is expected as the cross-spectral analysis makes no correction for anisotropy and the direction must therefore be very nearly perpendicular to the axis of elongation of the pattern. The same is true for ϕa, which is the apparent direction from the cross-correlogram. The value of Va determined from the shift of the peak of cross-correlogram takes into account mainly the highest frequency component of the record and hence agrees with the high frequency end of V(f). The low frequency components will contribute to the shapes of the functions at large time shifts (SPRENGER and SCHMINDER 1969) but will be relatively unimportant in influencing the positions of the maxima.

JAMES (1962) has shown that if a number of patterns moving with different speeds are superimposed, the value of Vc will be of the same order as the range of velocities involved. The present result for Thumba as well as other stations is not unexpected due to the dispersion effects. MCGEE (1966) has shown that the dispersion is associated with the showness of the cross-correlation functions. This aspect is discussed in details for Thumba in the next section of this chapter.

Origin of dispersion in the ionosphere

The most direct explanation could be the propagation of some kind of dispersive waves through the E and F regions of ionosphere. However this interpretation involves serious difficulties as the dispersion observed is very variable in magnitude and even reverses its sign occasionally (as can be seen from some of the results for Thumba). Also the dispersion is most often positive whereas internal gravity waves can give rise to only negative dispersion.

It therefore confirms that the movements observed in splaced receiver experiment are a type of plasma drift produced by the combined action of $\vec{E}$ and $\vec{B}$ fields (MARTYN 1959). On this theory, the variability and the effect of magnetic disturbances on the drift is readily expressed by the changes in the electric field strength. If an electric field E exists in the ionosphere, this will produce a bodily drift of ionization with a velocity $\vec{E} \times \vec{B}/B^2$, where B is the strength of earth's magneticfield. CLEMOW and JOHNSON (1959) have shown that weak cylinderal irregularities, aligned in the direction of B will also drift with the same velocity. The same authors have also derived the dispersion equation using a perturbation treatment, which gives the relation between frequency and wave number of a particular Fourier component of electron density

perturbation. The dispersion of velocity derived from this [illegible] is however negligible to account for the observed dispersion in the drift.

Other possible causes of the dispersion in the ionosphere which can be significant are discussed below:-

(i) Height gradient of the horizontal drift in the ionosphere

Height variation of the horizontal drift both on E and F regions at Thumba has been earlier indicated (MISRA and RASTOGI 1970). BEDINGER et al. (1968) have also shown by the rocket experiments that there are sharp gradients of drift speed around 100 km within a range of 5 Kms. Similar results have been obtained by RAO and RAO (1961) for F-regions at Waltair. As the electronic gate used for the selection of a particular echo for drift recordings has a finite width (2-5 kms), the record thus obtained is contaminated with the echoes from the very close ranges within this height interval and the dispersive nature of drift velocity is revealedin the cross-spectral analysis according to the relation $f = V/\lambda$. The fading imposed at different points will be of different frequencies.

Another possibility could be that apart from the vertical dispersion of the velocities, at any given height there exists a spectrum of wavelengths (BRIGGS and GOLLEY 1963). Therefore at any height V is definite, but due to

varying λ, we shall get according to the equator $f = V/\lambda$ different fading frequencies from different slant heights from the same level of reflection. Each reflecting height would produce one frequency spectrum shifted to the right or left depending on the velocity. The results of observed amplitude at frequency f_1, say, would now arise from superposition of the components coming from different heights, each having a different velocity and wavelength but all satisfying the relation $f_1 = V/\lambda_1$. The velocity at f_1 will therefore be an integrated mean of the velocities of all these components. Similarly for other frequencies.

(ii) Independently moving reflecting secreens

HAUG and PATTERSEN (1970) has generated mathematically the observed dispersion of drift velocities at Tromso (Norway) in terms of the velocities (V_1, ϕ_1), (V_2, ϕ_2) etc of a number of independently moving reflecting screens at the same height. Such an analysis was possible from the skewness of the cross-correlograms.

(iii) Dispersive nature of the vertical drift velocity

The component of non-horizontal drifts in the ionosphere is also measured by the closely spaced receiver method, alongwith the actual horizontal drift of the ionization. It is, therefore, possible that the dispersive

nature of this oblique movement of the ionospheric irregularities could give rise to the dispersion of the horizontal drift determined by the cross-spectral analysis. RASTOGI (1971) has shown evidence of the height variation of the vertical drifts from the upward moving kinks on the ionograms.

This effect will however be significant only when the magnitude of vertical drifts is comparable with that of the horizontal drift. For an equatorial station such as Thumba, this possibility is very rare as the horizontal drifts are of the order of 100-200 m/s whereas the vertical drift in F-region is nearly 16-20 m/s (see section 2.5 of Chapter VI). However, the vertical drift increases with height in F-region and reaches a magnitude of nearly 50 m/s near the peak F_2-region (at about 400 Km). Near the Sq focus, V_H and V_Z are of comparable magnitudes. For higher latitude V_Z is low and should not be taken as the contributing factor ($V_Z = Ey/B \cos I$).

(iv) Height gradient of scale size of irregularities

To account for the occasional observations in which the sign of dispersion is reversed, it is necessary to postulate that on these occasions the scale size of the irregularities also varies with height. Suppose, for example, that the irregularities have a larger scale size in the

regions where the drift velocity is large than in the regions where it is small. Then if the variation of scale size is sufficiently great, it will be found that the low frequency components give the higher velocities. In gerneral, the variations of scale size with height will introduce an additional cause of dispersion which may either add to or subtract from that produced by a vertical gradient of horizontal velocity. The above theory will still hold when the transmission is oblique instead of vertical with the only difference that the variation of V and scale size with height will be replaced by the variation along the line of sight.

(v) Gravity waves

Gravity waves are generated by the lower atmospheric disturbances such as thunderstorms, nuclear explosions and other man made disturbances. A considerable part of the energy of these oscillations is able to penetrate through the troposphere and effect the E and F-regions of the ionosphere. These waves have a period of 10 mins to 2 hrs and are amplified as they move upward due to decreasing density. There are two types of gravity waves, namely internal and external or surface gravity wave. A gravity wave is called internal when the wave number K is real and surface wave when it is imaginary. HINES (1960) and

SCORER (1953) have respectively discussed the properties of these two types of waves. HINES and RAO (1968) have discussed the possible effects of the gravity waves on the ionosphere in producing wavemotions. The velocity for for the internal gravity waves decreases with the increasing frequency and hence these are either not present in Thumba ionosphere or they are not detectable by the closely spaced receiver method as there is always a positive dispersion observed at Thumba. Surface gravity waves however have a positive dispersion and are produced by wind shears in the atmosphere. The Thumba results of cross-spectral analysis, similar to those for Adelaide, Cambridge and Aberysweth, show the presence of positive dispersion and hence the surface gravity waves.

(vi) Variability of Drift speed during the course of a record

BRIGGS (1967) and FELGATE and GOLLEY (1971) have shown that the positive dispersion will result if the record length analysed is larger than the period over which the drift is likely to remain constant. Experience shows that the drift at Thumba is fairly fixed in both magnitude and direction except around the reversal timings for a period of nearly one to two hours where as the length of the records used for anlysis are only half to one magnitude long.

It has however been shown by FELGATE and GOLLEY (1971) that the artificially introduced variations in the velocity of ionospheric drifts records also produce a positive dispersion, similar to the drift records with naturally occurring velocity variations. Three receiver dispersion analysis (cross-spectral analysis) must therefore be treated with some caution unless it can be shown that the records are statistically stationary. A two dimensional spatial dispersion analysis given by BRIGGS (1968) is not affected by these spurious velocity variations. However a very large array of receiving aerials is required for this method such as used by GOLLEY and ROSSITER (1970) at Buckland Park, Adeliade which consists of 89 receiving dipoles.

The wavelike character of the diffraction pattern on the ground is therefore confirmed from four indpendent measurements at different stations namely Adelaide, Thumba, Cambridge, and Billerica, Mass. Little can be said about the horizontal wavelength or period of atmospheric waves or their vertical excursion. Obviously a single smooth and well defined wave does not fit the observations. It could be a combination of a large internal gravity wave and a superposition of relatively short lived ripples moving essentially with the wave. The fact that the measurements of the receiver are limited practically to short distance, the picture of the reflection surface is incomplete.

This deficiency can be corrected with a relatively simple improvement in the data processing system by scanning the height gate in descrete steps as described by BIEL and GORMAN (1970). It then will be possible to determine slant range, dippler shift, and the direction of all the reflecting areas of a single frequency at a given instance and their variation with time. This should be lead to a realistic description of the motions and fine structures in the ionosphere.

Some other tests for the dispersion in the Ionospheric drifts

Though the full cross- spectral analysis is the best method to study the dispersion in the drift velocity, it requires very tedious and time taking mathematical computation. The idea of the dispersion in the drift can be had by studying the following three properties of the cross-correlograms, which are obtained while analysing the drift records by Phillips and Spencer's method. These are described in the following:

7.4 Comparision of apparent drift speed as determined by similar fades method and from the shift of the maxima of cross-correlogram

JONES and MAUDE (1968) have shown that the difference between V' and Va would be one of the indications of the presence of dispersion in the ionosphere. This is shown by

the analysis of artifically constructed fading record. On account of the presence of dispersion or the randomness, the fading records at any two aerials are similar but not identical in details. In the simple Mitra's method of similar fades which consists of the optical comparison of the similar features of the two records, the eye would unconsciously pick out the sharp definedfeatures for comparison so that the velocity thus obtained would correspond to the highest frequencies present in the record. The numerical correlation would on the other hand give an equal weightage to all the frequencies present. If the V' values are consistently higher than Va the positive dispersion is present and if V' < Va then the dispersion is negative.

This method was applied to the drift data for Thumba as shown in the Fig.7.7. It is seen that for both F and F-regions the deviation between two values is not much for smaller values but slightly more for the higher values of velocity.

As the points are distributed more or less equally on both sides of the 45° line, and as the spread is very small it can be concluded that in general there is very little dispersion at Thumba.

7.5 Skewness of the cross-correlograms

MCGEE (1966) has shown that the asymmetry of the cross-correlation curves is associated with the dispersion in the drift velocity along that direction. He defined an skewness parameter for the asymmetrical cross-correlation as follows:-

If M is the point of maximum cross-correlation and P is the foot of the perpendicular from M on a line AC drawn at half the height of maximum and B is the middle point of this line, then the Skewness of this curve is given by S = PB/BC.

The skewness is positive if B is further away from origin than the point P. In the given figure, the skewness would be negative. Same convention will hold if the asymmetry is in the other direction. The advantage of this technique has in the fact that it can be quickly applied to the existing cross-correlogram used for full correlation method, to determine the nature of ionospheric movements (i.e whether it is a ma movement or the wave motion).

If the random drift parameter is caused by the dispersion or the spread of V with frequency, as shown by the results discussed in the section 7.4 of this chapter, then the skewness (S) should be related directly to the ratio of random to steady drift (i.e.Vc/V)as determined from

the full-correlation analysis.

The skewness parameters for Thumba were studied in the light of above discussion. Only ten percent of the records studied, showed the skewness in the E-W cross-correlograms. The N-S cross-correlograms were mostly symmetrical. These were grouped in the day and night hours and the histograms for the percentage occurrence were made as shown in the Fig.7.8. The skewness was found to be predominantly positive during the day and negative during the night with the most probable values as + 0.12 and - 0.15 respectively.

This effect has been investigated by a few other workers for different stations. BRIGGS and GOLLEY (1968) have studied the distribution of skewness parameters for Cambridge, using the spaced scintillation records of the source casiopeia-A. They found a most probable value of this parameter to be + 0.03, though it was present in almost all their records. Kaushik studied the distribution of S for Ahmedabad and Halleybay.

The interrelation of S and Vc/V is shown in the Fig.7.9 for Thumba. There is a fairly linear relationship showing that the dispersion of the drift in ionosphere contributes directly to the randomness parameter Vc.

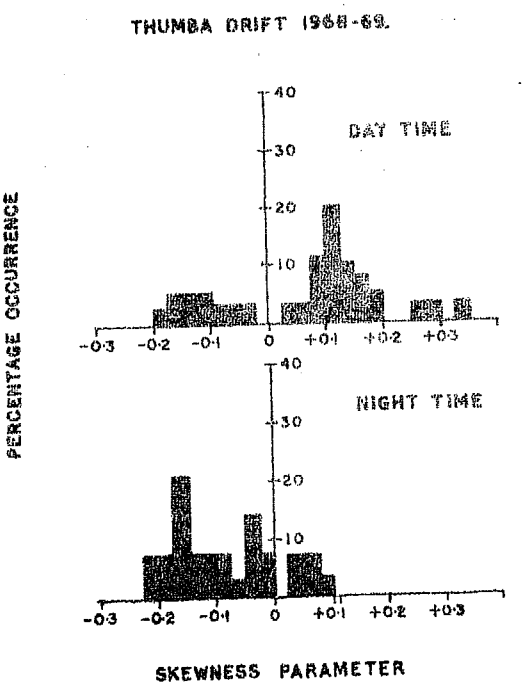

FIGURE 7.8

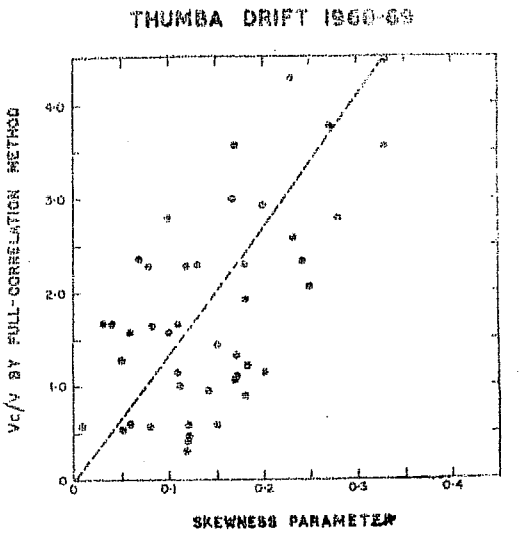

FIGURE 7.9

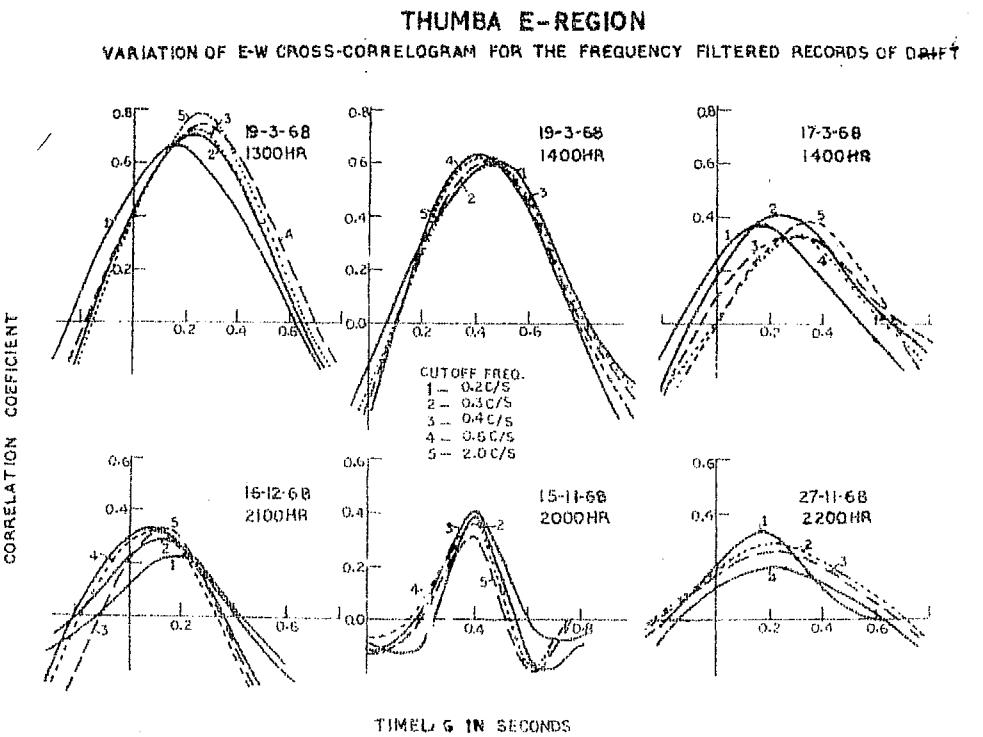

FIGURE 7.10

HAUG and PATTERSEN (1970) have explained the asymmetry of the cross-correlograms in terms of the individual reflecting screens moving with different velocities. They have calculated these velocities for a few observed asymmetric correlograms.

Cross-correlation functions for satellite scintillations at spaced receivers show a systematic skewness indicative of the dispersive motions (PAPAGIANNIS and ELKINS, 1970).

7.6 Analysis of frequency filtered drift records

From the investigation of the power spectrum of the reflected signals by theory of the auto-correlation functions, it is seen that there is always a considerable power in the fading components with periods shorter than the mean fading period. In order to study the behaviour of these short period fading components separately, SPRENGER and SCHIMINDER (1969) suppressed the long period fading componenets before subjecting the records to correlation analysis. This has been achieved by transforming the original fading functions X (t), Y(t) and Z(t) according to:

$$X(t)' = 1/T_f \int_{t-Tf/2}^{t + Tf/2} X(t) . dt$$

and similarly for Y(t)' and Z(t)'.

The deviations from a running mean are calculated over a given time interval T_f which is centered on the time t of the respective amplitude value. The new functions X(t)', Y(t)' and Z(t)' are then used for the computation of the correlation functions. This procedure acts as a high pass filter with a cut-off frequency $F_f = 1/T_f$ and suppresses fading components with frequencies $F < F_f$.

SPRENGER and SCHMINDER (1969) compared the cross-correlograms for these five filtered series of amplitudes. It was found that the width of the correlation functions decreases systematically with the increasing cut-off frequency but the time shifts of the maxima of cross-correlation function remained nearly unchanged (in contrast to the results of JONES / and MAUDE (1965). Thus the apparent drift speed V_w calculated from these time lags did not change with fading frequency. SPRENGER and SCHMINDER (1969) also calculated the steady drift speed V and the characteristic drift speed Vc, using the relations given by BRIGGS et al. (1950). The steady drift V showed a distinct increase with the increasing frequency of the fading components, whereas the random drift Vc showed only a slight decrease. The increase of V with frequency is interpreted by the short period fadings originating from a reflection level slightly higher than the long period fadings. The observed velocity increase may

therefore indicate a real velocity gradient with height. A gradient of nearly 1-2 m/s /km has thus been derived. Mean vertical wind gradients of this order of magnitude have been found from the radar meteor wind measurements (GREENHOW and NEWFIELD, 1961). The slight decrease of Vc with fading frequency can also be explained in terms of this concept of different reflecting levels for the components of different fading frequency, since the upper part of the reflecting region is near the turbo-pause level where turbulence vanishes.

A number of drift records for E and F region for Thumba were filtered mathematically using the cut off frequencies F_f = 0.2, 0.3, 0.4, 0.6 and 2.0 c/s. The resulting series of amplitudes x(t), y(t), and z(t) were used to compute the cross-correlograms in E-W and N-S directions. A set of E-W cross-correlograms for E-region for some of these records are shown in the Fig.7.10. The N-S correlograms showed no significant change with thevariation of F_f due to extremely high correlation in that direction at Thumba and hence are not shown here.

Two types of cases were observed. Firstly those in which the peak of the cross-correlogram did not shift with the increase in F_f, such as on 15th Nov, 2000 hr and 27th Nov 2200 hr. These were the cases when the ionization

moved as a whole as far as the apparent drift is concerned. In the second type of cases, the peak of the cross-correlogram shifted more and more away from the zero, as F_f increases. This indicated a positive dispersion in the apparent drift speed. Sometimes Va showed an irregular variation with the F_f when both positive and negative dispersions were present. The steady and random drift speeds V and Vc were also derived by using these correlograms (BRIGGS et al.1950) and a slight increase in V with F_f was noticed in a number of cases. Vc however did not show a definite dependence on F_f.

7.7 Variation in the shape of the cross-correlation curves with the receiver separation

The auto-correlation and the power spectrum of the fading signal are fourier transforms of each other. If the pattern on the ground is considered to behave as a number of sine waves moving with possibly different velocities, the signal recorded at a second nearby receiver will be the same as that at the first receiver except for a phase change for each sine wave. The cross-correlation curve will therefore be the same as the auto-correlation curve except for a phase change of the various frequencies of which the pattern is composed of.

It is possible to make use of a mathematical analogy to predict qualitatively how the cross-correlation curve will change if the separation of the two receivers is increased. DOWN and MAUDE (1968) derived mathematically the shape of this curve, at various separations in terms of the wave packet at various times. A wave packet too may be considered as being made up of a number of sine waves and its shape sometimes later may be found by imposing a phase change on each of these wave. If the wave packet is travelling through a non-dispersive medium, the phase change will be inversely proportional to the wavelength and the wave packet will move, undistorted to a new position. In the same way, if the phase change of the cosine functions which make up the auto-correlation curve is inversely proportional to their period, the cross-correlation curve will have the same shape as the auto-correlation curve but will be displaced sideways. This will be the case if the pattern moves as a whole over the ground.

If the wave packet travels through a dispersive medium, the phase and group velocity will differ and wave-packet will distort as it moves. In particular if the spectrum of the wave packet is sufficiently narrow for the packet itself to show oscillations around the principal wavelength, the individual peaks will travel through the

packet, growing as they enter from one side and dying away again as they leave from the other-side.

If the pattern of signal strength on the ground moves in a dispersive manner, the phase change which is imposed on each frequency in transforming the auto-correlation into cross-correlation function will not be inversely proportional to the frequency and some kind of distortion which occurs to the wave packet will occur to the shape of the correlogram too (see Fig.7.11 a).

Of particular importance is the case where the phase change imposed is independent offrequency as this is approximately the condition in the case described by MAUDE and JONES (1965). In this case the group velocity is zero and the individual peaks will pass through a stationary packet.

The above reason is general and does not depend on the power spectrum. Fig.7.11(b) shows a set of cross-correlation curves resulting for varying receiver separation, when the drift velocity is assumed to be proportional to the fading frequency. The theoretical variation of the delay of a maxima of cross-correlation curve with the increasing receiver separation will look-like the parallel line of Fig.7.11(c). This line will pass through the origin only if the ground diffraction pattern moves

as a whole . A few sets of multi-antenna records for E-region were taken for the investigation of this effect. Out of nearly thirty records studied for the cross-correlation curves with the increasing aerial separation in eastwest or noth-south direction, most of them showed no distortion in their shape with increasing separation. Only a few showed the distortions similar to what is discussed above. Some of the F-region cross-correlograms for different aerial separations in the east-west direction are shown in the Fig.7.12. A few actual records are reproduced in the accompanying plate. As the pattern is highly elongated along the north-south direction at Thumba, it was not possible to detect the presence of wave motion in this direction as the correlation value charged very little even with the large change in the receiver separation.

The plot of the time lag of maxima with increasing receiver separation is given in the Fig.7.13. Only two of these lines pass through origin indicating the mass movement of the ionization. The other two cases indicate a dispersive drift of ionization in accordance with the theoretical prediction of DOWN and MAUDE (1968).

KELLEHER (1966) has also studied the cross-correlation curves for F-region and JONES (1968) has studied the dispersion of E-region by this method. KELLEHER found

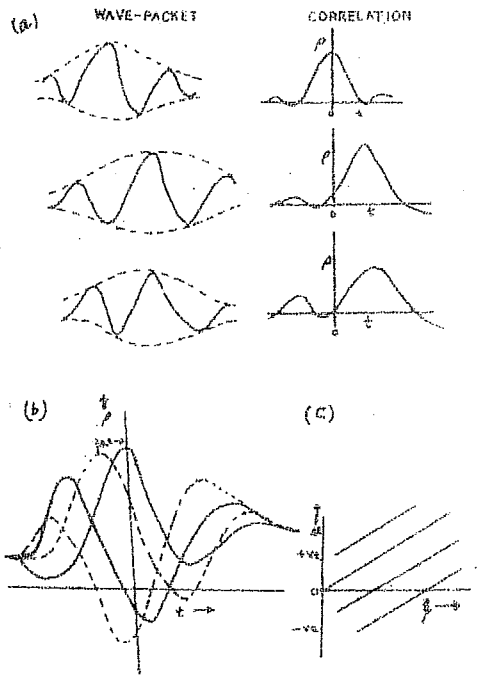

FIGURE 7.11

THUMBA DRIFTS

SHAPE OF EAST-WEST CROSS-CORRELOGRAMS WITH INCREASING SEPARATION
(PRESENCE OF WAVE MOTION)

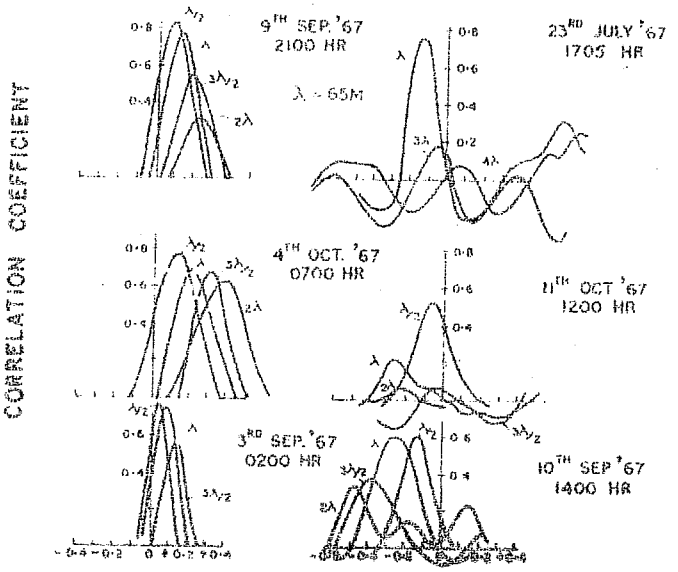

FIGURE 7.12

THUMBA DRIFT

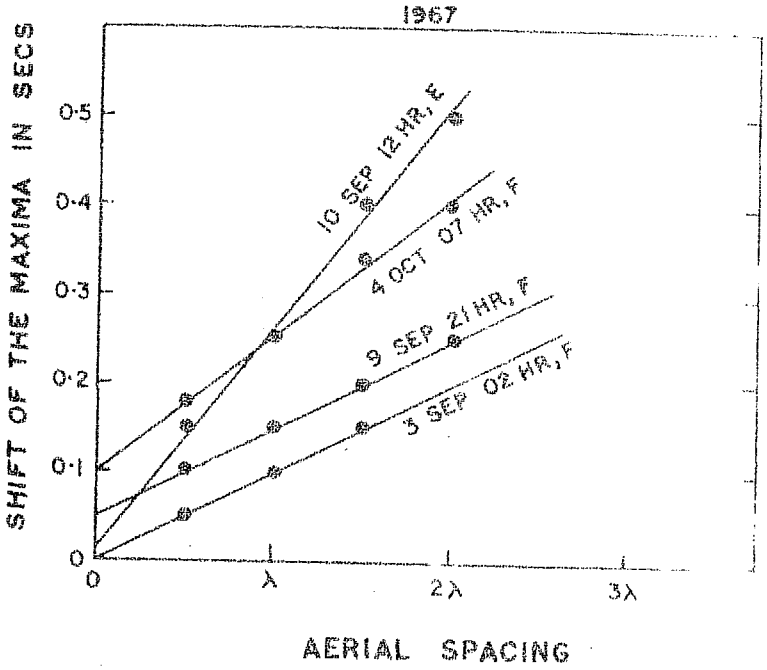

FIGURE 7.13

THUMBA E-REGION

MULTI FREQUENCY CORRELOGRAM

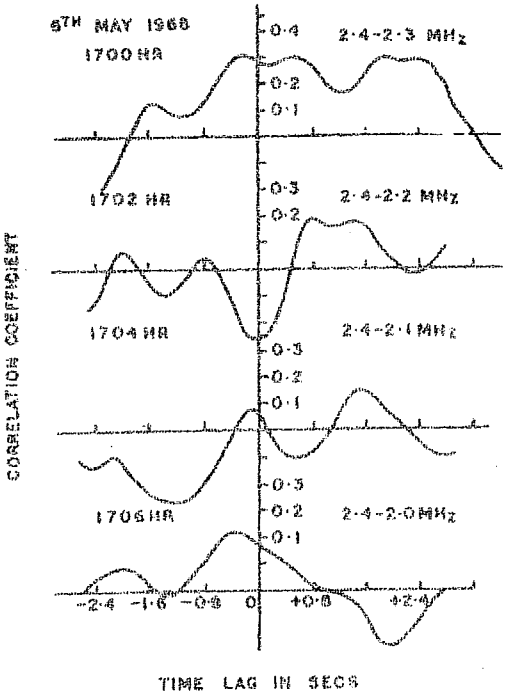

FIGURE 7.14

that only a quarter of the 66 records studied gave a straight line passing through the origin. In other cases these lines did not pass the origin, but were parallel to this. Jones too obtained similar results for E-region. Thumba results are of two types, one in which the plot of τ_{max} vs $\frac{1}{f}$ passesthrough origin and another in which it does not. ELKINS and PAPAGIANNIS (1970) have studied the multi-frequency cross-correlation curves instead of the multi-antenna curves, which show a similar variations of the shape as would be expected in the caseof dispersion. The frequency separation instead of receiver separation also causes the variation of total path length traversed by the wave-packet as the height of the reflection charges and hence is the manifestation of a similar phenomenon. Frequency separated cross-correlograms were studied for Thumba also for F-region in a limited number of cases. The E-region results are shown in the Fig.7.14. The maximum correlation is not significant, probably due to large height change by a change of only 0.1 MHz. Still thes shape of the cross correlograms is very much variable with the increasing difference of frequency, in the case of E-region. Due to low values of correlations involved, it is not possible to say definately by this result, that the dispersion is present in the drift speed.

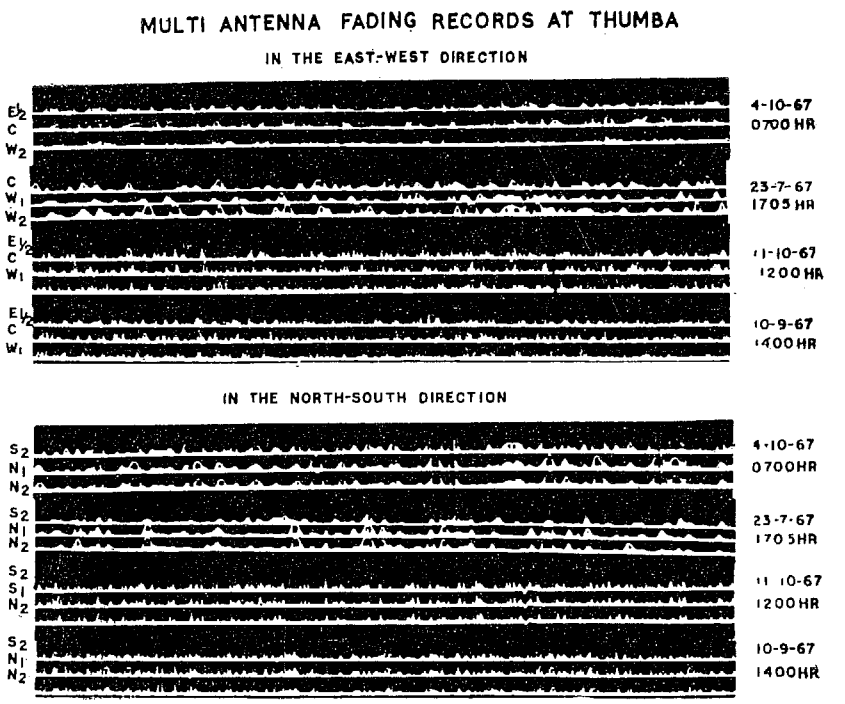
MULTI ANTENNA FADING RECORDS AT THUMBA
IN THE EAST-WEST DIRECTION
E½
C
W2
4-10-67
0700 HR
C
W1
W2
23-7-67
1705 HR
E½
C
W1
11-10-67
1200 HR
E½
C
W1
10-9-67
1400 HR
IN THE NORTH-SOUTH DIRECTION
S2
N1
N2
4-10-67
0700 HR
S2
N1
N2
23-7-67
1705 HR
S2
S1
N2
11-10-67
1200 HR
S2
N1
N2
10-9-67
1400 HR

Figure 7.15

7.8 Conclusions

It can be concluded from these results that the horizontal drifts at Thumba exhibit slight positive dispersion during day and slight negative dispersion during the night. The results of the similar fades analysis as discussed in Chapter II are reliable measurements of the drift speed and direction of the major wave component present in the fading of the signal. The height gradient of horizontal drift and presence of gravity waves may be the possible causes of slight dispersion in the drift speeds in E and F regions at Thumba.

CHAPTER VIII

THUNDERSTORM AND THE OCCURRENCE OF NIGHT-TIME SPORADIC E AT THUMBA

8.1 Introduction

The sporadic E layer of the ionosphere occurs broadly in three zones (1) the auroral zone in which the occurrence of E_s is predominantly a night-time phenomenon with little seasonal variation, (2) the mid-latitude zone in which it is a summer-time phenomenon occurring both during day and night but more intensely during day and (3) the equatorial zone in which sporadic E is a day-time phenomenon with little seasonal variation (RATCLIFFE, 1962).

Various theories have been suggested to explain the occurrences of temperate latitude sporadic E. DUNGEY (1956, 1959) had suggested that the ionization could be compressed by a north-south shear moving the ionization up and down along magnetic field lines. The idea has been further developed by WHITEHEAD (1960, 1961, 1962). The convergency of ionization has also been suggested due to the neutral wind shear (WHITEHEAD, 1967). LAYZER (1967) proposed that the gravity shock waves produce sudden changes in the vertical layer movement causing the convergency of the ionisation. The plasma instabilities in the

E-layer due to gravity as well as background electron density gradient have been suggested to cause the sporadic E ionization (LIU and YEH, 1965; TSUDA, 1966). The ionization by energetic particles have been also suggested one of the causes of sporadic E ionization.

The equatorial E-region have been shown to be closely associated with the equatorial electrojet currents, both in the diurnal and latitudinal variations (KNECHT and MCDUFFIE, 1962). FARLEY (1963a,b) suggested that when the electron drift velocities exceed the ion thermal speed, two stream plasma instabilities are created giving rise to E_s reflections. Meteor has also been suggested as a cause of the sporadic E ionization (GREENHOW, 1954).

Thunderstorms were suggested to cause the ionization of the regular ionosphere itself (WILSON, 1925), which was immediately proved to be untrue but the sporadic E have been found by various authors since then to be associated with the thunderstorms (RATCLIFFE and WHITE, 1934; BHAR and SHYAM 1937; STOFFREGEN 1944; MITRA and KUNDU 1954; RASTOGI 1957, 1962; DATTA, 1970). Many authors have found lack of correlation between thunderstorm and sporadic E ionization (APPLETON, NAISMITH and INGRAM, 1936; RANGARAJAN, 1954). It may be pointed out that

when there are possibilities of so many agencies causing the sporadic-E ionization, it is rather unlikely to obtain a high correlation between the sporadic E ionization and any index of thunderstorm. It was therefore stressed by RASTOGI (1957, 1962) that the relation between the thunderstorm and sporadic E should be studied only during the passage of isolated thunderstorms over the region of observation.

8.2 Ionospheric soundings during thunderstorm activity

The present chapter describes the occurrence of sporadic E ionization during individual thunderstorms at an equatorial station (Thumba 0.6°S dip) during the night-time. The period of study was May to July 1968. The occurrence of the thunderstorm and other related meteorological parameters were recorded by the meteorological section of the Thumba Rocket Launching Station. The occurrence of sporadic E ionization in the night-time were detected in the vertical pulse ionospheric drift equipment at Thumba but they were later confirmed from the ionograms recorded on C_4 vertical ionosonde situated nearby.

The number of occurrence of fEs during each of the months of the year 1968 in the evening (18 - 24 hr) is shown in Fig.8.1. June, July and August are the months

of highest occurrence of E_s. Again in the months of January and December, the fEs 2.0 occurs for fairly large number of times. RAMANATHAN (1921) has given the occurrence of thunderstorms for Trivandrum, according to which the thunderstorms are most active during the months of April, May, June and July and again in the months of October, November, December and January. The summer month occurrence of E_s in 1968, therefore, seems to have been caused by thunderstorms.

The daily variation of the occurrence of frequency of fEs greater than 3.0, 3.0 and 7.0 MHz as well as the monthly median fEs during the months of May, June and July 1968 at Thumba are shown in Fig.8.2. As well known, the sporadic E at the equator is predominantly a day-time phenomenon. It can be seen from these diagrams that fEs at Thumba occurs mostly between 06 and 18 hr. The monthly median value of fEs is around 7.0 MHz between 09 to 16 hr. The occurrence frequency of fEs $>$ 5.0 MHz is for more than 80% of occasions during the day while during the night-time fEs $>$ 5.0 MHz is either absent or occurs on less than 5% of the occasions. During June 1968, the occurrence of fEs between 3.0 and 5.0 MHz was roughly around ten percent.

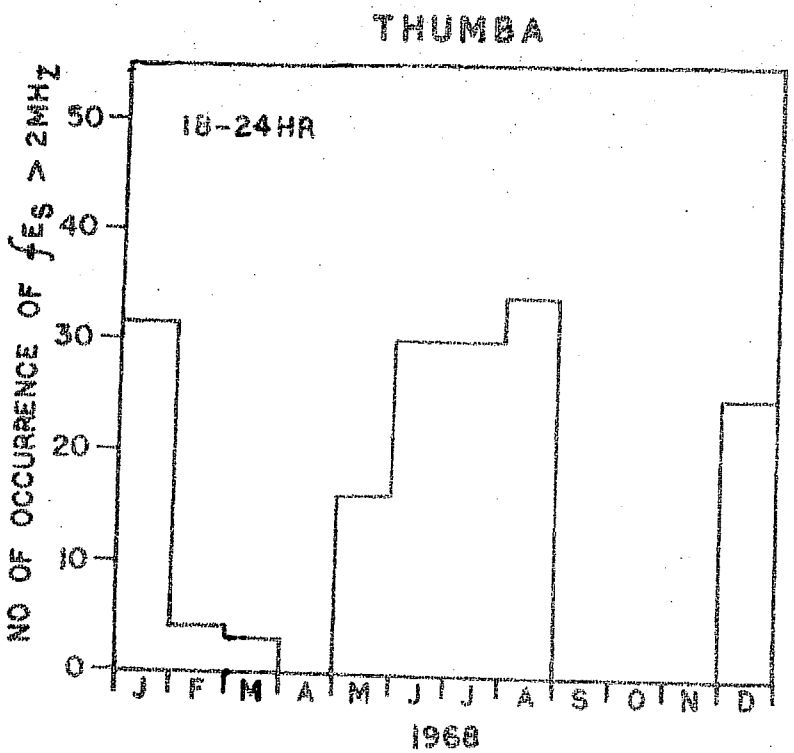

FIGURE 8.1

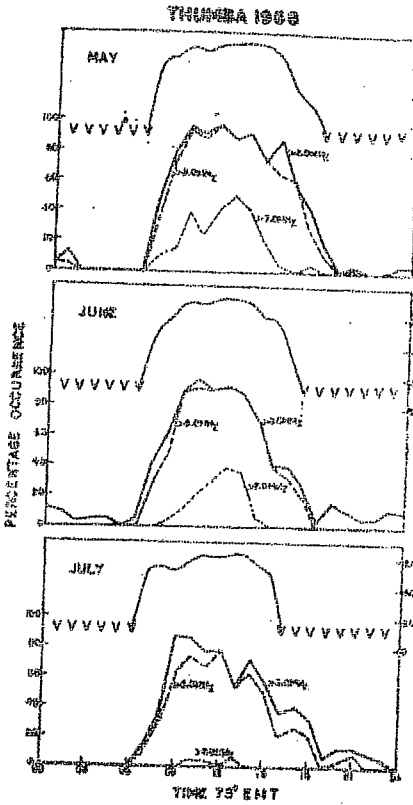

FIGURE 8.2

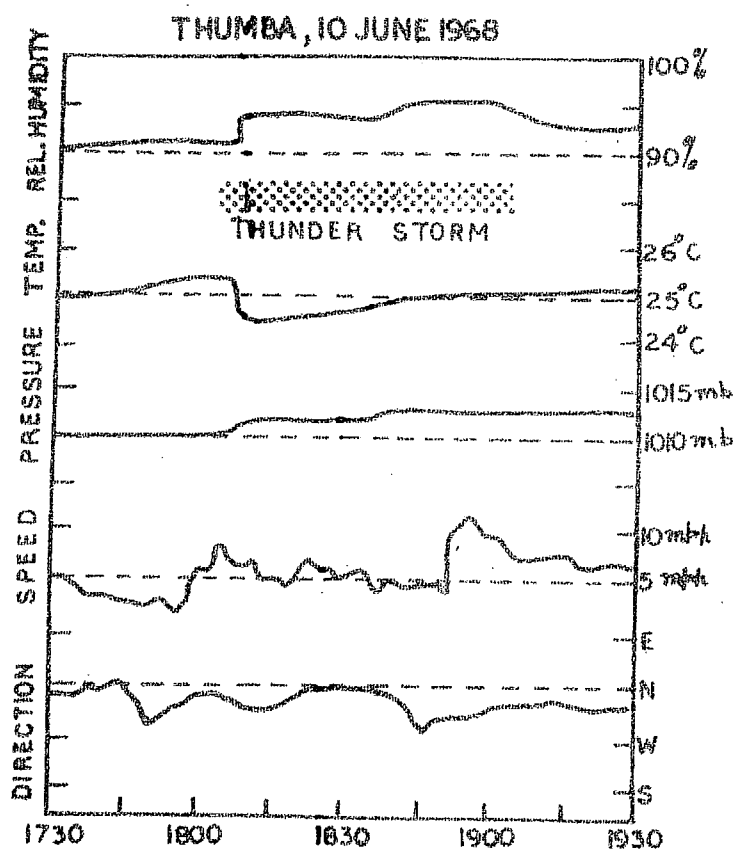

FIGURE 8.4

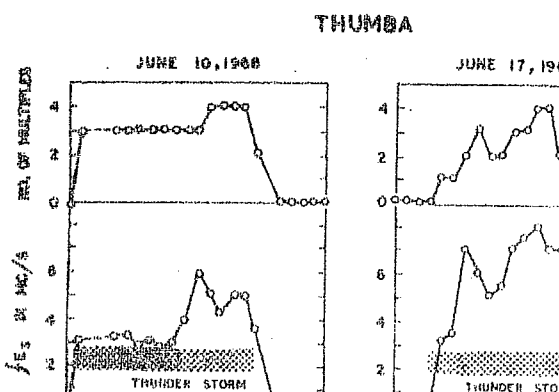

FIGURE 8.6

The ionograms taken at Thumba during the passage of thunderstorm on June 10 and June 17, 1968 are reproduced in Figs.8.3 and 8.4. The variation of fEs, number of multiples and the period of thunderstorm activity are shown in Fig. 8.5.

Referring to the thunderstorm on June 10, 1968 (Fig.8.2), it is seen that there is no sporadic E at 1800 hr, while at 1815 hr three multiples of E_s appeared with fEs of about 3.0 MHz. The E_s continued to remain at this level till 2015 hr after which fEs further increased attaining a maximum of 6.0 MHz with four multiples at about 2045 hr. The M and N type reflections between E_s and F layers are also present. The E_s layer decayed slowly disappearing completely at 2230 hr. The period of thunderstorm activity started at about 1800 hr and lasted till 2200 hr. The corresponding humidity, temperature, pressure and the wind speed and direction variations are shown in Fig.8.6. The shaded portion indicates the period of thunderstorm. There is seen to be a sudden increase in humidity and fall in temperature around 1745 hr. The pressure also shows a slight increase at the same time. These changes are not very large as the humidity at Thumba is almost always near 100% and the temperature variations are also small. The wind speed at 200' level

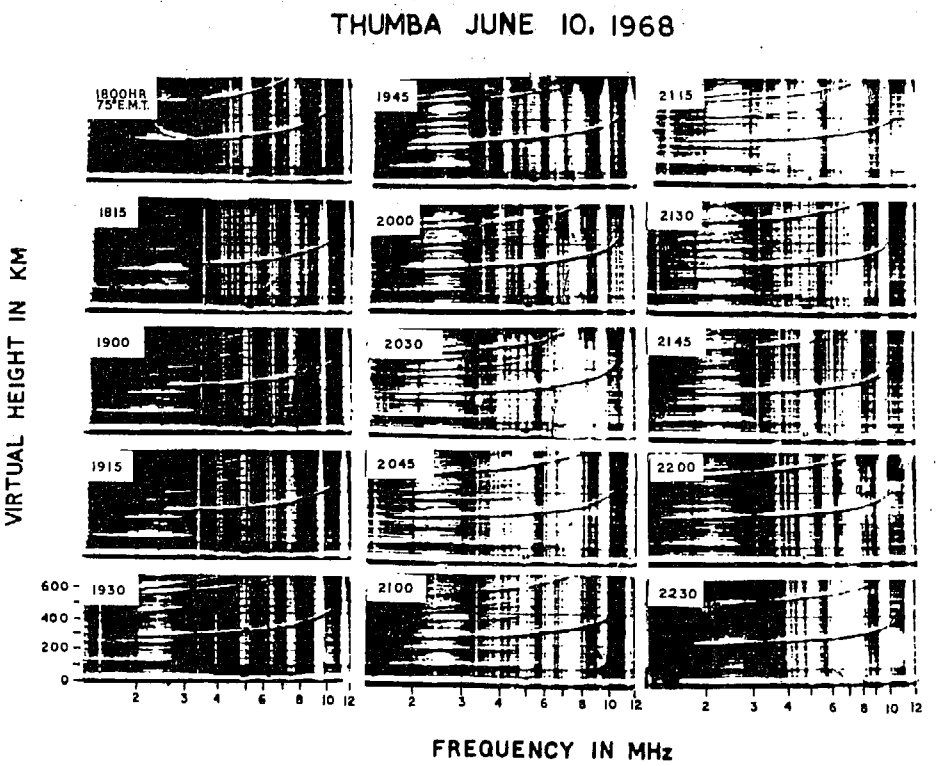

Figure 8.3

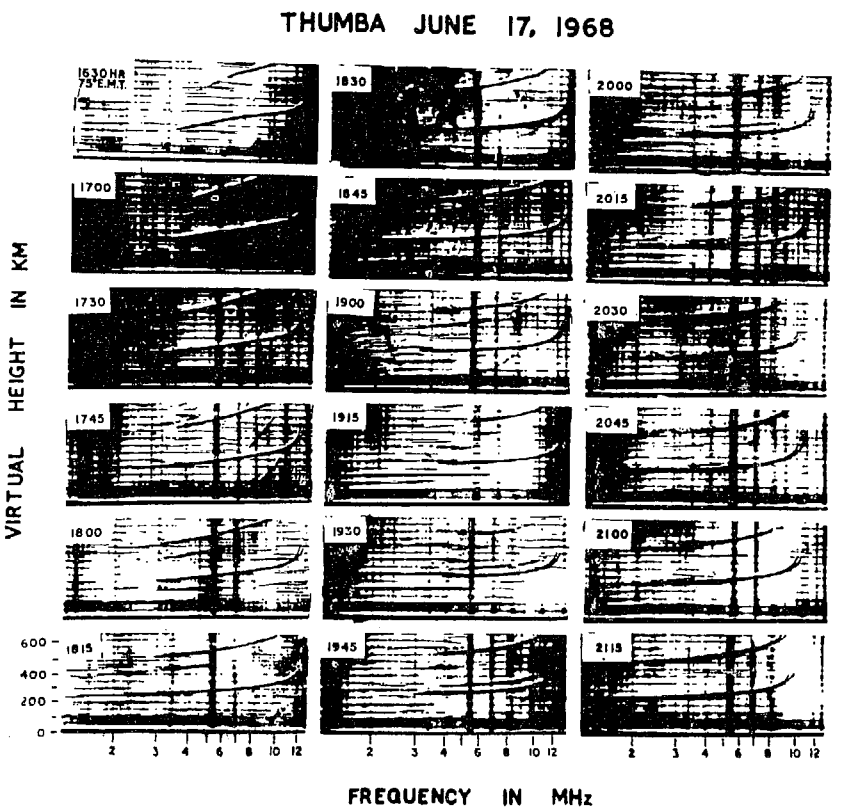

Figure 8.5

is seen to have increased from 5 to 10 mph around 1730 hr and then again fall to about 5 mph at about 1745 hr. Wind direction also shows fluctuations between North and West at these two times. All this points towards the onset of a thunderstorm over Thumba at about 1745 hr.

The thunderstorm on 17 June 1968 (Fig.8.4) was more severe and of shorter duration. It appeared from observing station at about 1720 hr and disappeared at about 2030 hr. The corresponding fEs and number of multiples (Fig.8.5) showed a sudden rise with the onset of thunderstorm (1730 hr) and a slow disappearance of sporadic E ionization after the passage of the storm. There were no sporadic E reflections till 1715 hr while at 1730 hr a strong E_s reflection was seen with fEs of about 3.2 MHz. It became more and more intense as the thunderstorm built up, reaching a maximum of about 8.5 MHz with four multiples at 1930 hr. The ionization started decaying slowly afterwards vanishing completely at 2115 hr.

Other cases of the passage of thunderstorm and the correspondingly changes in fEs and number of multiples are collected in Fig.8.7. The ionograms for some of these are reproduced in Figs.8.8 and 8.9. The corresponding meteorological parameters namely humidity, temperature and pressure are shown in Figs.8.10 and 8.11. The wind speed and

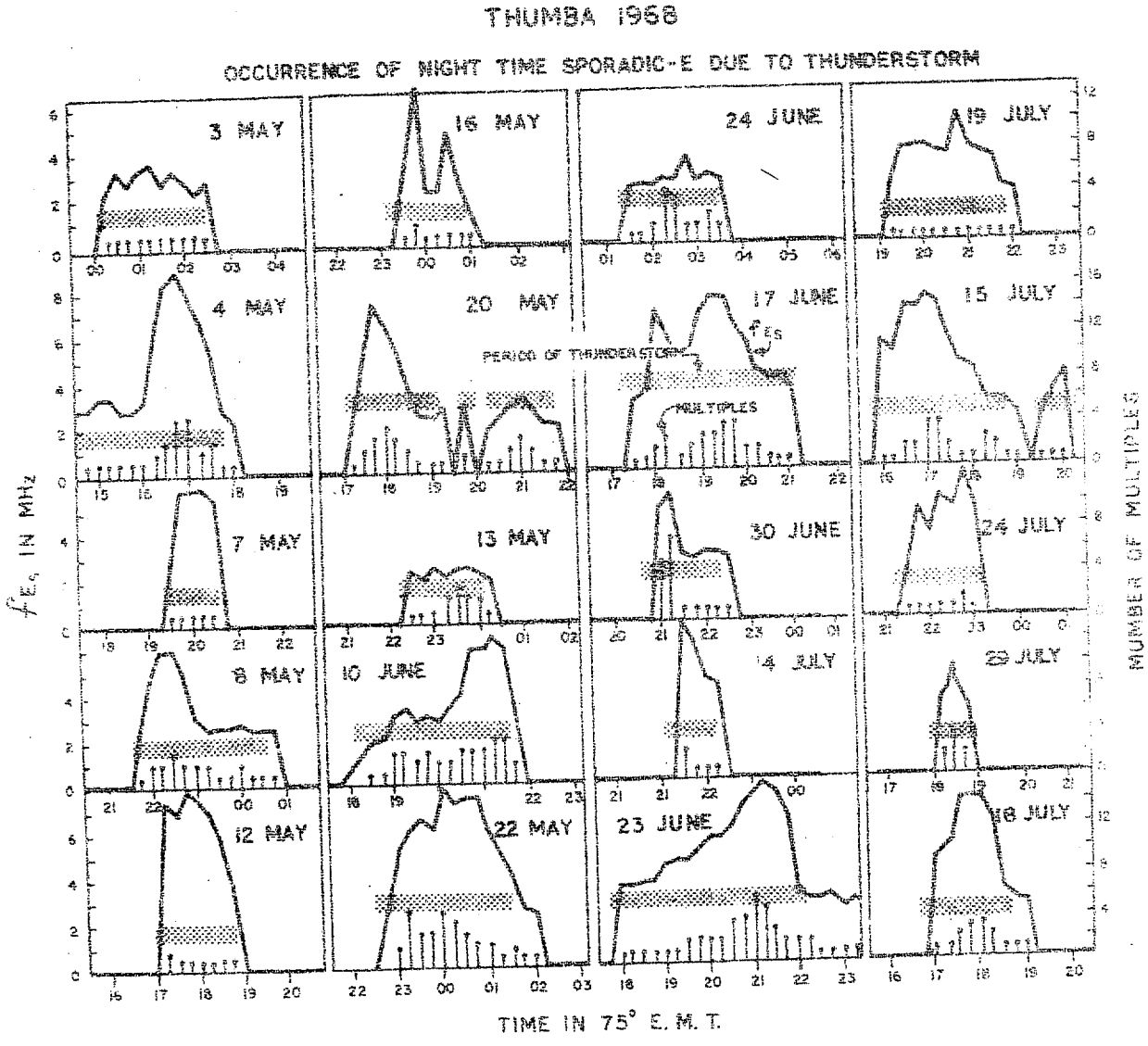
THUMBA 1958
OCCURRENCE OF NIGHT TIME SPORADIC-E DUE TO THUNDERSTORM
3 MAY
16 MAY
24 JUNE
19 JULY
4 MAY
20 MAY
17 JUNE
15 JULY
PERIOD OF THUNDERSTORM
MULTIPLES
7 MAY
13 MAY
30 JUNE
24 JULY
8 MAY
10 JUNE
4 JULY
29 JULY
12 MAY
22 MAY
23 JUNE
28 JULY
f_{Es} IN MHz
MUMBER OF MULTIPLES
TIME IN 75° E. M. T.

FIGURE 8.7

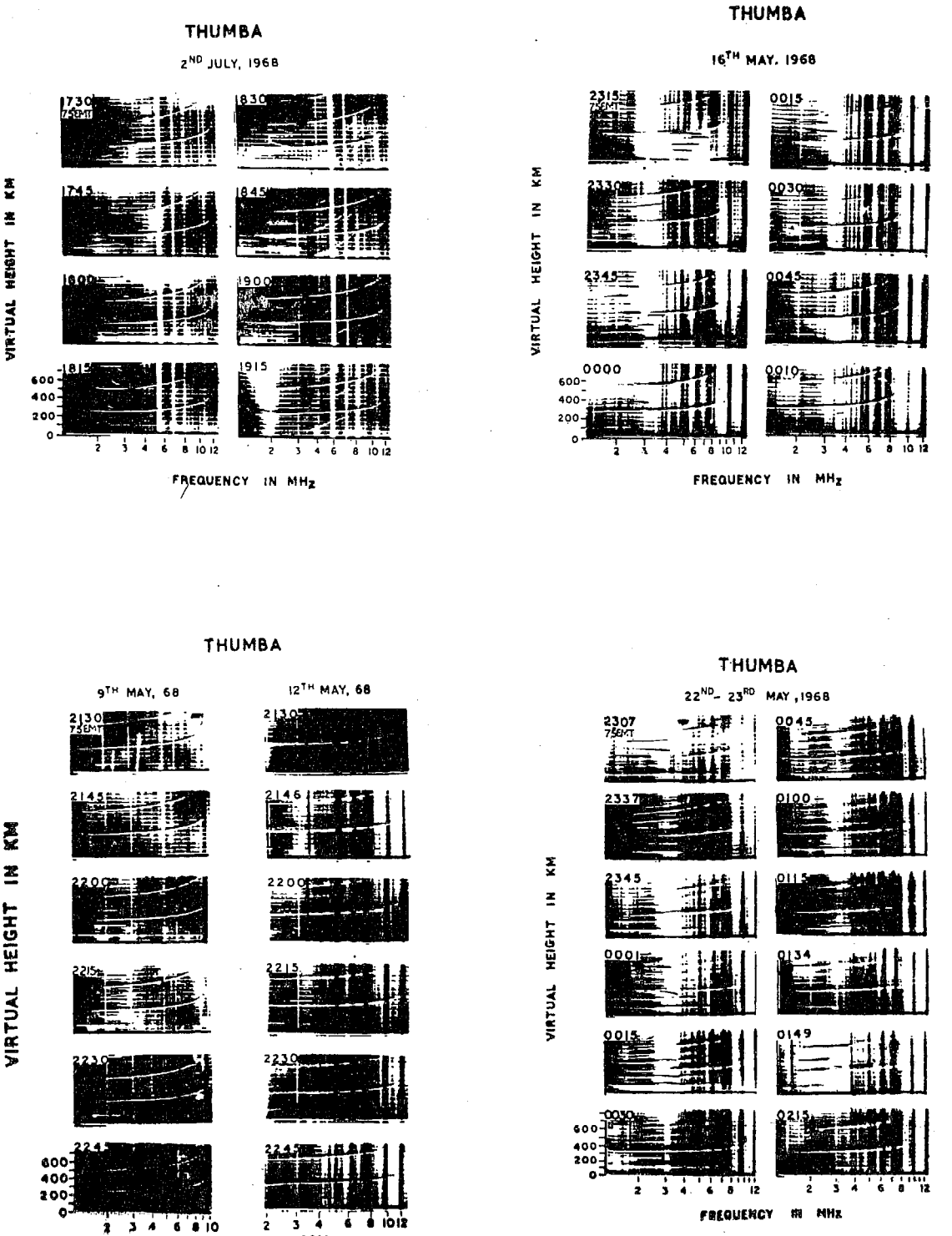
THUMBA
2ND JULY, 1968
1730 75EMT
1745
1800
1815
1830
1845
1900
1915
VIRTUAL HEIGHT IN KM
600
400
200
0
2 3 4 6 8 10 12
FREQUENCY IN MHz
THUMBA
16TH MAY, 1968
2315 75EMT
2330
2345
0000
0015
0030
0045
0010
VIRTUAL HEIGHT IN KM
FREQUENCY IN MHz
THUMBA
9TH MAY, 68
12TH MAY, 68
2130 75EMT
2145
2200
2215
2230
2245
2130
2146
2200
2215
2230
2245
VIRTUAL HEIGHT IN KM
600
400
200
0
2 3 4 6 8 10
2 3 4 6 8 10 12
FREQUENCY IN MHz
THUMBA
22ND- 23RD MAY, 1968
2307 75EMT
2337
2345
0001
0015
0030
0045
0100
0115
0134
0149
0215
VIRTUAL HEIGHT IN KM
600
400
200
0
2 3 4 6 8 12
FREQUENCY IN MHz

Figure 8.8

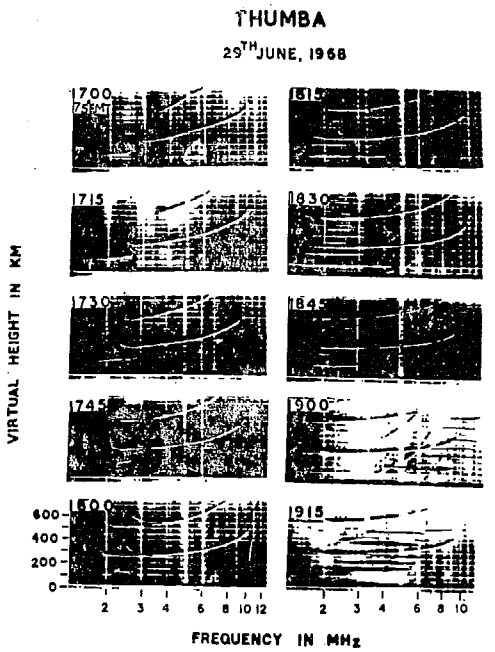
THUMBA
29TH JUNE, 1968
VIRTUAL HEIGHT IN KM
FREQUENCY IN MHz

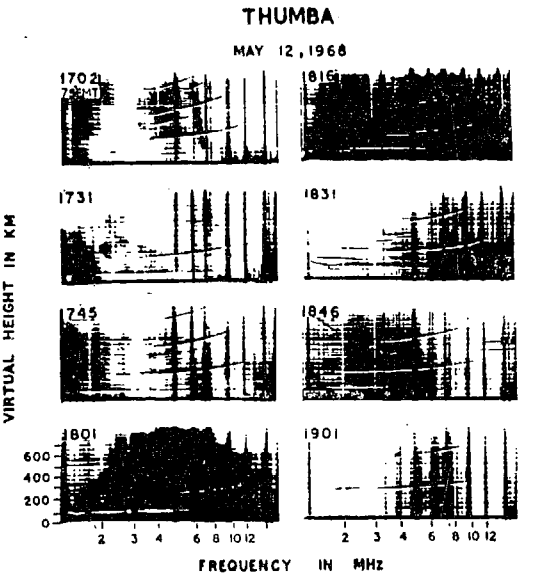
THUMBA
MAY 12, 1968
VIRTUAL HEIGHT IN KM
FREQUENCY IN MHz

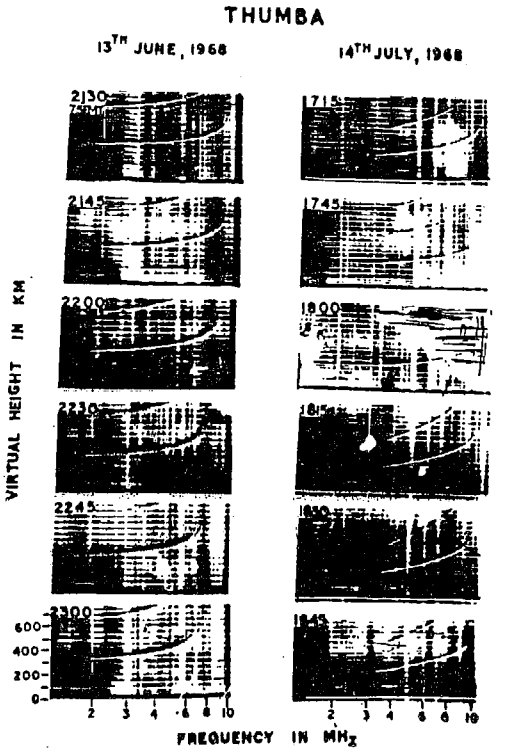
THUMBA
13TH JUNE, 1968
14TH JULY, 1968
VIRTUAL HEIGHT IN KM
FREQUENCY IN MHz

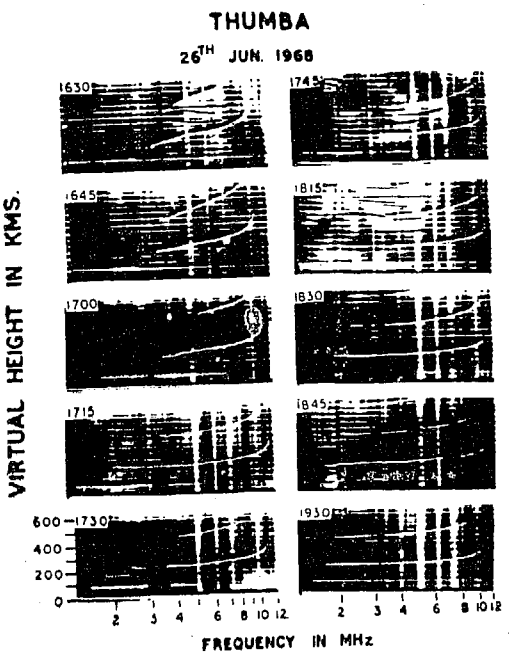
THUMBA
26TH JUN. 1968
VIRTUAL HEIGHT IN KMS.
FREQUENCY IN MHz

Figure 8.9

METEOROLOGICAL CHARTS DURING THUNDERSTORMS AT THUMBA

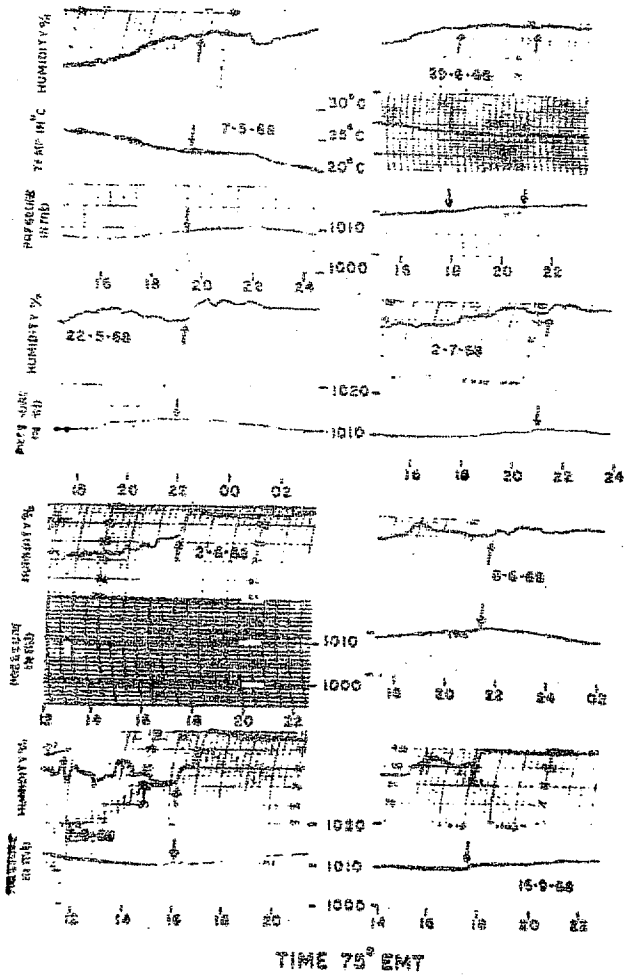

FIGURE 8.10

METEOROLOGICAL CHARTS DURING THUNDERSTORMS AT THUMBA

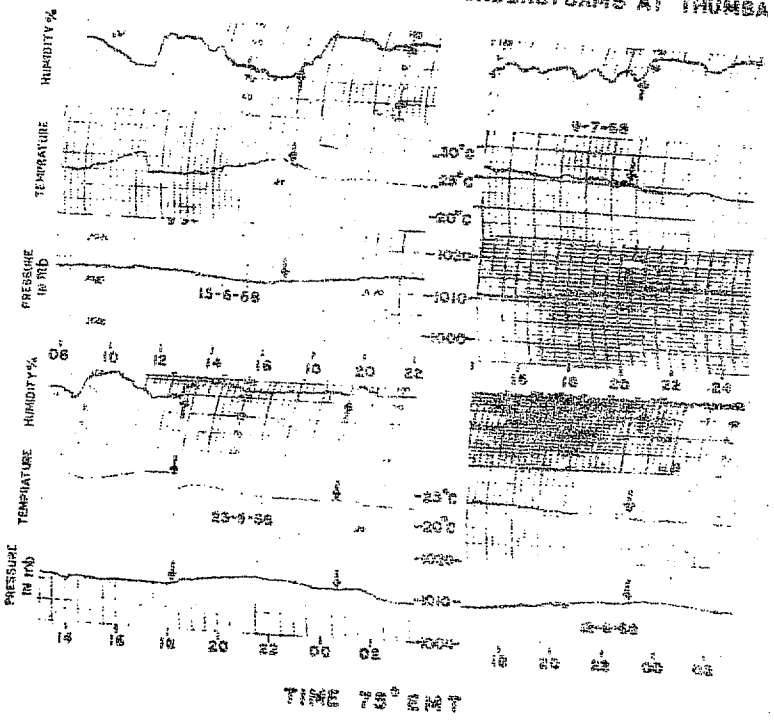

FIGURE 8.11

WIND SPEED AND DIRECTION AT 200 FT. LEVEL AT THUMBA DURING THE THUNDERSTORMS

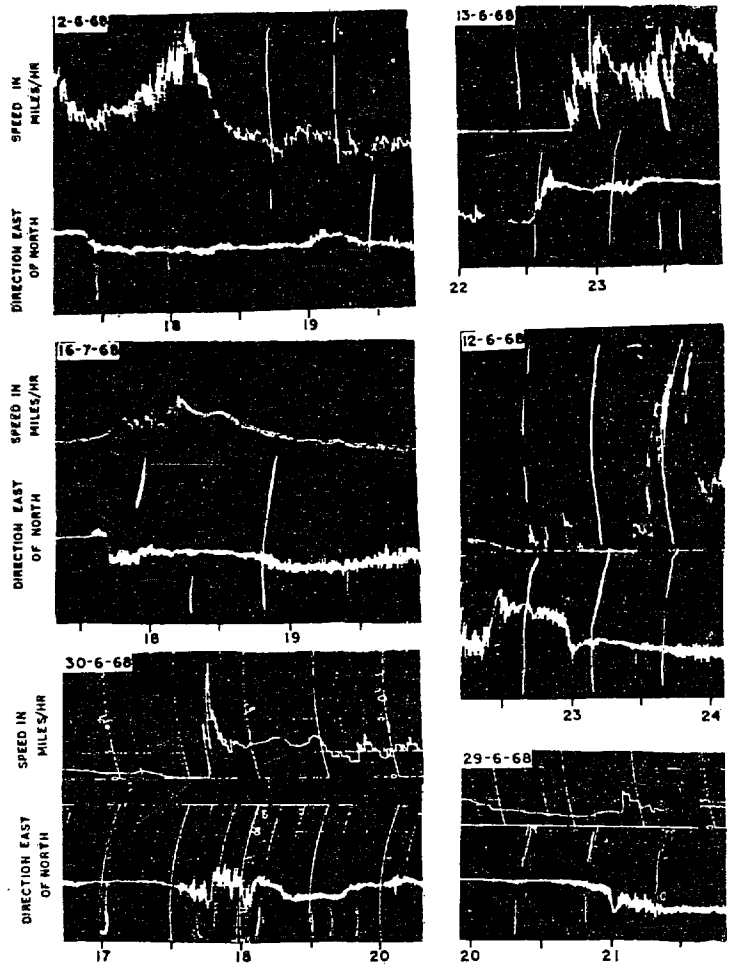

TIME 75° EMT

Figure 8.12

WIND SPEED & DIRECTION AT 200 FT. LEVEL AT THUMBA DURING THUNDERSTROMS

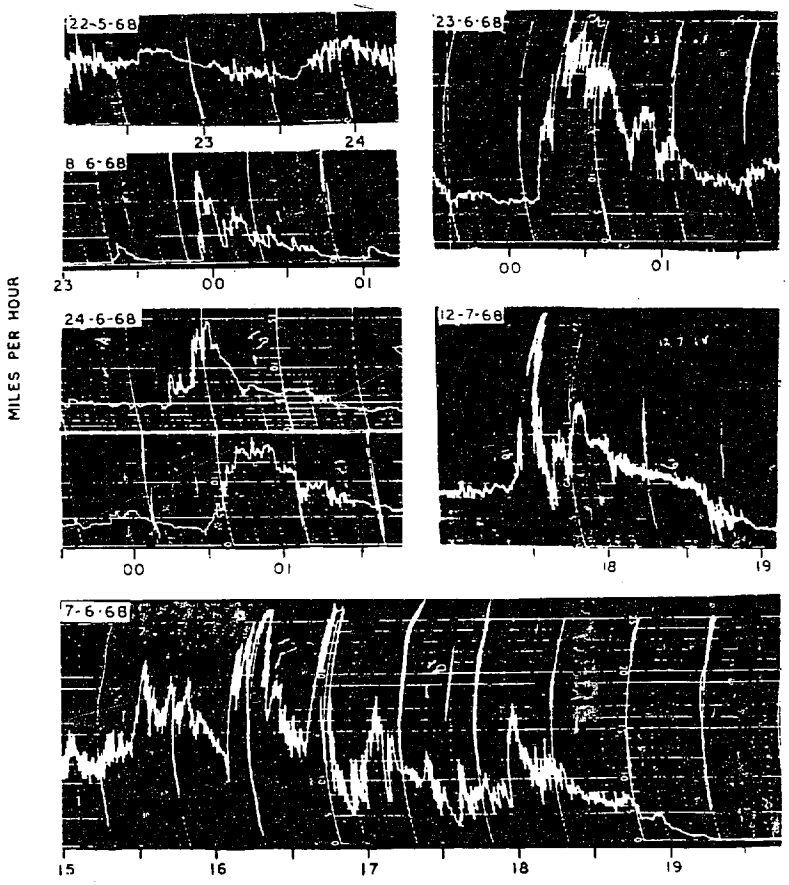

TIME 75° EMT

Figure 1.13

direction at 200' level are given in Figs. 8.12 and 8.13. The variation of fEs is shown by thick solid curve and the number of multiple echoes by the length of vertical lines and the period of thunderstorm activity by shaded portion.

8.3 Conclusion

It is seen from all these observations taken at Thumba that some of the thunderstorms which occur isolated at the equatorial station do produce an increase in fEs. These sporadic E reflections seem to be different from those observed during the day. The day-time E_s is always completely transperant to the reflection from the higher regions and normally no higher multiples are recorded. The thunderstorm produced E_s is on the other hand of a blanketing type and large number of multiple echoes as well as the reflections between the F and the top of E_s are observed. The day-time E_s is thus due to the scattering of radio waves by the irregularities in the normal E region whereas the thunderstorm E_s could be an irregular patches of ionization produced by the thunderstorm. In the case of an intense thunderstorm these could form a partly homogeneous layer.

More refined observations of the meteorological parameters of the thunderstorm in the changes produced

in the height and the ionization of the E_s at an equatorial station could greatly assist in explaining the coupling between the ionosphere and the lower atmosphere.

8.4 Discussions

These observations show for the first-time that the thunderstorms can produce the sporadic E ionizations at very low latitude station. Recent techniques enabling minute fluctuations in the height of the ionization in the ionospheric layer have shown that atmospheric disturbances like hurricanes affect even the higher F_2 region of the ionosphere (BAUER, 1958). GEORGE (1968) has found an apparent relationship between certain ionospheric disturbances with the occurrence of severe weather in the troposphere. SHRESTHA (1971) has shown for Brisbane that the enhanced sporadic E ionization is associated with the cold fronts and microbarometric activity. Generation of atmospheric waves in the frontal region and its leaking to the ionospheric heights is suggested as the possible cause of the enhanced E_s ionization. The original suggestion of WILSON 1925) about thunderstorm causing the ionospheric ionization was based on the discharge in the ionospheric region due to direct electrostatic field of the thundercloud or in terms of the stream of energetic electrons

flowing from the top of the thundercloud upto the E-region. WORMELL (1953) suggested that the enormous potential developed in the thundercloud could drive a vertical current upwards from the earth through the cloud and on into a highly conductive region above. This upward conduction current have been measured directly either by means of high altitude acroplanes flying over the thundercloud (GISH and WAIT, 1950) or by means of the radar echoes (RUMI, 1956). RASTOGI (1962) suggested that thunderstorms may generate gravity waves of enough energy which could affect the ionization in the sporadic E region. PIERCE and CORONITI (1966) have advanced the idea that E_s is caused by the transfer of acoustical energy produced by the top of the oscillating thundercloud to the ionosphere. GEORGE (1968) has discussed the propagation of these gravity waves through the ionosphere and has explained the wave-like ionospheric disturbances characterised by the periods in the range of 2 - 5 minutes in terms of the filtering of these gravity waves in its passage through the troposphere.

REFERENCES

Alpert, Ya.L.	1960	The Propagation of Radio Waves and the Ionosphere, Moscow, Izd-vo, ANSSSR.
Appleton E.V. & Ratcliffe J.A.	1927	Proc. Roy. Soc., A115, 315.
Appleton, E. V., Naismith, R., & Ingram, L.J.	1936	Phil.Trans., A236, 191.
Appleton, E.V.	1946	Nature, 157, 691.
Balsley, B.B.	1966	Ann. de. Geophys., 22, 460.
Balsley, B.B.	1969	J.A.T.P., 31, 475.
Balsley, B.B.	1965	J.Geoph. Res., 70, 3175.
Balsley, B.B. & Woodman, R.F.	1969	J.A.T.P., 31, 865.
Bailey, D.K.	1948	Terr.Mag.Atmos.Electr., 53, 3[illegible]
Banerji, R.B.	1958	Sci. Rep. No.81, Perm.Stat.Univ
Bauer, G.J.	1958	J. Geophy. Res., 63, 265.
Bhar, J.N., & Shyam, P.	1937	Phil. Mag., 23, 513.
Berg, H. Von.	1955	Physics of the Ionosphere, (Lond)., pp.4.
Bedinger, J.F., Knaflinch, H., Manring, E., & Layzer, D.	1968	Planet.Space Sci., 16, 159.
Berkner, L.V. & Wells, H. W.	1934	Terr.Mag.Atmos.Electr., 39, 21[illegible]
Barber, N.	1957	J. A.T.P., 31, 119.

Blackman, R.B., & Tuckey, J.W.	1958	Power spectrum analysis.
Balsley, B.B.	1969	J.G.R., 74, 1213.
Benynon, J.G. & Wright, J.C.	1969a	J.A.T.P., 31, 111.
Benynon, J.G., & Wright, J.C.	1969b	J.A.T.P., 31, 593.
Bibl, K., Harnischamacher,E. & Rawer, K.	1955	The Physics of Ionosphere, Phy. Soc. London, p.113.
Bibl, K., & Gorman,J.E.	1970	AFCRL, 70, 0259 (Report)
Booker, H.G., & Wells, H.W.	1938	Terrest.Mag. Atmos. Elec., 43, 249.
Booker, H.G., Ratcliffe, J.A. & Shinn, D.H.	1950	Phil. Trans. Roy.Soc.,242, 57.
Bowles, K.	1960	J. G. R., 57, 191.
Bowhill, S.A.	1956	J.A.T.P., 8, 120.
Brameley, E.N., & Peart,M.	1965	J.A.T.P., 27, 1201.
Brameley, E.N., & Young, M.	1968	J.A. T.P.,30, 99.
Brennon, D.G.	1969	Statistical methods in Radio Propagation, p.296, Pergamon Press, Oxford.
Briggs, B.H., Phillips, J. S., & Shinn, G.J.	1950	Proc.Phys. Soc., B63, 106.
Briggs, B.H., & Spencer, M.	1954	Rep. Prog. Phys,, 17, 245.
Briggs, B.H., & Golley, M.G.	1968	J.A.T.P., 30, 963.
Briggs, B.H.	1968a	J.A.T.P., 30, 1777.

Briggs, B.H.	1968b	J.A.T.P., 30, 1789.
Briggs, B.H. & Page	1955	Physics of the Ionosphere, Phy. Soc. (Lond).
Briggs, B.H.	1967	Proc.Phys. Soc.(Lond),77,305.
Bamgboye, D.K. & Lyon, A.J.	1968	Nature, 220, 15.
Budden,K.G.	1954	Rep.Camp.Conf.Ionosph.Phys. p.332., Physical Society,London.
Cahill, L.J.	1959	J.G.R. 64, 489.
Calvert,W., & Cohen, R.	1961	J.G.R. , 66, 3125.
Clemesha, B.R.	1964	J.A.T.P., 26, 91.
Chapman, S,	1951b	Compen.Met.Amer.Met.Soc.p.510.
Chapman, S., & Westfold, K.C.	1956	J.A.T.P., 8, 1.
Cohen, R., & Bowles, K.L.	1963	J.G.R., 68, 2503.
Cole, K.D.	1963	Planet.Space Sci., 10, 129.
Croom, S.A.,Robbins,A.R., & Thomas, J.O.	1959	Nature, 184, 2003.
Cook,A.C. & Price,A.T.	1969	Planet.Space Sci.,17, 471.
Datta, R.N.	1968	J.A.T.P., 30, 187.
Davis,T.N., Stolarik, J.D., & Heppner, J.P.	1965	J.G.R. 70, 5883.
Deshpande, M.R. & Rastogi, R.G.	1966a	Ann. de. Geophys., 23, 418.
Deshpande, M.R. & Rastogi, R.G.	1966b	Proc.IQSY Symp., New Delhi, p.
Deshpande, M.R., & Rastogi, R.G.	1967	Proc. Indian Academy of Sci., 66, 272.

Deshpande, M.R., & Rastogi, R. G.	1968	J.A.T.P., 30, 293.
Deshpande, M.R.	1966	Ph.D. thesis, Gujarat University
Datta, R.N.,	1970	Ind. J.Pure.Appl. Phys.,546.
Dungey, J.W.,	1956	J.A. T.P., 8, 39.
Dungey, J.W..	1959	J.G.R.,64, 2188.
Egadal, J.	1947	Terr.Mag.Atmos.Electr.52, 449.
Egadal, J.	1948	Nature, 161, 443.
Essex,E.A. & Hibberd, F.H.	1967	J.A.T.P., 29, 1025.
Farley, D.S.	1963a	Phys.Rev.Lett., 10, 279.
Farley, D.S.	1963b	J.G.R., 68, 6085.
Fedor, L.S.	1967	J.G.R., 72, 5401
Felgate, D.G.	1970	J.A.T.P., 32, 100.
Fooks, G.F.	1961	J.A.T.P., 22, 43-49.
Fooks, G.F.	1965	J.A.T.P., 27, 979.
Fooks, G.F. & Jones, I.J.	1961	J.A.T.P., 20, 229.
Fürth, R. & Mcdonald, D.K.C.	1947	Proc,Phys, Soc., 59, 388.
Gish,, O.H. & Wait, G.R.	1950	J.G. R., 55, 473.
George,T.M.	1968	J.A.TP. 30, 735.
Golley, M.G., & Dennison, P.A.	1970	Planet.Space Sci., 18, 95.
Golley, M.G., & Rossiter, D.E.	1971	J.A.T.P., 33, 701.
Golley, M.G. & Rossiter, D.E.	1970	J.A.T.P., 32, 1215.
Gouin, P & Maynud, P.N.	1967	Ann.De.Geopy. 23, 41.

Goodman, N.P. Katz,S. 1961 Krama, B.H. &Kuo,M.T.		Tatmometrics 5, 245.
Gossard, E.E.	1967	J.G.R., 72, 1563.
Greenhow, J.S., & Newfold, E.L.	1961	Q.J.R.Met.Soc., 87, 472.
Greenhow, J.S.	1954	Phil. Mag., 45, 471.
Hansoh,W.B. & Moffet,R.J.	1966	J.G.R. 71, 5559.
Harish Chandra	1969	Ph.D.theis, Gujarat University.
Haug, A., & Pattersen, H.	1970	J.A.T.P., 32, 397.
Hey,J.S.	1947	Nature, 159, 119.
Harang, L. & Pedersen, K.	1956	Geophys.Publ.Vol.XIX No.10
Hibberd, F.H.	1971	J.A.T.P. 33, 783.
Hirono, M. & Maeda, H.	1954	J.Geomag.Geoelec.,6, 122.
Hines, C.O.	1960	Can.J.Phys., 38, 144.
Hines, C.O. & Rao, R.R.	1968	J.A.T.P., 30, 979.
James, P.W.	1962	J.A.T.P., 24, 237.
Jones, D., & Maude, A.D.	1965	Nature, 206, 177.
Jones,D., & Maude, A.D.	1968	J.A.T.P., 30, 975.
Jones, D., & Maude,A.D.	1968	J.A.T.P., 30, 1487.
Kashin,A.A., & Mirkotan, S.F., & Rybalchenko, V.G.	1970	Geomagnetism and Acronom 10, 368.
Kelleher, R.F.	1966	J.A.T.P., 28, 213.
Kelleher, R.F.	1965	Proc.IInd.Int.Symp,on Equato Ionosphere, ed.F.ed.Mendonca p.272.

Keneshea, T.J.	1965	J.A.T.P., 27, 17.
Keneshea, T.J., Gardner, M.E., & Pfister, W.	1965	J.A.T.P., 27, 7.
Kent,G.S., & Koster,J.R.	1966	Ann.de.Geophys. 22, 405.
Kent,G.S., & Wright,R.W.H.	1968	J.A.T.P., 30, 657.
Knecht,R.W. & Mcduffie,	1962	'Sporadic E' Pergamon Press, Newyork, pp.215.
Krautkramer	1950	Archiv.Elekt.Upertragung,4,133
Krishnamurthy, B.V.	1965	Ph.D. theis, Andhra University.
Koster, J.R.	1963	J.G.R., 68, 2579.
Koster, J.R., & Katsriku, I.K.	1966	Ann.de.Geophys, 22, 440.
Kazimirovskiy, E.S.	1962	Geom.Aeronomy, 2, 897.
Layzer, D.	1967	Nature, 213, 576.
Liller, W. & Whipple, F.L.	1954	Space Supple.to J.A.T.P., 1, 1
Lyon, A.J. & Thomas, L.	1963	J.A.T.P., 25,373.
Lyon, .A.J, Morris,R.W. & Bamgboye, D. K.	1969	Scientific Report
Liu, C.H.,&Ych,K.E.	1966	Radio Sci., I, 1283.
Martyn,D.F.	1947	Proc. Roy.Soc., A190, 273.
Martyn,D.F.	1955	Proc,Phys.Soc.London.
McGee,C.R.	1966	JA.T.P., 28, 861.
McNicol, R.W.E.	1949	Proc.Instn.Elect.Engrs. Part III,96, 517.
McNish, A.G.	1937	I.A.T.M.E., Bull., 10, 271.

Martyn, D.F.	1950	Phil.Trans.Roy. Soc., London, A246, 306.
Manning, L.A., Villard, P.G., & Peterson, A.M.	1950	Proc.I.R.E., 38, 877.
Misra, R.K., & Rastogi, R.G.	1970	J.A.T.P., 32, 967.
Misra, R.K., Chandra, H. & Rastogi, R.G.	1971	J.of Geomag.Geoelect.(in press)
Misra, R.K., & Rastogi, R.G.	1971	Ind. J. Pure.Appl. Phys.,(in p
Misra, R.K., & Rastogi, R.G.	1971	J.I.T.E., (in press).
Misra, R.K., & Rastogi, R.G.	1971	J.I.T.E., (in press).
Mitra, S.N.	1949	J.I.E.E., 96, III, 441.
Mirkotan, S.F.,	1962	Geomag.and Aeronomy, 2, 578.
Maeda, K. & Matsumoto, H.	1961	Rep. Ionos. Space Res.,(Japan), 16, 1.
Morris, R.W. & Lyon A.J.	1963	Nature, 210, 617.
Madea, K.	1963	Phys.Rev.Letters, 11, 406.
Muller, H.G.	1968	Planet.Space Sci., 16, 6190.
Morris, R.W.	1967	J.A.T.P., 29, 651.
Munro, G.H.	1948	Nature, 162, 386.
Munro, G.H.	1963	J.G.R., 68, 1851.
Osborne, D.G.	1963	J.G.R., 68, 1851.
Onwumechilli, C.A. & Alexender, N.S.	1959a	J.A.T.P., 13, 222.
Onwumechilli, C.A. & Alexender, N.S.	1959b	J.A.T.P., 16, 115.
Putter, P.ST.	1955	Physics of the ionosphere, p.

Papagiannis, M.D.,& Elkins, T.J.	1970	J.A.T.P., 32, 383.
Pawsey, J.L.	1935	Proc.Camb.Phil.Soc., 31, 125.
Phillips, J.S., & Spencer,M.	1955	Proc. Phys. Soc., 68B, 106.
Phillips, G.T.	1952	J.A.T., 2, 141.
Pitteway,M.L.V., Wright, J. W., & Fedor, L.S.	1971	J.A.T.P., 3, 635.
Pfister, W., & Bibl,K.	1968	AFCRL Report, 68,0662.
Pfister, W.	1970	AFCRL Report, 70, 0461.
Rao, B.R. & Rao E.B.	1958	Nature, 181, 1612.
Rao, R.R. & Rao B.R.	1961	J.A.T.P., 22, 81.
Rao, .A.S & Rao,B.R.	1964a	J.A.T.P., 26, 399.
Rao, G.L.N. & Rao,B.R.	1965	J.G.R., 70, 667,
Rao, P.B. & Rao B.R.	1964	J.A.T.P., 26, 445.
Rao, B.R., Rao, P.B., & Murthy, Y.V.R.	1961	Proc.IGY Symp., New Delhi., 205-211.
Rastogi, R.G.	1959a	Can. J.Phys.37, 874.
Rastogi, R.G.,	1959b	J,G.R., 64, 727.
Rastogi, R.G., Deshpande, M.R., & Kaushika,N.D.	1966	J.A.T.P., 28, 137.
Rastogi, R.G., Deshpande, M.R., & Harish Chandra.	1968	J.A.T.P., 30, 1597.
Rastogi, R.G.	1970	Nature, 225, 258.
Rastogi, R.G.	1971	Proc.Ind.Academy, Sci. 73, 283
Rastogi, R.G., Chandra, H., & Chakravarty, S.C.	1971	Proc.Ind.Academy, Sci. 74, 62

Rastogi,R.G.	1957	Indian J.Met.Geophys,, 8, 43.
Rastogi, R.G.	1962	J.A.T.P., 24, 533.
Ratcliffe, J.A., & White, E.L.C.	1934	Proc.Phys.Soc., Lond, 46,107.
Ratcliffe,J.A.,	1962	'Sporadic E', Pergamon Press, Newyork, pp.28.
Ratcliffe, J.A.	1954	J.A.T.P., [illegible]
Ratcliffe, J.A.	1948	Nature, 162, 9.
Ratcliffe, J.A.& Pawsey, J.L.	1933	Proc.Camb.Phil. Soc., 29, 301.
Rawer, K.	1965	Annales IGY, 33, Compiled by K.Rawer.
Rice, S.O.	1949	Bell system Technical Journal, 24, 46.
Rishbeth, H.	1967	Planet.Space Sci., 15, 1261.
Rossiter, D.E.	1970	ADP Report No.88, 89, University of Adelaide.
Ramanathan,K.R.	1921	Proc.Indian Assen.Cultivation Sic., p.107.
Rangrajan, S.	1954	J.G.R., 59, 239.
Saguira, M., Cain,J.C.	1966	J.G.R., 71 , 1869.
Saguira, M. & Poros, D.J.	1969	J.G.R., 74, 4025.
Sastry,T.S.G.	1968	J.G.R. 73, 1789.
Sprenger, K. & Schiminder, R.	1969	J.A.T.P., 31, 1085.
Sivaraman,B.M.	1966	J.A.T.P., 28, 1025.
Singer, S.F. ,Maple,E & Bowen, W.A.	1951	J.G.R., 56, 265.

Skinner, N.J.yon, A.J. & Wright, R.W.	1958	Nature, 182, 1363.
Sen, N.N.	1964	J.A.T.P., 26, 25.
Swingerton-Dy, H.P.F.	1963	The Computer, Jr., 16, 23.
Stoffregen, W	1944	Ark.Mat.Astr.Fys., A30, 19.
Taubenheim, J	1957	J.A.T.P., 11, 14.
Tsuda, T., Sa, T., & Maeda, K.	1966	Radio Sci., I , 212.
Untied, J.	1967	J.G.R. 72, 5799.
Vollard, H., & Taubenheim, J.	1958	J.A.T.p., 12, 258.
Woodman, R.F	1970	J.G.R., 75, 6249.
Woodman, R.F & Hogfors	1968	
Wright, J.W., & Fedor, L.S.	1969	J.A.T.P., 31, 925.
Wright, J.W., & Fedor, L.S.	1967	Space Res., 7, 68.
Whitehead, J.D.	1961	J.A.T.P., 20, 49.
Whitehead, J.D.	1967d	J.A.T.P., 29, 285.
Wilson, C.T.R.,	1925	Proc,Phys.Soc.,London,37,320.
Wormell,T.W.	1953	Quart.J.R..Met.Soc., 79, 3.
Wic-Wall	1962	
Yerg, D.G.	1955	J.G.R., 60, 173.
Yerg, D.G.	1956	J. A. T. P 8 , 247
Yerg, D.G.	1959	J.Geophys. Res., 64, 27.